A Structure-Function Study of the TWIK-1 K2P Channel

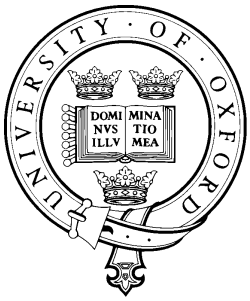

M Firdaus Abd-Wahab

Wolfson College

University of Oxford

A thesis submitted for the degree of

Doctor of Philosophy

Trinity 2015

Declaration of authorship

The work described in this thesis was carried out in the laboratory of Dr. Stephen Tucker, in the Clarendon Laboratory, Department of Physics , University of Oxford, between October 2011 and October 2015. All work within this thesis is entirely my own, unless otherwise stated and has not been previously submitted to this University or any other for the award of a degree. The Molecular Dynamics Simulations and analyses in Chapter 4 has been performed by Dr Prafulla Aryal from the Structural Bioinformatics and Computational Biochemistry Unit, Department of Biochemistry.

Mohd Firdaus Abd-Wahab

(October 2015)

Abstract

Two-pore domain potassium (K2P) channels play a role in regulating the resting membrane potential of cells and therefore play a major role in the function of both excitable and non-excitable cells. One of the K2P family members is the Tandem-pore Weak Inwardly-rectifying Potassium (TWIK-1) channel. It is mostly found in the kidney and heart. However, not much is known about the biophysical properties and regulation of this channel. In the first part of this study, the presence of a hydrophobic cuff at the inner pore side of the channel is identified and characterised. This cuff acts as a barrier to water permeation, and by extension, ion flow through the channel. Using molecular dynamic simulations and electrophysiology, two leucine residues, L146 and L261, were identified as the primary constituents of this hydrophobic cuff. Systematic mutagenesis of these residues reveals that the barrier against pore hydration can be overcome by introducing polar side chains into these positions.

This study also addresses the problem of TWIK-1 functional expression at the surface membrane. Suppression of TWIK-1 functional activity has been thought to be caused by binding of a small ubiquitin-like modifier (SUMO) to a lysine residue in the C-helix (K274). However, it has also been suggested that TWIK-1 at the surface membrane is rapidly internalised into endosomes via the endocytosis pathway. My results suggest that the latter explanation is more likely.

The second major part of this study focused on the structure and function of the amphipathic helix near the c-terminus of the protein. This 'C-helix' lies parallel to the intracellular membrane surface. Using scanning mutagenesis and electrophysiological measurements, a trio of positively-charged residues (K274/R277/K278) that faces the inner pore were identified as playing an important role in the functional expression of TWIK-1 currents by influencing the electrostatic charges at the intracellular pore mouth of TWIK-1. Overall this thesis provides new insights into the structural features which control the functional activity of the TWIK-1 potassium channel.

Acknowledgement

First and foremost, I wish to express my heartfelt gratitude to my supervisor, Professor Stephen J. Tucker, whose expertise, understanding and continued encouragement has tremendously added to my graduate experience in Oxford. I find his vast knowledge and skills inspirational, and has aspired me to someday become a great teacher and dad like him.

I would like to thank Prafulla Aryal who performed the molecular dynamics simulations in this thesis. A special mention to Juris Galvanovskis from the Department of Physiology, Anatomy and Genetics, who has been helpful with the fluorescence microscopy. I also thank them for their share of experience.

I would also like to take this opportunity to thank those who has been through my ups and downs in the electrophysiology lab. Particularly to Conor McClenaghan, Giovanna Bucci, Lejla Zubcevic, Laurianne Angue and Chetan Sharma, for the fruitful discussions, as well as for putting up to my bursts of insanity. We can do serious science and have fun at the same time!

My special thanks also goes to the LSIDTC, which has been instrumental to my development here in Oxford. But in particular, I am ever grateful to Elspeth Garman for her continued support and advice. To my DTC mates, Federico Garza De Leon, Emma Sadler, Lorenz Berger, Alexandra MacKenzie, Marc Szabo, Joe Martin, Aiman Entwistle, and many others, well, what would I do without you.

Not to forget Ilham Ramli, Firdaus Chin, Juliana, Syed Nooh, Nazri Bajuri and many others, thank you for the Malaysian hospitality. Also to Hakimi Kassim, I will always miss our breakfast conversations on receptors and channels at Zappi's. A cup of hot chocolate and a slice of banana bread is always good to get us going!

Finally, I know I owe it to my family back home for their undying encouragements and support. I wouldn't have come all this way without you, Mum and Dad. To Amanatuzzakiah, thank you for your patience and loving support. And to my little princess, Ayra Safiyyah, hopefully someday I can inspire you as much as I have been inspired by these people.

Dengan Nama Mu..

継続は力なり

Contents

1 Introduction **1**
1.1 Channels for the movement of ions across membranes 1
1.1.1 Potassium homeostasis is vital for body function 2
1.2 Bioelectricity 4
1.2.1 Membrane Potential 4
1.2.2 Resting Potential 5
1.2.3 The action potential 7
1.2.4 Rectification 8
1.2.5 Conductance 8
1.3 Potassium Channels 10
1.3.1 The selectivity filter 11
1.3.1.1 Structural arrangement of the selectivity filter 12
1.3.1.2 Ion selectivity 13
1.3.2 Classification of K^+channels 15
1.4 Two-Pore Domain Potassium Channels (K2P) 17
1.4.1 The unique structure of K2P 19
1.4.1.1 The extracellular cap 20
1.4.1.2 Twist and turn: Domain swapping 21
1.4.1.3 Lateral fenestration 21
1.4.2 TWIK-1 channel 22
1.4.3 Regulation of TWIK-1 expression 22
1.4.4 Crystal structure of TWIK-1 23
1.4.4.1 The C-helix 25
1.4.5 Physiological significance of TWIK-1 26
1.4.5.1 Dynamic ion selectivity in TWIK-1 27
1.5 Scope and Significance of Study 27

2 Materials and Methods **29**
2.1 Molecular Biology 29
2.1.1 Materials 29
2.1.1.1 Gene and Vector 29
2.1.1.2 Oligonucleotides 29
2.1.1.3 Synthesis, Extraction and Purification Kits 30
2.1.1.4 Sequencing Primers 31

2.1.2 Molecular Biology Methods 31
2.1.2.1 *Escherichia coli* 31
2.1.2.2 Subcloning 32
2.1.2.3 Site-Directed Mutagenesis 32
2.1.2.4 Gel Electrophoresis 33
2.1.2.5 Ligation 33
2.1.2.6 In-vitro RNA Transcription 33
2.1.3 pFAW vector construct 34
2.2 *Xenopus laevis* Oocyte Harvest and Preparation 35
2.2.1 Schedule 1 Procedure 36
2.2.2 Oocyte Preparation 36
2.3 Electrophysiology 36
2.3.1 The Voltage Clamp Technique 37
2.3.2 TEVC Materials 37
2.3.3 Microinjection and Incubation 39
2.3.4 TEVC Data Acquisition 39
2.4 Fluorescence Microscopy 40
2.4.1 Fluorescent-Tagged Plasmids 40
2.4.2 Wheat-Germ Agglutinin and CF633 40
2.4.3 Fluorescent Microscopy 41
2.5 Molecular Dynamics Simulation 42

3 Functional studies of TWIK-1 44
3.1 Introduction 44
3.1.1 SUMOylation of TWIK-1 45
3.1.2 Rapid Internalisation of TWIK-1 47
3.2 Results 49
3.2.1 Declaration of Authorship 49
3.2.2 Wild-Type TWIK-1 currents appear functionally silent 49
3.2.3 Mutations are inconsistent with SUMOylation hypothesis 50
3.2.4 Functional expression of TWIK-1 is increased by mutation of the trafficking motif 53
3.2.5 TWIK-1 structural observation at the C-helix 55
3.2.5.1 Possible interaction between K274 and E269 55
3.2.5.2 MD simulation suggests that the C-helix is stable 58
3.3 Discussion 59

3.3.1 SUMOylation or rapid internalisation? . . . 59
3.3.2 The C-helix formation is stable . . . 59
3.4 Conclusion . . . 60

4 A Hydrophobic Barrier in TWIK-1 62
4.1 Introduction . . . 62
4.1.1 Mechanism of the Hydrophobic Barrier . . . 63
4.1.2 Nanopores and Electrowetting . . . 64
4.1.3 Ligand-gated ion channels . . . 67
4.1.4 Bacterial mechanosenstive ion channels: Hydration of pores influences gating kinetics . . . 68
4.1.5 MthK channel lacks a helix-bundle crossing . . . 68
4.1.6 TWIK-1: Dewetting of the inner pore . . . 69
4.2 Results . . . 73
4.2.1 Declaration of Authorship . . . 73
4.2.2 Identification of a 'greasy doughnut' . . . 73
4.2.3 M2 Helix: Role of L146 . . . 76
4.2.3.1 L146D mutation . . . 76
4.2.3.2 L146N mutation . . . 76
4.2.3.3 Mutants retain inhibition by quinine and external pH . 81
4.2.3.4 L146I and L146V compared to L146T: Isosteric substitutions . . . 82
4.2.3.5 Reducing side-chain volume: L146A, L146G, L146S mutations . . . 84
4.2.3.6 Other substitutions: L146M and L146K . . . 86
4.2.3.7 Conclusion from L146 scanning mutagenesis . . . 88
4.2.3.8 Surface membrane expression levels of TWIK-1 mutants 89
4.2.3.9 Do mutations alter the permeation pathway? . . . 92
4.2.4 M4 helix: Role of L261 . . . 94
4.2.4.1 L261D/N mutations . . . 94
4.2.4.2 L261S/A and L261T/V mutations . . . 96
4.2.5 Pairwise mutations of L146 and L261 . . . 98
4.2.6 Other residues in the hydrophobic cuff: L264 . . . 100
4.2.7 Influence of lipids on the hydrophobic barrier . . . 103
4.3 Discussion . . . 105
4.3.1 L146 and L261 create the hydrophobic cuff . . . 105

4.3.2 Regulation and expression level unaffected by mutation 105
4.3.3 Mutating L146 and L261 alters permeation directly 106
4.3.4 Lateral fenestration sites and the L264 106
4.4 Conclusion 107

5 Scanning mutagenesis of the C-Helix 108
5.1 Introduction 108
5.2 Results 111
5.2.1 Declaration of Authorship 111
5.2.2 Functional effects of residues on the polar surface of the C-helix 111
5.2.2.1 Mutations of K274 113
5.2.2.2 Mutating R277 results in an increase of functional activity 115
5.2.2.3 MD simulation suggests a possible interaction between R277 and E265 117
5.2.2.4 Glutamate substitution on other lysine residues in the C-helix. 120
5.2.3 Other residues on the C-helix 121
5.2.4 Position of C-helix activatory mutations around the inner pore . . 122
5.3 Discussion 122
5.3.1 Role of pore-facing charged residues 123
5.3.2 Movement of the C-helix may influence inner pore gating 124
5.4 Conclusion 125

6 Conclusion and Future Directions 126
6.1 Summary of findings 126
6.1.1 TWIK-1 channels undergo endosomal distribution 126
6.1.2 Hydrophobic Barrier in TWIK-1 127
6.1.2.1 Scanning mutagenesis strongly support the presence of the hydrophobic cuff 127
6.1.2.2 The mutations alter the permeation pathway 127
6.1.2.3 Influence from the lateral fenestration on the hydrophobic cuff 128
6.1.2.4 Does mutating the cuff affect unitary conductance? . . . 128
6.1.3 Role of the C-helix 128
6.1.3.1 The activatory mutations on the C-helix face the pore . 129
6.2 Future Directions 129
6.2.1 Hydrophobic gating in other K2P channels 129

6.2.2 Other studies on TWIK-1 130
6.2.3 Future annotation of membrane protein structures 131
6.3 Concluding remarks 132

Appendix A: TWIK-1 sequence alignment **135**

Appendix B: DNA sequence for pFAW vector **136**

Appendix C: Electrophysiology buffers **140**

Appendix D: A hydrophobic barrier deep within the inner pore of the TWIK-1 K2P potassium channel **141**

Appendix E: Influence of lipids on the hydrophobic barrier within the pore of the TWIK-1 K2P channel **156**

References **162**

List of Figures

1.1 **Potassium secretion and sodium reabsorption by the principal cells in the late distal and cortical collecting tubules.** 3
1.2 **The Nernst potential.** 6
1.3 **The action potential.** 7
1.4 **A typical Goldman-Hodgkin-Katz rectification** 9
1.5 **Basic topology of a K^+channel.** 10
1.6 **The structure of KcsA.** 11
1.7 **The K^+-selective filter.** 12
1.8 **The different mechanisms of ion permeation at the selectivity filter.** 14
1.9 **The mammalian potassium channel family.** 16
1.10 **The mammalian K2P family.** 19
1.11 **X-ray crystallography structures of K2P channels.** 20
1.12 **The general architecture of TWIK-1.** 24
1.13 **The C-helix structure is unique to TWIK-1.** 25

2.1 **pBF plasmid containing the human TWIK-1 gene.** 30
2.2 **Constructing the pFAW plasmid.** 34
2.3 **pFAW vector map.** 35
2.4 **Recording whole cell currents on Two-Electrode Voltage Clamp.** . . . 38
2.5 **GFP-tagged TWIK-1 protein.** 40
2.6 **Fluorescent Microscopy.** 42

3.1 **The SUMO pathway.** 46
3.2 **The proposed TWIK-1 SUMOylation site.** 47
3.3 **TWIK-1 is being internalised and recycled.** 48
3.4 **Current density highlighting the effect of removing or mutating the di-isoleucine motif.** 48
3.5 **Lack of functional expression of wild-type TWIK-1.** 50
3.6 **The effect of mutating K274E and K274R varies.** 51
3.7 **Mutating K274 shows different level of currents.** 52
3.8 **Endocytotic mutation vs SUMOylation mutation.** 54
3.9 **The C-helix domain of TWIK-1 subunit.** 56
3.10 **E269Q mutation has no effect on TWIK-1 channel activity.** 57
3.11 **100ns MD simulation supports that the C-helix is stable.** 58

4.1 **Principle of hydrophobic gating.** 66

4.2 **100ns MD simulation shows stability of the C-helix** 70
4.3 **Stochastic wetting and dewetting of the inner pore.** 71
4.4 **Dewetting persists under different forcefields.** 73
4.5 **Identifying the 'greasy doughnut'.** 75
4.6 **Breaking the hydrophobicity barrier with polarity inclusion.** 77
4.7 **Introducing polarity is sufficient to improve permeation.** 79
4.9 **TWIK-1 L146N mutant channel retains normal functional activity.** . . 81
4.10 **Isosteric and hydrophobic mutations retain low channel activity, but not hydrophilic mutation.** 83
4.11 **Changing inner pore diameter around the hydrophobic ring with smaller amino acids.** 85
4.12 **Other substitutions: L146M and L146K.** 87
4.13 **Scanning mutagenesis of L146 shows higher activity for hydrophilic mutants.** 88
4.14 **Qualitative confirmation of TWIK-1 mutants expression level.** 90
4.15 **Comparison of surface expression level and electrophysiological recordings.** 91
4.16 **L146N mutation alters the permeation pathway directly.** 93
4.17 **Polarity at position 261 also relaxes the hydrophobic barrier.** 95
4.18 **Hydrophilic substitutions overcome the hydrophobic barrier for permeation to occur.** 97
4.19 **Pairwise mutations at the hydrophobic cuff.** 99
4.20 **Location of L264 in the structure may partially contribute to the hydrophobic barrier.** 100
4.21 **Mutations at L264 suggests a partial influence towards stabilising the hydrophobic barrier.** 102
4.22 **Influence of lipid tails in the ion conduction pathway of TWIK-1.** . . 104

5.1 **Surface electrostatics at the inner pore mouth.** 109
5.2 **Scanning Mutagenesis of the C-Helix.** 112
5.3 **Substitutions at K274 resulted in an increase in current.** 114
5.4 **Mutations at R277 also produce an increase in the level of functional expression of TWIK-1.** 116
5.5 **Interaction between R277 and E265.** 118
5.6 **Effect of substituting E265 on TWIK-1 channel activity.** 119
5.7 **Effect of K275E and K278E mutations on whole cell TWIK-1 currents.** 120

5.8 **Substitutions at the non-pore-facing residues of the C-helix have no significant effect.** 121
5.9 **Position of the three key residues.** 122
5.10 **Surface polarity at the inner-pore side of the C-Helix domain.** 123

6.1 **Hydrophilic substitutions in TREK-2 inner pore increases channel activity.** 130
6.2 **Inhibition of TWIK-1 L146N* by carvedilol.** 131

List of Tables

2.1 Kits from Qiagen Inc. used for DNA synthesis and purification. 30
2.2 Kits used for RNA synthesis and purification. 31
2.3 Primers used for DNA sequencing. 31

CHAPTER 1

Introduction

This thesis has studied the TWIK-1 ion channel, which is classified as a member of the two-pore domain (K2P) family of potassium channels. In this chapter, the general overview of potassium channels will be briefly introduced before the K2P channel family, including TWIK-1, is described. The physiological importance of potassium ions is also briefly highlighted here.

1.1 Channels for the movement of ions across membranes

Every living cell is enclosed within a membrane layer that is composed mainly of lipidic constituents. This generally protects the cell from its external surroundings, which typically contains a plethora of hydrophilic and charged molecules (Choe, 2002). Without the lipid bilayer, these molecules could easily penetrate into the cell body and disrupt the intracellular conditions, which could lead to detrimental consequences. This epitomises the importance of the membrane bilayer.

However, exchange of molecules across the lipidic bilayer milieu is still required to maintain cell function. In order to allow this process to take place in a regulated manner, pore-forming macromolecules are embedded on the membrane surface. For

ions, ion-selective channels are the main units that catalyse ionic movement into and out of the cells (Hille, 2001).

Ion channels exist in abundance. The roles they play are diverse and pivotal to maintaining proper bodily functions. The most evident role of ion channels is in the control of cell electrical excitability, although they are also present in non-excitable cells (Hall, 2010a). Ion channels are most often preferentially permeant to a certain species of ion, and can change between open and closed states. Therefore, potassium ion channels have a higher preference for potassium ions over sodium, or other ions. Potassium channels have been diversely characterised in terms of their functional roles and modulations, which highlight the importance and need to regulate the flow of potassium ions across cells.

1.1.1 Potassium homeostasis is vital for body function

Potassium is the major cation in the body intracellular fluid. At a concentration of 140-150mM, 98 percent of potassium is contained within body cells. The remaining 2 percent can be found in the plasma, interstitial fluid and other extracellular fluid (Cheng et al., 2013). This cationic gradient created by potassium across the cell membrane is balanced by sodium, which is more abundant in the extracellular fluid than in the intracellular fluid. Several factors can influence potassium distribution, either by stimulating potassium uptake into cells or its release into the extracellular space. These include insulin and aldosterone levels, osmolarity and acid-base balance (Pohl et al., 2013; Palmer, 2015). The control of potassium distribution is important for our body to withstand sudden changes in extracellular potassium concentration, particularly during hyper- and hypokalaemic conditions.

Potassium homeostasis mostly occurs in the kidney. In the proximal tubule and the ascending loop of Henle, potassium is reabsorbed through the renal interstitium and into the blood, whereas potassium secretion takes place in the late distal and cortical

collecting tubules (Hall, 2010b). The latter process is controlled by principal cells, a group of cells that constitute the majority of epithelial cells in those parts of the renal tubule (Figure 1.1), and the TWIK-1 channel was suggested to influence the regulation of K^+ions here (Cluzeaud et al., 1998; Millar et al., 2006). In an ATP-driven process, the Na^+-K^+-ATPase pump at the basolateral region maintains a low concentration of Na^+ions inside the cell, while actively transporting K^+ions from the blood into the cell. This creates a concentration gradient that drives passive transport of K^+across the membrane. In a counterbalance act, intracellular $Na^+$is replenished by transport through the epithelial Na^+channel (ENaC).

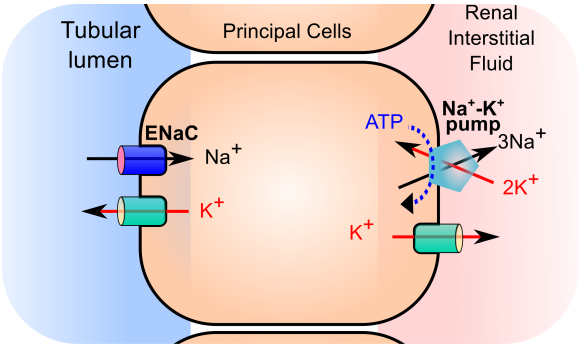

Figure 1.1: Potassium secretion and sodium reabsorption by the principal cells in the late distal and cortical collecting tubules. As the Na^+-K^+-pump energetically increases the intracellular potassium concentration, K^+ions then moves along its gradient and exits the cell by passive transport. In turn, Na^+ion are replenished back into the cell through the ENaC channel.

Regulation of potassium movement is also important in the nervous system. In the central nervous system (CNS), tight regulation of the potassium is crucial for various neuronal processes, including electrogenic transport and synaptic transmission (Kofuji and Newman, 2004). This strict maintenance is achieved through the activity of the abundant K+ channels present in the nerve. In glial cells, potassium homeostasis is achieved by mitigating excess extracellular K^+ions from sites of elevated concentration through adjacent cell members and released into sites where the extracellular K^+ion concentration is low. This so-called *spatial buffering* mechanism redistributes extracellu-

lar K^+ions from locations where neuronal activity just occurred to sites where the cells are at rest (Kofuji and Newman, 2004; Noori, 2011).

A stable and well regulated level of potassium is also crucial for the heart to function normally, because excess potassium in the extracellular fluid may not only disrupt electrical signalling but also lead to dilated cardiomyopathy and arrhythmia. Conversely, hypokalaemia can also lead to other cardiovascular diseases, or even sudden cardiac death (Kjeldsen, 2010). This is, in part, due to the change in potassium concentration gradient across the muscle tissues, which affects the membrane potential.

Regulating the ionic flux across the plasma membrane in excitable cells are equally important, even when cells are electrically at rest. Ion channels continuously mediate the movement of ions, always creating and dissipating the electrochemical gradient across the membrane.

1.2 Bioelectricity

1.2.1 Membrane Potential

The main determinant that separates the extracellular and intracellular environment of a cell is its membrane. It is mostly composed of lipids, but also contains ion channels that make it selectively permeable to different ions. The concentration of individual ions between the extracellular and intracellular environment are unequal. The concentration of K^+ions, for example, is much higher inside the cell than outside. This generates a chemical potential across the membrane, which causes an efflux of K^+ions down the chemical gradient. Movement of K^+ions through the membrane is mediated by channels that are K^+-selective. Since K^+channels are permeable to K^+ions only, this causes negative charges to be left behind and remain inside the cell. As more K^+ions leave, the intracellular environment becomes more negative. Gradually, this generates an electrical potential that resists any further movement of K^+ions. As a result, the

concentration gradient is counterbalanced by the electrical potential at the membrane. Eventually, an equilibrium is reached between the chemical and electrical potentials. For an individual ion species, its equilibrium potential is given by the Nernst equation. This equation correlates the equilibrium potential of an ion species to its concentration gradient as follows;

$$E_{ion} = \left(\frac{RT}{zF}\right) \ln \frac{[ion]_o}{[ion]_i}, \tag{1.1}$$

Where:

E_{ion} : the equilibrium potential for the ion species :

R : gas constant T : temperature

z : ion valence F : Faraday constant

$[ion]_o$: extracellular ion concentration $[ion]_i$: intracellular ion concentration

1.2.2 Resting Potential

When cells are at rest, they maintain a membrane potential of -80mV. The equilibrium potential for $K^+$is -90mV. This close approximation between the resting membrane potential and the K^+Nernst potential is because the membrane contains a high population of K^+channels. However, movements of other ions across the membrane also occur. Sodium ions move in the opposite direction to K^+ions, thus introducing back positive charges into the intracellular side. This shifts the equilibrium potential rightward, or depolarises, to a lesser negative potential. A better estimation of the equilibrium potential to the Nernst potential is given by the Goldman-Hodgkin-Katz (GHK) equation. This equation takes into consideration the intracellular and extracellular concentrations

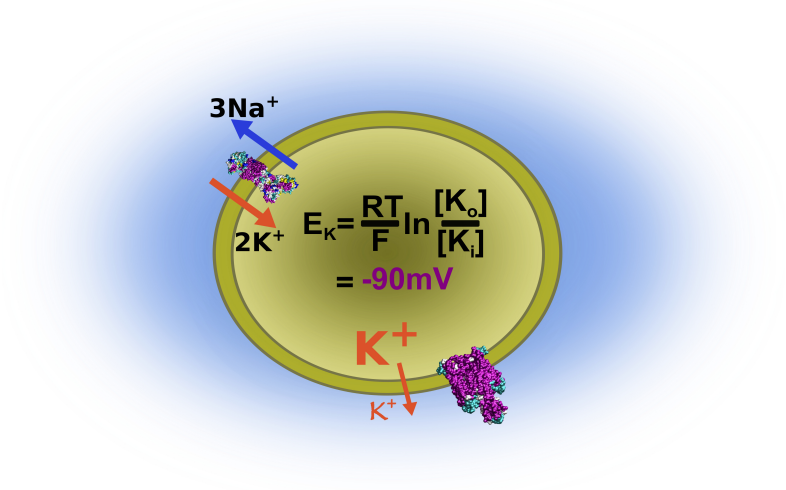

Figure 1.2: The Nernst potential. As the Na^+-K^+ATPase actively transport Na^+ions out and K^+ions in, it increases the K^+concentration inside the cell. This causes $K^+$to diffuse out through K^+-selective channels. The concentration gradient of $K^+$is counterbalanced by an electrical gradient across the membrane. The magnitude of the potential is proportional to the ratio of $[K]_o$ and $[K]_i$. A typical resting membrane potential inside a cell is approximately -80mV. Potassium tends to move out down its concentration gradient.

of the different ions, along with their relative permeability. For a membrane that is permeable to K^+, sodium and chloride ions, the GHK equation is as follows;

$$V_m = \left(\frac{RT}{F}\right)\ln\left(\frac{[K]_o}{[K]_i} + \frac{[Na]_o}{[Na]_i} + \frac{[Cl]_i}{[Cl]_o}\right), \tag{1.2}$$

Where:

V_m : Equilibrium membrane potential F : Faraday constant

R : gas constant T : temperature

$[]_o$: extracellular ion concentration $[]_i$: intracellular ion concentration

The permeability of the membrane to each ion at a given point in time forms the basis for the action potential in an excitable cell.

1.2.3 The action potential

The opening and closing of different ion channels influence changes in membrane relative permeability. When the cells are at rest, their membrane potential is maintained by the constitutive activity of 'leak K^+channels'. As a consequence, the membrane is mostly permeable to K^+ions, setting the cell at its resting potential. After voltage-gated sodium ion channels open the membrane depolarises. This is followed by the opening of voltage-gated K^+channels and inactivation of the sodium channels. Consequently, the cell returns to its resting potential. An overview of an action potential is shown in figure 1.3.

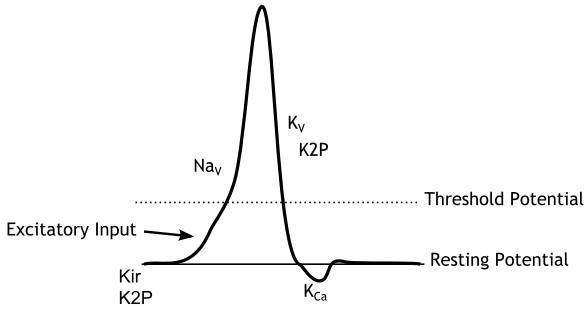

Figure 1.3: The action potential and ion channels involved during its propagation. While cells are at rest, the membrane potential is maintained at its resting potential by background K^+channels (Kir and K2P). When stimulus triggers the ligand-binding ion channels, an influx of mostly $Na^+$and Ca^{+2} cause the membrane to depolarise. If sufficient depolarisation occurs and brings the membrane potential above the threshold limit, voltage-gated sodium (Na_V) channels are activated. This initiates a sharp increase in membrane potential, the action potential. Depolarisation also activates the voltage-gated K^+channels, although their kinetics are much slower than that of the Na_V channels. The membrane potential then reaches a plateau, and repolarisation begins to take place. The membrane eventually reaches back to its resting potential, ready for the next firing.

The major role of the two pore domain (K2P) K^+channels, including TWIK-1, is to maintain and regulate the resting potential of the cell. Classically, this role has been attributed to leak channels. They help regulate excitability in cells by stabilising membrane voltages in the sub-threshold range. This sets the voltage magnitude a

membrane needs to be stimulated to before an action potential can take place. They also determine the duration, amplitude and frequency of action potentials.

1.2.4 Rectification

One of the main assumptions in the Goldman-Hodgkin-Katz equation is that ions move independently of each other. This allows one to predict the conductance based on the differences in ionic concentration across the membrane. The conductance for ions flowing against the concentration gradient will be lower than flowing down its gradient. Consequently, under physiological concentrations, K^+channels were expected to show an outward rectification when current (I) is plotted against voltage (V). On the other hand, when the concentrations on both sides are equal, the I-V plot would be linear, resembling the Ohm's law. This GHK-resembling I-V plot that was previously predicted of leak channels, including K2Ps, are shown in figure 1.4. Although ions do not move independently, but interact with the selectivity filter region of the ion channel, the GHK equation still describes the behaviour of K^+channels reasonably well.

However, rectification may not simply only be conferred by differences in inside and outside ion concentrations, but may also be due to gating in channels that are voltage-dependant, or even blockers that act in a voltage-dependant manner (Goldstein et al., 2001)

1.2.5 Conductance

Measuring the ionic flux is therefore imperative to characterise the intrinsic property of an ion channel. As described earlier, we can see that the activity of an ion channel is related to the flow of its permeating ions (currents) at a certain voltage. This allows us to plot an I-V curve. In general, current, I is linearly proportional to voltage, V, and

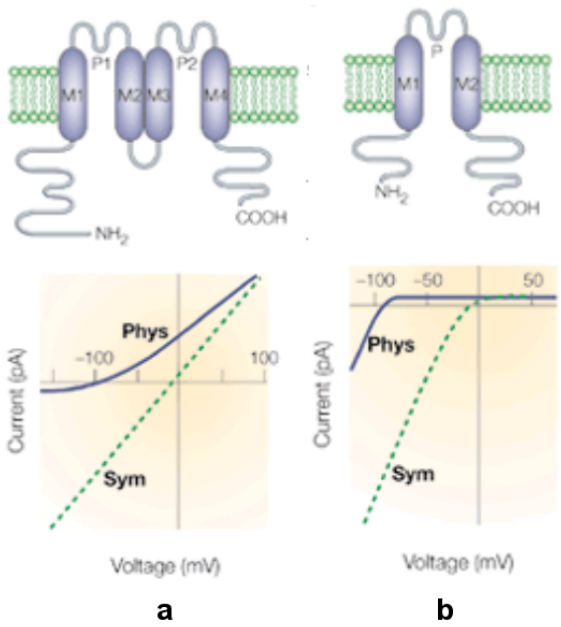

Figure 1.4: A typical Goldman-Hodgkin-Katz rectification. a) Classically, conductance of K2P channels under physiological conditions (Phys) are regarded to be outwardly/openly rectifying, and linear in symmetrical K^+solutions (Sym), which is different to (b) the conductance of a typical Kir channel, which is inwardly-rectifying. Figure adapted from (Goldstein et al., 2001).

inversely proportional to resistance, R, in accordance to the Ohm's law.

$$I = \frac{V}{R} \tag{1.3}$$

Since conductance (g) is the inverse of resistance, we can then rearrange the equation as;

$$I = V \times g \tag{1.4}$$

Conductance then represents a measure on the intrinsic ability of an ion channel to permeate ions.

1.3 Potassium Channels

The first K channel cloned was from the Drosophila Shaker gene (the Shaker K channel). The discovery of this voltage-gated K channel by cloning led to genome projects that revealed other K channels, including those from the mammalian family. Today, K channel genes constitute the largest family of ion channels known to date, and more than 80 mammalian genes that encode for K channel subunits have been found (Feliciangeli et al., 2015).

Although varying in certain topology and form, K channels share certain common features that can be recognised with. The most important feature is that they contain at least one pore-lining loop (P-loop) in each subunit. Within this P-loop is a conserved sequence of amino acids ('TXGYG') that signifies the K-channel family, and is known as the selectivity filter motif. In addition to this feature, K-channel subunits also typically contain at least two transmembrane domains, which flanks the P-loop (Figure 1.5). The basic module of a K-channel subunit, therefore, consists of two transmembrane domains and one P-loop (2TM/1P) (Hille, 2001).

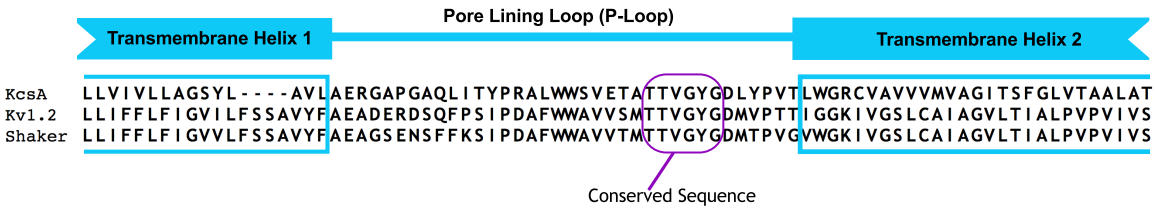

Figure 1.5: Basic topology of a K^+channel.. A K^+channel generally has at least two transmembrane domains that span the membrane and flank a pore-lining loop (P-loop). Within this P-loop is a consensus amino acid sequence that forms the selectivity filter region of the channel. It also serves as a signature sequence for recognising K^+channels, as exemplified by the sequence alignment of KcsA, Kv1.2 and Shaker channels.

Structurally, the functional K-channel assumes a tetrameric formation (figures 1.6a, 1.6b), as exemplified by the structure of KcsA (Doyle et al., 1998). This usually involves an assembly of four subunits, with a pore lumen located at the centre axis of the channel. In the outer membrane side of the channel, the P-loop from each subunit lines the pore,

and forms a narrow passage that is highly selective of K-ions. Due to this selective manner, the region is known as the selectivity filter.

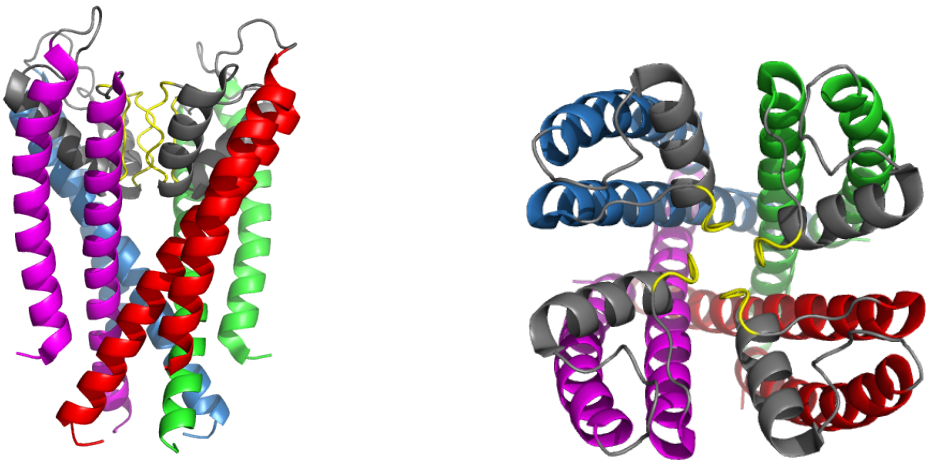

(a) (b)

Figure 1.6: The structure of KcsA (PDB: 1K4C) exemplifies the tetrameric formation of a K^+channel. Four subunits (coloured separately; red, purple, green and blue) assemble to form a pore cavity at the centre. The pore is lined at the outer-membrane side by the selectivity filter motif (yellow) from the P-loop (grey). Each subunit consists of two transmembrane helices, with the P-loop located in between. Left: side-view, right: top-view.

1.3.1 The selectivity filter

The most intriguing element about potassium channels is the fact that although they conduct K^+rapidly at a rate near to its diffusion limit, the channels are still capable of selecting K^+ions several thousand times over Na^+ions (Hille, 2001). The Pauling diameter of a K^+ion is 2.66Å, which is larger in size when compared to 1.90Å of a Na^+ion (Varma et al., 2011b). Thus, this remarkable degree of ionic selectivity would require a mechanism that is capable of filtering out smaller ions.

Suggestions on the mechanism of ion selectivity had been provided before (Eisenman and Horn, 1983). But it was not until the crystal structure of a prokaryotic potassium channel had been resolved, that we were able to visually describe the mechanics behind ion selectivity with great detail (Doyle et al., 1998).

1.3.1.1 Structural arrangement of the selectivity filter

The KcsA potassium channel forms a tetrameric structure consisting of four subunits encompassing a central pore (figures 1.6a, 1.6b). Each subunit contributes to one pore-forming helix domain, the channel pore therefore also contains four pore loops that form a narrow opening, known as the selectivity filter, near the outer membrane. The residues lining this pore arrange themselves in such a way that the backbone carbonyl oxygens from each of these residues point towards the axis of the channel (Figure 1.7b).

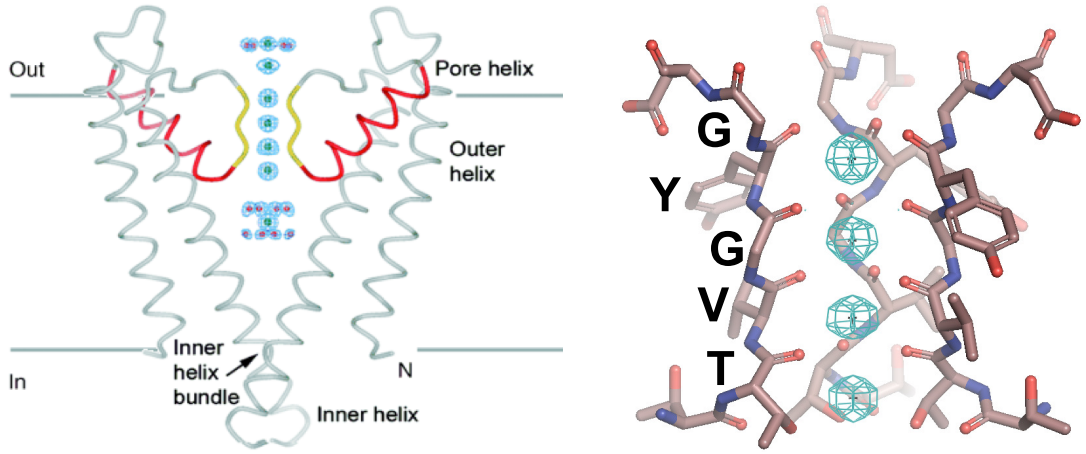

Figure 1.7: The K^+-selective filter. Based on the KcsA structure that Mackinnon group solved (Doyle et al., 1998), they were able to characterise the nature of potassium ion selectivity, especially over sodium ion. a) K^+ion is dehydrated as it enters the selectivity filter, and rehydrated again once it exits from the other side of the filter (MacKinnon, 2003), yellow: selectivity filter domain, red:pore helix, atoms; green:potassium, red:water. b) Averaged position of potassium in the selectivity filter from the crystal structure of KcsA, which displays the four sites formed by the oxygens of the filter motif backbone carbonyl and side-chain hydroxyl groups. The signature sequence (TVGYG) is shown next to each residue (PDB id: 1K4C).

1.3.1.2 Ion selectivity

As shown in figure 1.7a, we can see that as the hydrated potassium ion enters the outer pore mouth of the channel, it sheds its bound water molecules. The now dehydrated ion then interacts with the carbonyl groups of the selectivity filter. Figure 1.7b reveals this tight packing between the ion and the carbonyl groups, rendering this process to be energetically favourable. This is the pivotal point that denotes selectivity of potassium over sodium ion. Sodium ions have a smaller ionic radius than potassium (0.95Å vs 1.33Å). Therefore, the ionic hydration energy for sodium is higher than potassium (-105 kcal/mol vs -85kcal/mol) (Hille, 2001). It is therefore, energetically less favourable for sodium ions to release their bound water molecules in order to permeate through potassium channel pores.

The selectivity filter forms the narrowest passage throughout the pore, and permits ion conduction in a single file. Intriguingly, this asserts the same idea that Hodgkin and Keynes concluded with from their experimental observation 40 years before (Hodgkin and Keynes, 1955). From the structure, four cation binding sites are formed by the carbonyl groups (figure 1.7b). At low extracellular potassium concentration, ions pass through the selectivity filter in turn with water molecules, cationic repulsion then moves the adjacent ion to the next binding site (Egwolf and Roux, 2010; Zhou et al., 2001). A recent molecular dynamics simulation has, however, proposed another mechanism of ion permeation that rarely requires water to be present in the filter (figure 1.8). It was suggested that potassium ions may render adjacent ion movement in the selectivity filter by coulomb repulsion. Arguably, this highly energetic repulsion is still considered feasible due to the counterbalancing effect of the negative charges on the carbonyl groups of the filter (Köpfer et al., 2014).

As potassium permeates pass the selectivity filter, it then once again gets rehydrated with the water molecules that occupy the inner pore of the channel. The presence of hydrophobic residues at the mouth between the selectivity filter and the inner pore is sig-

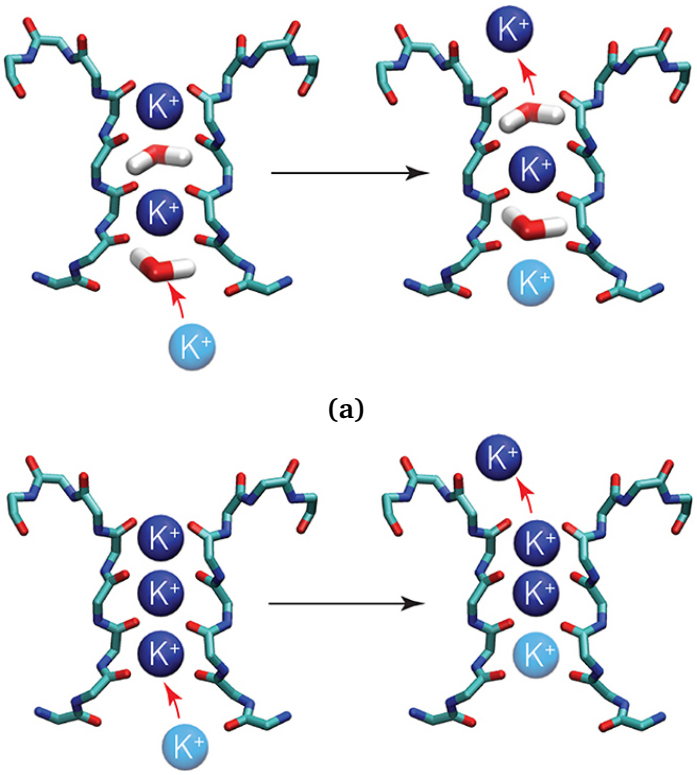

Figure 1.8: The different mechanisms of ion permeation at the selectivity filter. a) The soft knock-on mechanism, where water molecules are present in between each permeating potassium ion in the filter. This is thought to absorb some repulsion energy between two adjacent potassium ions. b) The hard knock-on mechanism, where instead of having water molecules present in alternate, potassium ions occupy all the spaces inside the selectivity filter. As another potassium ion enters, adjacent K^+ions are being knocked out by coulomb repulsion (Hummer, 2014). Light blue: Incoming K^+ion.

nificant in allowing water molecule to bind to potassium ions without steric competition from the surrounding amino acids (Zhou et al., 2001).

1.3.2 Classification of K^+channels

K^+channels represent the largest group of ion channels identified from the humane genome. In general they can subdivided into three major categories: Voltage-gated K^+channels (Kv), Inward rectifiers (Kir), and the Two-pore domain K^+channels (K2P) (Miller, 2000). With the structure being resolved, and supported by functional studies of the potassium selectivity signature sequence (TVGYG) (Heginbotham et al., 1992), our understanding of the basis of a potassium channel has been significantly increased. From sequence alignment, a vast number of potassium channels have now been characterised, leading to the identification of the canonical potassium channel architecture. The archetypal pore-forming structure of a potassium channel consists of a short loop (the pore loop) flanked by two transmembrane helices. This 2TM/1P (two transmembrane helices and one pore loop) topology has been well-conserved across all potassium channels identified thus far (Lu et al., 2001). Further classification of the diverse members of the potassium channel is then based on other distinct topology and phenotype. In mammalian cells, the potassium channel family can generally be categorised into three groups, based on their membrane spanning topology; 6TM/1P, 2TM/1P and 4TM/2P (Figure 1.9).

Voltage-gated potassium (Kv) channels have six transmembrane domain (S1 to S6) and one pore helix in each α-subunit. The selectivity filter loop lies between the S5 and S6 domains. Therefore, the S5 and S6 transmembrane domains line the pore conduction pathway, while the other remaining four transmembranes of each subunit are arranged at the periphery of the pore. These form the voltage-sensing domain, and movements of these domains, especially the S4 domain, are coupled to the lower activation gate of the Kv channel, a helical bundle crossing. The S4 domain is unilaterally lined with

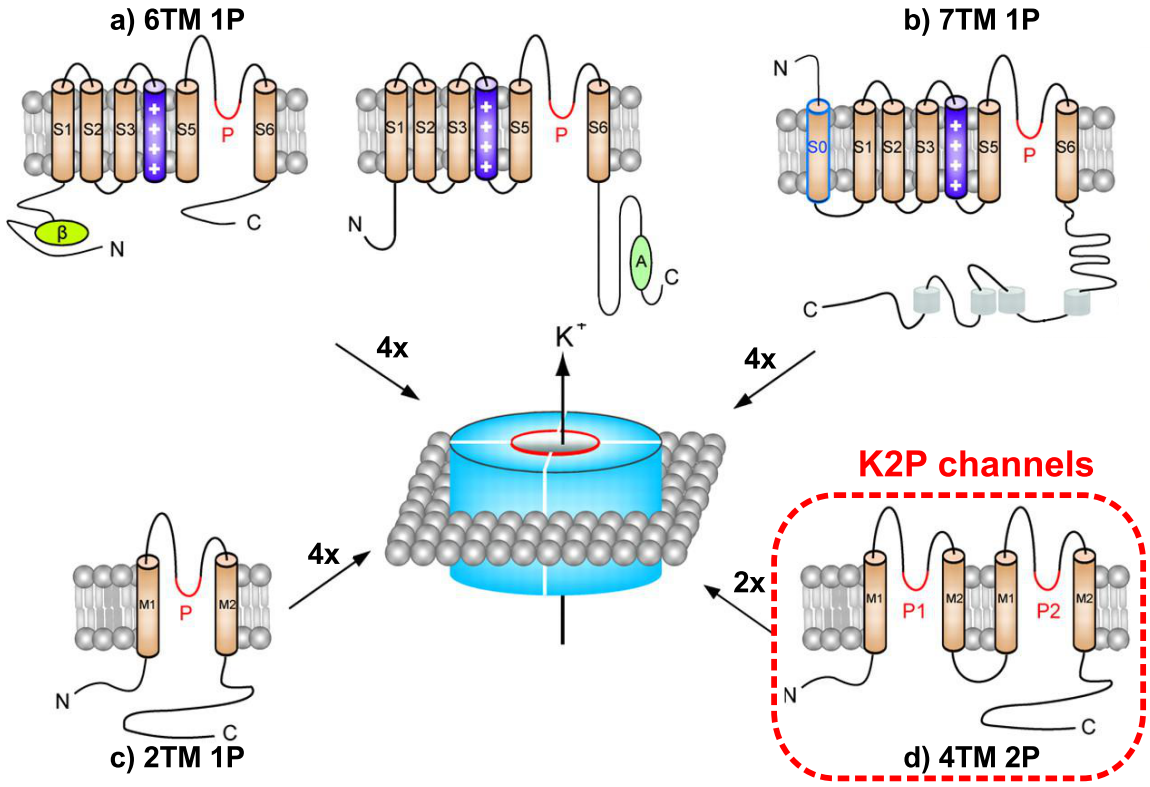

Figure 1.9: The mammalian potassium channel family. Potassium channels are categorised based on the number of their membrane-spanning domain (TM) and pore helix (P). a) Voltage-gated (Kv) channels are members of the 6TM/1P, b) Calcium-activated K^+ channels are 7TM/1P, c) Inwardly-rectifying (Kir) channels are 2TM/1P, and d) Two-pore domain (K2P) channels are 4TM/2P. Members of the 4TM/2P family form dimers, whereas others form tetramers. Figure adopted from Benarroch (2009)

positively charged residues on one side, rendering it sensitive to changes in membrane potential (Long et al., 2005).

The group of potassium channels whose subunits comprise of two transmembrane domains and a pore helix (2TM/1P) are the inwardly rectifying potassium channels (Kir). These channels are characterised by a large cytoplasmic domain that moves in a twisting manner to help gate the channel at the helical bundle crossing (Nishida et al., 2007; Bavro et al., 2012). Interestingly, this constriction is formed by four leucine residues that sterically act as a hydrophobic barrier against ion permeation (Bavro et al., 2012).

Finally, the two-pore domain (K2P) potassium channel family have four membrane-spanning domains and two pore helices (4TM/2P) in each subunit. The unconventional stoichiometry of having two pore loops in a subunit makes the architecture of this group unique from other potassium channel family. Since the characteristic form of a potassium channel is to have four pore loop domains in the core to constitute the selectivity filter, the subunits of this channel group dimerise, instead of tetramerise, to form a functional protein with a pseudo-tetrameric pore.

1.4 Two-Pore Domain Potassium Channels (K2P)

Among the subgroups of different K^+channels, the K2P clades were the last addition to the family. Their discovery was sparked by the cloning of TOK1, a channel with eight transmembrane helices and a tandem pore domain (8TM/2P) from *Saccharomyces cerevisiae*, in 1995 (Ketchum et al., 1995). This later led to the first discovery of the mammalian *tandem-pore domain in a weak inwardly rectifying* K^+ (TWIK-1) channel, in 1996, by Lesage and colleagues (Lesage et al., 1996a). Most K2P channels produce currents over the whole range of the membrane potential, lending them the fitting role as 'regulatory K^+channels' for stabilising the resting membrane potential (Renigunta et al., 2015). In excitable cells, establishing the resting membrane potential sets a depolarising

range that the membrane has to undergo to reach the firing threshold for an action potential to occur. This regulates the frequency for an action potential to take place (Lesage et al., 1996a). Regulating the resting membrane potential in non-excitable cells is equally important, although their resting potential does not change as rapidly and frequently as excitable cells.

To date, 15 mammalian K2P channels have been characterised and categorised into 6 subfamily based on their sequence homology (figure 1.10a). Functional studies with various stimuli on these channels have shown that they are not merely leak channels. Instead, K2P channels are regulated by a multitude of modalities that range from various physical and chemical stimuli (Feliciangeli et al., 2015; Renigunta et al., 2015). TWIK-1, for an instance, is inhibited by intracellular acidification. However, study on the regulation of TWIK-1, and the other two TWIK members (TWIK2 and KCNK7) are still limited compared to the other K2Ps (Feliciangeli et al., 2015). This is mainly due to the difficulty in obtaining detectable currents from these channels, especially KCNK7 (Bichet et al., 2014).

As shown in figure 1.10b , the selectivity filter sequence in the K2P channels are slightly different from the consensus sequence. Most notably is the presence of phenylalanine in place of tyrosine in the 'GYG' sequence. This was, however, not thought to have a significant effect on K^+-selectivity. A previous study has suggested that the hydroxyl group in tyrosine is not critical for ion selectivity (So et al., 2001). Moreover, in TWIK-1, TWIK-2 and KCNK7, a leucine residue was found in the second filter motif (SF2), whereas tyrosine is still present in the first motif (SF1). The same study by So et al. (2001) showed that while having tyrosine or phenylalanine present in the motif is essential, a four-fold symmetry of the aromatic amino acids is not. Therefore having leucine in two places at the selectivity filter does not change ion selectivity, as long as the other two residues are still tyrosine or phenylalanine.

Secondly, an isoleucine amino acid can be seen in the selectivity filter sequence of

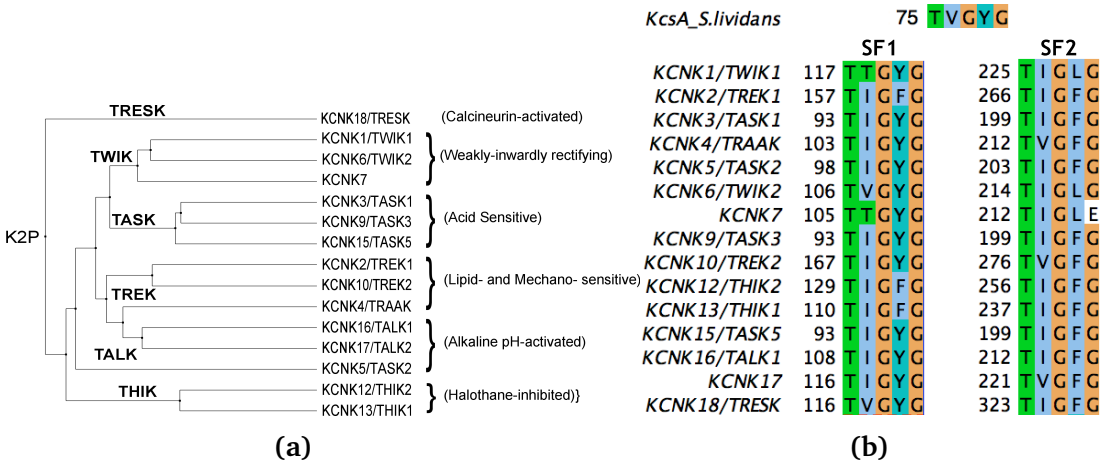

Figure 1.10: The mammalian K2P family. a) The K2P phylogenetic tree illustrates the relative identity of the 15 K2P family members, grouped into six clades. The tree was generated by taking an averaged-distance measure of each pair-group that was calculated based on percent identity. General properties of each clade are shown in brackets on the right (based from (Renigunta et al., 2015))b) Alignment of the K2P family at the selectivity filter sequence, compared to the selectivity filter sequence of KcsA. Both images were generated in Jalview.

most K2Ps where valine is normally expected under the consensus amino acid sequence. The presence of isoleucine instead of valine in the selectivity filter sequence is quite common in other K channels and the selectivity of the channels remain intact (Chatelain et al., 2012; Chen et al., 2014). On the other hand, the presence of the second threonine in TWIK-1 was suggested to lend the channel its dynamic selectivity behaviour, whereby under hypokalemic condition, TWIK-1 has a higher permeability to Na+ ions (Chen et al., 2014).

Notably, KCNK7 has a glutamate amino acid in place of glycine in SF2. However, study on the effect of this difference in sequence on ion selectivity has yet to be determined, mainly due to the channel being non-functional.

1.4.1 The unique structure of K2P

Quite recently, there has been a rapid advancement in x-ray crystallography structures of K2P channels. The first two crystal structures published were for the TWIK-1 and

TRAAK channels (Brohawn et al., 2012; Miller and Long, 2012), which did confirm several expectations pertaining to its structure. Firstly, the structures did confirm that K2P channels could form a pseudo-tetrameric structure by the assembly of two subunits, and secondly, the pore forming region around the selectivity filter resembles the typical structure of a potassium channel. However, several unusual features were also observed in the K2P crystal structures.

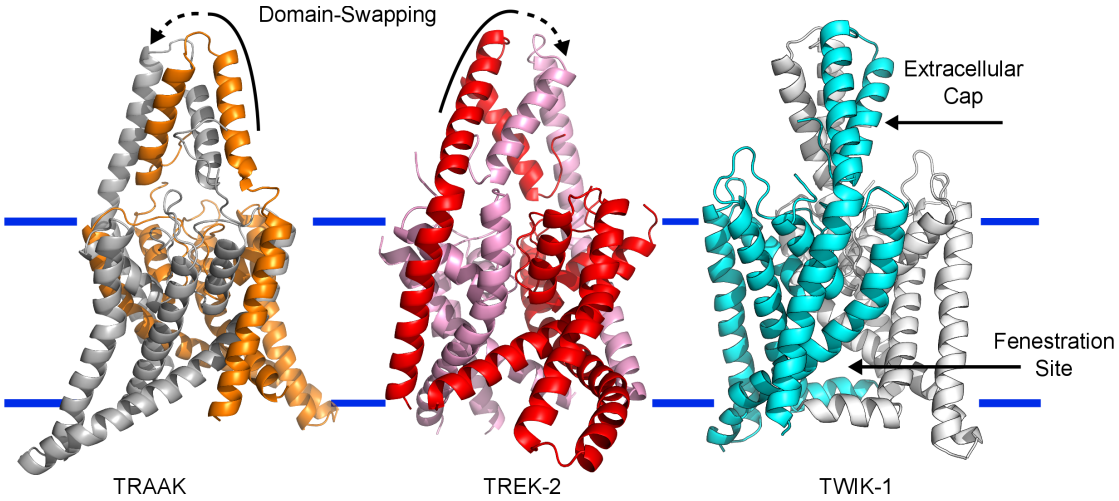

Figure 1.11: The mammalian K2P family and x-ray crystallography structures of members of the K2P. The crystal structure of three K2P members displays the common features of all K2P channels, including the pseudo-tetrameric dimerisation of the channel (different colour represents separate subunit), and the presence of an extracellular cap and a fenestration site. Left: TRAAK (pdb:4I9W), middle: TREK-2 (pdb:4BW5) and right: TWIK-1 (pdb:3UKM). Blue lines indicate the membrane bilayer boundaries.

1.4.1.1 The extracellular cap

From the crystal structure, the presence of a helical cap was evident, which extends beyond the extracellular membrane (figure 1.11b). This has been previously predicted by Lesage et al. (1996b), referred to as the M1P1 loop. In these structures, two cap helices (C1 and C2) run parallel to each other and form the extracellular cap domain. They are linked by a short linker that contains a cysteine residue, located at the top end of the cap formation. This residue, one from each subunit, forms a disulphide bridge

that holds the dimer formation of the channel. Down the end of the extracellular cap, it covers two openings that leads to the selectivity filter. This serves as an extracellular entryway for K^+ions to permeate. The exact role of the extracellular cap is still unclear. However, it has been suggested that the cap may be preventing inhibition of the pore by extracellular toxins (Brohawn et al., 2012). While the presence of the extracellular cap is observed in all the K2P structures, previous studies have also suggested that it could be a conserved feature in other mammalian K2Ps (Enyedi and Czirják, 2010).

1.4.1.2 Twist and turn: Domain swapping

Subsequent to the structures of TWIK-1 and TRAAK, three additional crystal structures of the K2P family have also been reported. One of these is another TRAAK structure, which was co-crystallised with antibody-antigen binding fragments (Fab) (Brohawn et al., 2013). The remaining two crystal structures are of TREK-1 (PDB: 4TWK) and TREK-2 channels (PDB: 4BW5) (Dong et al., 2015). Compared to the initial K2P structures, an interesting feature appeared in these later additions.

It was discovered that the first membrane-spanning helix (M1), as well as the C1 cap helix, were shifted to the opposite side of its own subunit, and swapped with the M1 and C1 helices of the other (figures 1.11). Brohawn et al. (2013) argued that this was not evident in their first crystal structure due to the low resolution obtained back then (3.8Å compared to 2.5Å of the later structure). Therefore, it is possible that domain swapping is common feature of all K2P structures, including TWIK-1.

1.4.1.3 Lateral fenestration

Another unique feature that appeared in the K2P structures, is the presence of large lateral portals at the interface between the M2 helix of one subunit and M4 helix of the other. These openings were located at a position that would expose the channel to the lipid core of the membrane bilayer (figure 1.11b). This likelihood is also being

demonstrated in the structure by the presence of a long tubular density (∼11Å) that propagates from the fenestration, and into the K2P structure (Miller and Long, 2012). This could potentially serve as a point of entry for any lipid soluble effectors to influence ion permeation in K2Ps, although this is still unclear. But recent studies have suggested that lipid involvement in channel gating is possible (Aryal et al., 2014b).

1.4.2 TWIK-1 channel

The TWIK-1 channel belongs to the TWIK subfamily, which also consists of TWIK-2 and KCNK7. The protein subunit is composed of 336 amino acids, and is encoded by the KCNK1 gene. The sequence of TWIK-1 is highly conserved among known species, especially at the transmembrane helices. The highest variation in sequence across these species occur at the C-terminus end of the protein (refer Appendix A).

Functionally, TWIK-1 was initially reported as weakly-inwardly rectifying (Lesage et al., 1996a). However, the ionic currents produced by expression of TWIK-1 were very small and it was thought the channel was 'silent', thus prompting studies focusing on its lack of functional activity (Rajan et al., 2005; Feliciangeli et al., 2009).

1.4.3 Regulation of TWIK-1 expression

TWIK-1 also contains a consensus sequence for N-glycosylation (in humans and rodents) near the N-terminus (sequence: $95-NAS-97$) (Lesage et al., 1996a). N-glycosylation occurs in the endoplasmic reticulum, and modulates protein trafficking and stability.

However, the low level of TWIK-1 functional activity was thought to be regulated by other factors. It was firstly suggested that the channel undergoes another post-translational modification that binds a small ubquitin-like modifier (SUMO) protein to TWIK-1. This process, known as SUMOylation, was thought to be the reason behind TWIK-1 inactivity, despite being expressed on the membrane (Rajan et al., 2005). But it was later argued that TWIK-1 is instead being rapidly internalised by endocytosis

factors that removes it from the surface (Feliciangeli et al., 2009). The conundrum encompassing TWIK-1 silent activity remains a subject of intense investigation, but I have attempted to test these competing ideas as part of this thesis. Further description of the two processes, and my observations are detailed in Chapter 3.

1.4.4 Crystal structure of TWIK-1

The crystal structure of TWIK-1 was obtained from a truncated construct that was expressed and purified from *Pichia pastoris*. The construct was truncated at both termini, to contain residues 19-288 of the human TWIK-1 protein. Diffraction data were collected to 3.4Å resolution (Miller and Long, 2012).

The basic architecture of TWIK-1 was similar to that described earlier, as shown in figure 1.12. It contains four transmembrane domains, M1-M4, that span the bilayer. Two pore forming helices, P1 and P2, are respectively located between M1 and M2, and M3 and M4. After the M1 domain, two helices extend beyond the membrane into the extracellular space. These domains, known as the extracellular cap, are important in holding the two TWIK-1 subunits together in the dimeric formation. These aforementioned structural architecture are similar to the general K2P structures described before. In addition to these, TWIK-1 has a unique structural conformation, that became apparent from the TWIK-1 crystal structure Miller and Long (2012). This motif, known as the C-helix, lies at the intracellular side of the membrane, and comes after the M4 domain.

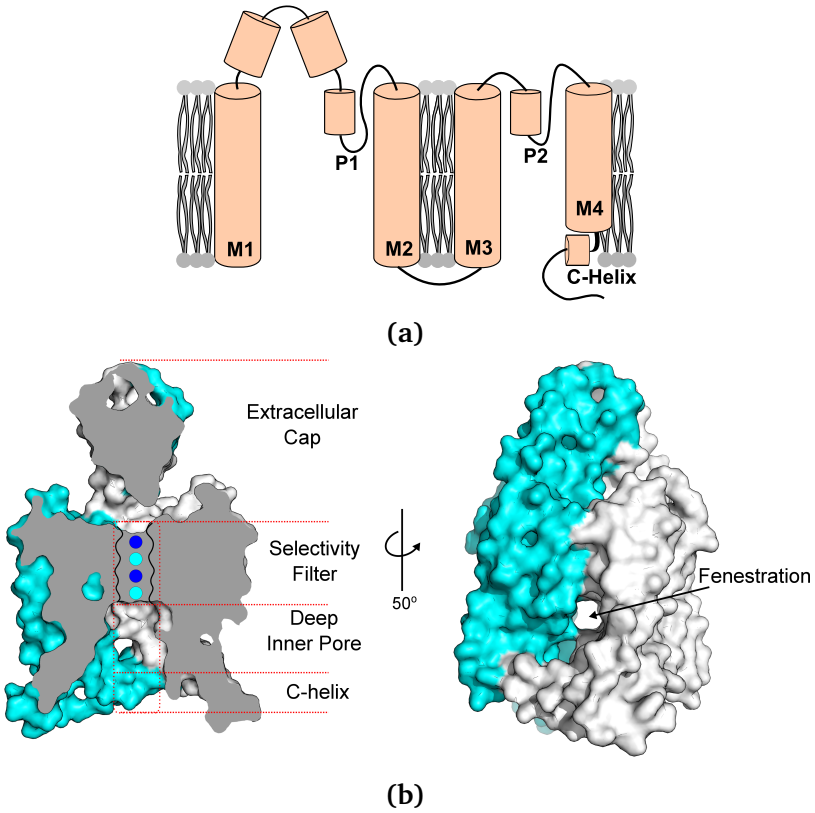

Figure 1.12: The general architecture of TWIK-1. a) The topology diagram of a TWIK-1 subunit.Similar to other K2Ps, it contains 4 transmembrane domain (M1-M4), and 2 pore-forming helices (P1 & P2). TWIK-1 also has a C-helix motif after the M4 helix. b) Left; Vertical slice through the axis of symmetry of the TWIK-1 pore, illustrating the main regions discussed in this thesis, with surface rendering of the structure. Right; The fenestration site of the TWIK-1 is close to the deep inner pore region.

1.4.4.1 The C-helix

The most striking difference between the TWIK-1 structure and the other K2P structures is the arrangement of the cytoplasmic domain (figure 1.13). In the TRAAK and TREK structures, the helices at the cytoplasmic side appear to be splayed open and away from the central pore axis (Brohawn et al., 2012, 2013; Dong et al., 2015).

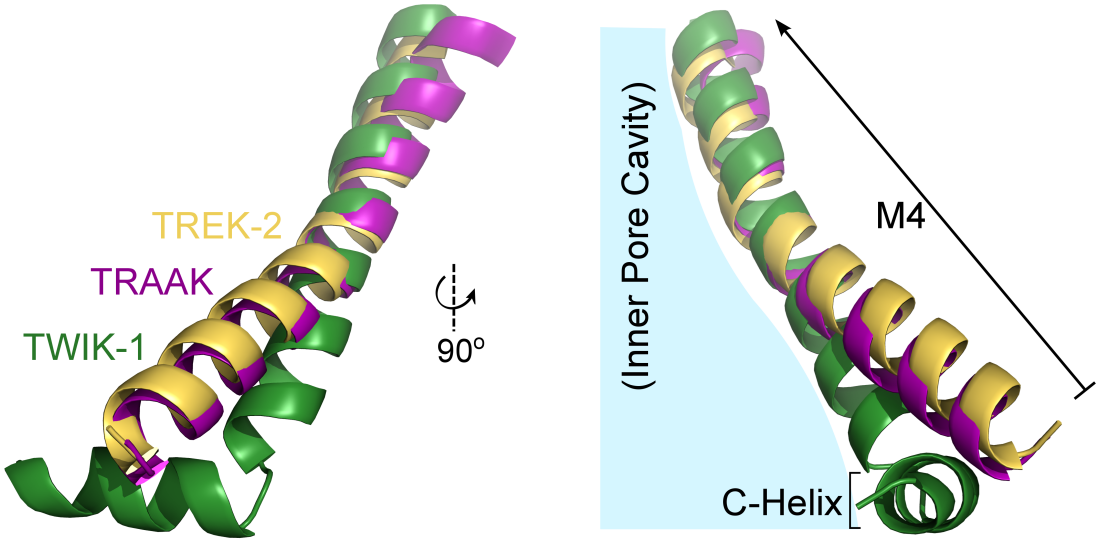

Figure 1.13: The C-helix structure is unique to TWIK-1. Structural comparison between the distal M4 membrane domains of TWIK-1 (green), TRAAK (purple) and TREK-2 (yellow) K2P channels shows that, while the other two M4 domains splay away from the pore axis, the end of the TWIK-1 M4 helix kinks by $\sim 80^o$, forming the C-helix structure that is parallel to the cytoplasmic membrane surface.

In both TREK-2 structures, the different conformations showed an upward and downward movements of the M4 helices (Dong et al., 2015). But both conformations still showed the structure to be splayed away from the pore axis.

On the contrary, a sharp kink is formed at the end of the TM4 region of the TWIK-1 structure. Consequently, the helix bends by $\sim 80^o$ inwardly, and lies at the interface between the membrane bilayer and the cytoplasmic region, forming the C-helix. Further study on this domain is detailed in Chapter 5.

1.4.5 Physiological significance of TWIK-1

TWIK-1 expression is quite ubiquitous, and its major function is implicated in several specific organs. In the kidney, TWIK-1 is expressed in the proximal tubule, ascending limb, distal tubule, as well as the medullary collecting duct. The absence of TWIK-1 has been shown to disrupt renal phosphate transport and water reabsorption (Nie et al., 2005). Functional studies on TWIK-1 gene knockout principal cells also shows that the cells down-regulate a quinidine-sensitive cation conductance in response to the TWIK-1 knockout (Millar et al., 2006).

A role for TWIK-1 in the brain has also been reported. The passive conductance in hippocampal astrocytes has been suggested to resemble that of TWIK-1 and TREK-1 channels when expressed in Chinese Hamster Ovary (CHO) cells (Zhou et al., 2009). It has also been shown that TWIK-1 can contribute to the Cs^+permeability in astrocytes, which was supported by a reduction in Cs^+permeability in the TWIK-1 knockout mice (Zhou et al., 2009; Wang et al., 2013). The absence of TWIK-1 also resulted in a reduction in inward rectification and a more hyperpolarised resting membrane potential. However, another interesting finding from the same study suggested that TWIK-1 is mostly localised in the internal compartments of astrocytes. Only 5% of the TWIK-1 was detected on the membrane surface in native cells. This low level of surface expression was suggested to correlate proportionally to the degree of depolarisation seen in these cells (Wang et al., 2013).

TWIK-1 is also found in the heart, where it plays a fascinating role. In a typical cell, the Na^+-K^+-pump maintains the high internal K^+concentration which allows K^+ions to then flow out of the cells through the potassium channels. Along with a much lesser influx of Na^+ions, the resting membrane potential inside the cell is maintained around -70mV. The membrane will shift towards a less negative potential, or depolarise, if we increase the extracellular K^+ion concentration, as this reduces the concentration gradient of K^+. Conversely, reducing the extracellular K^+concentration would cause the resting

potential to hyperpolarise, or become more negative.

However, the conundrum arising in cardiac cells is that when the K^+ion concentration in the serum was reduced, the cells did not hyperpolarise, but depolarise (Goldstein, 2011). Clues to this paradox was unveiled when a study on TWIK-1 found that it changes selectivity as K^+concentration is depleted.

1.4.5.1 Dynamic ion selectivity in TWIK-1

In the study by Ma et al. (2011), they maintained that under physiological K^+ion concentration, TWIK-1 is highly selective for $K^+$and cells expressing this channel depolarises with increasing extracellular K^+ion concentration, in agreement with the Nernst equation. However, when TWIK-1 was perfused with solutions containing K^+ion concentrations below 2mM, it was revealed that the reversal potential remained depolarising. It was then shown that the relative permeability, an indicator of ion selectivity, of $Na^+$to K^+slightly increased. It was also shown that the change in ion selectivity was due to a threonine located in the P1 selectivity filter loop, (T118). In other K2Ps, this was found to be an isoleucine instead. It was then proposed that the paradoxical depolarisation occurring in cardiac cells could actually be partly due to the change in ion selectivity in TWIK-1.

1.5 Scope and Significance of Study

The conundrum underlying the apparent 'silent' functional expression of TWIK-1 has been a matter of great interest and controversy amongst those studying this channel. Even when expressed in heterologous overexpression systems, wild-type TWIK-1 channel activity is poorly detectable by standard electrophysiological recording methods. Various hypotheses have been proposed to explain the reason behind the scanty detection of TWIK-1 channel activity. While one study suggested TWIK-1 to be 'silenced' at the surface membrane by the post-translational modification (SUMOylation), another

study proposed an endosomal distribution of the channel, which results in the rapid internalisation of channels expressed at the membrane surface.

I therefore designed a set of experiments to try and reproduce the findings from these different studies by examining many of the same mutations. The results of this comparative study are described in chapter 3.

As part of this analysis we also performed state-of-the-art molecular dynamics (MD) simulations and noticed that the inner cavity of the TWIK-1 pore was prone to dewetting, thereby acting as a possible barrier to ion permeation. I conducted extensive functional studies of TWIK-1 to validate the existence of this hydrophobic barrier within the inner pore cavity beneath the selectivity filter region. These results are described in chapter 4.

Another unusual feature of the channel is the presence of an amphipathic C-helix attached to the end of the M4 helix. Since this region is located at the intracellular entrance to the pore, it could potentially influence the permeation of ions through the channel. Mutations within this region provide a novel interpretation on the role of the C-helix and the results are described in Chapter 5.

Together, these studies contribute to our understanding of why TWIK-1 remains functionally silent under normal physiological conditions and the major influence that hydrophobic surfaces have on the movement of water and ions through channels and related nanopores.

CHAPTER 2

Materials and Methods

2.1 Molecular Biology

2.1.1 Materials

2.1.1.1 Gene and Vector

The human KCNK-1 gene (Gene ID: 3775) encodes for the TWIK-1 channel protein. For the purpose of this study, the gene is subcloned into a pBF vector. A Kozak sequence that is optimised for Xenopus oocytes was appended to the 5' end of the KCNK-1 gene (figure 2.1).

2.1.1.2 Oligonucleotides

Primers were designed using DNADynamo (Bluetractor software) and purchased from Sigma-Aldrich. The dry, desalted pellet is resuspended in elution buffer (Qiagen Kit) to 100mM stock concentration.

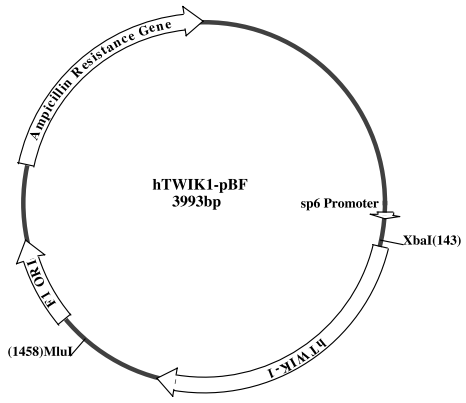

Figure 2.1: pBF plasmid containing the human TWIK-1 gene. The gene is appended with a *Xenopus* Kozak sequence at the 5' end before being subcloned into the pBF vector.

2.1.1.3 Synthesis, Extraction and Purification Kits

Our lab utilises kits from the Qiagen Inc. to facilitate most of our molecular biology works, especially for DNA synthesis (Table 2.1).

Table 2.1: Kits from Qiagen Inc. used for DNA synthesis and purification.

Qiagen Kit Name	**Usage**
QIAprep Spin kit	rapid extraction of plasmid DNA from *e.coli*
QIAquick PCR purification kit	rapid DNA purification
QIAquick Gel Extraction kit	Extracting and cleaning linear DNA from agarose gel

All of our plasmids are encoded with either SP6 or T7 promoter for use in In-vitro transcription. The kits used for RNA synthesis are supplied by Cellscript™, whereas the RNA purification kit is obtained from Qiagen Inc (Table 2.2).

Methods for using each kits were as per described in the protocols provided by the suppliers, with alterations made on elution volumes to ensure high throughput after purification.

Table 2.2: Kits used for RNA synthesis and purification.

Cellscript Kit Name	Usage
AmpliCap™SP6 High Yield Message Maker Kit (Cellscript™)	RNA synthesis for pBF-based DNA
AmpliCap-Max™T7 High Yield Message Maker Kit (Cellscript™)	RNA synthesis for pFAW-based DNA
Rneasy Mini Kit	Purification of RNA Transcripts

2.1.1.4 Sequencing Primers

All of our DNA samples are sequenced by the Source Bioscience Sequencing team based in the Biochemistry Department, University of Oxford (Source Bioscience plc). The primers used to sequence our DNA are listed in table 2.3.

Table 2.3: Primers used for DNA sequencing. The plasmid on which the primer is used is referred.

Primer Name	Sequence	Plasmid
SP6	GATTTAGGTGACACTATAG	pBF
T7F	TAATACGACTCACTATAGGG	pFAW and pFAW-AcGFP
pBFr7	GTTGTCCCCCAAAATGTAG	pBF, pFAW and pFAW-AcGFP
pFAW_Linker_R	GCCCTTGCTCACAACCTTTTG	pFAW-AcGFP
pFAW-R	CAAAAGGTTGTGAGCAAGGGC	pFAW

2.1.2 Molecular Biology Methods

2.1.2.1 *Escherichia coli*

The Subcloning Efficiency™$DH5\alpha$ competent cells (Invitrogen) was used for transformation and retansformation of plasmids. Cultivation is done overnight in a 37°C incubator

agitated at 200rpm.

Culture Media 25g/L of premixed Luria Bertani (LB, Sigma) medium is used for growing overnight cultures of *e.coli* cells. For LB agar, 15g/L of agar (Sigma) was added onto the LB. The culture media were liquid-sterilised by autoclave.

Antibiotic selection Both pBF and pFAW plasmids contain an ampicillin resistant gene. To utilise this selection gene, all LB media were added with 1mg/ml of carbenicillin, an ampicillin analog, prior to use.

2.1.2.2 Subcloning

Every clone used in this work is firstly subcloned into the pBF vector. To do this, primers were designed to amplify the gene of interest, as well as include a Xenopus optimised Kozak sequence at the 5'-end of the gene. Restriction sites were also added to the primers for better ligation. For subcloning hTWIK-1, hTWIK-2 and hTRESK genes into pBF, EcoRI and XhoI were added to the forward and reverse primers, respectively.

2.1.2.3 Site-Directed Mutagenesis

A pair of complementary oligonucleotides carrying the required mutation is added to the reaction mixture, which also contains the target DNA as the template. After amplification by polymerase chain reaction (PCR), DpnI is added to digest the template DNA. The product is then cleaned and transformed into *e.coli*.

For the hTWIK-1 DNA, an internal restriction site, PstI, was abolished by mutating one of its nucleotide (c.19T>G). The mutation does not change the amino acid at this position. This DNA is used as the master DNA for hTWIK-1.

2.1.2.4 Gel Electrophoresis

Gel electrophoresis was used for diagnosing restriction digest outputs and in-vitro transcription products, as well as purifying PCR products prior to ligation. 1% (w/v) agarose (Sigma) in Tris-acetate-EDTA buffer is normally used for these purposes. 0.5μg/ml of ethidium bromide is added for later UV-visualisation. The electrophoresis is run for 30mins at a constant voltage of 110V (10V/cm). After that, the gel is observed under UV-lamp and the DNA lane is compared to the 1kb DNA Ladder lane (Promega) for approximate size. For gel purification protocol, the desired band of DNA is sliced out of the gel before proceeding to the "Qiagen Gel Extraction" protocol.

2.1.2.5 Ligation

Ligation of DNA fragments is done using the T4 ligase (Promega) and its ligation buffer. The vector:insert ratio used are either 1:1, 1:2 or 1:5. The reaction mixture is incubated in 18°C for at least 6 hours. As a control, an insert-free ligation mixture was also made. All reactions are then transformed, plated onto LB media and incubated overnight at 37°C. The DNA product is eventually checked by gel electrophoresis for the correct band size before sequencing it.

2.1.2.6 In-vitro RNA Transcription

Before transcription, the plasmid DNA is linearised with MluI restriction enzyme (Promega) at 37°C for one hour, and purified using the "QIAquick Purification Kit" protocol. The elution step was done by adding 27μl of RNase-free Water into the filter column. For the transcription protocol, 8.5μl of the linearised DNA is added to the SP6 reaction mixture (5.5μl for T7 Kit). After cleaning, the RNA products are loaded onto agarose gel to check for purity, and onto Nanodrop chamber for RNA concentration.

2.1.3 pFAW vector construct

pFAW vector was constructed to obtain a more versatile plasmid (figure 2.2a). In particular, this vector is aimed at enabling us to express our gene of interest in *Xenopus* oocytes as well as mammalian cell lines. Essentially, this plasmid is a hybrid between a mammalian (pRAT) and a Xenopus expression system (pBF).

The pRAT vector was digested with ApaI enzyme, resulting in two fragments of 5kb and 1.5kb in size. DNA Polymerase I, Large (Klenow) Fragment (New England Biolabs) is then used to fill in the 5' overhang of the fragments. The DNA pieces are loaded onto 1% agarose gel, and the 5kb fragment is extracted and purified (figure 2.2b). Following this, the DNA product is once again digested, this time with HindIII to form a 5'-sticky end. The pBF vector is double-digested with HindIII and PmlI to produce a 3' overhang

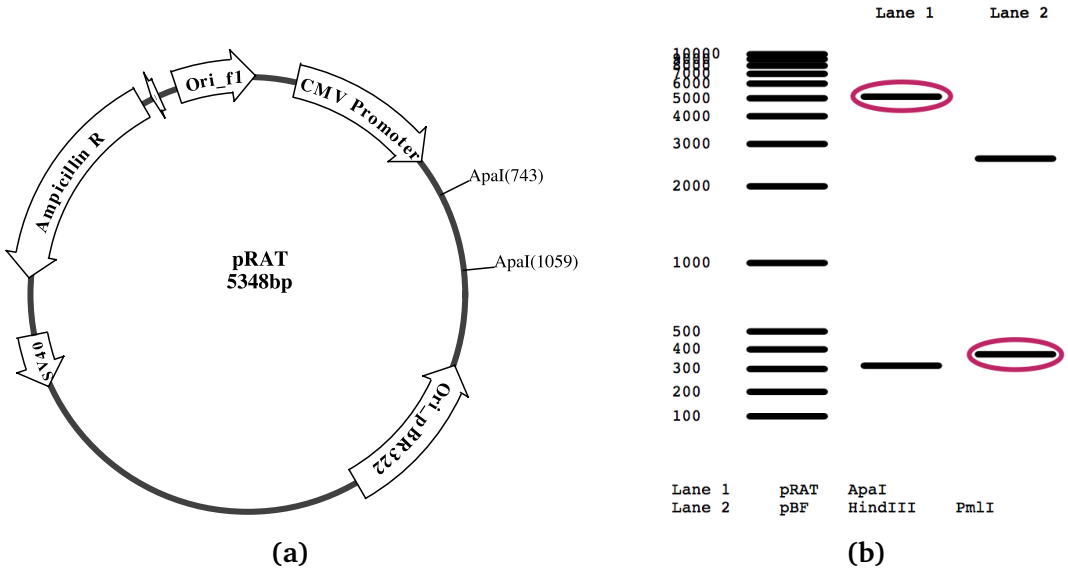

Figure 2.2: Constructing the pFAW plasmid. a) The mammalian expression vector, pRAT. The digestion site used (ApaI enzyme) is shown. b) The digestion of both vectors used to construct the pFAW vector. Lane 1: pRAT digested with ApaI, and Lane 2: pBF digested with HindIII and PmlI. Bands picked and cut are circled in red. The DNA marker is shown on the left.

and a 5' blunt-end, respectively. After running the sample on a 1% agarose gel, the smaller fragment (400bp) is extracted and purified.

Finally, the two isolated fragments were ligated to each other using the T4 DNA ligase (Promega), by incubating the mixture at 18°C for 6 hours, followed by a 20mins incubation at 37°C, to inactivate the ligase. The product is then transformed into *E.coli*. Following plasmid preparation, the DNA was digested with several restriction enzymes to check for correct DNA size. The rightly sized DNA is then sent for DNA sequencing. For this purpose, T7F, pBFr7 and and pFAW-R primers were used.

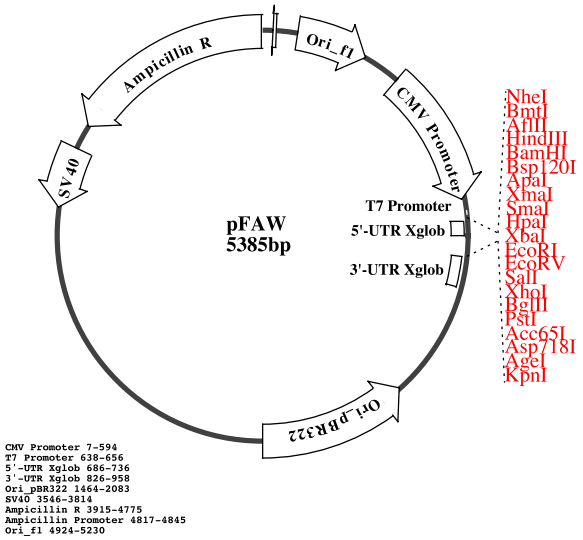

Figure 2.3: pFAW vector map. The plasmid contains elements that allows expression in mammalian cell-lines, as well as for in-vitro transcription for injection into *Xenopus* oocytes.

Thus far, the pFAW vector has only been used in *Xenopus* oocytes in our lab. However, it has been successfully used in mammalian cell lines by another group in the University of Kiel, Germany.

The pFAW is used in this study for fluorescence imaging of TWIK-1.

2.2 *Xenopus laevis* Oocyte Harvest and Preparation

Mature *X. laevis* toads were supplied by the European Xenopus Resource Centre in Portsmouth. The toads were kept and maintained at the Biomedical Sciences Building, University of Oxford.

2.2.1 Schedule 1 Procedure

Tricaine Methanesulfonate (MS-222) was used to anaesthetise toads for this procedure. 5g of MS-222 (Sigma-Aldrich) is dissolved in 1L (0.5% w/v) of tank water and titrated to pH7 - pH8 by adding approximately 15g Sodium Bicarbonate (Sigma-Aldrich). To perform humane killing of the toad, it is first fully submerged into MS-222 for 10 to 20 minutes, or until the toad does not respond to a toe-pinch reflex and remains belly-side up when turned. Toad euthanasia is confirmed by decapitation as a secondary measure.

A small incision on the abdomen is then made to the skin and fascia layer of the toad. This exposes the ovary sac. Pieces of the ovary is cut and collected in a tube containing calcium-free ND96 buffer.

2.2.2 Oocyte Preparation

The collected ovary chunks are then cut into smaller pieces, and incubated in Ringer's solution containing 2mg/ml Collagenase A (Roche) for 45 minutes. It is then washed several times with Ringer's solution before digesting for another 30 minutes with fresh Collagenase A. After that, the oocytes are washed several times with Ringer's solution until the Collagenase is completely removed (cloudy solution becomes clear). Healthy, stage V-VI oocytes are isolated and manually defolliculated using a pair of fine-tip forceps. They are placed in an antibiotic-rich storage buffer and kept in the 17°C incubator.

2.3 Electrophysiology

The majority part of this thesis is based on data recorded from a Two-electrode Voltage Clamp (TEVC) system. This system utilises a voltage electrode to measure the immediate membrane potential of the cell. The current electrode, on the other hand, passes current to clamp the cell at a set voltage and records back the membrane current as a function of channel activity.

2.3.1 The Voltage Clamp Technique

Studying the conductance through channels is difficult mainly because they change over both time and voltage. The advantage of the voltage clamp technique is that it 'clamps' the voltage across the membrane at a certain set point, thus allowing us to study the changes in ionic conductance that occur with time.

The voltage clamp technique involves measuring the membrane voltage, V_m, of a cell relative to an external, or bath, potential (Figure 2.4). The obtained V_m value is then compared to a command voltage (V_c) which is the desired membrane voltage that we can set accordingly. If the value between V_m and V_c is not equal ($V_m \neq V_c$), the amplifier will then generate an instantaneous current that is injected into the cell, in order to compensate the differences, making $V_m = V_c$. This generated current is measured and recorded. Therefore, current that is measured by the amplifier at any point in time corresponds to the change in V_m that occurs in response to changes in activity of the ion channels in the cell membrane.

2.3.2 TEVC Materials

The main components for TEVC recordings are:

- Amplifier where the main operation is controlled here. The voltage, current and bath electrodes are connected here.
  - **OC-725C oocyte clamp amplifier** (Warner Instruments)
  - **OC-725C headstages and bath probe** (Warner Instruments)
  - Ag electrodes bleached in Sodium Hypochlorite solution (10-15% chlorine, Sigma Aldrich)
- Analog to Digital converter to relay data acquisition between the amplifier and the computer with high sampling rate.

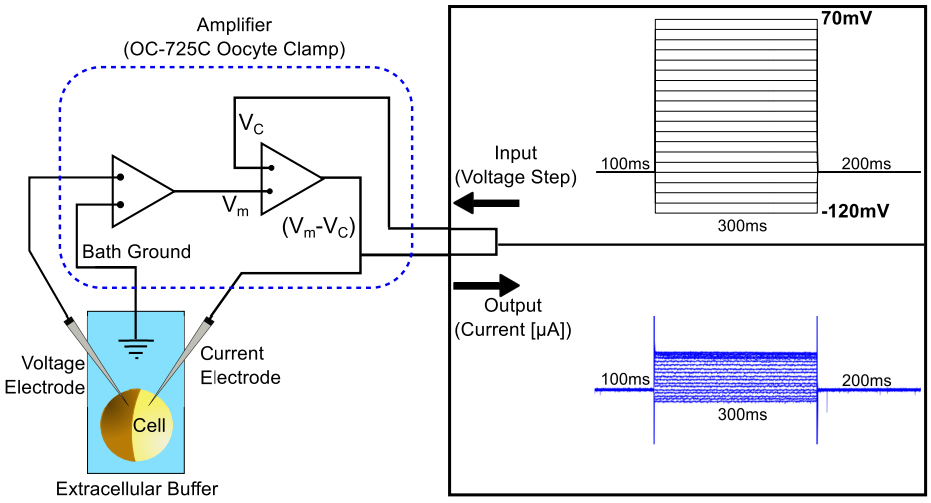

Figure 2.4: Recording whole cell currents on Two-Electrode Voltage Clamp. As the oocyte cell is impaled and electrically clamped with both electrodes, the amplifier (OC-725C Oocyte Clamp (Warner Instruments)) then passes current to the cell through the current electrode. The magnitude of the current to be injected is determined from the difference between the command potential (from the voltage step protocol) and the membrane potential (from the voltage electrode). The amount of current injected to the oocyte is then measured from the bath electrode and displayed as the current recorded from the channel proteins expressed on the oocyte, in response to the command potential given. This voltage-step protocol illustrated here is used throughout most of the experiments done in this study. A 10mV-step increment, from -120mV to +70mV, follows an initial 100ms of resting potential at -80mV. The step voltage runs for 300ms before returning back to -80mV. An interval of 1.5ms is applied between each step.

  - **Axon Digidata 1440A** (Molecular Devices)
  - **PClamp 10 Software**, licensed (Molecular Devices)

- Perfusion system for passing solutions onto oocytes.
  - **Ismatec 829 *REGLO* Analog Peristaltic Pump** (IDEX Health & Science GMBH)
  - **Perfusion Chamber**: This was designed using SolidWorks 2005 (Dassault Systemes), and milled on a Modela MDX-40A (Roland DG) desktop CNC machine with the assistance of Mr Marc Szabo from the Department of Chemistry.

2.3.3 Microinjection and Incubation

The Nanoliter 2000 system (World Precision Instruments) was used for microinjection. Borosilicate capillary pipettes were pulled using the PC-10 micropuller (Narishige) and tips were manually broken to a fine diameter (approx. 15μm). The whole pipette length was backfilled with mineral oil (Promega) and any trapped air bubble was purged out. 1-2μl of RNA was loaded into the capillary. Oocytes were then lined onto an injection chamber and individually turned to expose the bright pole. 50.6nl of RNA is injected into each oocyte, and they are incubated in ND96, pH7.4 buffer at 17°C. Whole cell currents are recorded 1-2 days after injection.

2.3.4 TEVC Data Acquisition

Oocyte was placed in the chamber and perfused with ND96 bath solution (2mM KCl), titrated to pH7.4 with NaOH. Microelectrodes were pulled and filled with 3M Potassium Chloride and set to zero values with respect to the bath electrode. Both voltage and current electrode resistances were made sure to be between 0.3 and 2MΩ. Recordings were done from a holding potential of -80mV. Unless stated otherwise, the standard acquisition protocol involves a 10mV step increase from -120mV to +70mV, each step running for 300ms with a 2 seconds holding interval between each step (figure 2.4).

Due to a rapid time-dependent inactivation of the TWIK-1 currents at depolarised potentials (beyond +40mV), the current values quoted for comparing the different TWIK-1 mutants are taken at 0mV, where the I-V relationship is linear.

2.4 Fluorescence Microscopy

2.4.1 Fluorescent-Tagged Plasmids

Green fluorescent protein (GFP) tagged TWIK-1 plasmid (pFAW) was obtained from Prof. Thomas Baukrowitz group in Kiel, Germany. The GFP, derived from *Aequorea coerulescens* (AcGFP), is linked to TWIK-1 at the C-terminus by a 19-amino acid long linker (IPVRPCKTNDLKQKVVSKG). The construct is shown in figure 2.5.

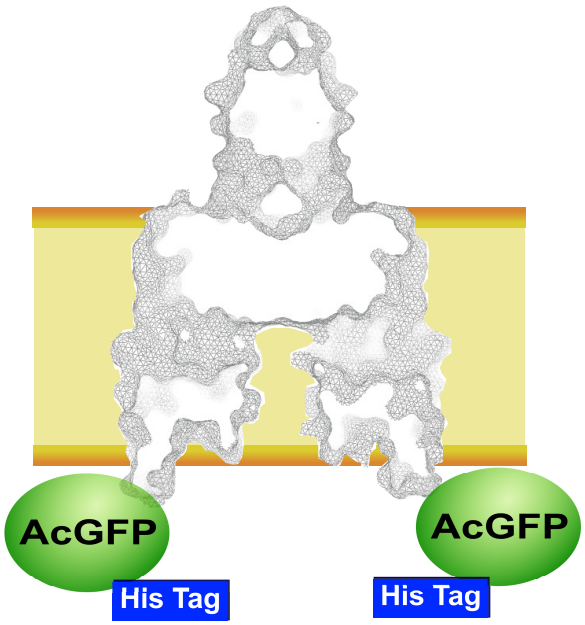

Figure 2.5: GFP-tagged TWIK-1 protein. The GFP is attached to the c- terminal end of TWIK-1, via a 19-amino acid long linker; sequence:IPVRPCKTNDLKQKVVSKG. 10x Histidine tag is attached to the end of GFP.

2.4.2 Wheat-Germ Agglutinin and CF633

Wheat Germ Agglutinin (WGA) is a 36kDa dimeric plant lectin that naturally protects wheat from other organisms by binding to sugar constituents in their membrane. WGA can bind oligosaccharides containing N-acetylglucosamine, which are common in many membrane constitutents. It can also bind to the sialic acid residues of some glycoproteins.

Due to this, WGA has been commonly utilised as part of a tracer for labelling cell membranes (El-Jouni et al., 2008).

In our study, the CF633-WGA (Biotium Inc.) labelling dye was used to label the Xenopus oocyte membrane surface. This marker uses the far-red fluorescent dye that is excited at a wavelength of 633nm. The emission peak is at 650nm.

For labelling purposes, the oocytes were incubated for three minutes in 1xPBS, pH7.4, containing 5μg/ml of CF633-WGA. Then the oocytes were washed completely with fresh 1xPBS.

2.4.3 Fluorescent Microscopy

An inverted confocal microscope was used to generate images of our fluorescent dyes on the oocyte membrane. The green fluorescent dyes tagged to the TWIK-1 proteins were excited by the 488nm line of the argon source from the Laser Scanning Module, LSM510. The emitted wavelengths were then filtered at a wavelength between 501-522nm. This allows us to detect and capture images of the GFP-tagged TWIK-1 proteins if they are expressed on and near the membrane surface.

As for the red-dye CF633, the fluorophore was excited by the helium-neon laser from the LSM510, at 633nm, and emitted light were sampled at a wavelength between 645-680nm. Images captured from this emission informs us of the oocyte membrane surface region, which, when overlaid with the GFP images, allows us to detect surface expression of the TWIK-1 proteins.

Co-localisation of the two fluorescent signals were analysed by the Zen Imaging software (Zeiss). An Overlap Coefficient was obtained from the analysed images as a measure of colocalisation of the two signals. The Overlap Coefficient was based on the calculations developed by Manders et al. (1993), which considers the signal intensities from both channels (CH1 and CH2) that are proportional to the co-localised pixels, and dividing them to the overall signal intensity, as follows;

$$\text{Overlap Coefficient} = \frac{\sum(CH1_i)(CH2_i)}{\sqrt{\sum(CH1_i)^2(CH2_i)^2}} \tag{2.1}$$

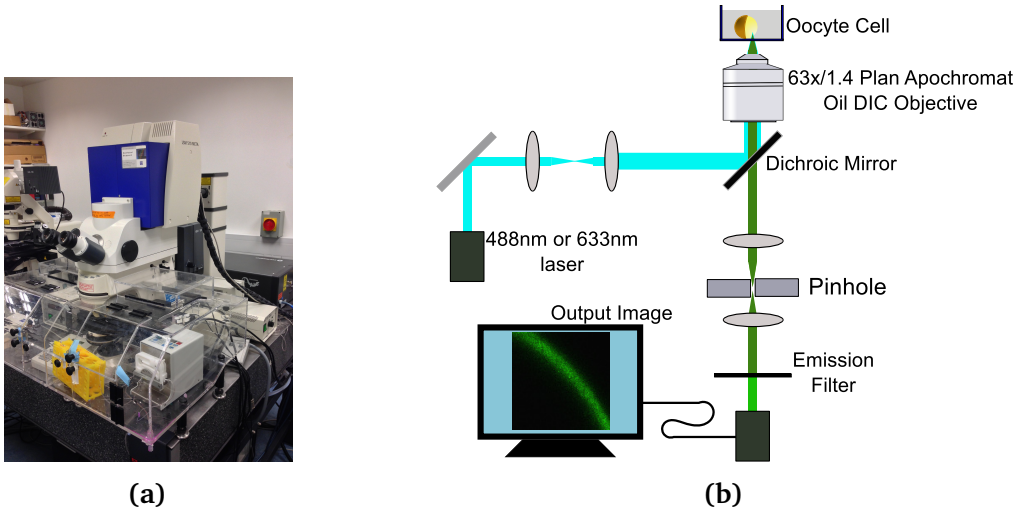

Figure 2.6: Fluorescent Microscopy. a) The inverted confocal microscope (Carl Zeiss®) used in this study to capture fluorescent images from the oocytes. The light source is supplied to the system by a laser scanning module, LSM510 (Carl Zeiss®). b) Schematic diagram of the confocal microscope (example shown for GFP detection). Blue-argon (488nm; for GFP detection) or Helium-Neon Red (633nm; for CF633 detection) lasers are supplied by the LSM510 module, collimated and reflected by a dichroic mirror. The light is then focused onto the oocyte cell using an oil-immersion objective (63x, NA 1.4, Plan Apochromat Oil DIC (Carl Zeiss®)). Emitted light then passes through the dichroic mirror and focused onto a pinhole for spatial filtering, recollimated and filtered through the emission filter. The output is then sent through the CCD sensor (AxioCam MRm, Carl Zeiss®) for image acquisition.

2.5 Molecular Dynamics Simulation

The MD simulations done in this study were performed by Dr Prafulla Aryal from the Structural Bioinformatics and Computational Biochemistry Unit, Department of Biochemistry. Briefly, the methods underlying these simulations were as follows: The TWIK-1 crystal structure (PDB ID: 3UKM) was used as the base structure for this work.

The crystal structure includes residues 19 to 281 of the protein sequence. Missing and incomplete structures (residues between 94-99 and 169-174) were modelled using the Modeller9.9 software. The TWIK-1 model was then converted into coarse-grained (CG) representations, which reduces the all-atoms level of resolution into fewer representations by treating groups of co-localised atoms as a single particle. CG molecular dynamics (CGMD) simulations developed were then run for 500ns at 323 K to allow for structure assembly and equilibration in a bilayer of 1-palmitoyl,2-oleoyl-sn-glycero-3-phosphocholine (POPC) lipids. The resultant assembly was next converted to atomistic structures, an all-atom representation, using the CG2AT package (Stansfeld and Sansom, 2011). This atomistic system was later solvated with simple point charge (SPC) water and 150mM NaCl. The SPC water model considers the basic three point interactions (H, O and H) of the water molecules, and assumes an ideal tetrahedral HOH angle of 109.47^o. K^+ions were then introduced into the assembly, by placing them in the selectivity filter, at positions S2 and S4, and the inner pore. Water molecules were also placed in the selectivity filter between the K^+ions. Initial simulations performed on the system uses the GROMOS96 43a1 forcefield, with SPC water, at 323K. Firstly, the system was equilibrated at 1atm and 323K for 1-ns with the non-hydrogen atoms of the protein restrained with a spring constant of $10kJ.mol^{-1}.A^{-2}$. It is then simulated for 100-ns, unrestrained, with a timestep of 2fs. Both the restraint and unrestrained simulations were repeated with a different, random initial velocity. For *in-silico* mutations, the residue of interest in the initial atomistic TWIK-1 model was mutated using pyMOL mutagenesis scripts. Energy minimization was then performed on the mutant system, before the 1-ns positional restraint and 100-ns MD simulations were run

CHAPTER 3

Functional studies of TWIK-1

3.1 Introduction

This chapter addresses the challenges in obtaining functional expression of TWIK-1, and initial attempts to improve this functional expression based on analysis of its x-ray crystal structure.

Functional studies of TWIK1 has been plagued with problems since it was first identified. Although it was the first mammalian K2P channel to be discovered, the difficulty of obtaining reproducible functional expression in heterologous systems has dampened much progress from being made in characterising its functional and biophysical properties.

Two different hypotheses have been proposed with regards to the problem of TWIK-1 expression. Both proposals agree that a subcellular mechanism suppresses the functional expression of TWIK-1 on the membrane surface. But the specific mechanism involved have been a matter of intense debate. One hypothesis argues that TWIK-1 is SUMOylated at the membrane surface, causing it to be non-functional, whilst the other argues that TWIK-1 is rapidly internalised by endocytosis.

3.1.1 SUMOylation of TWIK-1

One of the first studies to address the lack of functional TWIK-1 activity in the plasma membrane proposed that it was being rendered inactive by SUMOylation (Rajan et al., 2005). SUMOylation is a form of post-translational modification, whereby a small ubiquitin-like modifier (SUMO or sentrin) protein forms a covalent bond with a lysine residue of the target protein. SUMO proteins are small-sized proteins, with approximately 100 residues, that have been typically implicated in various cellular processes. These include nuclear localisation, transcription regulation and cellular stress response (Gareau and Lima, 2010).

The SUMOylation pathway involves a series of complex-forming processes, in the presence of several cofactor enzymes (figure 3.1). It starts with a sentrin/SUMO-specific protease (SENP) cleaving the pro-form of SUMO to reveal its di-glycine linkers, and SUMOylation of the target substrate ends with the glycine residue from the SUMO protein forming a peptide bond with the lysine residue of the substrate. This step is catalysed by a SUMO-conjugating enzyme, Ubc9, which recognises a specific motif on the substrate and appends the SUMO protein to this motif. The widely recognised consensus motif for Ubc9 binding, and thus SUMOylation, to occur is of the form; ψ-K-x-[D/E], where ψ is a bulky aliphatic amino acid and x is any amino acid (Geiss-Friedlander and Melchior, 2007).

TWIK-1 was the first ion channel, or indeed membrane protein, to be reported as a target substrate for SUMOylation (Rajan et al., 2005). Prior to this finding, SUMO binding is normally restricted to the nucleus. It was proposed that expression of TWIK-1 was suppressed through covalent modification by the SUMO1 protein, which binds covalently to the ϵ-amino group of the lysine residue at position 274 in the C-Helix region. In the crystal structure, this amphipathic helix lies at the intracellular membrane interface. The critical lysine residue (K274) is positioned within a sequence that supposedly resembles the consensus motif for Ubc9 binding (figure 3.2). Noticeably in TWIK-1, a phenylalanine

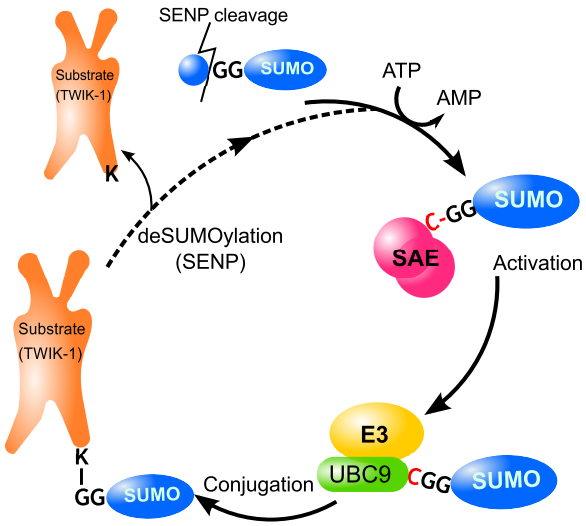

Figure 3.1: The SUMO pathway. SENP cleaves the precursor form of the small ubiquitin-like modifier protein (SUMO) to expose its glycine residue (The GG sequence appended to the SUMO figure), which can then bind to the E1 complex (SAE1/SAE2). Once activated, SUMO binds to Ubc9, which then catalyses the conjugation process of SUMO to the lysine (K symbol at the bottom of TWIK-1 model figure) residue of the target substrate. DeSUMOylation of the substrate may occur when SENP cleaves it off the SUMO protein. TWIK-1 was proposed to be SUMOylated by SUMO-1, making it silent at the plasma membrane.

lies in place of the negatively charged residue (D/E) on the consensus motif. Furthermore, it has also been argued that the consensus motif needs to be located in an intrinsically disordered region of the target protein for Ubc9 to bind (Henley et al., 2014).

Rajan et al. (2005) reported that when K274 was mutated to glutamate (K274E), an increase in current was observed, with a magnitude comparable to the high wild-type current observed when co-expressed with a SUMO protease (SENP1). This was associated to the inability of SUMO1 proteins to bind and inhibit the mutant (Rajan et al., 2005). It was therefore concluded that SUMO proteins are an important regulator for TWIK-1 channels to yield currents at the surface membrane. Moreover, it was also shown that only a single lysine at position 274 was necessary for SUMOylation to suppress channel activity (Plant et al., 2010, 2012). However, other groups were reportedly unable to observe the increase in TWIK-1 current when K274 was mutated into other amino acid besides glutamate (Feliciangeli et al., 2009).

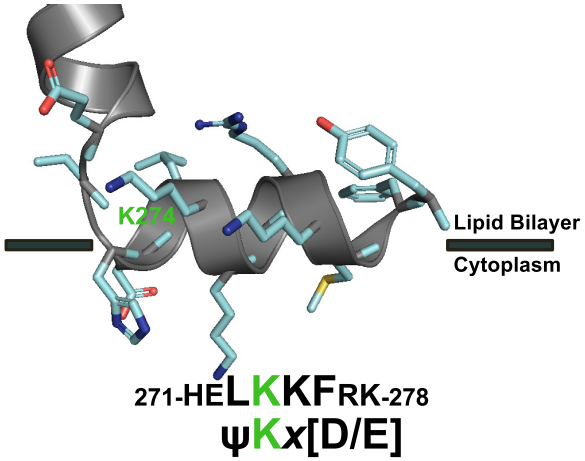

Figure 3.2: The proposed TWIK-1 SUMOylation site. View of the C-helix domain of TWIK-1 that shows the position of K274. Also shown is the sequence pattern of the TWIK-1 site recognised as its SUMOylation site, and compared to the consensus sequence below it. ψ is a bulky aliphatic amino acid and x is any amino acid.

3.1.2 Rapid Internalisation of TWIK-1

The proposition that TWIK-1 is being SUMOylated was, however, highly controversial, with several groups appearing unable to reproduce the results. Instead, TWIK-1 was shown to interact with EFA6A, an exchange factor for the small G-protein ADP-ribosylation factor 6 (ARF6) (Decressac et al., 2004). ARF6 is known to modulate endocytosis at the apical surface of Mabin-Darby Canine Kidney (MDCK) cells, and TWIK-1 was shown to only interact with EFA6A bound to ARF6 (figure 3.3). A cascade of further interactions were then suggested to cause TWIK-1 internalisation from the plasma membrane to the recycling endosome. Retrieval of TWIK-1 back into the plasma membrane appears possible by the activation of Gi-coupled receptors (Feliciangeli et al., 2009), although little is known of this step (Bichet et al., 2014).

Another study was also unable to reproduce the currents obtained from an arginine substitution (K274R) at the proposed SUMOylation site, and biochemical characterisation did not show any evidence of TWIK-1 SUMOylation (Feliciangeli et al., 2007, 2009). Instead, it was found that a di-isoleucine motif located at position 293-294 was critical for TWIK-1 endocytosis. When both isoleucines were mutated to alanines (I293A/I294A),

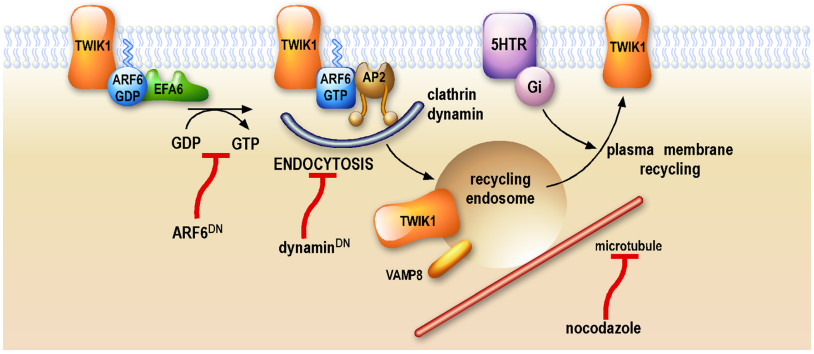

Figure 3.3: TWIK-1 is being internalised and recycled.A schematic diagram illustrating how TWIK-1 is trafficked in the cell. As TWIK-1 becomes available at the plasma membrane, it is rapidly internalised by the forming complex with ARF6-EFA, which is then internalised into the recycling endosome in a dynamin-dependant manner. TWIK-1 then concentrates in the recycling endosome. Rescue to the plasma membrane in CHO and MDCK cells is possible through the activation of Gi-coupled receptor. (Adapted from Bichet et al. (2014))

the channel appeared to be retained at the membrane surface, and currents were able to be recorded from cells expressing this mutant (figure 3.4) (Feliciangeli et al., 2009; Chatelain et al., 2012). It was proposed that this motif resembles a di-leucine-based recognition site for internalisation (Feliciangeli et al., 2009).

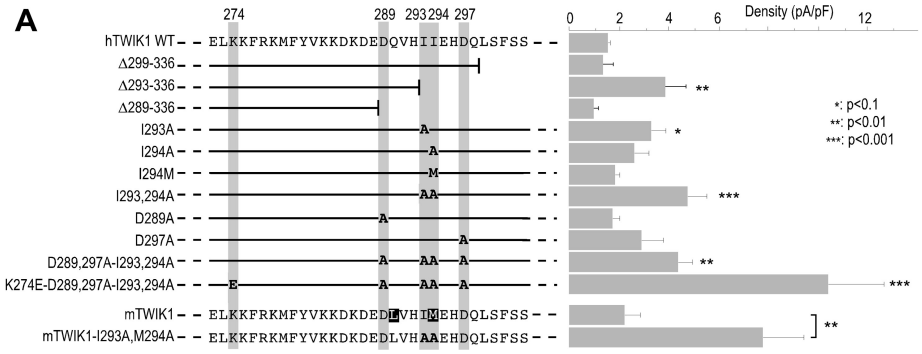

Figure 3.4: Current density highlighting the effect of removing or mutating the di-isoleucine motif. Currents recorded at +40mV shows that when TWIK-1 C-terminus was partially deleted from residue 293, an increase in current was observed. Similar effect was also seen when the di-isoleucine motif at 293 and 294 was mutated to alanines, suggesting that this motif may have been a trafficking signal for endocytosis. (Feliciangeli et al., 2009)

In general, internalisation involves a similar recognition motif as those destined for

lysosomal-targetting, and can be classified into two major categories; tyrosine-based and dileucine-based signals. The canonical dileucine motifs are either a [D/E]xxxL[L/I] or a DxxLL, notably with an acidic residue nearby. The AP-2 clathrin-adaptor has also been shown to bind to the di-isoleucine motif of an inwardly-rectifying potassium channel, Kir2.3, resulting in its internalisation(Mason et al., 2008). However, it is possible that AP-2 binding to this motif may adopt a different strategy than binding to the canonical di-leucine motif, which is more typical for lysosomal-targeting (Ortega et al., 2012). It was therefore concluded that the lack of functional expression of TWIK-1 at the plasma membrane was instead due to the rapid internalisation rather than post-translational modification by SUMOylation. However, the subject was, and remains, controversial. We therefore decided to determine whether the structure of TWIK-1 could provide any insight into this controversy.

3.2 Results

3.2.1 Declaration of Authorship

In addition to the declared role mentioned in the "Declaration of Authorship" section in the beginning of this thesis, I hereby declare that all the molecular biology works and two-electrode voltage clamp experiments done in this chapter are solely done by me. The molecular dynamics simulations and analyses discussed in section 3.2.5.2 have been performed by Dr Prafulla Aryal.

3.2.2 Wild-Type TWIK-1 currents appear functionally silent

Consistent with all previous reports, we found that no recordable currents could be observed from the wild-type TWIK-1 when expressed in *Xenopus* oocytes. When compared to basal currents recorded from uninjected oocytes, there was no significant difference

between the two sets of recordings (Student t-test p-value > 0.1) (figure 3.5).

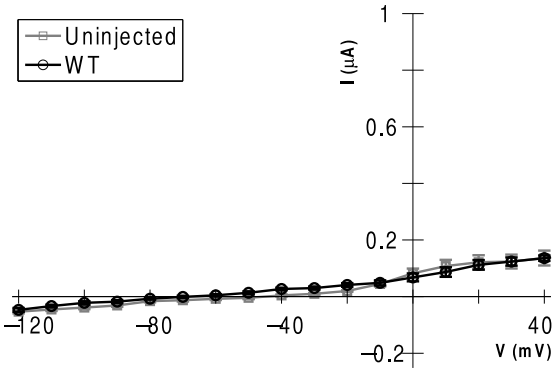

Figure 3.5: Lack of functional expression of wild-type TWIK-1. The currents recorded from oocytes injected with TWIK-1 RNA (n=10) are virtually non-existent when compared to uninjected cells (Student t-test: p-value>0.1). Currents were recorded in 10-step increment from -120mV to 70mV, and in physiological bath solution at pH7.4; 2mM KCl, 96mM NaCl, 2mM $MgCl_2$, 1.8mM $CaCl_2$, 5mM HEPES.

3.2.3 Mutations are inconsistent with SUMOylation hypothesis

In order to test for the possibility that TWIK-1 is SUMOylated, mutations were carried out on the lysine residue at position 274. This is aimed at reproducing some of the previously reported observations (Rajan et al., 2005; Plant et al., 2010). When glutamate substitution was introduced (K274E), a slight improvement in current was observed. This concurs with the increase in current observed by other studies on the K274E mutant (Rajan et al., 2005; Feliciangeli et al., 2007). However, contrary to previous reports, when arginine substitution was introduced (K274R), the level of current did not improve (figure 3.6).

This raises the possibility that the K274E mutation is affecting TWIK-1 activity in a way that is different to the K274R mutant. This implies that replacing lysine with another amino acid may not be rescuing the channel from being SUMOylated. Instead, it may be affecting the ability of the channel to conduct ions. It is plausible that by changing the electrostatics at position 274 might favour the movement of cations such

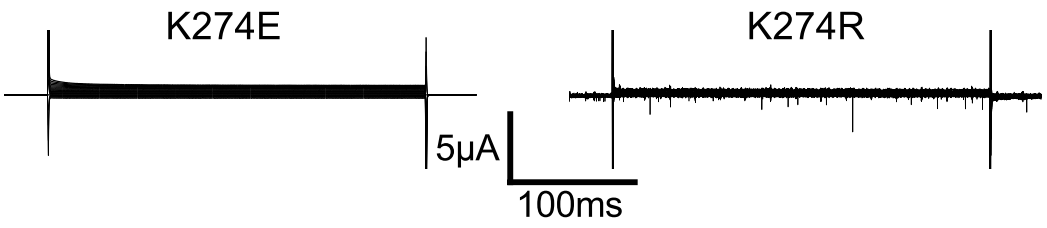

(a)

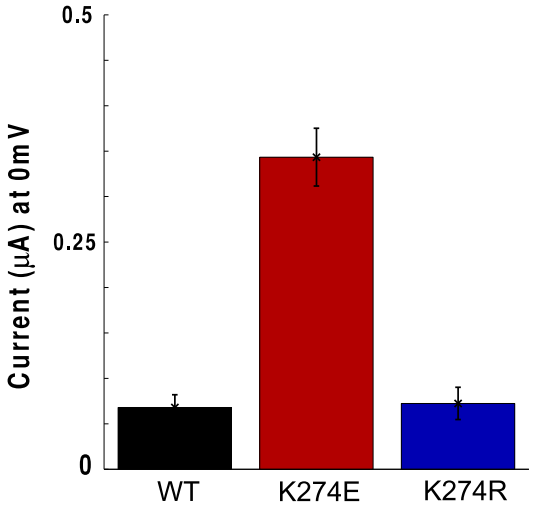

(b)

Figure 3.6: The outcome of mutating K274E and K274R varies. a) Representative current traces from -120mV to +40mV shows the different effect of mutating K274. While K274E leads to higher channel activity, K274R appears to have no change in basal activity. This difference in effect can be seen in (b) the averaged bar plot for recordings taken at 0mV. Currents are recorded from oocytes after 24 hours of incubation, and perfused in physiological buffer at pH7.4; 2mM KCl, 96mM NaCl, 2mM $MgCl_2$, 1.8mM $CaCl_2$, 5mM HEPES.

as potassium to flow through.

Further mutations at position 274 were therefore tested, to see if other amino acid substitution would result in an increase in current. These results are shown in figure 3.7, and demonstrate that neither a glutamine nor alanine substitution were capable of increasing functional expression. Our observations, therefore, argue against the hypothesis that TWIK-1 is functionally suppressed by SUMOylation at K274.

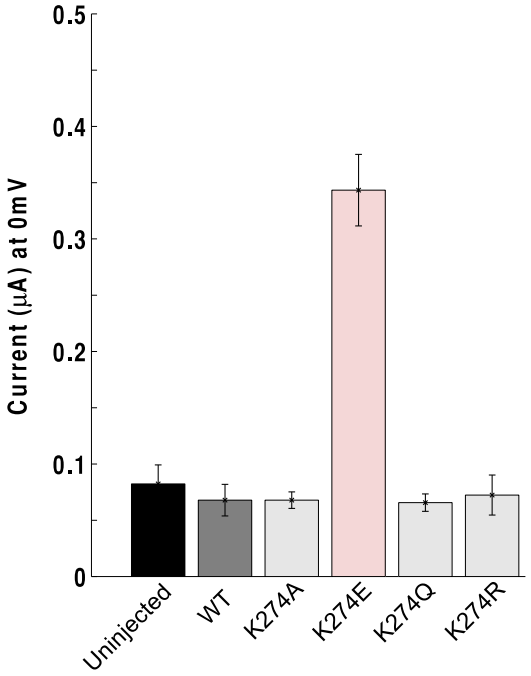

(a)

Figure 3.7: Mutating K274 shows different level of currents. The bar plot shows the mean±SEM current value at 0mV of each mutant and compared to wild-type TWIK-1, as well as uninjected oocytes. Only the K274E mutant (light red) had a significant effect (Tukey's test, $p<0.05$), while other K274 mutants did not improve the level of currents. Oocytes (n=5-12) were recorded 24 hours after incubation and perfused in physiological bath at pH7.4.

3.2.4 Functional expression of TWIK-1 is increased by mutation of the trafficking motif

We next examined whether TWIK-1 is in fact being internalised and recycled by endocytosis, by mutating the di-isoleucine motif into alanines (I293A/I294A). As previously reported (Feliciangeli et al., 2009; Chatelain et al., 2012), this resulted in an increase in functional activity. The level of whole-cell currents recorded form the oocytes expressing this mutant was even higher than the one recorded from oocytes expressing K274E TWIK-1 mutants (figure 3.8).

These observations are, therefore, consistent with the fact that it is more likely for TWIK-1 to be rapidly internalised by endocytosis. This does not rule out the possibility that SUMOylation can still affect TWIK-1 functional activity at the plasma membrane in other cell types, but it seems unlikely, at least in oocytes. Due to this, we have decided to use this endocytosis-insensitive mutation as our pseudo-wild-type TWIK-1 (WT*) for further studies of TWIK-1. II293/294AA mutation done on TWIK-1 will therefore be denoted as *(asterisk) throughout the rest of this thesis, unless specified otherwise.

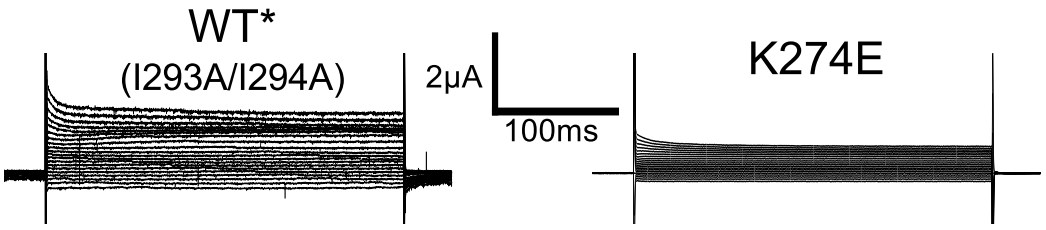

(a)

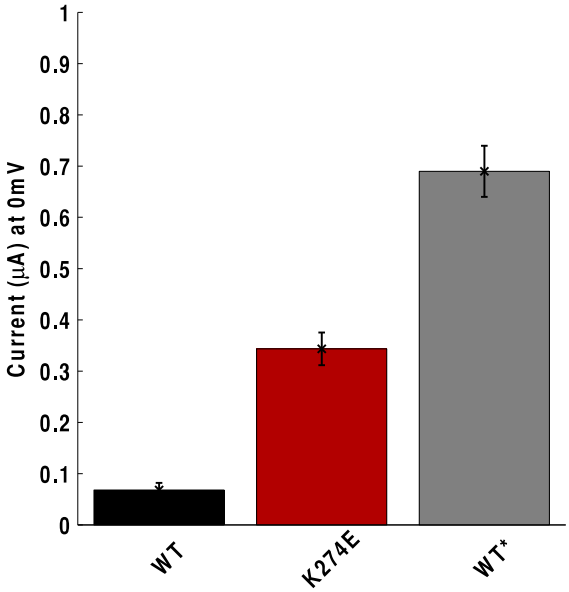

(b)

Figure 3.8: Endocytotic mutation vs SUMOylation mutation. a) Currents recorded from oocytes expressing TWIK-1 de-SUMOylating mutant(K274E) is compared to those expressing TWIK-1 internalisation-insensitive mutant. The mean±SEM current is recorded in a voltage step from -120mV to +70mV. b) The higher channel activity is recorded from the trafficking mutation WT* (I293A/I294A).

3.2.5 TWIK-1 structural observation at the C-helix

Although functional analysis of the TWIK-1 K274 mutations does not support the SUMOylation hypothesis, they may still impose a different effect on TWIK-1 activity. As observed earlier, the TWIK-1 K274E mutant resulted in an increase in current, whereas retaining the positive charge at the same position with the K274R mutant did not. This might reflect an electrostatic effect that can, in turn, affect either gating at the cytoplasmic region of the channel, or movement of ions within the pore. Further study on the effects of mutating this position toward channel activity is described in Chapter 5.

Looking into the x-ray crystal structure of TWIK-1, the region where K274 is positioned appears to be an amphipathic helix that lies parallel to the membrane surface (figure 3.9a). The amphipathic nature of this helix allows it associate and conform stably at the membrane surface. This domain hinges at L270, and kinks inwardly towards the M2 helix of the adjacent subunit. Typically, kinks arise when there is a presence of a flexible glycine residue, or a proline that lacks the ability to form a complete hydrogen bonding network necessary for a helical structure. However, neither of these amino acids were present nearby L270, prompting us to consider that the kink may be unstable or non-permanent.

When the electron density is mapped onto the TWIK-1 structure, an extra density is seen at the kink of the C-helix (pointed by an arrow in figure 3.9b). This small density propagates further down the M4 helix, which could indicate an alternative conformation for the C-helix structure. If this extra density represents a physical movement of the C-helix, it may suggest that TWIK-1 channel activity could be regulated by this movement.

3.2.5.1 Possible interaction between K274 and E269

Upon examining the K274 in the structure, it was noticed that E269 appears to be in close proximity to this residue. The distance between the two residues suggests that

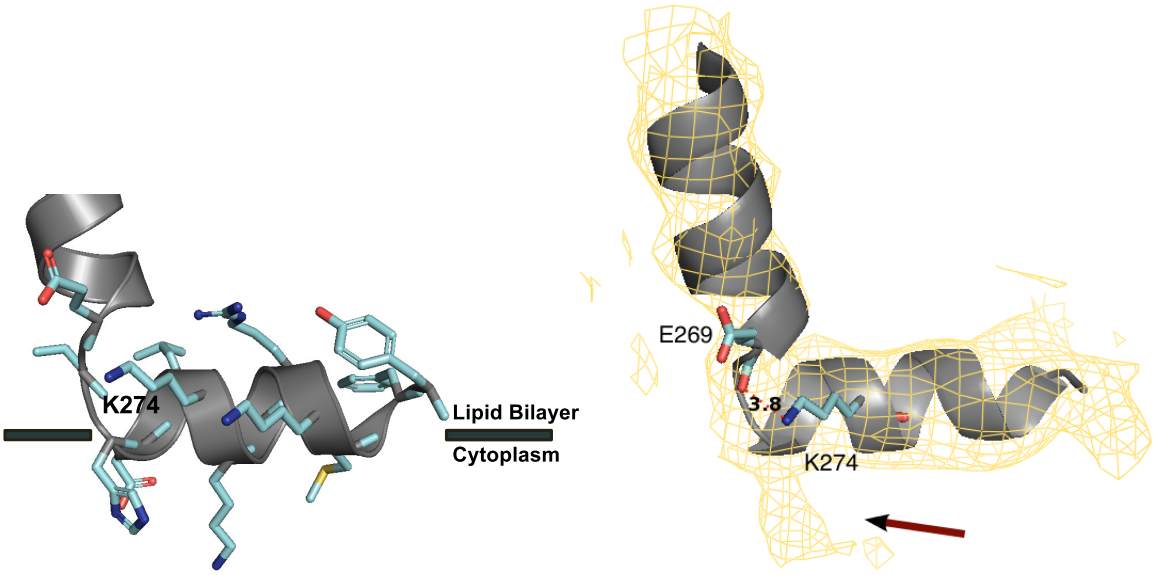

Figure 3.9: The C-helix domain of TWIK-1 subunit. a) The C-helix is formed by a sharp kink at the end of M4 helix. The structure is composed of 10 residues from position 271-281. This includes the K274 residue. b) The electron density around the C-helix structure reveals an extra density near the kink (shown by arrow). Also shown is the close contact (3.8Å) between K274 and E269 (shown as sticks), making it possible for them to interact.

they could be in contact with each other. Visualisation of the structure suggests that this kink may be held by the interaction between K274 and E269. This assumption is consistent with the observed outcome from mutating K274E and K274R. Substituting K274 with a negatively charged residue (K274E) could break this putative interaction, resulting to the increase in functional activity previously mentioned (figure 3.7). On the contrary, maintaining the positive charges with the arginine substitution (K274R) could retain the interaction, leading to the restricted channel activity described before.

If this putative interaction does occur, it is then possible to replicate the above observations by mutating E269 instead. However, when mutated to E269Q, channel activity remained at the same level as the wild type. Similar outcome was also seen when the same mutation was done on TWIK-1 with the trafficking mutation background (E269Q*). Mutating E269 to a lysine (E269K*) also did not improve channel function,

neither the alanine substitution (E269A*).

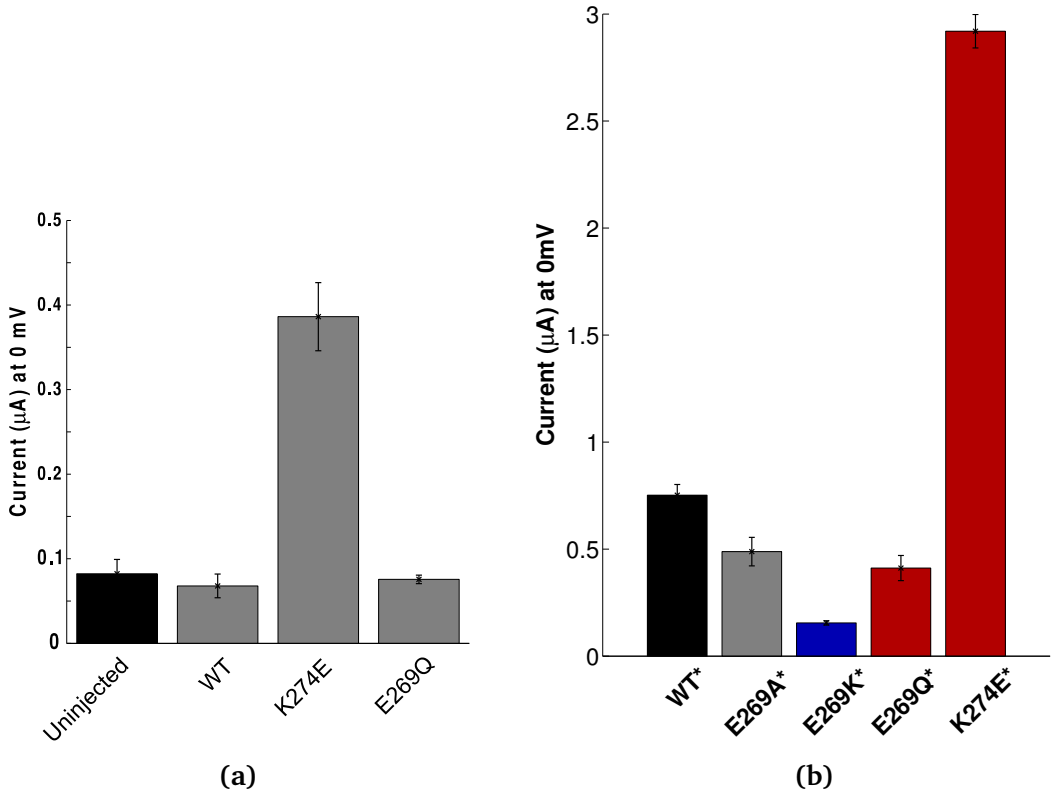

Figure 3.10: E269Q mutation has no effect on TWIK-1 channel activity. a) The bar plot compares the mean±SEM current value at 0mV between K274E and E269Q. E269Q appears to have no significant effect on TWIK-1 activity, suggesting that the C-helix structure is not formed by the K274-E269 interaction. No significant effect was also observed from other E269 mutations as shown in (b), even with the trafficking mutations being present. Oocytes (n=7-11) were recorded 24 hours after incubation and perfused in physiological bath at pH7.4.

These observations suggest that E269 could not be interacting with K274 in a manner that contributes to the kink formation. Instead, the stability of the kink formation could be mainly due to the strong amphipathic nature of the C-helix, which associates strongly with the membrane at the intracellular side.

3.2.5.2 MD simulation suggests that the C-helix is stable

We then shifted to test this stability by means of molecular dynamics (MD) simulation. A 100ns MD simulation, performed by Dr Prafulla Aryal, was run for the TWIK-1 model and fluctuations at the C-helix was observed. As can be seen in figure 3.11a, the C-helix appeared to be stable throughout the simulation. This is also shown by the root-mean-square fluctuations (RMSF) plot of the TWIK-1 structure, taken as an average throughout the simulation (figure 3.11). While movements were mostly occurring at the end of M2 helix, the C-helix movement were mainly subtle and stable. This suggests that the formation of the C-helix is possibly part of the TWIK-1 native structure, and not an artefact.

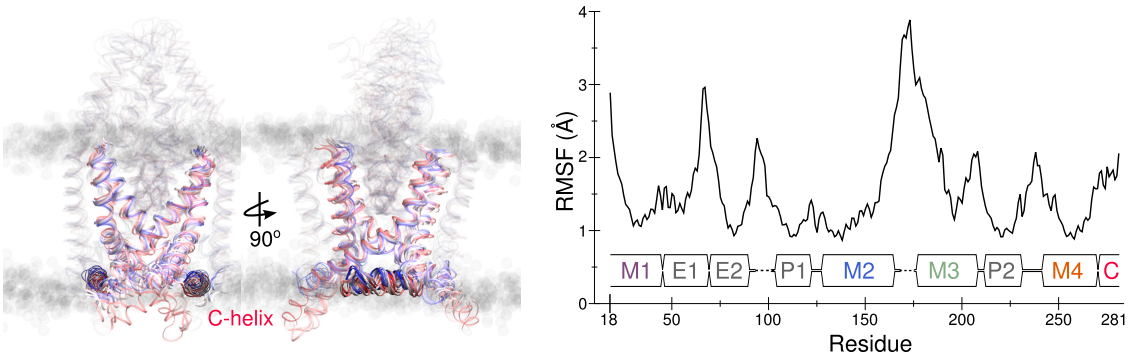

(a) **(b)**

Figure 3.11: 100ns MD simulation supports that the C-helix is stable. 100ns-simulation of the TWIK-1 model suggests that the C-helix structure is stable, as shown by snapshots of the structure throughout the simulation. The C-helix remains intact in this simulation. b) The structure stability is also illustrated by the averaged root-mean-square-fluctuation (RMSF) plot from the simulation. Figures have been prepared by Dr Prafulla Aryal Aryal et al. (2014a).

3.3 Discussion

3.3.1 SUMOylation or rapid internalisation?

In this chapter, the ongoing debate regarding how TWIK-1 channel expression is being regulated was addressed. On one side, the expression of TWIK-1 was argued to be present at the membrane surface, but the channel activity itself was thought to be suppressed by SUMO proteins. On the contrary, another opinion suggest that TWIK-1 expression itself was being regulated by the endocytosis machinery that internalises TWIK-1 away from the membrane surface. Both contesting opinions were built on observations from valid experiments.

However, upon testing ourselves the TWIK-1 expression, we are prone to agree that TWIK-1 is more likely to be regulated via the endocytosis pathway, at least in Xenopus oocytes. When the di-isoleucine trafficking motif was removed from TWIK-1 by mutagenesis (I293A/I294A), better functional activity was obvious.

On the other hand, when the postulated SUMO-related lysine residue in TWIK-1 was mutated, mixed levels of channel activity was observed. While K274E does improve functional activity, other mutations (K274A/Q/R) did not. As SUMOylation only occurs by binding to a lysine residue located within a certain motif, replacing the lysine residue with any amino acid should rescue channel activity. This is inconsistent with our observation, making SUMOylation less probable to occur. Moreover, it has been suggested that the SUMO-conjugating enzyme, Ubc9, binds preferentially to an intrinsically disordered region of the target protein (Henley et al., 2014). This makes K274 the lesser candidate, since it is located in the C-helix domain.

3.3.2 The C-helix formation is stable

Nonetheless, the increase in current observed from the K274E mutant could indicate a gating mechanism for TWIK-1. Therefore we postulated that it may be forming an

interaction with another residue, E269, in a manner that could cause the helix to kink and form the C-helix structure.

However, mutating E269 did not improve channel activity. In particular, E269K, which was thought to cause a similar repulsion as mutating K274E, did not lead to any increase in channel activity. Therefore, it is thought that the C-helix formation is intrinsically part of the TWIK-1 structure, and K274 influences TWIK-1 functional activity in a different manner. The effect of K274 and other residues on the C-helix is studied further in Chapter 5.

The stability of the C-helix is also highlighted in the MD simulation of the TWIK-1 model, where only minimal movement is observed at the c-terminal end of TWIK-1, and the C-helix structure never diminished throughout the simulation.

On the contrary, a separate, yet interesting, development was observed in the TWIK-1 structure. Water was seen to be entering and leaving the inner pore structure as the simulation runs through. This phenomena has been described before in simulations of nanopores and other ion channels as a 'wetting and dewetting' event. Such observation became part of an interesting study that proposes a novel mechanism by which K2P channels may be gated at the deep inner pore region. This study is described in the next chapter.

3.4 Conclusion

From our initial study, it can be concluded that expression of TWIK-1 in Xenopus oocytes is regulated via the endocytosis pathway that internalises the channel from the membrane surface. Its expression can be rescued by removing the di-isoleucine motif near the C-terminus end of the channel.

The formation of the C-helix is also shown to be stable and is intrinsically part of the channel. However, water oscillations observed in the simulation could be a mechanism

by which channel activity is regulated.

CHAPTER 4

A Hydrophobic Barrier in TWIK-1

4.1 Introduction

Ionic hydration is a key factor to how an ion channel operates. Studies have previously shown that the thermodynamics of ion solvation are a major determinant that enables potassium channels to discriminate and favour K^+ions over Na^+, despite the latter being smaller in size (Noskov and Roux, 2007; Nimigean and Allen, 2011; Varma et al., 2011a). It was suggested that the total energy cost of dehydrating an ion, and allowing it to form a snug-fit interaction with the carbonyl groups on residues at the selectivity filter, enables K^+channels to favour potassium ion permeation (Noskov and Roux, 2007). This therefore highlights the importance of ionic hydration in facilitating ion permeation. In this chapter, the close relationship between ion hydration and permeation is extended, and the possible effect of altering water permeability on ion permeation inside the channel pore is described.

It was shown in the previous chapter that, while the C-helix structure at the cytoplasmic region of TWIK-1 remained stable during the molecular dynamics simulation,

the inner pore side of the channel was dewetted and void of water for most of the time. In this chapter, we shall be looking into this phenomenon much closer, with focus on the region at the inner pore where the void was observed in the simulation. I demonstrate here that the presence of a hydrophobic barrier inside the channel pore is likely to impede ion permeation, thus limiting functional activity. This barrier may be overcome by introducing polarity in the region, or increasing pore dimension, therefore allowing more ions to permeate. Work detailed in this chapter has been published. Prafulla Aryal, Firdaus Abd-Wahab, Giovanna Bucci, Mark S P Sansom, and Stephen J Tucker. A hydrophobic barrier deep within the inner pore of the TWIK-1 K2P potassium channel. Nature Communications, 5, July 2014 (See Appendix).

4.1.1 Mechanism of the Hydrophobic Barrier

Water possesses a unique characteristic that enables it to solvate and hydrate a plethora of substances, including ions. The dynamic formation of hydrogen bonds between water and ion molecules helps stabilise the ions in their hydrated forms, which then allows them to diffuse along space (Grossfield, 2005). Ion transport through channels is, therefore, greatly facilitated by the presence of water.

However, water molecules in the bulk configuration have been suggested to behave differently when confined to the nano-scale space. Not only are the thermodynamic properties between bulk and nano-confined waters different, some biophysical terms that are negligible in the bulk water becomes more significant in the confined arrangement (Sendner et al., 2009; Pérez-Hernández et al., 2012; Chiavazzo et al., 2014). This includes interfacial interactions between water and the substrate surface (Hummer et al., 2001; Sendner et al., 2009). Therefore, the shape and dimensions of narrow pores like ion channels, and their pore-lining constituents, may influence the behaviour of water as it comes into contact.

Capillary effects too tend to have a significant implication on water in small pores.

Under conditions where the surface to volume ratio is high, microscale water tend to be in a metastable liquid state. This state is generally an extended state that mostly lies in between the liquid and vapour states in the water phase diagram. It has also been described that water at the interface of hydrophobic surfaces could result in the formation of a depletion monolayer, which when confined to a channel, forms nanobubbles (Ball, 2003). Given the large ratio between wall surface to water volume in a channel, the weak adhesive force from the hydrophobic surface competing with the cohesive force of adjacent water shifts the phase of the interfacial water into forming gas bubbles. This formation could shift back in phase and become condensed once more as the surface becomes less hydrophobic (Roth et al., 2008). Consequently, capillary actions then causes water to shift between the liquid and vapour states by means of condensation and evaporation (Beckstein and Sansom, 2004).

4.1.2 Nanopores and Electrowetting

In nanopores, water was observed to oscillate between two states when subjected to a narrow hydrophobic pore. As water passes through the pore, the cavity is either filled with bulk-liquid density, or empty in a vapour-like manner. These states have been associated with the opening and closing of the narrow pore, since opening of the pore means allowing water to occupy the confined space and facilitating ion permeation, and closing otherwise (Aryal et al., 2014c).

The principle of hydrophobic gating may be defined as dependent on two main features of the pore; size, and hydrophobicity. These key components can be deduced from studying simplified nanopores (Beckstein et al., 2001). Firstly, the diameter of a pore can induce physical occlusion to permeation if the constriction is sufficiently tight. This may be achieved when, ideally, the pore diameter is smaller than the size of a water molecule or a hydrated ion. However, as has now been numerously shown, most nanopores and ion channels are in the close state even when the constriction diameter

can still physically allow water molecules to pass (Beckstein et al., 2001; Beckstein and Sansom, 2003).

This leads us to the second feature of the hydrophobic gating. Hydrophobicity may play a more significant role than pore size in generating a hydrophobic gate. This could then explain the reason behind most pores being closed to permeation even when the pore opening is still larger than the size of a water molecule. The capillary effect between water and the hydrophobic surface causes the formation of nanobubbles at the vicinity of the pore, which in turn impedes water entry (Beckstein and Sansom, 2004; Aryal et al., 2014c). Recently, it has been shown that stochastic wetting (water-filling) and dewetting (water-leaving) can be simulated in nanopores by introducing a ring of hydrophobic leucine residues at the central pore, surrounded by hydrophilic residues (figure 4.1a) (Trick et al., 2014).

On the other hand, if the opening of the pore diameter is wide enough, then water may freely pass through and behave in a bulk water manner. Beyond this maximal pore size, the effect of hydrophobicity become less significant. The role of pore size is illustrated in figure 4.1b, whereby as the pore size increases, the oscillations become less frequent and the channel remains open more often. The correlation between pore size, or openness, and hydrophobicity is then shown in figure 4.1c. This plot depicts the probability of finding a pore in an open state, given its radius and hydrophobicity. Therefore, the possibility of shifting an ion channel into its open state would then rely on either increasing its pore size, or shifting its surface profile into becoming less hydrophobic (Beckstein and Sansom, 2004; Aryal et al., 2014c).

However, another study suggests that the energetic barrier induced by the hydrophobic gate may also be overcame if and when the electric potential is sufficiently high to drive the pore to be functionally open. This concept, known as electrowetting, illustrates that the hydrophobic gate may also be voltage-dependent (figure 4.1d) (Powell et al., 2011).

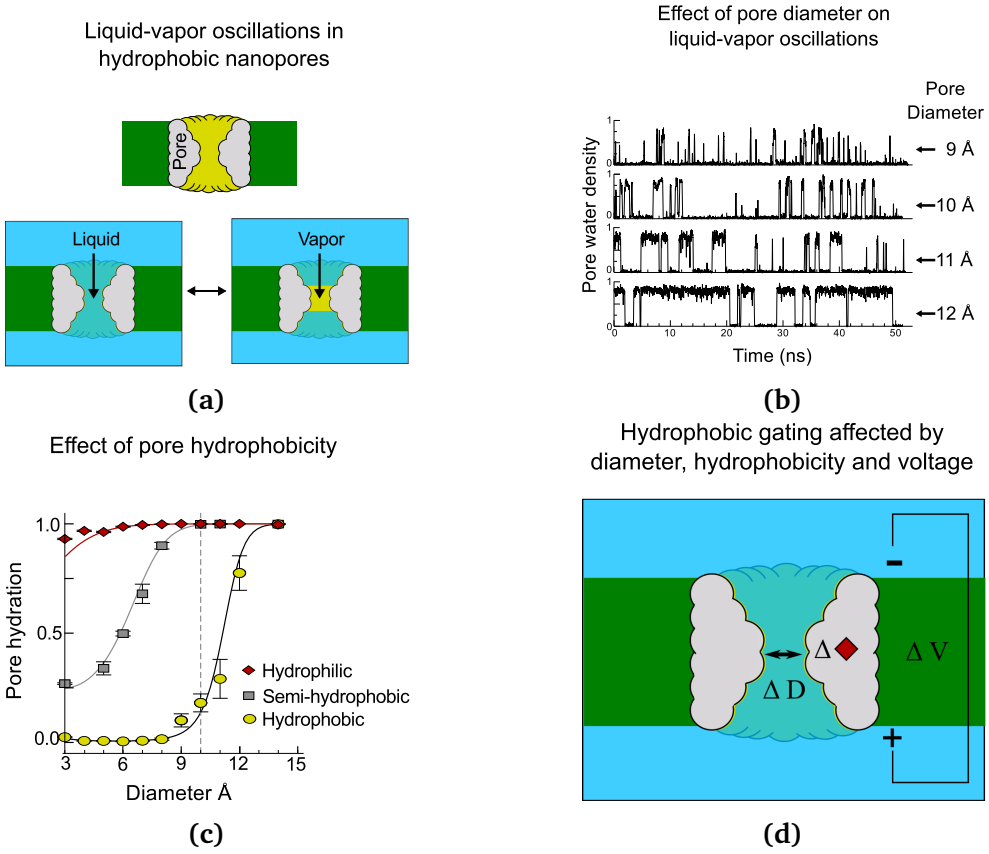

Figure 4.1: Principle of hydrophobic gating. a) Illustration of a model hydrophobic nanopore. The hydrophobic surface is shown in yellow. The image depicts the oscillation of water between its two states; liquid and vapour, as it passes through a narrow hydrophobic pore. b) The effect of pore diameter causes rapid fluctuations between water states, depending on pore size. As the diameter increases and reaches a minimum size for pore hydration, the oscillations begin to relax and favour water in the liquid state. This dependence on pore diameter, as well as pore surface hydrophobicity strength is summarised in (c). Complete hydration occurs for hydrophobic pores when its diameter increases beyond 14Å. But as it goes below the 10Å threshold (dashed vertical line), the pore gets dewetted more frequently. d) Hydrophobic gating can not only be affected by pore size and hydrophobicity, but also transmembrane potential. Figure adapted from Aryal et al. (2014c).

4.1.3 Ligand-gated ion channels

In the nicotinic-acetylcholine receptor (nAchR), a pentameric ligand-gated ion channel (pLGIC) found at the nerve-muscle synapse, a tight constriction of 3Å radius was observed in the middle of the pore (Miyazawa et al., 2003). Such a narrow pore is too small for a hydrated ion to flow through. The effective diameter of an ion with its first hydration shell intact is approximately 8Å (Miyazawa et al., 2003). Therefore, it is not possible for the ion to pass this region without having to lose its hydration shell. De-solvating an ion would be energetically costly, taking more than 300kJ/mol (Beckstein and Sansom, 2006), but it can be reduced if the absence of water can be replaced by a snug-fit polar surface, as is the case for the selectivity filter. However, the narrow pore in nAChR is lined by symmetrical interactions between hydrophobic residues. This creates an energetic barrier to ion permeation, known as a hydrophobic gate. Therefore, even without any physical occlusion, this mechanism is sufficient to gate the pore of a channel functionally closed. Hydrophilic substitution on leucine and valine residues located near the cytoplasmic-side inner pore was shown to shift nAchR to an open state, which was suggested to be caused by an increase in pore hydration (Jha et al., 2009).

A similar hydrophobic barrier was also reported to exist in the pore of a bacterial homologue of the pLGIC family, the GLIC ion channel. By running an MD simulation on the high resolution structure (2.99Å), water was found to diminish completely from the long, but narrow, segment of the pore. The free energy required to hydrate the pore in the closed-state was found to be ∼11.4kcal/mol, which is ∼28-fold greater than if it was to be hydrated in the open-state (Zhu and Hummer, 2012). On the contrary, the free energy difference for passing an ion through a pre-hydrated pore in the closed state is only 3.9kcal/mol. This signifies the greater barrier for ion permeation is, in fact, pore hydration.

4.1.4 Bacterial mechanosenstive ion channels: Hydration of pores influences gating kinetics

The presence of a hydrophobic gate was also reported in bacterial mechanosensitive ion channels, MscL and MscS (Aryal et al., 2014c). Both channels are activated when stretched upon osmotic stress. However, despite being functionally similar, they are structurally distinct. While MscL is a pentamer of two-transmembrane subunits, MscS is formed by heptameric assembly of three-transmembrane subunits. Nevertheless, MscL and MscS both contain a narrow constriction site at the inner pore cavity that can energetically exclude water from filling inside the site. In MscS, this constriction is lined by leucines, a L105 and L109 pair from seven subunits. Whereas MscL is lined by five pairs of leucine and valine, L19 and V23, from each subunit. Even in the closed state, the constriction site of both channels were not occluded completely, but they were found to be dewetted for most of the simulation period (Sukharev et al., 2010). When hydrophilic substitutions were introduced into the constrictions, hydration at the pore appears to occur more often. It was suggested that the iris-like opening of the pore in both channels is dependant on the gradual exposure of the polar groups, and mediated by nearby glycine residues (Sukharev et al., 2010; Aryal et al., 2014c).

4.1.5 MthK channel lacks a helix-bundle crossing

Recent studies have ruled out the possibility that gating of the MthK channel is regulated by an intracellular helix bundle crossing. It was shown that quaternary ammonium blockers were still able to access and bind the inner cavity of the channel when it is inactivated (Posson et al., 2013, 2015). Quaternary ammonium (QA) blockers are commonly used to study the kinetics of potassium channels, since QA blockers can access the inner cavity of potassium channels when they are open (Armstrong, 1971). Therefore, for a QA blocker to still be able to enter the inner pore of MthK in its inactivated state,

indicates that its entryway into the pore is not physically occluded by the helix-bundle crossing.

However, it was also shown that the kinetics for QA block of the closed-state channel is slower than it would in the open-state (Posson et al., 2015), suggesting a change in the inner pore profile when closed. It has also been previously suggested that the channel gating and conductance may be regulated by an alanine residue (A88) located near and below the selectivity filter (Shi et al., 2011). Mutating this residue to larger hydrophobic amino acids appears to cause a decrease in current. On the contrary, hydrophilic substitutions, such as mutating it into aspartate or asparagine, causes an increase in conductance and open probability of the channel. Such observation is consistent with the presence of a hydrophobic barrier at the inner pore region of the channel, which may play a role in the gating of the channel.

4.1.6 TWIK-1: Dewetting of the inner pore

The major part of the molecular dynamics simulations and analyses of TWIK-1 described in this chapter were performed by Dr Prafulla Aryal, with some analysis by me. The X-ray crystal structure of TWIK-1 (Miller and Long, 2012) was equilibrated into a POPC lipid bilayer environment. Prior to assembly and equilibration, missing residues on the crystal structure (atoms at positions 94 to 99, and 169 to 174) was modelled in by Modeller. Subsequently, an atomistic system was created with water and ions included in, and the simulation was run for 100ns. The potential function for this simulation utilises the Gromos 43A1 forcefield set at temperature 323K.

From the simulation, the kinked structure of the C-helix domain appeared stable throughout, and only slight movements at the M2 helices were observed (Figure 4.2a). This movement, consequently, causes the fenestration site, which was initially present on both sides of the structure, to gradually close.

A striking phenomenon, however, was observed at the deep inner pore region of the

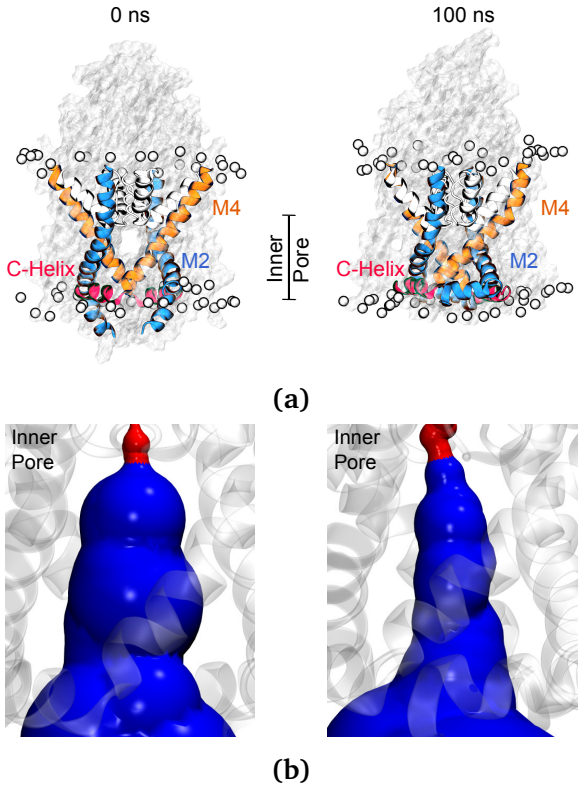

Figure 4.2: 100ns MD simulation shows stability of the C-helix. a) TWIK-1 structural conformation at the before (0 ns) and after (100 ns) the MD simulation. b) HOLE surface profile shows that the inner cavity pore remains open throughout the simulation (blue:radius>1.2Å,red:radius<1.2Å). Figure adapted from Aryal et al. (2014a).

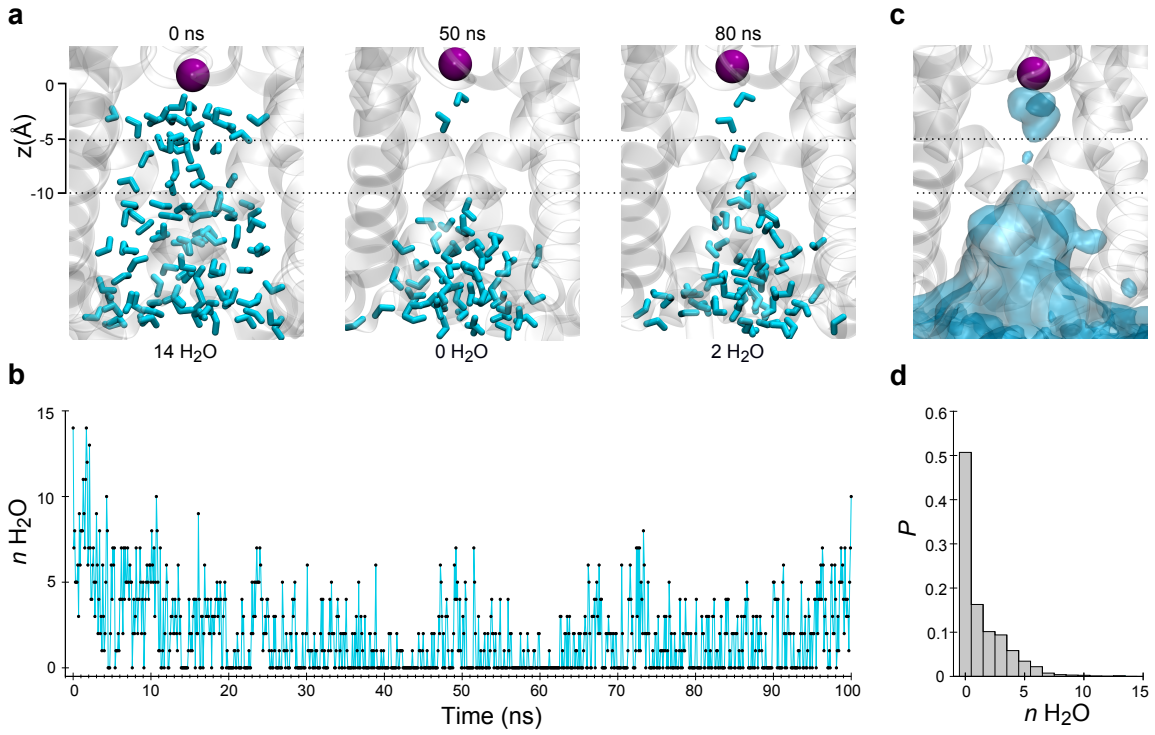

Figure 4.3: Stochastic wetting and dewetting of the inner pore. a) Snapshots from the 100ns MD simulation of the WT TWIK-1 deep inner pore, illustrating the wetting and dewetting process. The overall description of this oscillation events is shown in (b), whereby water counts throughout the 100ns simulation shows the rapid drop in water counts in the first few nanoseconds of the simulation, followed by fluctuations between wetting and dewetting processes. The averaged water occurrence in the inner pore is shown in (c), highlighting the water void region in the deep inner pore region (-10Å$\leqslant$ z $\leqslant$-5Å). d) Normalised probability histogram of the water counts emphasises dewetting as the most common event occurring in the pore. Figure adapted from Aryal et al. (2014a).

structure. Instantly within the first 10-20ns of the simulation, the region approximately 5-10Å below the selectivity filter became void of water molecules (figures 4.3a and 4.3b) . The water density within this volume oscillated rapidly between 0 to 10 number of water molecules at a time. However, throughout the 100ns simulation, the deep inner pore was empty of water for half of the time (figure 4.3d).

This clear absence of water molecules was also reproducible in a second, independent, duplicate run of the simulation, and the dewetting events were even observed in other MD simulations, employing different forcefields (figure 4.4). Using the same GROMOS 43A1 forcefield as above but reducing temperature to 310K, the deep inner pore was void of water for almost 80 percent of the time. On the other hand, it was only empty of water for 30 percent of the time in the other two forcefields (GROMOS 53A6 and OPLS-AA), also simulated at temperature 310K. In all instances, water was always present at the cytoplasmic pore mouth region of TWIK-1. Both the Gromos 53A6 and Gromos 43A1 forcefields were used in conjunction with the 3-site simple point charge (SPC) model for liquid water, whereas the TIP4P water model was used with the OPLS-AA forcefield. Moreover, the OPLS-AA forcefield includes representation for every atoms in the system, but both the Gromos forcefields do not include an explicit representation of the non-polar hydrogens.

As described earlier, dynamic oscillations of water wetting and dewetting the pore surface is a common feature observed in hydrophobic nanopores. Similarly, random fluctuations of liquid water seen in the deep inner pore of TWIK-1 in this simulation resembles such feature. In this chapter, I therefore set out to experimentally validate whether dewetting of the inner pore was related to the low functional activity of TWIK-1 and whether this might act as a functional hydrophobic gate.

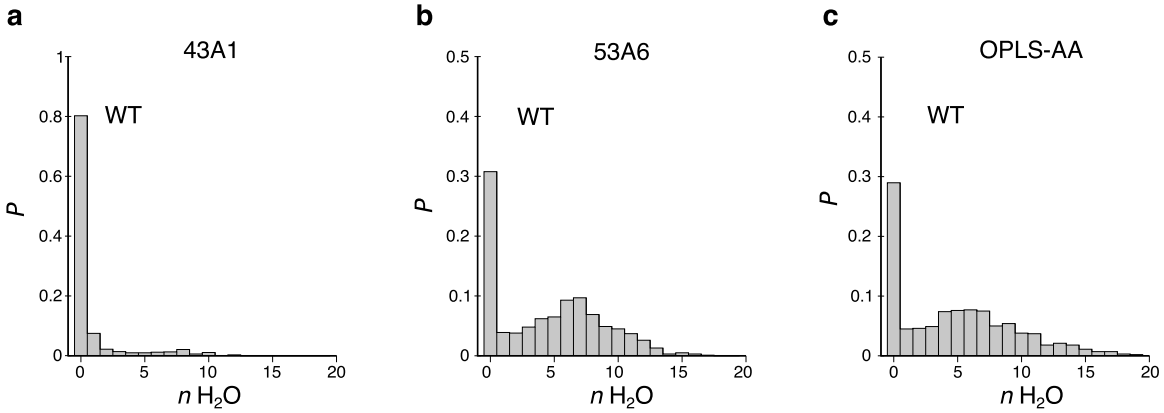

Figure 4.4: Dewetting persists under different forcefields. Normalised probability histogram of water counts from simulations done on the WT structure, using different forcefields; a) GROMOS43A1, b) GROMOS53A6 and c) OPLS-all atoms. The dewetting event still persist as the more common event occurring under these forcefields. Figure adapted from Aryal et al. (2014a).

4.2 Results

4.2.1 Declaration of Authorship

In addition to the declared role mentioned in the "Declaration of Authorship" section in the beginning of this thesis, I hereby declare that all the molecular biology works and two-electrode voltage clamp experiments done in this chapter are solely done by me. The molecular dynamics simulations and analyses done in this chapter have been performed by Dr Prafulla Aryal. The excised patch-clamp experiments in section 4.2.3.9 was done by Dr Giovanna Bucci.

4.2.2 Identification of a 'greasy doughnut'

In order to begin to test the idea of hydrophobic gating highlighted above, I first examined the structure of the TWIK-1 deep inner pore. A section through the inner pore shows that the region where dewetting is most prominent is composed of hydrophobic residues that encircles a certain region of the inner pore, and forming a cuff with a narrow opening of ∼8.5Å in diameter (figure 4.5). These residues were identified to be a pair of leucines

from each subunit. L146 lies in the M2 helix, whereas L261 is in the M4 helix.

The role of hydrophobic residues, especially leucines and valines, in influencing ion pore conduction have been highlighted previously in bacterial ion channels (Doyle et al., 1998; Miyazawa et al., 2003). In Acetylcholine receptors (AchR), the leucine L251 and valine V255 contributes significantly to the hydrophobic surface of an 8A long hydrophobic girdle inside the pore. This was suggested to create an energetic barrier to ion permeation by preventing cation from passing through while retaining its first hydration shell (Miyazawa et al., 2003).

In other human K2Ps, the residues equivalent to TWIK-1 L146 are mostly hydrophobic (Figure 4.5d) , but leucine is only conserved in TASK channels and KCNK7. THIK channels have an isoleucine residue at the analogous position, which is an isomer of leucine. Mutating the isoleucine into aspartate has been shown to increase the intrinsic activity of THIK channels (Chatelain et al., 2013). On the other hand, glycine residues can be found in TREK-1, TREK-2 and TRAAK. Aspartate substitution of glycine at the equivalent position, but in KCNK0, has been previously shown to lead to an increase in current (Ben-Abu et al., 2009). These findings affirm the significant role L146 may play towards ion permeation in the TWIK-1 channel.

Meanwhile, residues at the equivalent position to L261 are less conserved among the human K2P family. Only KCNK7 maintains a leucine at this position, whereas TWIK-2 has a near-isosteric valine residue at this analogous position. The TREK/TRAAK and TASK channels contain an Alanine and Glycine, respectively, which are small-sized residues.

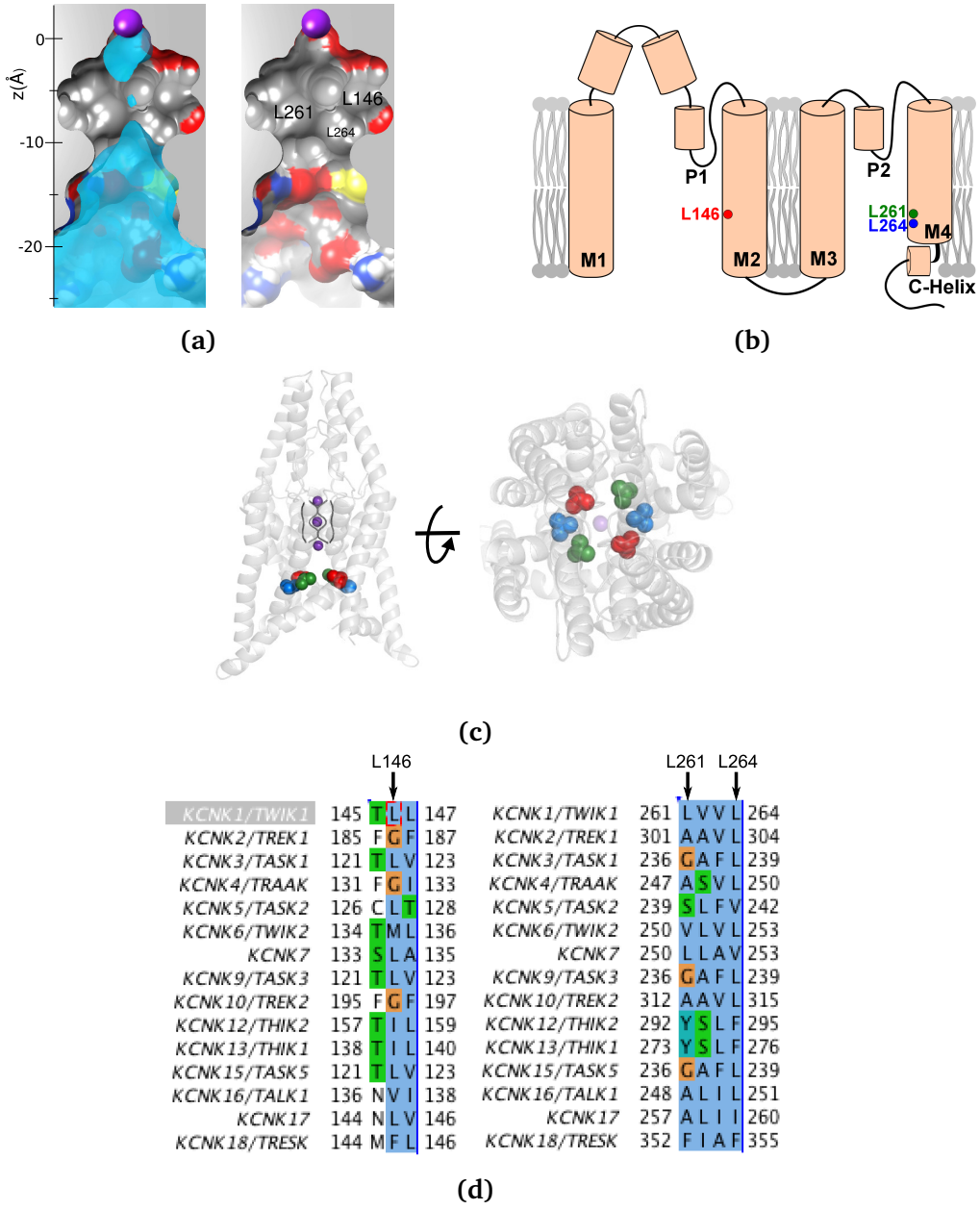

Figure 4.5: Identifying the 'greasy doughnut'. a) Cross-sectional view of the TWIK-1 inner pore shows the water void (dewetted) region underneath the selectivity filter (-10Å⩽ z ⩽-5Å). Identifying residues around the dewetted area reveals a hydrophobic cuff that is lined with leucine residues; L146, L261, and to a lesser extent, L264. The cytoplasmic pore mouth is constantly filled with water throughout the simulation. Figure prepared by Dr. Prafulla Aryal (Aryal et al., 2014a). b) Topology view showing L146 at the M2 helix, and L261 and L264 at the M4 helix. All three residues are located at the inner pore side of TWIK-1, also shown in (c) the structural-view. L146 (red) and L261 (green) lies on a similar plane-axis inside the pore of the channel, forming a hydrophobic cuff underneath the selectivity filter (black). purple: K^+ions. d) Sequence alignment at positions equivalent to TWIK-1 L146, L261 and L264 in other K2Ps.

4.2.3 M2 Helix: Role of L146

One of these leucine residues, L146 lies in the M2 helix domain of TWIK-1, with its side chain pointing straight into the permeation pathway and towards the other L146 from the second subunit.

4.2.3.1 L146D mutation

The effect of mutating L146 into a negatively-charged aspartate side-chain (L146D) on TWIK-1 functional activity has been initially tested by Chatelain et al. (2012). In their study, the large increase in current that was observed with the L146D mutant was described to be due to channel being locked in a constitutively open state, an observation similar to the G134D mutation in KCNK0 (Ben-Abu et al., 2009). Although glycine is replaced by leucine in TWIK-1 (L146), it is conserved in the TREK K2P family (Ben-Abu et al., 2009).

In our hands, we were able to reproduce this high level of channel activity in TWIK-1 with the L146D mutation. With 8μA of current at 0mV, the increase is nearly 16-folds higher than that of the WT* channel current (figure 4.6b).

When the TWIK-1 structure was modelled with the L146D mutation and a 100ns MD simulation was run, the inner pore passage remained hydrated (see figure 4.6c). The diameter of the inner pore remained the same as the wild-type model, at 8.5Å. This suggests that the pore hydration could be mostly due to reducing the hydrophobicity at the greasy cuff with the negative charge from the aspartate.

4.2.3.2 L146N mutation

Although mutating leucine into aspartate does show an increase in channel activity, this substitution may arguably introduce other effect due to the negative charge carried by its side-chain.

It is therefore desirable to check if we can replicate a similar outcome with a different

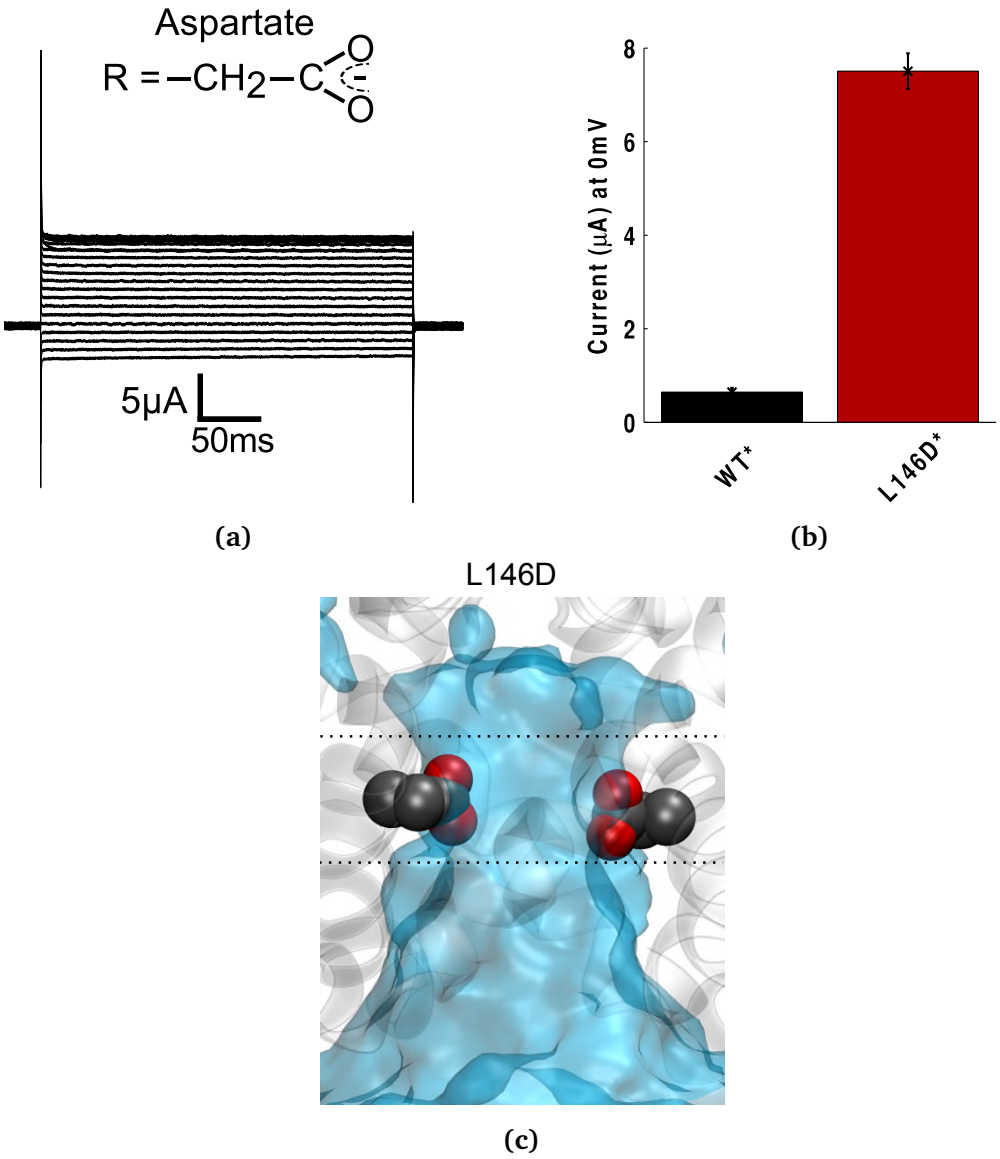

Figure 4.6: Breaking the hydrophobicity barrier with polarity inclusion. a) Whole cell current trace of TWIK-1 L146D mutant, clamped between -120mV and 70mV, and perfused with ND96 2mM KCl, pH7.4. b) Average whole cell current level when the cells were clamped at 0mV, showing the large difference in channel activity between the L146D mutant and the wild-type. c) MD simulation showing the spontaneous opening of the inner pore to water permeation (blue). Figure (c) was prepared by Dr Prafulla Aryal.

residue. If the hydrophobic ring restricts water permeation as predicted in figure 4.1c, then a mere introduction of polarity should suffice, and we may observe a similar outcome to introducing a charged side-chain.

Encouragingly, when mutated to L146N, with asparagine being isosteric to aspartate and polar but uncharged, an increase in channel activity was also observed. Furthermore, the averaged whole cell current was also very similar to that of mutating L146D (figure 4.7b). This suggests that introducing polarity, and no charges, is sufficient to draw water into the deep inner pore region and, in effect, allow permeation of ions through the channel pore.

This concept is also supported by the MD simulation that was done on the L146N mutant model (figure 4.7c). Water molecules were found to hydrate the deep inner pore more than the wild-type model, even without putting a strong charge at the hydrophobic cuff. Also, the L146N mutant pore is constantly hydrated throughout the simulation, whereas intermittent wetting and dewetting process occured within the inner pore of the wild-type (figure 4.8a-d).

Given that the difference in water events between the two channels is not due to any minor structural changes, retention of water in the wild-type channel could then be caused an energetic barrier that prevents hydration, and by extension, K^+ ion movement through the pore. By calculating the potential of mean force (PMF) to estimate the free energy profile for a K^+ ion to move through the inner pore of equilibrated MD structures, we were able to map the energetic barrier that needs to be overcome in order for an ion to move freely through the inner pore. From figure 4.8f, it can be seen that by introducing a polar group in the hydrophobic cuff such as L146N, the overall barrier is reduced by $\sim$4kT. Thus, hydrophilic substitutions at L146 appear to directly alter the permeation pathway.

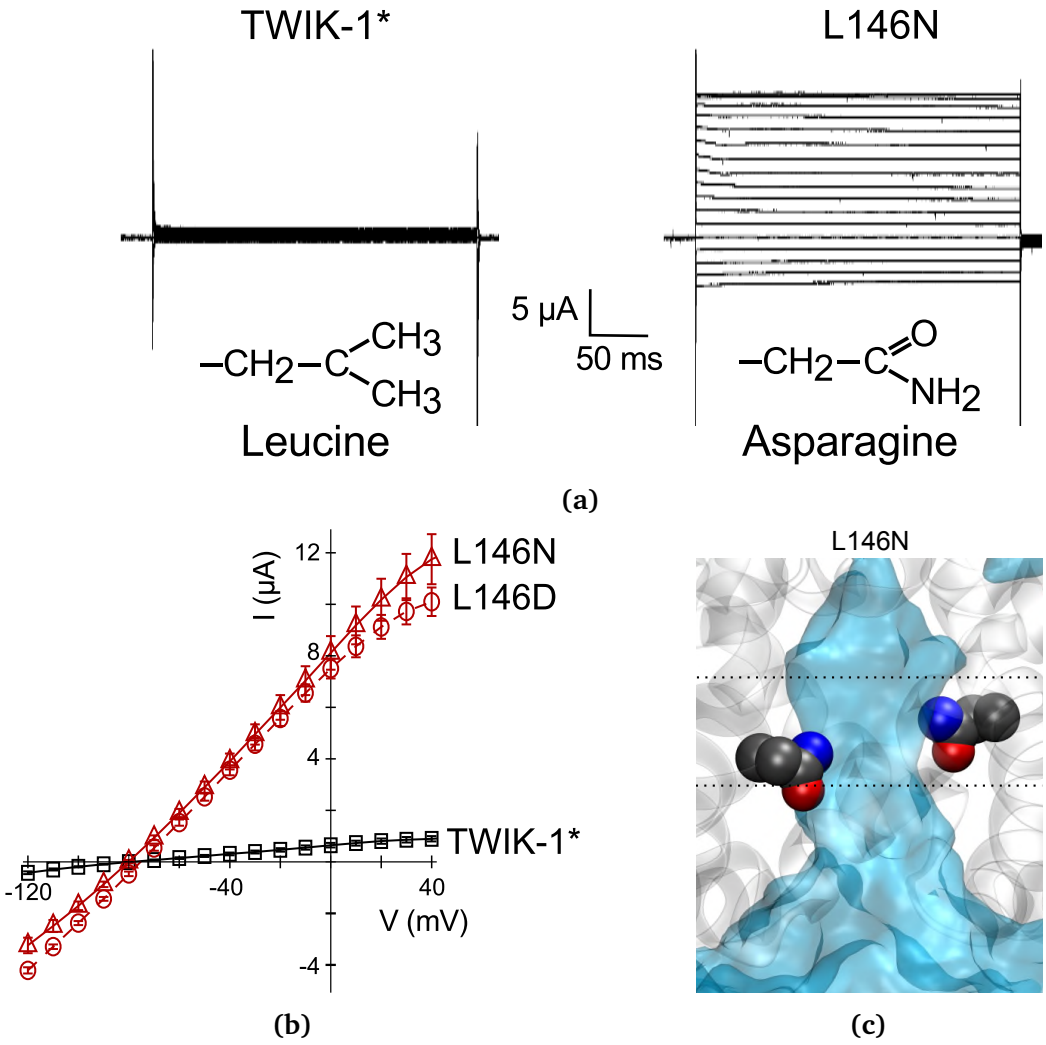

Figure 4.7: Introducing polarity is sufficient to improve permeation. a) Current trace of L146N when perfused under physiological ND96 (2mM KCl) buffer, at pH7.4. The large increase in current can be seen when compared to the trace of the wild-type TWIK-1 current. b) I-V plot of the L146N compared to L146D shows the similar level of current obtained from both mutations, thus suggesting that introducing polarity is sufficient to hydrate the deep inner pore of TWIK-1. c) MD simulation of the L146N supports that introducing polarity is sufficient to allow water molecules to enter the deep inner pore region. Figure (c) was prepared by Dr Prafulla Aryal.

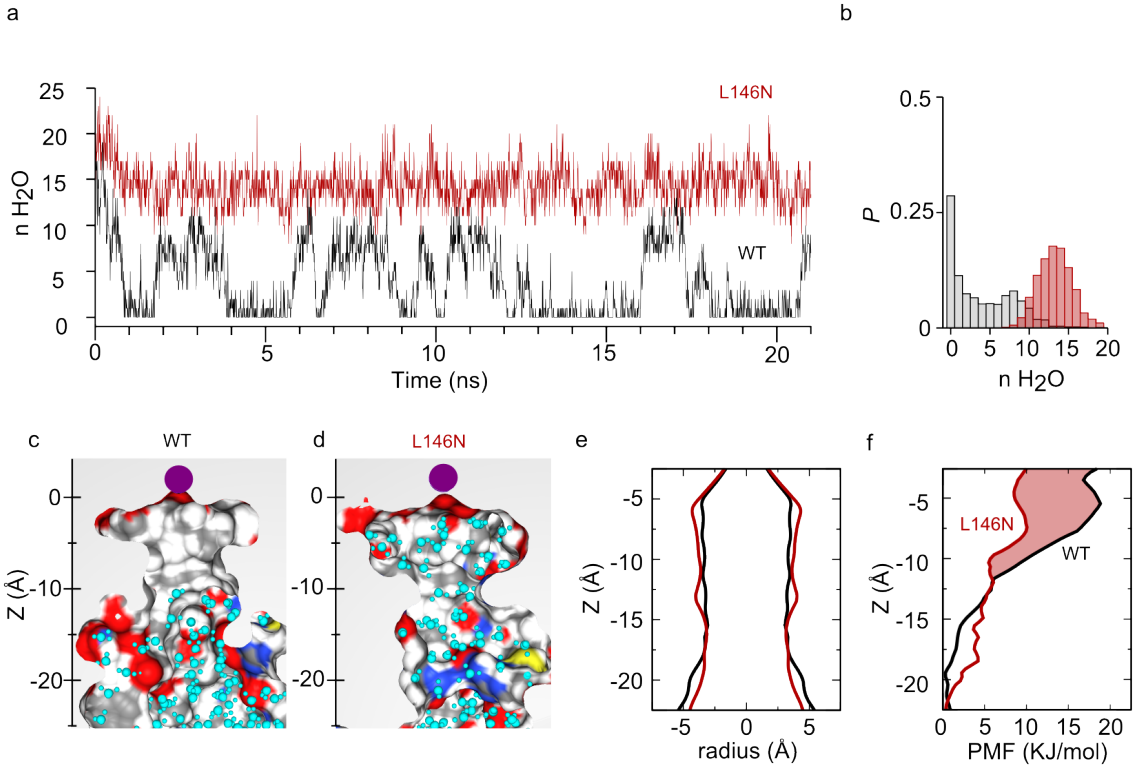

Figure 4.8: Positional restraint simulations and energetic profiles. a) Water count within the deep inner pore region of WT (black) and L146N (red) , sampled every 0.01ns, during a positional restraint simulation. A force constant of 10 KJ mol^{-1} $Å^{-2}$ was applied to the backbone carbons. The wetting and dewtting oscillations were obvious for the WT, whereas L146N is consistently hydrated. This difference is water presence can also seen from the normalised probability histogram for water occurrence shown in (b). c) and d) Cross-section of the inner pore of starting structures for WT and L146N. e) The potential of mean force (PMF) of the starting structures, showing that both WT (black) and L146N (red) structures share a comparable radius profile. f) PMF of K^+ ion along the inner pore axis of WT (black) and L146 (red), respectively. The shaded area represents the difference in free energy barrier between an ion moving along the two structures. Simulation and analysis done by Dr Prafulla Aryal

4.2.3.3 Mutants retain inhibition by quinine and external pH

One of the concerns that may arise is as to whether introducing these mutations at the deep inner pore would alter the channel in a way that could "break" it, and respond in an unpredictable manner.

However, when the TWIK-1 bolcker, 1mM Quinine was applied, the level of TWIK-1 (L146N) current was inhibited (figure 4.9). This concurs with previous studies, which showed that TWIK-1 is sensitive to quinine, a general potassium channel inhibitor (Ma et al., 2011; Lesage et al., 1996a).

Moreover, functional activity of the mutant (L146N) was also inhibited when the extracellular pH was lowered to pH6.0, shown here in figure 4.9. Previous studies have supported this observation on the wild-type TWIK-1 current, whereby it was suggested that TWIK-1 is indeed sensitive towards extracellular acidification. When extracellular pH is lowered beyond pH6.5, the channel becomes inhibited (Rajan et al., 2005; Chatelain et al., 2012; Chen et al., 2014).

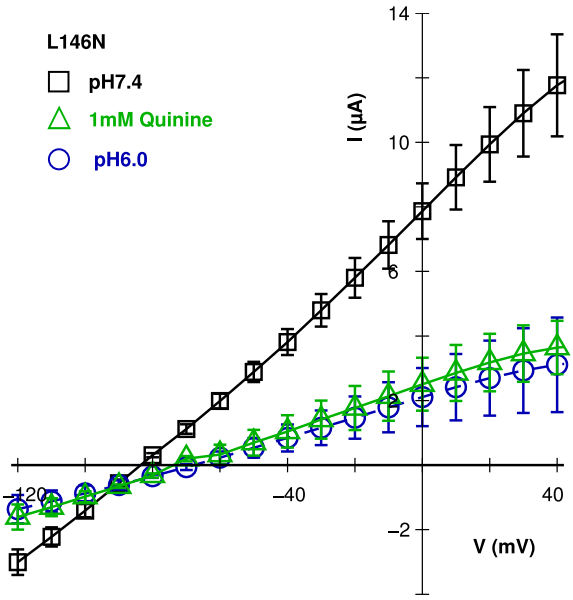

Figure 4.9: TWIK-1 L146N mutant channel retains normal functional activity. Inhibition by quinine and extracellular acidification of TWIK-1 L146N mutant suggests that the channel still retains its normal function.

These functional responses of the L146N mutant, which are relatively similar to the inhibition of wild-type TWIK-1 to quinine as well as extracellular acidification, therefore illustrates that the channel still retains a typical functional activity, despite the mutation.

4.2.3.4 L146I and L146V compared to L146T: Isosteric substitutions

In order to test the hypothesis further that a hydrophobic barrier may exist, it is necessary to see if we can retain the hydrophobicity of the greasy cuff by introducing other isosteric, hydrophobic amino acids. It is, therefore, plausible to replace the leucine with its other naturally occurring isomer, the isoleucine residue. This L146I mutation retains the hydrophobicity of the inner pore, and consequently, I found that the channel activity remains similar to that of the wild-type (figure 4.10c).

Similarly, mutating L146 into valine (L146V) also resulted in a low activity as the wild-type channel (figure 4.10a). Valine is one carbon-chain shorter than leucine, but they both share the similar branched methyl ends form. We can then compare the effect of having a hydrophobic residue at position 146, on channel activity, to having a polar side chain, without having to consider major differences on side chain size. This can be achieved by comparing the L146V mutant to a threonine substitution (L146T). Threonine differs from valine by having a hydroxyl group in place of one of the methyl ends.

Intriguingly, when L146T was tested, the increase in channel activty was high, comparable to the L146D and L146N mutants. This highlights the significance of the surface profile at position 146 to TWIK-1 channel activity. By having a hydrophilic surface at this position in the deep inner pore region, channel function can be significantly improved. Conversely, having a hydrophobicity at position 146 impedes traceable activity from TWIK-1.

These isosteric mutations, along with L146N and L146D, illustrates that inducing polarity around the hydrophobic cuff significantly helps in increasing TWIK-1 channel

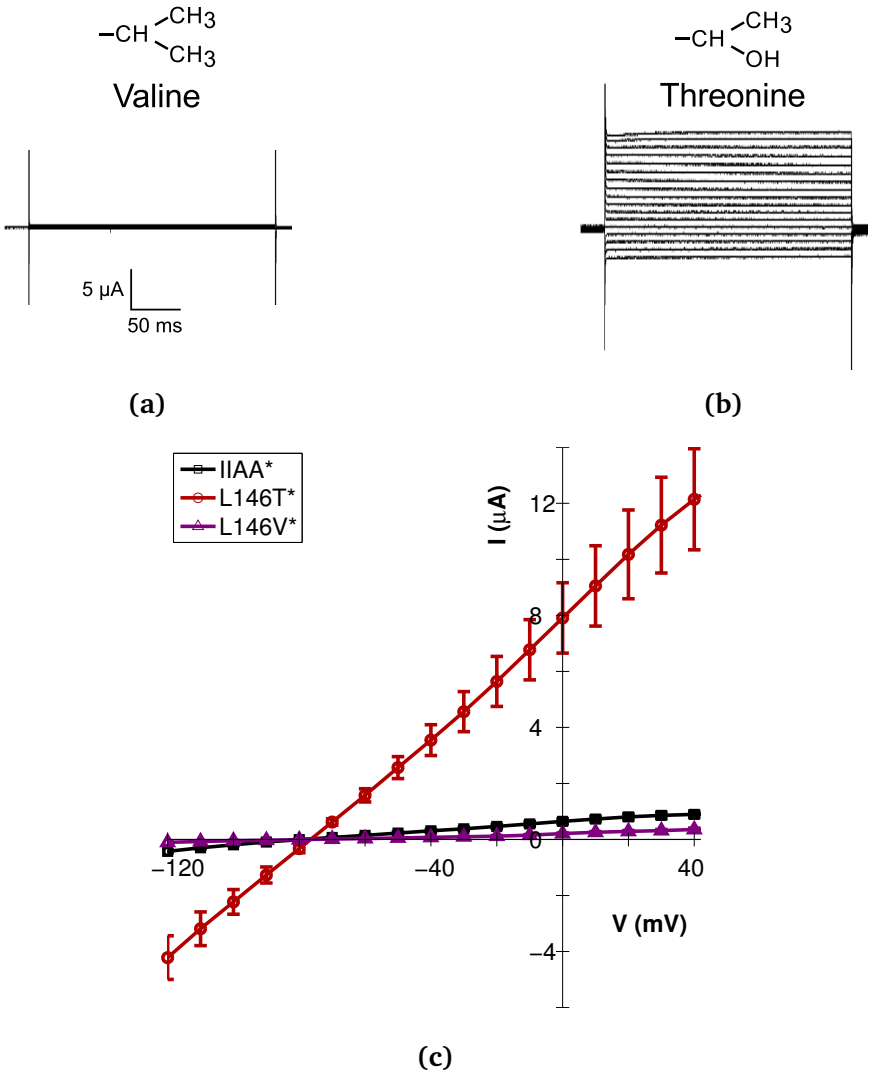

Figure 4.10: Isosteric and hydrophobic mutations retain low channel activity, but not hydrophilic mutation. a) L146V mutation shows low TWIK-1 current level under physiological condition in ND96 (2mM KCl, pH7.4) buffer, but not when mutated to b) L146T. c) I-V plot highlights the large increase in current with the L146T mutation, as compared to wild-type, as well as L146V and L146I.

activity. It also implies that a hydrophobic barrier may be at work in the deep inner pore region of TWIK-1, such that ionic permeation is being obstructed by means of impeding water passage into the inner pore.

4.2.3.5 Reducing side-chain volume: L146A, L146G, L146S mutations

As shown in figure 4.1c, apart from polarity, another parameter that could potentially influence pore hydration is diameter of its opening. A minimum opening for pore hydration to occur in hydrophobic pores is predicted to be ∼10Å in diameter. Even so, complete pore hydration is achieved only when the pore diameter opens beyond 12Å.

On this perspective, one possibility to increase pore diameter in the deep inner pore region of TWIK-1 is by substituting leucine to smaller sized amino acids. Given that the smallest naturally occurring amino acid available is glycine, we therefore substituted leucine to this residue (L146G). However, even with this mutation, the functional activity did not improve much.

Instead, substituting L146 with another smaller, yet hydrophilic, amino acid resulted in high levels of channel activity (figure 4.11). Serine mutation (L146S) introduces a hydroxyl group into the hydrophobic cuff, and thus increases current level of the TWIK-1 mutant. This greater effect with polarity can also be seen when compared to the alanine mutation of L146 (L146A). Therefore, increasing polarity in the hydrophobic cuff has a more significant effect towards ion permeation than increasing pore diameter. This observation appears to agree well with the prediction of pore hydration in relation to pore diameter and hydrophobicity strength.

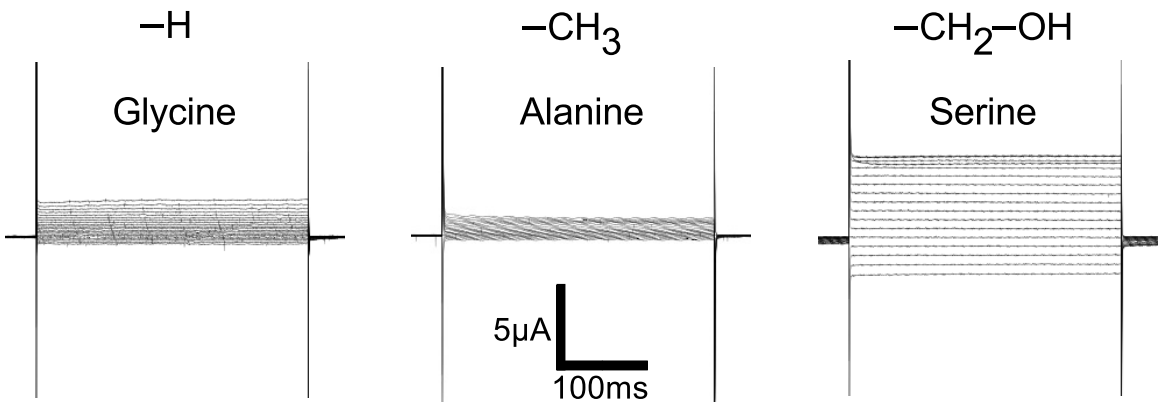

(a)

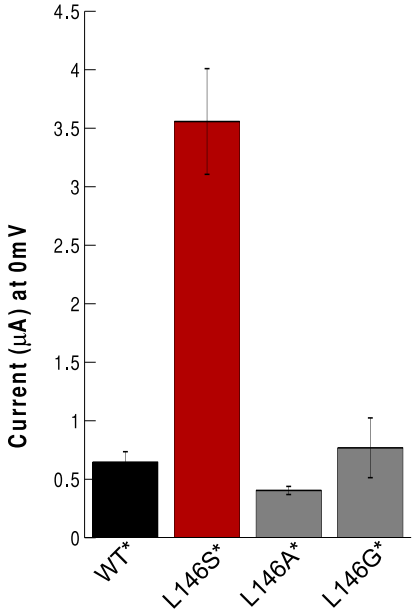

(b)

Figure 4.11: Changing inner pore diameter around the hydrophobic ring with smaller amino acids. a) Current traces of L146G, L146A, and L146S mutants under physiological buffer, ND96 (2mM KCl, pH7.4). Improved channel activity is yet most apparent when polar groups are included in the hydrophobic ring, as demonstrated by the L146S mutant, and compared to the L146A mutant, also illustrated in the bar plot in (b).

4.2.3.6 Other substitutions: L146M and L146K

Other substitutions that was also introduced were the L146M and L146K mutants. While it can now be predicted that methionine substitution (L146M) may retain the hydrophobicity of the pore, mutating L146 with a positively-charged residue such as lysine (L146K) is particularly interesting.

When these TWIK-1 mutants were injected into oocytes and their channel activity obtained, L146M expectedly resulted in a similarly low level of functional activity as that of the wild-type (figure 4.12). Intriguingly, L146K also has a relatively low activity, albeit slightly improved from the wild-type channel activity. While having a charged residue in place of leucine ought to induce polarity to the hydrophobic cuff, the positive charge from the lysine side chain may not be favourable for permeating K^+ions. This may instead introduce a different energetic barrier to ion permeation.

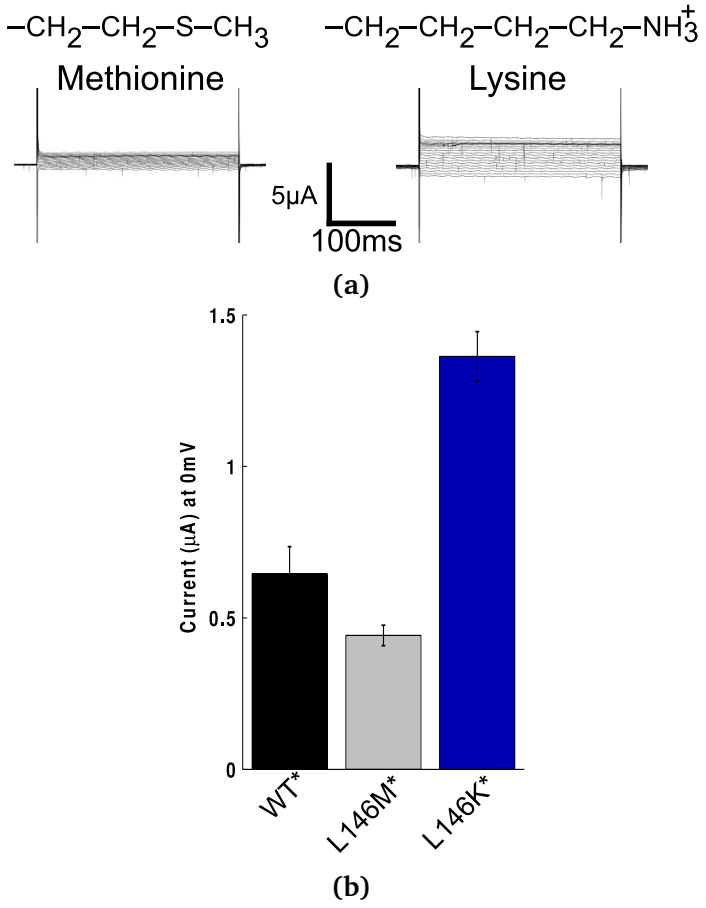

Figure 4.12: Other substitutions: L146M and L146K. a) Current traces of the L146M and L146K mutants. b) Average whole cell currents recorded at 0mV showing the low activity of TWIK-1 L146M and L146K mutants, although L146K is slightly higher than that of the wild-type.

4.2.3.7 Conclusion from L146 scanning mutagenesis

Based on the functional data collected from mutating L146, it becomes clear that introducing a hydrophilic substitution here results in an increase in channel activity (figure 4.13). The amplification of channel function by polar substitutions is consistent throughout, which demonstrates that introduction of a polar group in the hydrophobic cuff mitigates the energetic barrier inside the pore. This in turn improves pore hydration, and allows better permeation.

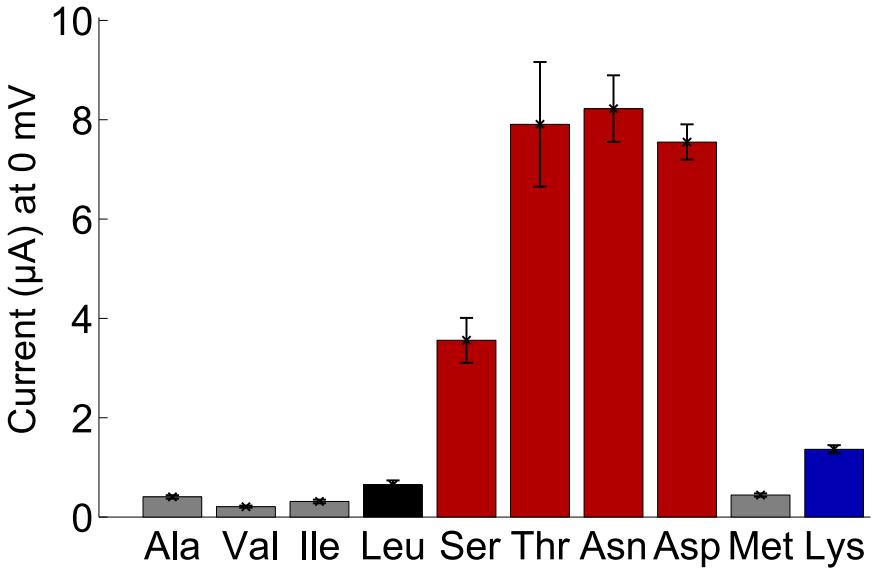

Figure 4.13: Scanning mutagenesis of L146 shows higher activity for hydrophilic mutants. Substituting L146 with polar amino acids increases channel activity, whereas hydrophobic substitutions leads to no significant effect on channel activity.

4.2.3.8 Surface membrane expression levels of TWIK-1 mutants

Another concern that arises from mutating residues at the hydrophobic cuff, or any mutagenesis in that matter, is whether these mutations would affect the expression level of ion channels at the plasma membrane. Particularly for TWIK-1, membrane surface expression has always been a contested issue, as described in Chapter 3.

TWIK-1 channels, wild-type and mutants, were therefore tagged with green-fluorescence proteins (GFP) and injected into oocytes. Under confocal microscopy, the GFP-tagged channels were observed, and their localisation compared to the red-dye tagged wheat germ agglutinin bound to the oocyte membrane surface. These were done for both wild-type TWIK-1 (WT and WT*), as well as the L146N and L146A mutants (in WT*). From our observations, the expression levels for all variants of the injected TWIK-1 channel are present and comparable to each other (figure 4.14).

This can also be seen in the bar graph shown in figure 4.15a. The overlap coefficients of the trafficking mutants (WT*, L146A* and L146N*) appeared similar, indicating that the expression level of the respective TWIK-1 mutants are comparable. When this is compared to the level of currents recorded from the individual mutants (figure 4.15b), it can be seen that only the hydrophilic mutant has a high channel activity compared to L146A* and WT*. This suggests that mutating L146 does not alter the expression level at the surface membrane, but rather affects the intrinsic activity of the channel itself.

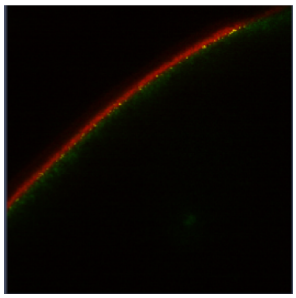

(a). Uninjected

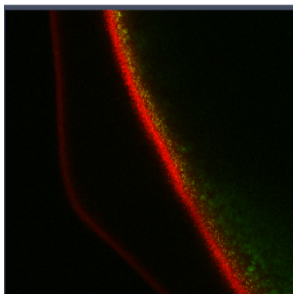

(b). WT

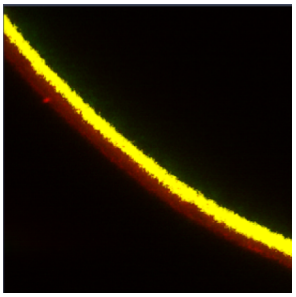

(c). WT*

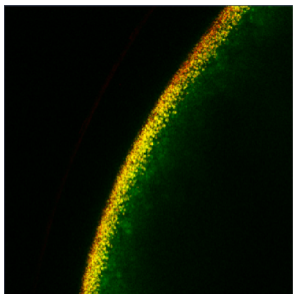

(d). L146A*

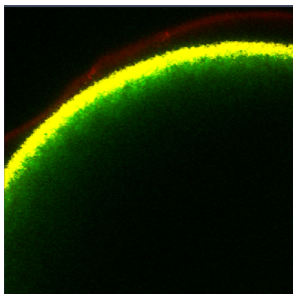

(e). L146N*

Figure 4.14: Qualitative confirmation of TWIK-1 mutants expression level. Different TWIK-1 channel variants were tagged with green fluorescence protein (GFP), injected into oocytes, and observed under confocal microscopy for localisation at the membrane surface. a) Uninjected oocytes, b) native wild-type TWIK-1 (WT), c) pseudo wild-type TWIK-1 (WT*) d) L146A* and e) L146N*. Yellow-coloured images confirms the presence of channel proteins on the membrane surface with no obvious increase in expression.

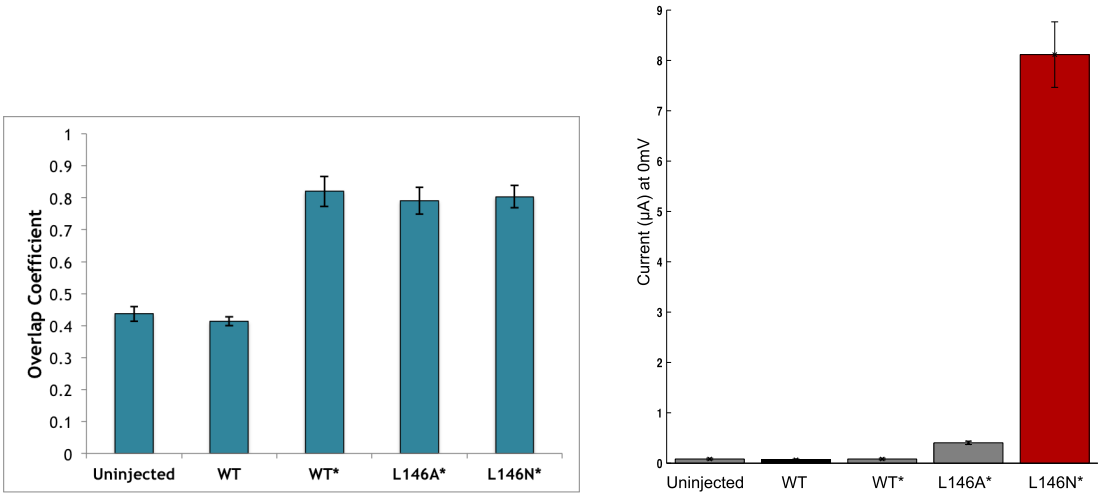

(a) **(b)**

Figure 4.15: Comparison of surface expression level of TWIK-1 mutants and their corresponding electrophysiological recordings. The plots compare and correlate the level of surface expression of the various TWIK-1 mutants with their respective level of current recorded. (a) Overlap Coefficients plotted from detection of the GFP-tagged TWIK-1 on the surface of Xenopus oocytes, as exemplified in figure 4.14. (b) The averaged-level of currents recorded for the TWIK-1 mutants. Sample n=3 for each batch. By comparing (a) and (b), especially for L146A* and L146N*, it can be seen that mutating L146 does not alter the level of surface expression of TWIK-1, but rather affecting its intrinsic activity.

4.2.3.9 Do mutations alter the permeation pathway?

Since the expression level of TWIK-1 does not appear to be altered by mutations at L146, the increase in whole-cell currents are thus thought to be due to a direct effect on the inner pore structure. To understand this effect, we employed giant excised patches of oocytes injected with wild-type TWIK-1 (WT*) or L146N mutant. The experiments that entails in this section are performed by Dr. Giovanna Bucci (Aryal et al., 2014a). This experiment utilises quaternary ammonium blockers, in this case tetrahexylammonium (THexA), as a tool to access the deep inner pore region of TWIK-1.

In giant excised patches, WT TWIK-1* currents are essentially negligible in symmetrical potassium solutions. Instead Rb^+ currents were used to test for channel activity, since Rb^+ ions contributed towards enhancing TWIK-1 currents. An increase in TWIK-1 channel activity by Rb^+ ions has been previously reported (Ma et al., 2012). Similarly, L146N currents are also enhanced in the presence of Rb^+ ions (figure 4.16a).

Interestingly, when the giant excised patches of L146N mutants were perfused with solution containing 50μM THexA, more than 90% of the channels were blocked. This was in marked contrast to the wild-type patches that appears insensitive to THexA blockade of the same concentration. Furthermore, 1μM THexA was sufficient to block L146N mutants by more than 70%. This high sensitivity of L146N towards THexA blockade suggests that L146N mutation directly alters the permeation pathway from within the deep inner pore cavity. Moreover, the higher voltage that is required to activate TWIK-1*, as compared to L146N in figure 4.16b, suggests that a greater driving force is required to overcome the hydrophobic barrier. This is consistent with the concept of electrowetting (Powell et al., 2011), and supports the notion that the hydrophobic ring is important for ion permeation.

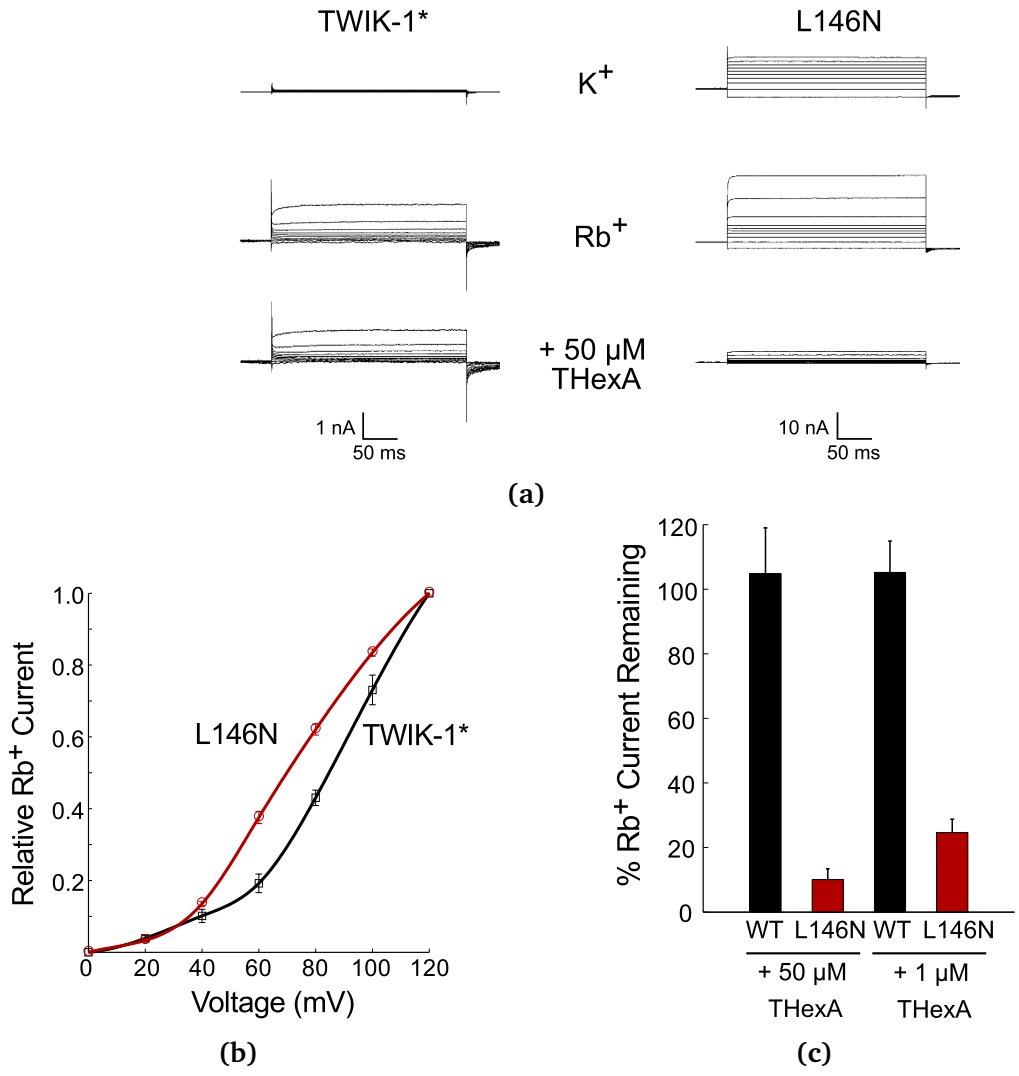

Figure 4.16: L146N mutation alters the permeation pathway directly. a) Example traces of current recorded from giant excised patches expressing TWIK-1*, or L146N, when perfused with either symmetrical K^+, or intracellular Rb^+ (Rb^+_{int}). Higher currents were detected from TWIK-1* when Rb^+_{int} is present. While TWIK-1* was insensitive to 50μM THexA, L146N mutant was already blocked by >90%. b) Voltage dependence of Rb^+ currents normalised to currents recorded at +120mV for TWIK-1* and L146N. c) Percent current remaining from TWIK-1* and L146N after block by 50μM and 1μM THexA, showing a high sensitivity to THexA in L146N mutant. These experiments described in these figures were done by Dr Giovanna Bucci. The figures were prepared by me.

4.2.4 M4 helix: Role of L261

The other leucine residue that lines the greasy cuff in the deep inner pore is L261, from the M4 helix domain. Similar to L146, the side chain of L261 also points straight into the inner pore cavity and towards the other L261 residue from the second subunit.

4.2.4.1 L261D/N mutations

The presence of a hydrophobic barrier relies on the surface profile at position 261 as much as it is dependent on L146. Due to this symmetrical role for both residues, validating the hydrophobic cuff from the M4 domain side utilises the same strategy as has been done to validate L146.

The MD simulations done on L261D and L261N mutant models showed a similar wetting of the deep inner pore region to L146D and L146N (figures 4.17a and 4.17b). This is somehow expected, since polarity is being introduced at the same region as before, albeit originating from another helix domain. In order to functionally test the activity of these mutants, I therefore introduced L261D and L261N substitutions in TWIK-1. Encouragingly, these mutants displayed a similar pattern of large increase in channel activity compared to the wild-type (figure 4.17c). This indeed supports our hypothesis that the leucine residues at this region are forming a hydrophobic ring, and having a hydrophilic residue in place of the leucine breaks the hydrophobic barrier.

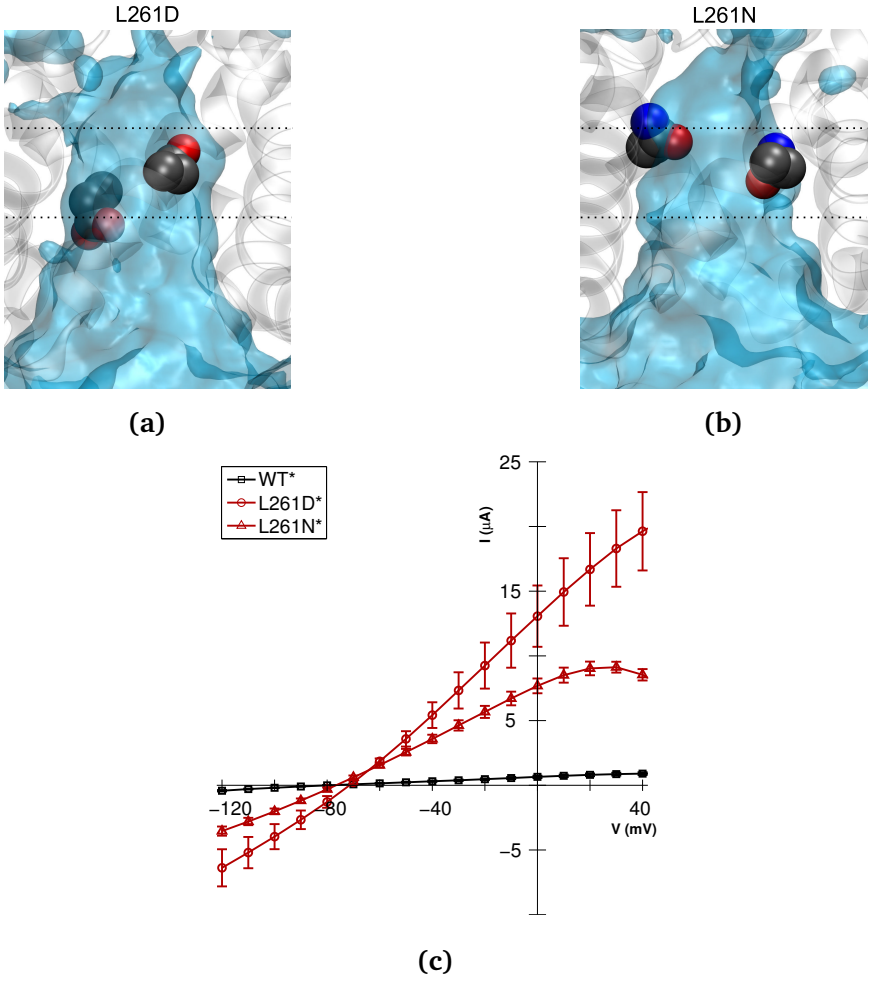

Figure 4.17: Polarity at position 261 also relaxes the hydrophobic barrier. When 100ns MD simulations were run on (a) L261D and (b) L261N mutant models, water also appears to hydrate the deep inner pore region of TWIK-1. c) Functional activity of the TWIK-1 channel were also increased when L261D and L261N mutations were done. Figures (a) and (b) were prepared by Dr. Prafulla Aryal Aryal et al. (2014a).

4.2.4.2 L261S/A and L261T/V mutations

I then sought to test whether isosteric substitutions, as well as reducing amino acid size, on L261 would replicate the observations from L146. Mutating L261 to isoleucine and valine (L261I and L261V) retains the low level of channel activity in TWIK-1, thus supporting that hydrophobicity in this region can be maintained in this channel with these isosteric amino acids. Substituting it with threonine (L261T), however, causes an increase in TWIK-1 function, although the level of activity observed here is lesser than L261D or L261N (figure 4.18a).

Substituting L261 with smaller amino acids (L261G, L261A, L261S) also resulted in a similar observation as mutating L146G, L146A and L146S, respectively. Only when mutated into serine (L261S) that the channel activity was significantly increased (figure 4.18b). Once again, this suggests that the increasing the pore diameter at the deep inner pore region may not be as effective as having a hydrophilic residue in overcoming the energetic barrier for pore hydration.

In summary, functional activity that is seen in mutating L261, and illustrated in figure 4.18c, reitrates our previous observation, that the presence of a polar group at the hydrophobic cuff contributes significantly towards hydrating the deep inner pore cavity, thus encouraging ion permeation.

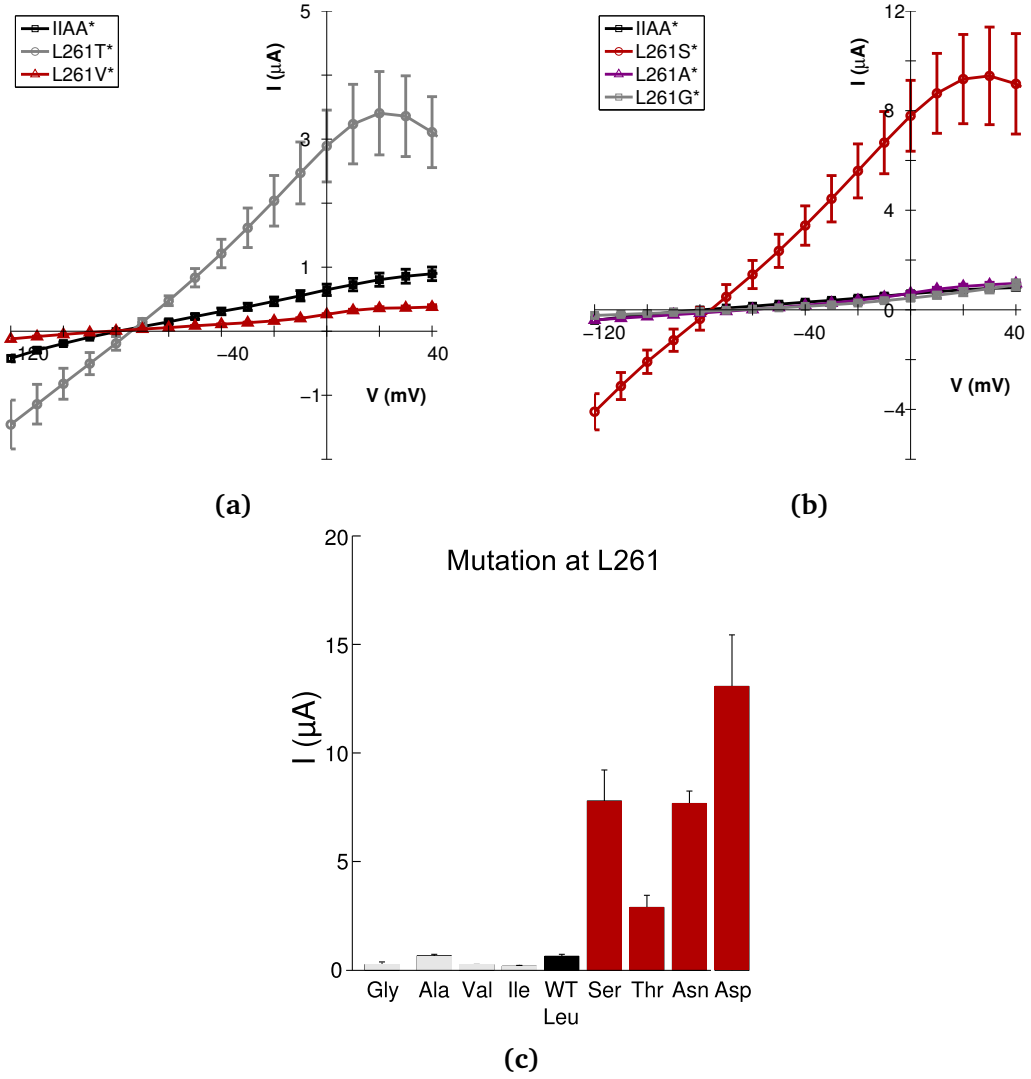

Figure 4.18: Hydrophilic substitutions overcome the hydrophobic barrier for permeation to occur. I-V plots in (a) and (b) supports that hydrophilic substitutions at position 261 lowers the energetic barrier at the deep inner pore region for permeation to occur. c) Bar chart summarises the overall effect observed from various mutations at position 261, comparing the effects of hydrophilic vs hydrophobic substitutions, as well as altering pore size.

4.2.5 Pairwise mutations of L146 and L261

As described earlier (figure 4.1c), pore hydration can also be dependent on the radius of the pore, which could potentially allow for better solvent accessibility. Thus far, however, the effect of increasing pore radius, by substituting L146 and L261 with smaller amino acids, have been barely minimum. Moreover, it has also been mentioned before that for complete pore hydration, the opening needs to be more than 12Å in diameter.

I therefore introduced a pairwise mutation on L146 and L261. When both positions were substituted with aspartate or asparagine, a substantial increase of channel activity was observed, with each pairwise mutation giving 15μA and 12μA of current, respectively, at 0mV (figure 4.19a). The mutant channel remained sensitive to extracellular acidification and quinine block, indicating that its regulation was unchanged, as compared to the wild-type channel (figure 4.19c).

L146 and L261 were then jointly mutated to smaller amino acids, glycine, alanine or serine, to test for effects of increasing pore diameter further. Interestingly, substituting both leucines with alanine (L146A/L261A) or glycine (L146G/L261G) resulted in a slight increase in channel activity, although still in lower than other polar substitutions (figure 4.19b). It can be argued that such pairwise mutations with these small amino acids should have broadened the pore opening at this constriction beyond the limit for hydrophobic gating (figure 4.1c). However, its effect on ion permeation is unlikely to be as profound as having a polar group in the pore. This can be deduced by comparing these two hydrophobic mutants to that of serine mutation (L146S/L261S). The level of functional activity with this substitution was comparable to the other hydrophilic substitutions (figure 4.19a).

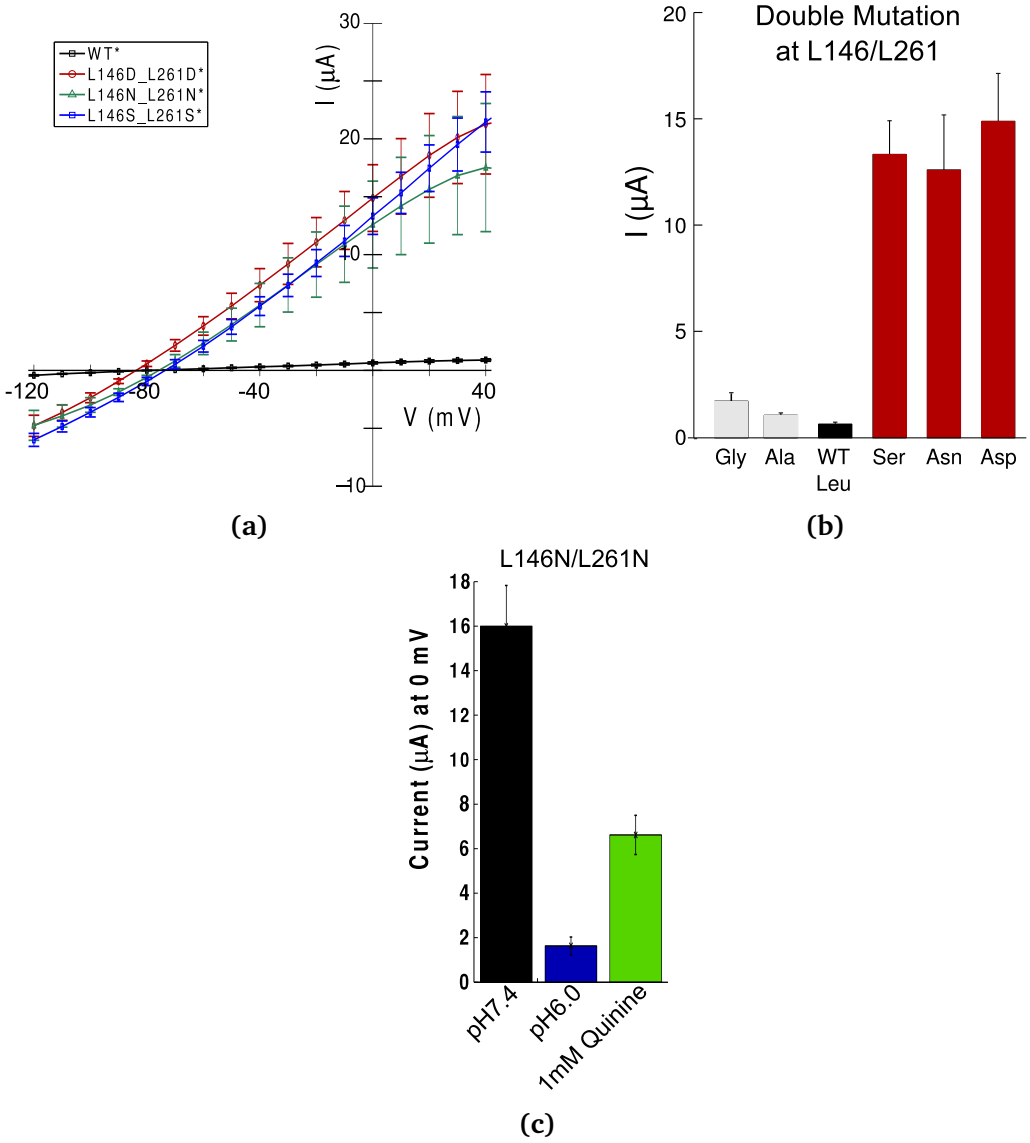

Figure 4.19: Pairwise mutations at the hydrophobic cuff. a) I-V plot of the polar group pairwise mutations; Aspartate(D), Asparagine(N) and Serine(S) on TWIK-1 shows markedly high level of channel activity. On the contrary, slight increase in current was observed when L146/L261 were substituted with glycine or alanine, as shown in (b). c) The TWIK-1 pairwise-mutant channel (L146N/L261N) is still sensitive to acidification and quinine block.

4.2.6 Other residues in the hydrophobic cuff: L264

Another residue that caught our attention from the TWIK-1 crystal structure is also a leucine in position 264 (L264). Although the side chain of this residue does not completely point into the pore cavity as L146 and L261, one of its branched δ-methyl group is exposed to the inner pore. Furthermore, L264 is tucked in between L261, from the same M4 helix, and L146 of the other subunit (figure 4.20). It is therefore located at the intersection between M2 and M4 of the adjacent subunit, and near the fenestration area. In the MD simulation, movement of the M2 domain closes the fenestration, which also brings L264 closer to L146 of the adjacent subunit. This may help stabilise the hydrophobic barrier in the deep inner pore region. I therefore examined whether mutating L264 with polar amino acids would lead to the same observation as mutating L146 and L261.

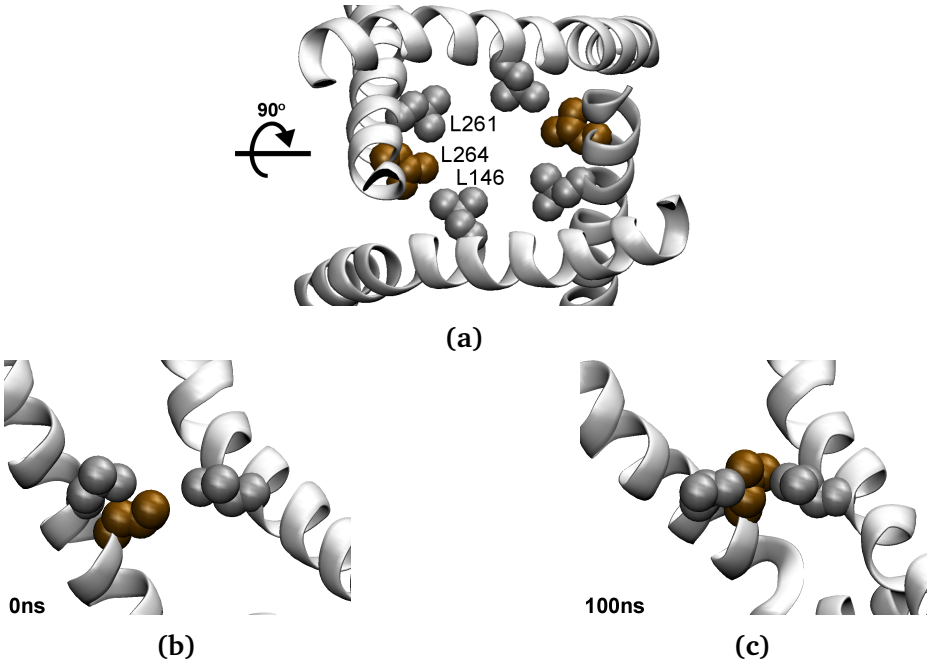

Figure 4.20: Location of L264 in the structure may partially contribute to the hydrophobic barrier a) L264 is located between the L261 (M4) and L146 (M2) of the adjacent subunit. The structure is viewed from the bottom of TWIK-1. b) AND c) Movement of the M2 helix during the simulation brings L264 closer to L146, which may lead to the stabilisation of the hydrophobic cuff.

When L264 was mutated into aspartate and asparagine (L264D and L264N), the increase in channel activity was found to be large. This was also in marked contrast to the level of current observed when L264 was substituted with isoleucine (L264I). Low level of functional activity, comparable to that of wild-type, was seen with the L264I mutant (figure 4.21b). MD simulation of the L264D mutant model also supports the notion that having a hydrophilic group in this region renders the pore cavity favourable to water, and by extent,ion permeation (figure 4.21a).

However, mutating L264 into valine led to a significantly higher channel activity than wild-type. Its magnitude is also larger than valine substitutions of the other leucine residues (L146V and L261V), although when compared to the threonine mutation (L264T), L264V is still considerably lower (figure 4.21c).

Similarly, a slight increase was also observed when L264 was mutated to alanine (L264A), although not as high as the serine substitution (L264S) (figure 4.21c). This suggests that mutating this residue may also induce other structural changes in TWIK-1, that may be translated into other conformational changes. Given the position of L264 that faces the intersection between M2 and M4, it is more possible that gating of the channel itself could be affected, rather than just an effect on the hydrophobic inner pore itself.

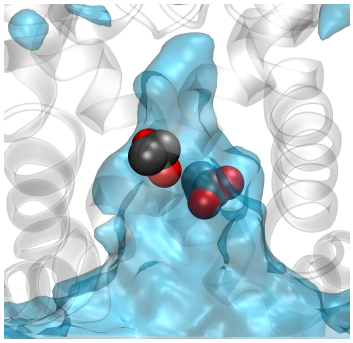

(a). L264D

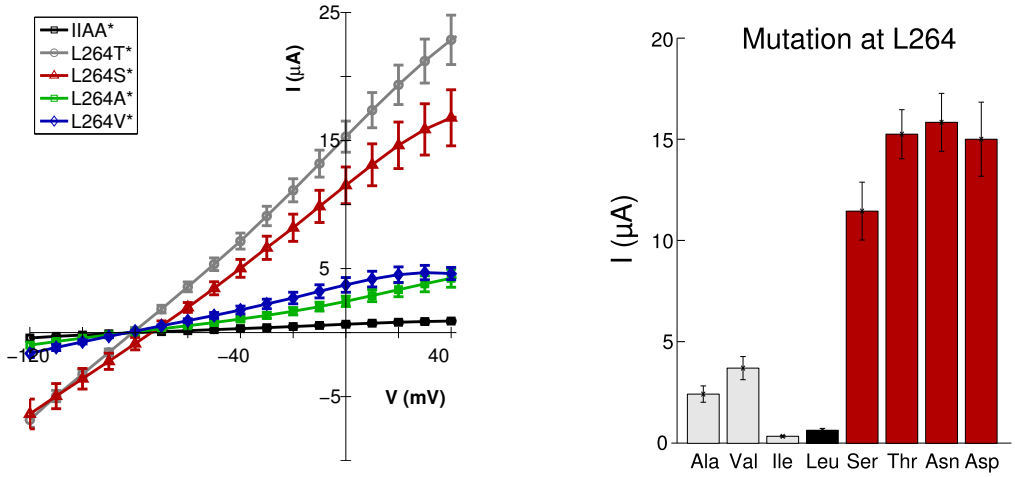

(b) **(c)**

Figure 4.21: Mutations at L264 suggests a partial influence towards creating the hydrophobic barrier. a) MD simulation of L264D mutant model supports the notion that polar substitution at this position may still disrupt the hydrophobic barrier. b) I-V plot shows the high channel activity of the polar/charged L264 mutants, compared to their isosteric partners. Of particular interest, however is the high increase in channel activity for L264V and L264A mutants, which can also be seen from the summary plot in (c). Figure (a) was prepared by Dr. Prafulla Aryal.

4.2.7 Influence of lipids on the hydrophobic barrier

As an addendum to this study, we also examined the potential effect of lipids on the hydrophobic barrier. It is important to remember that membrane proteins cannot be considered independent of their lipid environment. One of the key features of TWIK-1, that is also present in other K2Ps, is the fenestrations on both sides of the channel. Since this fenestration sites provide direct access to the bilayer, it is possible that lipids may enter these fenestrations and influence channel pore. This is particularly relevant as it has been proposed that entry of lipids into fenestration sites may gate mechanosensitive K2P channels (Brohawn et al., 2014). Although TWIK-1 is not mechanosensitive, this may shed some light on the role of lipids in regulating other mechanosensitive channels. Another possible effect of lipid entry, with respect to the TWIK-1 channel, is that lipids might also influence the hydrophobic barrier by inducing greater hydrophobicity via the fenestration. This has been shown by simulating lipid movements around the TWIK-1 channel (Aryal et al., 2014b).

In brief, analysis of MD simulations done by Dr Prafulla Aryal shows that lipid tails could enter the fenestration and thereby penetrate into the cavity to form part of the pore lining near the hydrophobic barrier region. Consequently, dewetting occurs more frequently when the lipid tails are present in the cavity, illustrated by the heatmap in figure 4.22c.

When the L146N mutant model was simulated in the presence of lipids, the cavity remained hydrated throughout, consistent with our previously shown results (figure 4.7c). It was also shown that the presence of lipids in the pore is lesser than that of the wild-type model (figure 4.22f). Pore occupancy of lipid carbon atoms was found to decrease from 55% in the wild-type to 35% in the L146N mutant model. From this observation, it can be deduced that lipid presence could influence the hydrophobic barrier in TWIK-1, but it may not sterically occlude the pore. Moreover, while dewetting might occur more frequently in the presence of lipids, the pore could still be dewetted in

the absence of lipid tails. Therefore, the constriction caused by the hydrophobic barrier is still an intrinsic nature of the TWIK-1 channel.

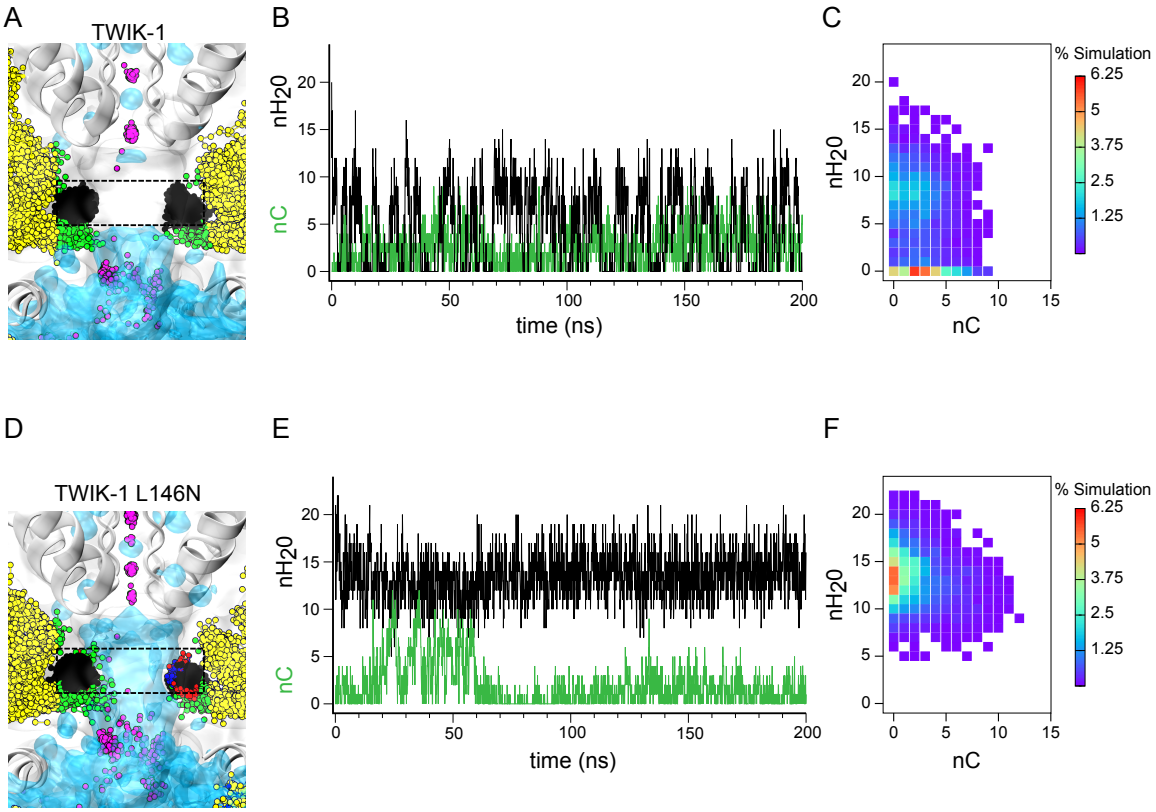

Figure 4.22: Influence of lipid tails in the ion conduction pathway of TWIK-1. Average water density, taken every 1ns, from a 200ns simulation from TWIK-1 (a) wild-type and (d) L146N mutant. L146 and L264 sidechains are shown as ball and sticks. Green: Lipid carbon atoms lining and inside the pore; yellow: carbon atoms outside the pore lining; black: L146 and L264 sidechain carbons. (b) and (e) Number of water molecules (black plot) from every 0.1ns of the MD simulation for wild-type and L146N, respectively. Count is taken from within the black-dashed box region in (a) or (d). Also shown is the count of lipidic carbon atoms (green plot) taken from inside the green box region in (a) or (d). The correlation heatmap is generated from atom count traces for (c)wild-type and (f)L146N mutant, respectively. The difference in heatmap contour between the (c) and (f) illustrates that lipid occupancy in wild-type is higher than in L146N Aryal et al. (2014b).

4.3 Discussion

The results obtained in this study presents us with significant evidence to suggest that a hydrophobic cuff exists deep within the inner pore of TWIK-1. The nature of this cuff prevents the pore from being fully hydrated, and consequently, preventing ion permeation. This constriction possibly generates an energetic barrier that 'gates' the permeation pathway without the need of a physical gate. This is illustrated by the difference in free energy between an ion passing through the inner pore of the WT channel and L146N.

4.3.1 L146 and L261 create the hydrophobic cuff

Two key residues that have been identified from this study are L146 and L261, both contributed by each channel subunit. When both residues were substituted with polar amino acids, channel activity increase significantly. However, changing one or the other into smaller, hydrophobic amino acids, little to no change in channel activity was observed. It could be that the minimum pore diameter required for full pore hydration is not achieved by merely mutating the residues. On the contrary, pore hydration is easier to obtain when the profile of the pore is shifted from being hydrophobic to hydrophilic.

4.3.2 Regulation and expression level unaffected by mutation

TWIK-1 channel has been previously shown to be sensitive to block by quinine (Ma et al., 2011; Lesage et al., 1996a). Here, we have also showed that TWIK-1 L146N and L261N mutants are also blocked by quinine. In addition, these mutants are inhibited by extracellular acidification at the same pH that inhibits wild-type TWIK-1. This implies that mutating L146 and L261 does not affect channel regulation.

Similarly, channel expression of TWIK-1 in oocytes are not affected by these mutations. The level of expression for L146N mutants in oocytes are comparable to that of the

wild-type. Therefore, it is unlikely that the increase of TWIK-1 channel activity is due to changes in expression.

4.3.3 Mutating L146 and L261 alters permeation directly

Instead, it was shown that mutating L146N alters permeation directly. By utilising Rb^+ ions as a channel activity reporter, wild-type TWIK-1 currents can be compared to L146N.

Changes in THexA affinity of the pore suggested a direct effect of the mutations on the conduction pathway, thus indicating that the mutations alter the permeation pathway directly.

This is also supported by another observation, whereby the wild-type TWIK-1 is only activated at higher voltages than that for L146N. This is consistent with the greater energy threshold that needs to be overcome in order to activate hydrophobic pores compared to the hydrophilic ones, an electric-inducing concept known as 'electrowetting' (Powell et al., 2011).

Hence, it is most likely that polar substitutions at the hydrophobic cuff improves TWIK-1 channel activity by directly disrupting the energetic barrier to allow water and ions to permeate.

4.3.4 Lateral fenestration sites and the L264

Lateral openings, or fenestration sites, are located on the part of the channel protein that is embedded inside the membrane bilayer. Lipid-like density was observed at these sites in the TWIK-1 crystal structure. Therefore lipid tails were able to penetrate through the fenestration and influence the hydrophobicity at the cuff.

L264 is located near the fenestration site. It lies between L146 of one subunit and L261 of the other. The aliphatic side chain of L264, therefore, partially contributes to the hydrophobic cuff. Hydrophilic mutations at L264 significantly increases channel

activity. While these substitutions could influence the hydrophobic cuff directly, it may also sterically affect the fenestration site by preventing lipid tails from penetrating.

4.4 Conclusion

In this study, a hydrophobic cuff has been identified in the deep inner pore region of TWIK-1. Water density within the volume of the cuff oscillates rapidly between wetting and dewetting states. Thus, the hydrophobic cuff creates an energetic barrier to pore hydration. By extension, this also prevents ions from permeating through the cuff. Hydrophilic substitutions at this cuff alleviates this energetic barrier, leading to an increase in channel activity. The presence of lipid tails at the fenestration sites could also influence the hydrophobicity of the cuff.

CHAPTER 5

Scanning mutagenesis of the C-Helix

5.1 Introduction

In chapter 3, the effect of mutations at the putative SUMOylation site, K274, on TWIK-1 expression were addressed, and it was suggested from our observations that SUMOylation may not be occurring at this position. In this chapter our study on TWIK-1 is extended to characterise the role of the entire C-helix on channel activity.

The crystal structure of TWIK-1 presents us with a unique and interesting arrangement of the C-helix, the domain where K274 is located. The surface structure of TWIK-1 at the inner membrane side forms an almost symmetrical square shape (figure 5.1b). This formation is unlike other K2P crystal structures reported so far. In TREK-1, TREK-2 and TRAAK structures, the cytoplasmic membrane surface of the channel is described as a rhomboid shape (Renigunta et al., 2015), which can be attributed to the arrangement of the distal M2 and M4 parts of the channel that splay away from the pore.

By contrast, the lower section of M4 in TWIK-1 kinks by approximately 80°, forming a separate domain known as the C-helix. This kink results in the C-helix positioning parallel to the inner membrane leaflet and around circumference of the channel pore mouth.

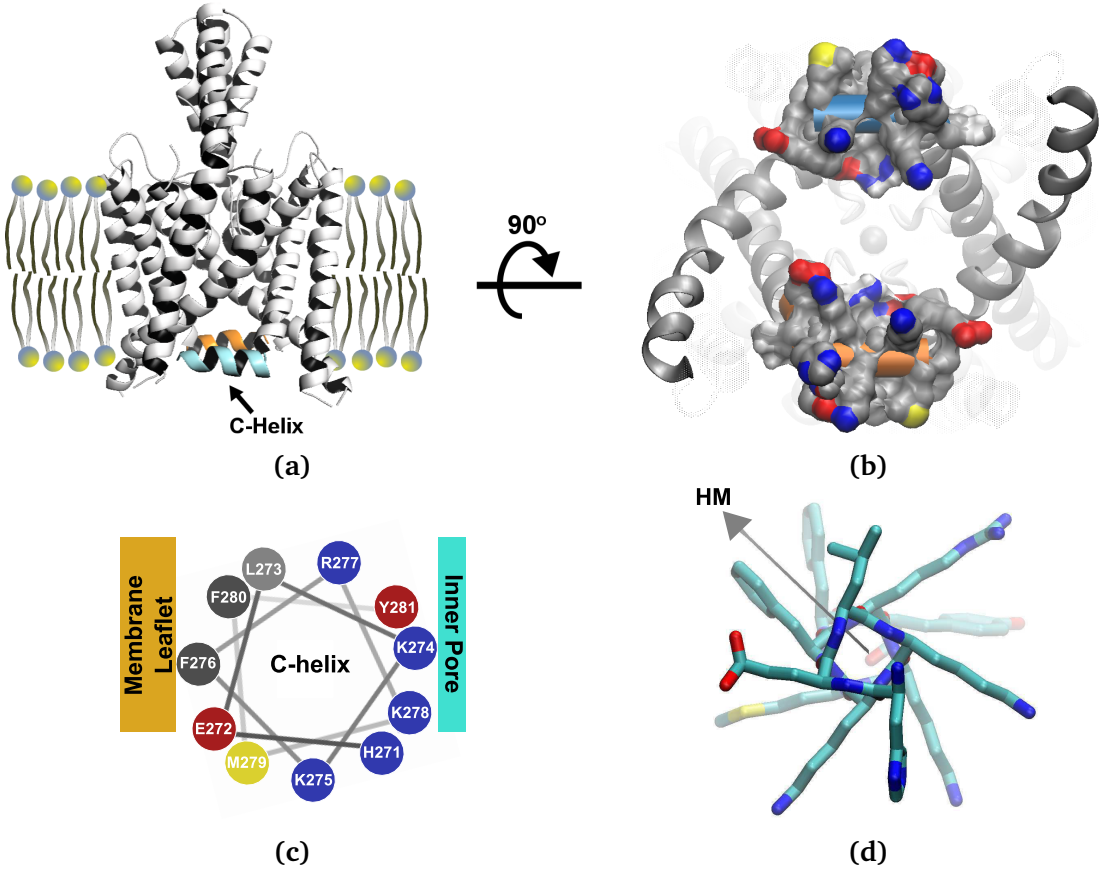

Figure 5.1: Surface electrostatics at the inner pore mouth. a) Side view of the TWIK-1 structure, highlighting the C-helix of each subunit (blue and orange). b) View of the TWIK-1 cytosolic region, going through the inner pore and up to the selectivity filter. The C-helix is shown in surface-rendered view, and its side chains are coloured by elements; red:oxygen, blue:nitrogen, yellow:sulphur. c) The helical wheel diagram illustrates the amphipathic arrangement of the C-helix, with the polar face residing at the inner membrane pore of TWIK-1 and the non-polar side facing the membrane lipidic environment. d) The C-Helix is calculated to have a Hydrophobic Moment (HM) vector of 10.67Å.kT/e in magnitude, and points in the direction of the hydrophobic residues. The HM is shown here as the grey arrow. The C-helix is viewed from the N-terminus side (starting from H271 on the nearest side) (Reisser et al., 2014).

This arrangement has been related to a similar α-helix structure reported in a eukaryotic voltage-gated potassium channel, Kv1.2 (Miller and Long, 2012). The S4-S5 linker-helix in Kv1.2, which also lies in parallel to the membrane surface, is thought to mechanically couple the movement of the voltage sensing domain to the movement of the inner helix (Long et al., 2005).

Another feature that the TWIK-1 C-helix shares with the linker-helix of Kv1.2 is the amphipathic nature of these domains that allows the C-helix to assume its position at the membrane-cytosol interface.

The presence of amphipathic helices at the cytoplasmic membrane region are quite common among potassium channels, and the various roles they play have been described. In inwardly-rectifying K^+ channels, both mammalian and bacterial, an amphipathic "slide helix" runs parallel to the membrane-cytosol interface (Kuo et al., 2003). This helix is involved in propagating movement between the cytoplasmic domain (CTD) and the transmembrane-pore domain(TMD), and forms a complex network for channel gating (Bavro et al., 2012; Bollepalli et al., 2014; Fowler et al., 2014). In hERG channels, an amphipathic helix in the N-terminus is also thought to be involved in regulating slow deactivation (Tan et al., 2012). These, and various other studies highlight the important functional role these amphipathic helices play in channel gating and regulation.

In the TWIK-1 structure, the C-helix is amphipathic, with the hydrophobic residues pointing up towards the membrane, whereas some, but not all, hydrophilic residues point downwards away from the channel. Interestingly, a few charged residues in the polar surface of the C-helix point towards the inner mouth of the pore. These may interact with the ions as they pass through the conduction pathway. The electrostatic distribution of charges within the pore might, therefore, play a role in regulating local potassium ion concentration near the pore entrance (Cai and Jordan, 1990), and overall conduction.

In this chapter, I have investigated the role of the residues within the entire C-helix

and studied their effects on the ability of TWIK-1 to form functional channels.

5.2 Results

5.2.1 Declaration of Authorship

In addition to the declared role mentioned in the "Declaration of Authorship" section in the beginning of this thesis, I hereby declare that all works in this chapter are done by me. The analysis in figure 5.5a and b was based on the MD simulations done Dr. Prafulla Aryal, which has been described in Chapter 4.

5.2.2 Functional effects of residues on the polar surface of the C-helix

Scanning mutagenesis was performed throughout the entire length of the C-helix domain (H271-M279). Amino acid substitutions were based on either removing or switching the native charge on the residues, or by changing the size and/or polarity of the amino acids.

Basal currents under physiological conditions were recorded from oocytes expressing TWIK-1 channels mutated at the C-helix domain. From these recordings, most of the mutants appeared to result in current levels either similar to or less than that of the wild-type TWIK-1 current.

However, mutations of three of these residues produced an increase in current amplitude compared to the wild-type (WT*) current. These residues were K274, R277, and K278. From the crystal structure, these positively-charged residues appear to be on one side of the C-helix and face the inner pore cavity.

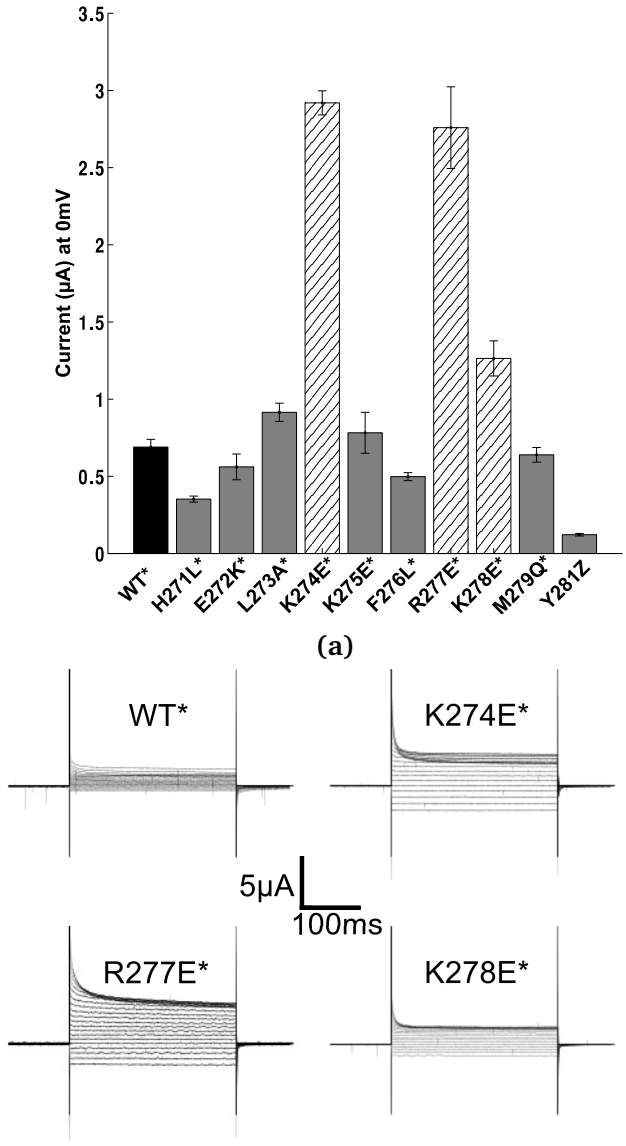

Figure 5.2: Scanning Mutagenesis of the C-Helix. a) Bar chart showing the effect of mutating different residues in the C-helix domain on the functional activity of TWIK-1. The whole cell currents were recorded at 0 mV under physiological conditions (ND96 buffer, pH7.4). Current amplitudes that are significantly higher than that of the wild-type TWIK-1 are hatched ($p<0.05$). Significance testing were done by ANOVA,($F(13,164)=47.753$). b) Representative current trace for TWIK-1 channel mutants that yield significantly higher current output than wild-type TWIK-1.

5.2.2.1 Mutations of K274

Consistent with the results described in Chapter 3, K274 appears to be one of the three residues that, when substituted with glutamate, significantly increased the level of whole cell current under physiological conditions. The mean current level at 0 mV was I_{0mV}=2.92 μA ± 0.08 μA, which is a four-fold increase from the wild-type current.

The other substitutions previously studied at K274 (K274A/Q/R) were also repeated here, by including these mutations in the wild-type TWIK-1*, as compared to the mutations of K274 shown in chapter 3, which were previously studied in wild-type TWIK-1 without the trafficking mutation. Interestingly, basal current was also significantly improved in the K274A TWIK-1 mutant. The averaged current level was almost as high as that of the K274E substitution, resulting also in a four-fold increase.

K274Q also showed some increase in current level compared to its wild-type (WT*), though, at I_{0mV}=1.74 μA ± 0.19 μA, the amplitude was lower than K274E and K274A. On the other hand, substituting K274 with arginine has no significant effect on TWIK-1 basal current levels. This reaffirms the previous conclusion that mutation of K274 is more likely to affect the biophysical properties of the channel than to be SUMOylated.

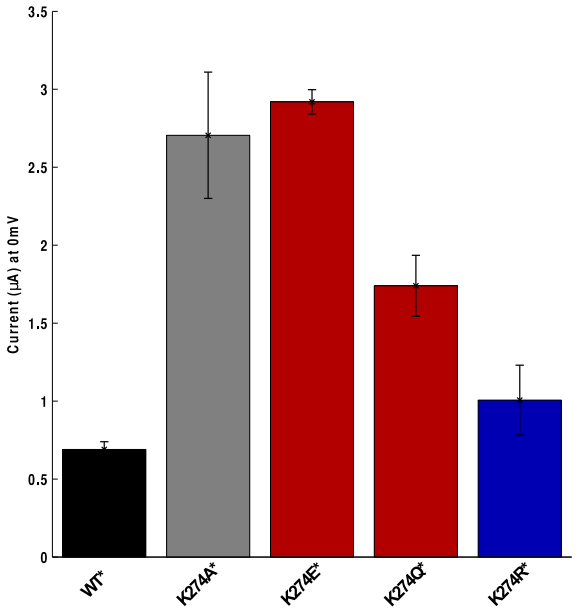

Figure 5.3: Substitutions at K274 resulted in an increase in current. When lysine is mutated to alanine or glutamate, approximately threefold increase in current were observed (Tukey's test, $p<0.01$). An increase in current was also observed in K274Q mutant, but no significant increase in current was seen when lysine was mutated to arginine.

5.2.2.2 Mutating R277 results in an increase of functional activity

The other residue that resides on the polar surface of the C-helix, and showed an increase in current amplitude when mutated, was R277. When mutated into glutamate (R277E), the mean whole cell current recorded at 0 mV was I_{0mV}=2.76 μA ± 0.26 μA. This magnitude was comparable to that of the K274E mutant described earlier (figure 5.2). In the crystal structure, R277 is located next to K274 on the C-helix, and its side chain also points into the pore cavity (figure 5.4c). This suggests that the presence of a negative-charge around the vicinity of the pore entrance may affect permeation, perhaps by affecting the local concentration of potassium ions. Consistent with this, substituting this arginine with alanine (R277A) also generated an increase in whole cell current, though to a lesser extent. However, this increase in macroscopic current with the R277A mutant may be due to a reduction in the positively-charged surface near the pore mouth, which would otherwise reduce cation entry into the pore.

Intriguingly, however, when R277K mutation was performed and tested functionally, the whole cell current was also enhanced by nearly threefold compared to the wild-type current. This suggests that by merely shortening the positively-charged side chain, permeation can be enhanced similarly to the effect of the R277A mutation.

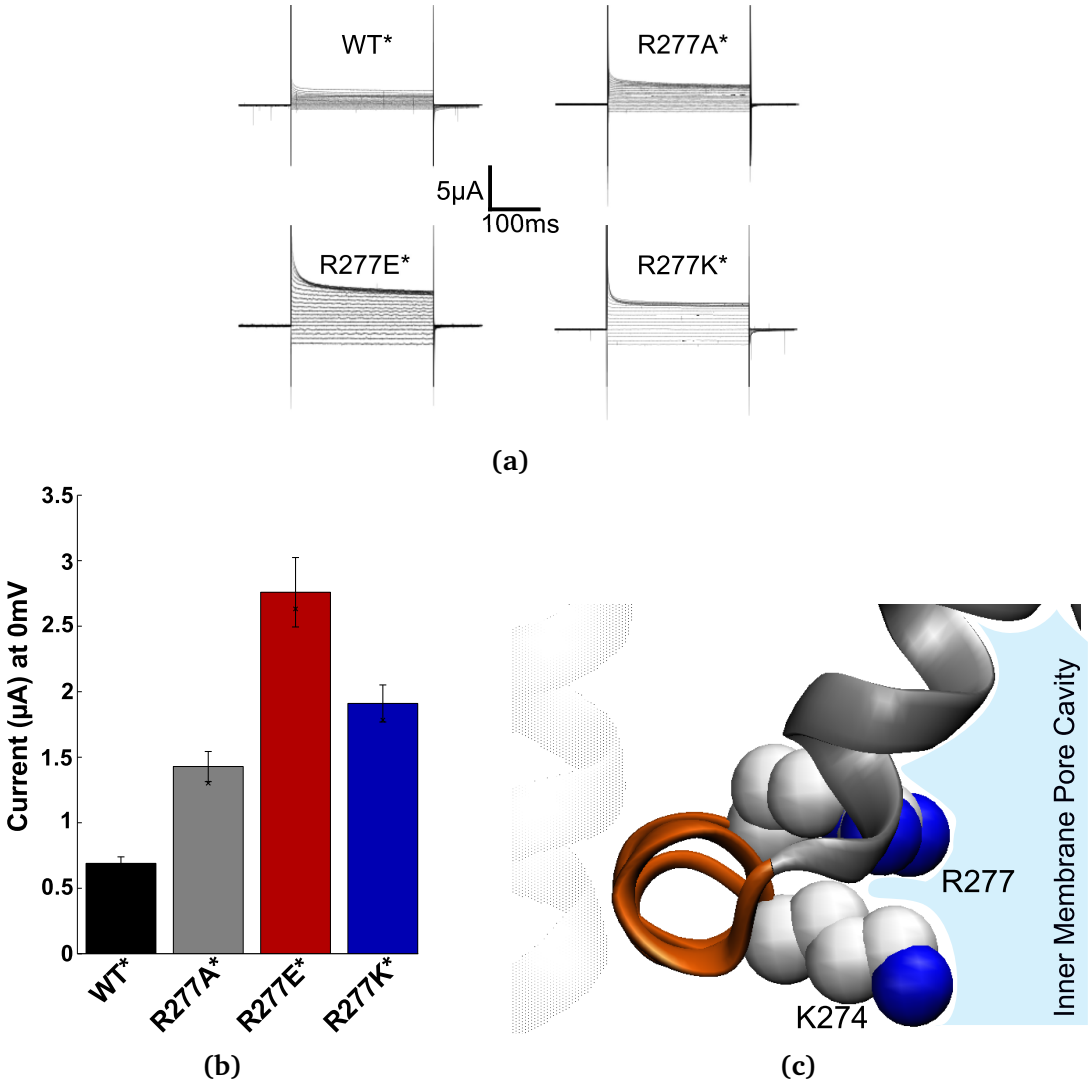

Figure 5.4: Mutations at R277 also produce an increase in the level of functional expression of TWIK-1. a) Current trace of the different R277 mutants. Currents were recorded from oocytes perfused in physiological ND96 buffer at pH7.4, and clamped between -120mV and +70mV in a 10mV voltage step. b) Average current (±SEM) recorded at 0mV for R277 mutants. The level of currents, when compared to WT*, shows a significant increase in current (Tukey-Test $p<0.05$), particularly for R277E and R277K. c) The crystal structure shows that R277 is located adjacent to K274 in the C-helix (orange), and it also points into the inner pore cavity. Blue: nitrogen.

5.2.2.3 MD simulation suggests a possible interaction between R277 and E265

In order to obtain further insights into any possible interactions between these residues, I returned to the molecular dynamics (MD) simulation originally performed on the TWIK-1 crystal structure, described in chapter 4 (Aryal et al., 2014a). As previously highlighted, the backbone of the C-helix domain was relatively stable throughout the simulation (figure 3.11a). This can be seen in the averaged root-mean square fluctuation (RMSF) plot of TWIK-1 around the distal part of the TWIK-1 model (residues 271-281), shown in figure 5.5a. Previously in chapter 3, it was shown that an interaction between K274 and E269 was observed in the MD simulation. However, when I re-analysed the MD simulation, another possible interaction involving R277 was also noticed here, which is shown in figure 5.5b. Within the first few nanoseconds of the 100-ns simulation, R277 in the C-helix was seen to rapidly interact with E265 from the distal end of M4. They form a strong interaction throughout the simulation.

I therefore sought to alter this interaction by means of substituting the glutamate at E265 with a different amino acid, which could result in a similar effect as seen with mutating R277.

However, mutating E265 to aspartate (E265D) maintained almost the same level of functional expression as that of the wild-type current. On the other hand, substituting this residue with a glutamine or alanine silenced channel activity even further (figure 5.6). This suggests that the presence of a negatively charged residue may be required at this position for the channel to function properly. It is also possible that removing the negative charge from the E265 (E265Q or E265A) may lead to a decline in functional activity or expression.

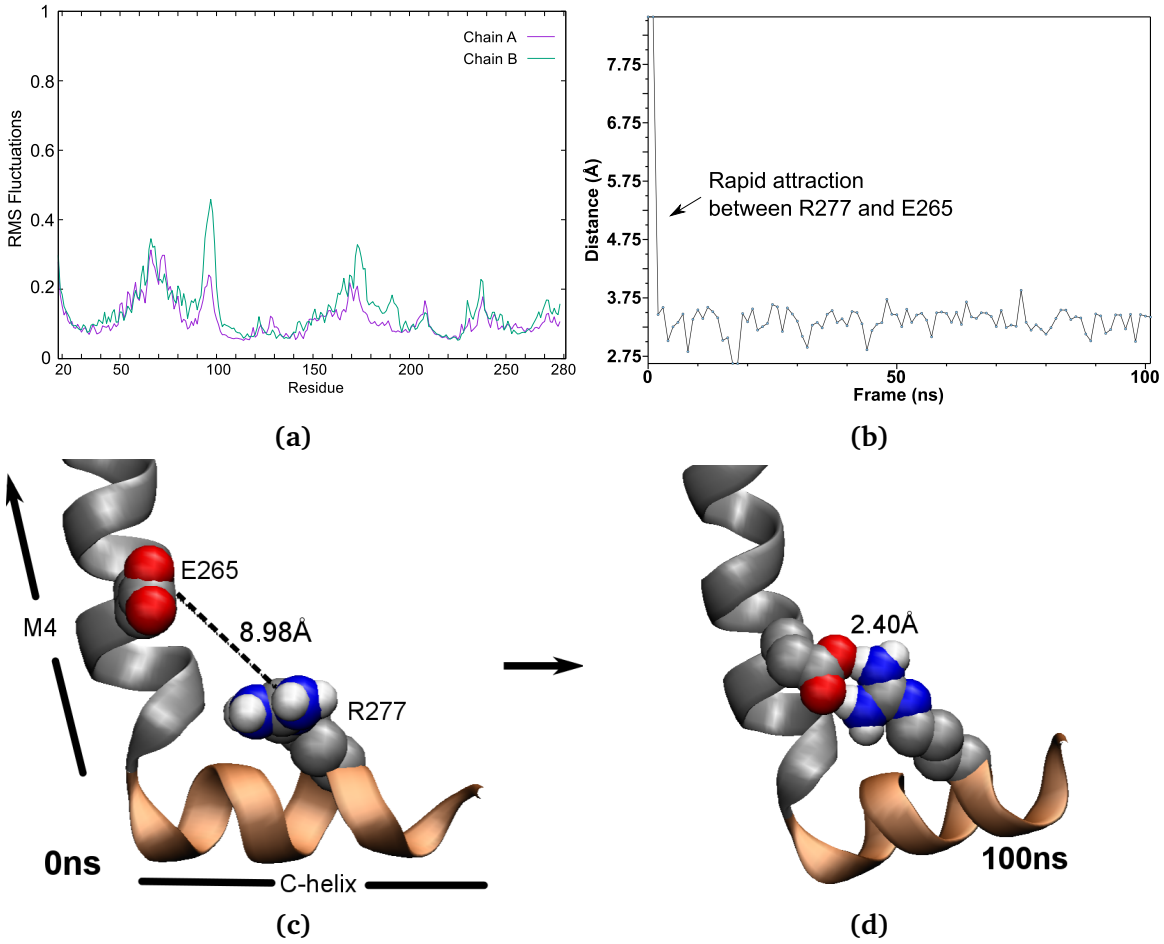

Figure 5.5: Interaction between R277 and E265. a) Root-mean square fluctuation analysis over the 100ns frame window shows the stability of the TWIK-1 backbone structure, particularly at the C-helix domain. b) Plot showing the distance between E265 and R277 in each frame throughout the 100-ns simulation. It can be seen here that the two residues came closer to each other almost instantly from the beginning of the simulation. The 100-ns MD simulation reveals that the R277 residue becomes attracted to E265 and forms a strong bond with it. This can be seen by comparing the distance at c) 0ns and d) 100ns. Dark grey: M4 domain, Orange: C-Helix, Purple: K^+ ions. The analysis in (a) and (b) are based on MD simulations performed by Dr Prafulla Aryal, which was described in Chapter 4.

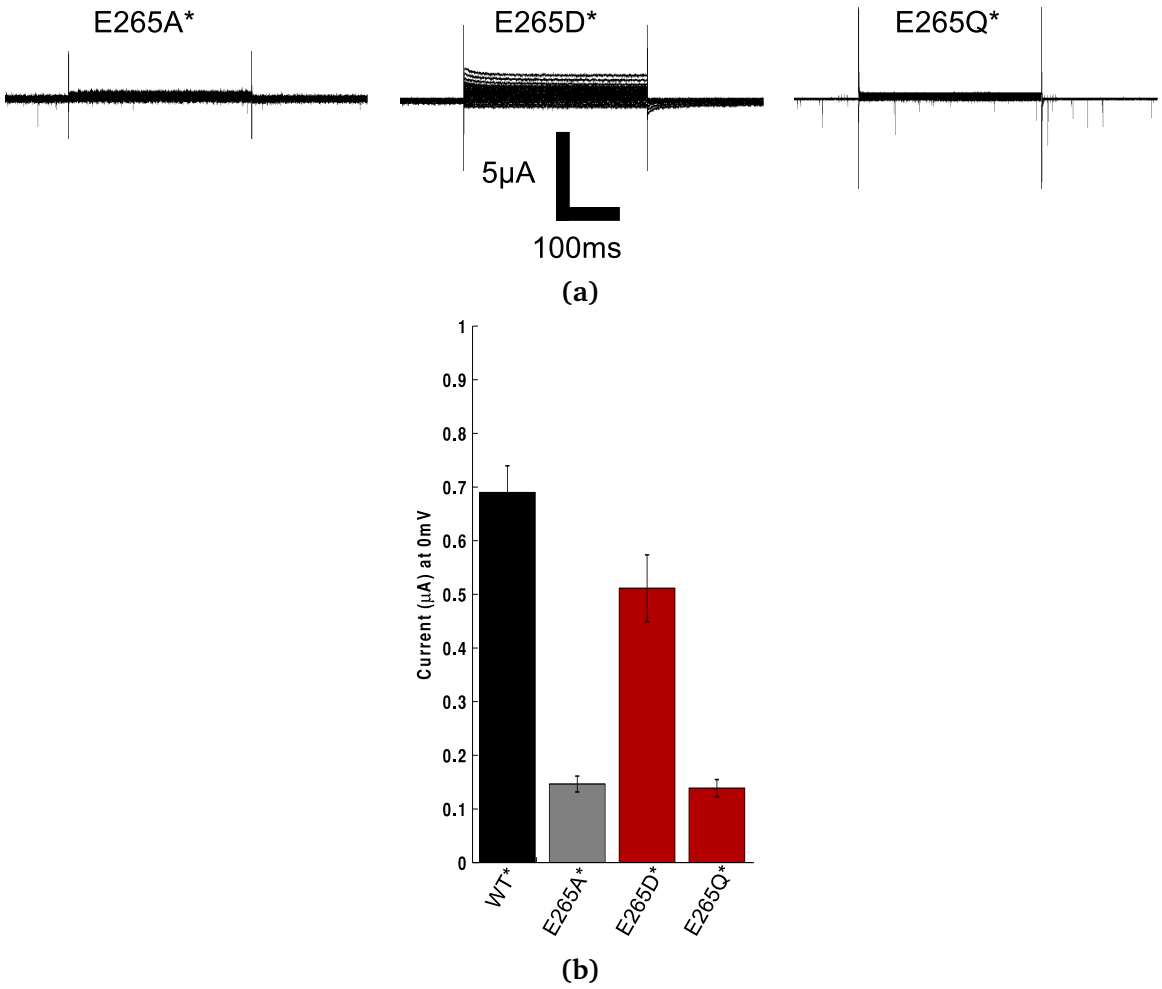

Figure 5.6: Effect of substituting E265 on TWIK-1 channel activity. a) Representative traces of each E265 mutant currents. b) The bar chart shows the level of currents recorded at 0mV, under physiological buffer, for TWIK-1 channels substituted at E265 with alanine, aspartate and glutamine, respectively. Mutant E265D does not result in a significant change in current level, compared to that of the wild-type. However, E265A and E265Q mutants cause a loss of channel activity. The statistical difference in current level of these mutants compared to wild-type are significant, with $p<0.01$.

5.2.2.4 Glutamate substitution on other lysine residues in the C-helix.

The lysine side chain of K278 in the crystal structure also points into the pore cavity of the channel, suggesting that it may also affect ion permeation in a similar manner to K274 and R277 (figure 5.7c). When mutated to glutamate (K278E), a slight increase in whole cell current was observed, with a mean value at 0mV of I_{0mV}=1.27μA±0.11.

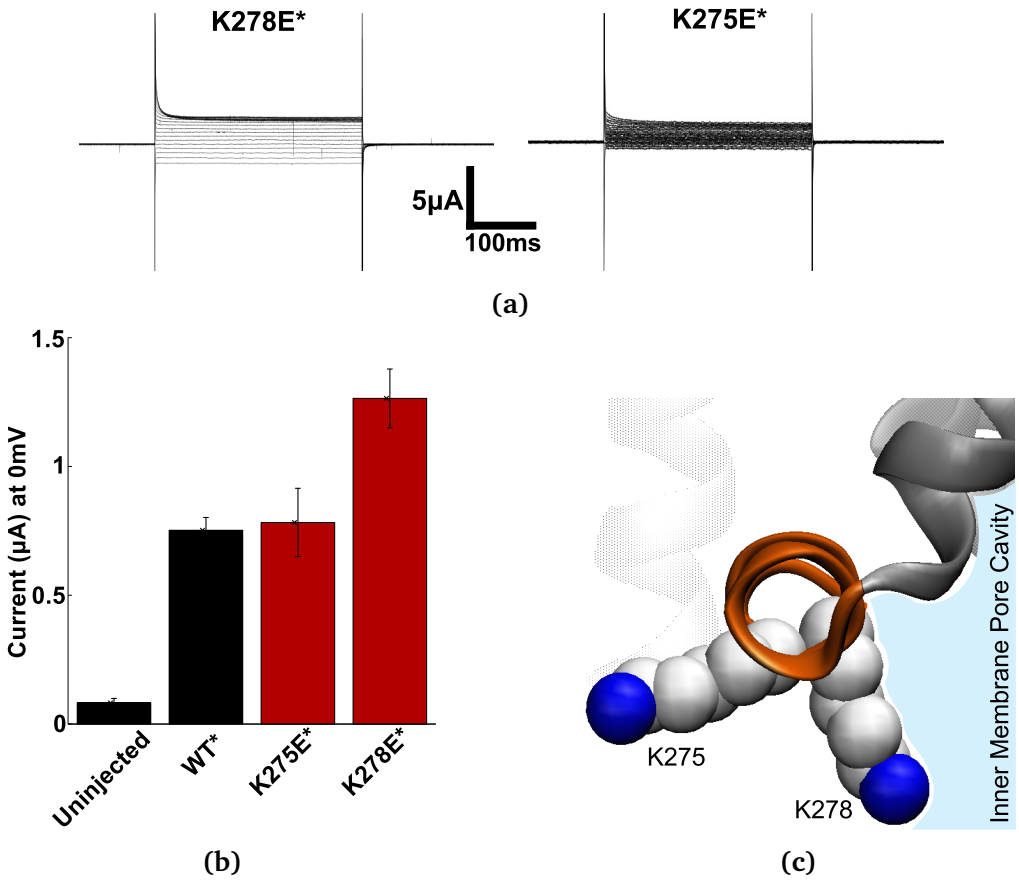

Figure 5.7: Effect of K275E and K278E mutations on whole cell TWIK-1 currents. a) Representative current traces show the different effects of substituting K275 and K278 with glutamate. b) Bar plot for mean current recorded at 0mV, illustrating the different effect between mutating K275E and K278E to whole cell current. While K278 faces the inner pore cavity similarly to R277 and K274 in the TWIK-1 structure, K275 resides oppositely away from the cavity, as shown in (c).

The other lysine residue in the C-helix domain is K275, whose side chain faces away from the channel's inner pore cavity. When K275 was mutated into glutamate (K275E), the level of whole-cell currents remained the same as that of the wild-type. A comparison

between the effect of K275E and K278E mutations is shown in figure 5.7.

5.2.3 Other residues on the C-helix

Further scanning mutagenesis of the C-helix revealed no mutations other than K274, R277 and K278 produced a significantly different level of mean current compared to wild-type (WT*). When E272 was substituted with lysine, no significant difference in the mean current was observed (figure 5.2). Similarly, mutating L273 to asparagine (L273N) or alanine (L273A) also did not have any significant effect on the mean current level.

Also, mutating F276 to leucine (F276L) did not improve the mean current level significantly. However when mutated to arginine (F276R), the mean currents were reduced instead, although, the reasons underlying this effect are unclear and could be due to a number of different reasons.

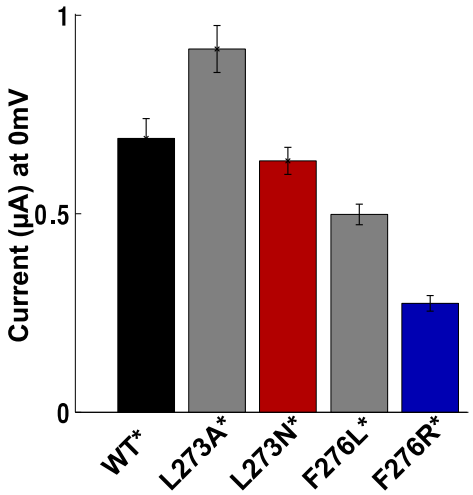

Figure 5.8: Substitutions at the non-pore-facing residues of the C-helix have no significant effect. Bar graph showing the low level of currents recorded at 0mV in physiological conditions for the TWIK-1 channels mutated at the non-polar surface of the C-helix. There were no significant difference in mean current determined from these mutants.

5.2.4 Position of C-helix activatory mutations around the inner pore

From these mutagenesis experiments, three key positions on the C-helix were identified, which have activatory effects on the channel when mutated. These positions pertain to residues K274, R277 and K278. In the crystal structure, these residues are positioned in and near the vicinity of the inner membrane pore cavity, as shown by the TWIK-1 cross-section in figure 5.9.

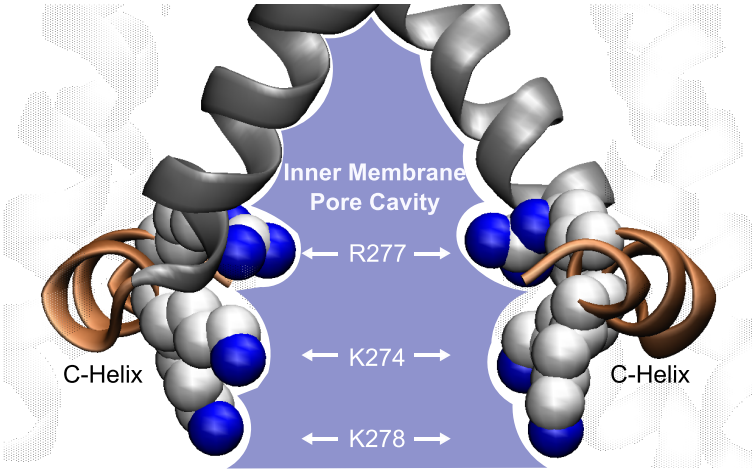

Figure 5.9: Position of the three key residues. The cross-sectional view at the entrance to the inner cavity shows that the activatory mutations observed in this study are located in TWIK-1 at positions 274, 277 and 278. These positions correspond to the residues in the C-helix of each subunit that points into the inner membrane pore cavity. Such arrangement is likely to allow any changes occurring on these residues/positions to affect channel activity significantly.

5.3 Discussion

In this chapter, a number of residues on the amphipathic C-helix have been identified, that influence channel activity. Firstly, we have confirmed that mutations at the putative SUMOylation site (K274) leads to varying degrees of magnitude in whole cell current for different amino acid substitutions. This supports our previous observation that K274 is unlikely to be SUMOylated, at least in the *X.laevis* expression system.

5.3.1 Role of pore-facing charged residues

Since K274 appears to point into the pore, it may instead, influence the behaviour of ions near the entrance of the channel. K274, along with R277 and K278, line the inner pore surface of the C-helix with positive charges. This can be seen from the electrostatic potential distribution on the surface in figure 5.10.

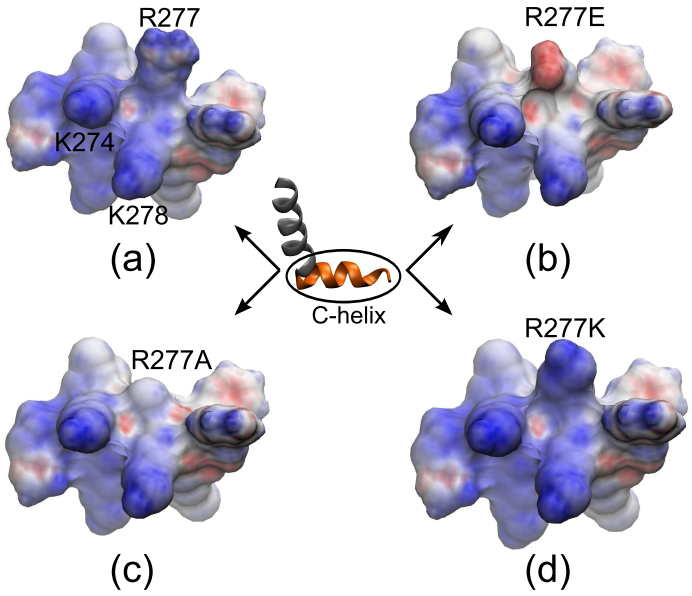

Figure 5.10: Surface polarity at the inner-pore side of the C-Helix domain. The electrostatic potential is illustrated for a) wild-type, b) R277E, c) R277A, and d) R277K. The charge distribution is modelled only on the C-helix, and based on the model system described by Reisser et al. (2014). Blue: $\delta+$, Red: $\delta-$ and Grey: nonpolar.

The results also suggest a role for R277 in the regulation of channel activity. When the charge on the R277 side chain was either reversed or removed with R277E or R277A,respectively, current levels increased. Therefore, these substitutions are predicted to lower the electropositive effect on the inner surface.

Intriguingly, a significant increase in current was also observed with the R277K mutation. Arginine has a long side-chain which consists of a guanidinium group at the distal end of its side chain. This provides arginine with three amino (-NH) groups that is available to form interactions in a larger number than lysine, which only has a single -NH group on its side chain.

The role of charged residues lining the pore of a potassium channel in affecting local ion concentration has been previously implied in other channels. A recent study, for instance, reported on increase in unitary conductances in Shaker channels when charged residues were introduced at the cytoplasmic entrance of the channel (Díaz-Franulic et al., 2015). It was suggested that these mutations cause an increase in local K^+ ion concentration. It is therefore possible that the presence of positively charged residues at the C-helix may also affect local ion concentration, and changing one of them into being negatively charged renders it to be more favourable for potassium ions to conduct past the pore entrance and through the channel. However, single channel recording of unitary conductances for TWIK-1 are needed to justify this hypothesis.

5.3.2 Movement of the C-helix may influence inner pore gating

Movement of inner helices at the cytoplasmic domain have also been previously associated with gating of channel activity by ion pathway occlusion. Intracellular helices may tilt, bend or rotate to induce a tight constriction at the intracellular ion pathway (Doyle, 2004). In some potassium channels, conformational changes at the intracellular helix bundle crossing is regarded as the final gate before the channel is activated, as exemplified by the helix bundle crossing gate of the KcsA channel (Cuello et al., 2010).

In contrast, movement of the inner portion of K2P channels is suggested to be coupled to the selectivity filter (Goldstein, 2011), although this movement is not thought to restrict ion permeation (Zilberberg et al., 2001; Piechotta et al., 2011). Therefore, it also appears that it is most likely that TWIK-1 is probably not gated by an inner helix bundle crossing.

Instead, recent findings suggest that transition between open, closed and inactivated states of a K2P channel may be caused by interhelical movements of the membrane helices at the intracellular region. The crystal structures from TREK-2 ion channel suggest a concerted movement of the TM2, TM3 and TM4 helices that renders the

channel into different conducting states (Dong et al., 2015).

Although the intracellular helix structures of TREK-2 do not kink, but bend outwardly and opposite to that of the TWIK-1 C-Helix, it still highlights that intracellular helix domain movement is probably critical to channel gating. If such structural rearrangements are important, then the C-helix in TWIK-1 may play a crucial role in this process. One possibility is that movement of the C-helix helps change the aperture (i.e. radius) of the inner pore, and thus, move the channel from a dehydrated to a hydrated state. It could also be possible that changes in the orientations of the K274-R277-K278 side chains may affect the energy barrier for ion permeation and/or the hydrated state of the inner pore.

5.4 Conclusion

In summary, the C-helix domain has been screened to identify functionally important residues that may influence TWIK-1 activity. The results show an apparent asymmetry to the C-helix surface that appears to influence TWIK-1 functional activity more significantly than others. Residues identified from the screening are K274, R277 and, to a lesser extent, K278. These residues appear to point into the pore at the cytosolic region of the channel, and when mutated to alanine or glutamate, channel activity was found to increase. This may be due to change in the ability of ions to enter the mouth of the pore, but it may also be due to changes in channel gating caused by these mutations.

CHAPTER 6

Conclusion and Future Directions

6.1 Summary of findings

In this thesis, I have described the results obtained from functional studies of TWIK-1. By examining the available crystal structure of TWIK-1, and with the help of simulations thereof, various regions of TWIK-1 were identified that could functionally contribute to channel activity. The major findings reported here are the identification of a hydrophobic cuff that creates an energetic barrier for permeation, as well as the characterisation of the C-helix domain that influences channel gating.

6.1.1 TWIK-1 channels undergo endosomal distribution

From this study, it has been shown that the evidence supporting the concept of TWIK-1 SUMOylation is weak. Instead, this study indicates that endocytosis may play a more potential role in regulating the surface expression of the channel. By mutating the di-isoleucine motif near the C-terminus end (I293/I294), this removes the endocytosis signalling motif and rescues TWIK-1 from being internalised, thus maintaining a stable expression at the membrane surface.

6.1.2 Hydrophobic Barrier in TWIK-1

In chapters 3 and 4, the structure of TWIK-1 was shown to be stable, especially at the C-helix region. Further analysis on the simulation has revealed a region within the structure that was void of water density. Thus, the presence of a hydrophobic cuff in the inner pore cavity was described. The key residues that make up the hydrophobic cuff are a pair of leucines, L146 and L261, from each subunit of the homodimer.

6.1.2.1 Scanning mutagenesis strongly support the presence of the hydrophobic cuff

Scanning mutagenesis of residues within the cuff supports the view that hydrophobicity of the pore lining affects channel function. By substituting L146 and/or L261 with polar residues, such as asparagine and threonine, channel activity significantly increased. Structurally, this was thought to be the consequence of removing the energetic barrier at the cuff. Increasing pore diameter, by simultaneously mutating L146 and L261 into smaller amino acids, contributed to a slight increase in current, but not sufficient to completely remove the hydrophobic barrier. Hydration of the inner pore therefore, appears inversely proportional to the hydrophobic strength of the pore lining.

6.1.2.2 The mutations alter the permeation pathway

It has also been shown in chapter 4 that expression level of the mutant TWIK-1 channels were not affected by the mutations, neither were the typical regulation that has been previously reported for TWIK-1. Extracellular pH and quinine block of the L146N remained similar to that of the wild-type TWIK-1 channel.

On the other hand, quaternary ammonium blockers were able to bind intracellularly the L146N mutant, but not wild-type TWIK-1. This illustrates our significant finding that access into the inner pore becomes more feasible once the hydrophobic barrier was removed. Therefore, it is concluded that mutations at the hydrophobic cuff directly

alters the permeation pathway, most likely by alleviating the energetic barrier for pore hydration.

6.1.2.3 Influence from the lateral fenestration on the hydrophobic cuff

Another leucine potentially influences the hydrophobic cuff despite not completely facing into the inner pore cavity; L264 was found to be located near the fenestration and between the pore-forming helices of different TWIK-1 subunits. Hydrophilic substitutions of this residue also cause an increase in channel activity. Therefore L264 too could affect pore hydration at the inner pore. However, mutating L264 is also likely to affect the fenestration sites of the channel, which could serve as an entry point for lipid tails. The presence of lipids at the fenestration site and nearby the hydrophobic cuff could, in turn, influence the pore hydration by strengthening the hydrophobic cuff. Thus hydrophilic substitutions at L264 could prevent lipids from entering, and reducing the hydrophobicity of the pore.

6.1.2.4 Does mutating the cuff affect unitary conductance?

The challenge for us in determining whether mutating the hydrophobic cuff affects the unitary conductance is the difficulty in obtaining recordable currents from single-channel patches. This problem has also been widely acknowledged by other groups studying the TWIK-1 channel. However, once single-channel recordings of TWIK-1 become accessible, this may provide a more direct insight to understanding the effects of mutating the hydrophobic cuff on the properties of the permeation pathway.

6.1.3 Role of the C-helix

In chapter 3, it has also been shown that the C-helix appears structurally stable in the simulation, and that its location at the inner membrane interface may play a key role in influencing permeation from the intracellular side.

6.1.3.1 The activatory mutations on the C-helix face the pore

Scanning mutagenesis has revealed an apparent side to the C-helix that, when mutated, could improve channel activity. Residues that were identified on this side of the C-helix surface are three positively-charged amino acids; K274, R277, and K278. Structurally, their side chains point into the inner pore region. Therefore, these residues serve as the cytoplasmic entryway for permeants entering the channel pore. Switching their side chains to being negatively-charged activates the channel. This supports the idea that these residues may play their role by either affecting the local ion concentration at the pore mouth, or by orchestrating a domain movement, interacting with the M4-domain. These effects may influence ion permeation at the intracellular side.

6.2 Future Directions

The current findings reported in this thesis could be further expanded to deepen our understanding on the mechanics of ion conduction and selectivity in TWIK-1 channel, as well as to extend these findings to other K2P channels. Suggestions for such endeavours are described as follows.

6.2.1 Hydrophobic gating in other K2P channels

A recent study on another member of the K2P channel, THIK-2, have showed that mutating an isoleucine into aspartate (I158D) leads to an increase in channel activity. It was shown that I158 is located at the position similar to L146 in TWIK-1 (Chatelain et al., 2013). It is therefore possible that THIK-2 also may possess a hydrophobic cuff below and near the selectivity filter region.

In TREK-2, the equivalent residues with the hydrophobic cuff are a glycine (G201) and an alanine (A317). My preliminary studies on these residues encouragingly indicated that hydrophilic substitutions lead to an increase in channel activity (figure 6.1). This

suggests that TREK-2 could also be modulated by the hydrophobic cuff, although further tests are needed. However, TREK channels are more amenable to electrophysiological recording and may therefore allow single channel recordings to be performed.

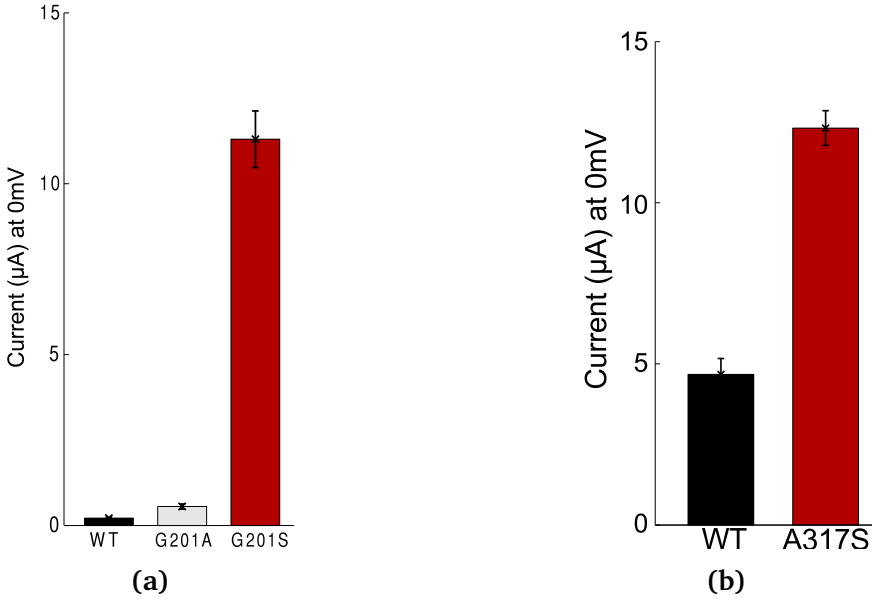

Figure 6.1: Hydrophilic substitutions in TREK-2 inner pore increases channel activity. Substituting (a) G201 and (b) A317 with serine, an isosteric but hydrophilic partner, causes an increase in TREK-2 channel activity.

6.2.2 Other studies on TWIK-1

Intracellular pH regulation of TWIK-1 may also shed some light to the native internal movements of the C-helix residues, particularly R277 and K274, that may influence the surface charge effect at the pore mouth and regulate ion localisation at and permeation through the pore.

Regulation by drugs or other molecules could also be extended on TWIK-1. Recent study on TREK-2 suggested that fluoxetine derivatives were able to bind into the channel by accessing its lateral fenestration site (Dong et al., 2015). Since it has been shown that TWIK-1 too has a fenestration site where lipids could potentially enter, it is possible that other drugs could penetrate these fenestrations and bind to TWIK-1.

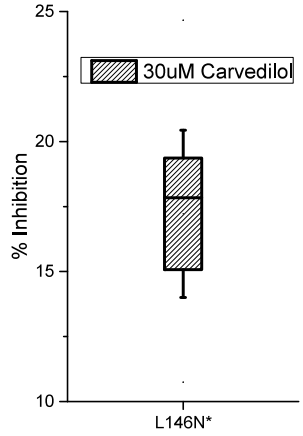

(a)

Figure 6.2: Inhibition of TWIK-1 L146N* by carvedilol. Initial tests suggests that TWIK-1 could be sensitive to carvedilol inhibition. At 30μM carvedilol, the L146N* mutant is inhibited by ∼17%.

Initial tests done on TWIK-1 has shown that channel activity is partially blocked by the drug carvedilol (figure 6.2), which is a common beta-blocker for treating cardiovascular diseases. It is possible that carvedilol can also penetrate the lipid bilayer and access the channel through its fenestration site. Further studies of this blocking effect may be useful.

In this thesis, attention has been given to connecting TWIK-1 functional activity to its structural features from the cytoplasmic half of the channel. Understanding the complete characteristic of the TWIK-1 structure is pivotal to unveiling its paradoxical behaviour. This includes focusing on the dynamic ion selectivity of its filter. Studies have indicated that hydration properties at the selectivity filter could also play a role in determining ion selectivity (Noskov and Roux, 2007; Varma et al., 2011a).

6.2.3 Future annotation of membrane protein structures

The results shown in this study and the functional validation experiments I have performed also demonstrate that the simulation of the unusual behaviour of water in a 'nanopore' can be used to determine whether the pore is likely to be permeable to ions

or not. Normally, computationally expensive free energy calculations are required to determine this, but with the recent advances in the use of graphics processing units (GPUs), MD simulations of water can be performed almost in a matter of hours. These relatively inexpensive simulations can yield important information on whether a pore is likely to be open, and future development of this methodology is likely to have a major impact in the field of membrane protein structural biology.

6.3 Concluding remarks

I have presented in this thesis an interesting finding that unlocks TWIK-1 channel from being functionally silent. The presence of a hydrophobic cuff that prevents pore hydration was described, and alleviating this energetic barrier by introducing polarity directly alters the permeation pathway.

From this study, it was also concluded that TWIK-1 channel is not 'silenced' by SUMOylation at the K274 position but internalised by endocytosis. Instead, K274, may be involved in channel gating from the cytoplasmic side, along with R277 and K278. These triad of positively-charged residues lie unilaterally on the C-helix domain, and faces the inner pore cavity of the channel. Mutations of these residues assert certain activatory effects.

A close collaboration between computational and functional studies have also been demonstrated here. With the advent of current technology, computational biology has become more useful and reliable in rapidly advancing our understanding the relationship between protein structure and function.

Thus far, this thesis have focused on the bottom half of the channel. Complete understanding of the relationship between structure and function of TWIK-1 might provide us a better insight of the role of the extracellular cap, as well as the dynamic selectivity of the channel. Moreover, since the presence of the hydrophobic barrier

in TWIK-1 is still a newly-found phenomenon, the biological relevance of this gating mechanism remains unclear. This study has empirically indicated that this energetic barrier does exist, which may be applicable to other subnanometer pores that could be further investigated.

Appendices

Appendix A

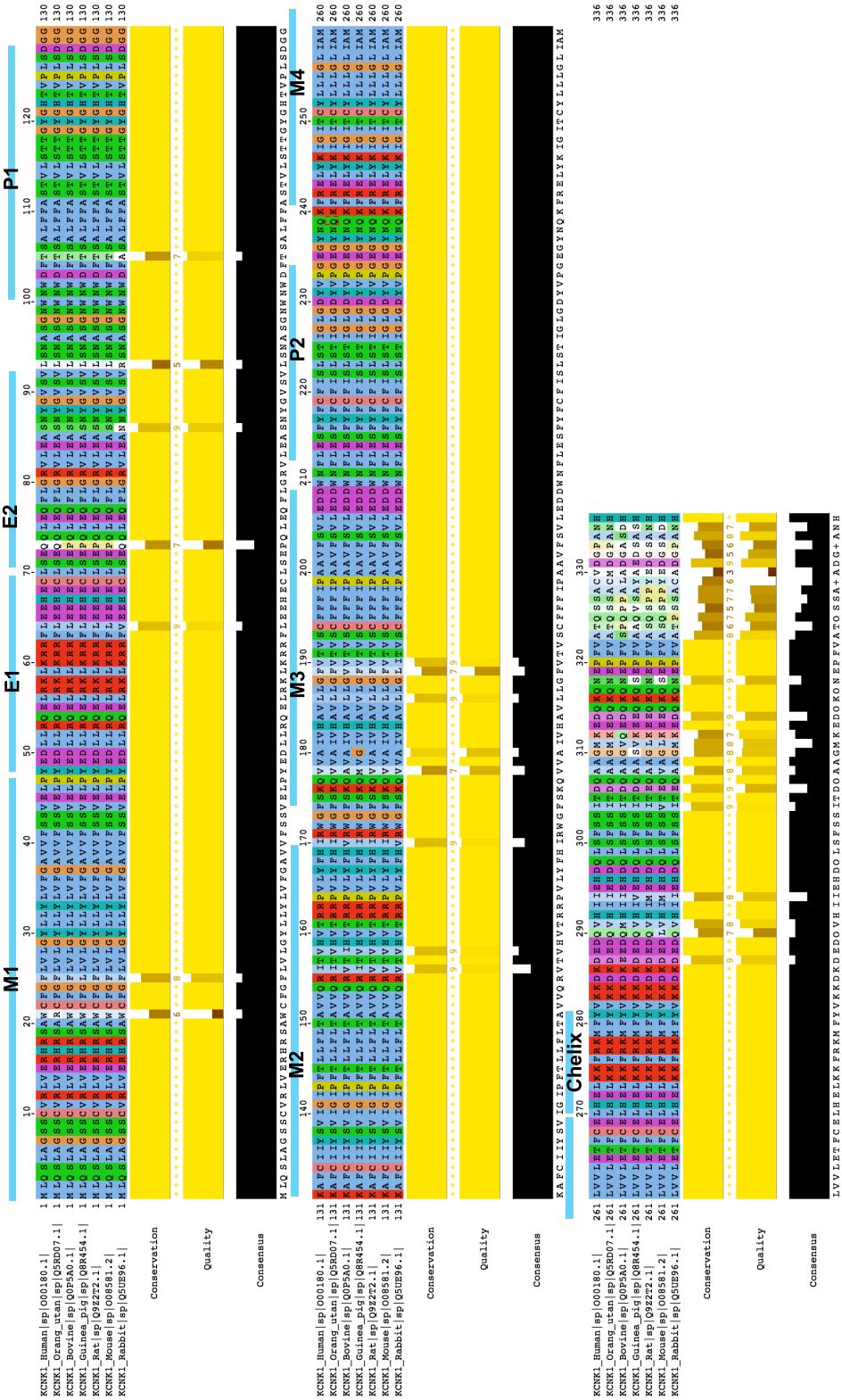

Sequence alignment of TWIK-1. The alignment highlights the highly conserved sequence of the TWIK-1 channel across species available from the National Center for Biotechnology Information (NCBI) database.

Appendix B

DNA sequence of the pFAW vector - T7 promoter (blue), multiple cloning site (green) and ampicilin resistance gene (yellow) are highlighted.

```
   1 GCGCGCGTTG ACATTGATTA TTGACTAGTT ATTAATAGTA ATCAATTACG
  51 GGGTCATTAG TTCATAGCCC ATATATGGAG TTCCGCGTTA CATAACTTAC
 101 GGTAAATGGC CCGCCTGGCT GACCGCCCAA CGACCCCCGC CCATTGACGT
 151 CAATAATGAC GTATGTTCCC ATAGTAACGC CAATAGGGAC TTTCCATTGA
 201 CGTCAATGGG TGGACTATTT ACGGTAAACT GCCCACTTGG CAGTACATCA
 251 AGTGTATCAT ATGCCAAGTA CGCCCCCTAT TGACGTCAAT GACGGTAAAT
 301 GGCCCGCCTG GCATTATGCC CAGTACATGA CCTTATGGGA CTTTCCTACT
 351 TGGCAGTACA TCTACGTATT AGTCATCGCT ATTACCATGG TGATGCGGTT
 401 TTGGCAGTAC ATCAATGGGC GTGGATAGCG GTTTGACTCA CGGGGATTTC
 451 CAAGTCTCCA CCCCATTGAC GTCAATGGGA GTTTGTTTTG GCACCAAAAT
 501 CAACGGGACT TTCCAAAATG TCGTAACAAC TCCGCCCCAT TGACGCAAAT
 551 GGGCGGTAGG CGTGTACGGT GGGAGGTCTA TATAAGCAGA GCTCTCTGGC
 601 TAACTAGAGA ACCCACTGCT TACTGGCTTA TCGAAATTAA TACGACTCAC
 651 TATAGGGAGA CCCAAGCTGG CTAGCGTTTA AACTTAAGCT TGCTTGTTCT
 701 TTTTGCAGAA GCTCAGAATA AACGCTCAAC TTTGGCAGGG ATCCGGGCCC
 751 CGGGTTAACT AGTCTAGAAT TCATCGATAT CCATGGTCGA CGAGCTCGAG
 801 ATCTGCAGCT GGTACCGGTT ACCACTAAAC CAGCCTCAAG AACACCCGAA
 851 TGGAGTCTCT AAGCTACATA ATACCAACTT ACACTTTACA AAATGTTGTC
 901 CCCCAAAATG TAGCCATTCG TATCTGCTCC TAATAAAAAG AAAGTTTCTT
 951 CACATTCTAA AAAAAAAAAA AAAAAAAAAA AAAAAAAAAA AAAAAAAAAA
1001 AAAAAAAAAA AAAAAAAAAA AAAAAAAAAA AAAAAAAAAA AAAAAAAAAA
1051 AAAAAAAAAA AAAAAAAAAA AAAAAAAAAA AAAAAAAACG CGTCACCGTT
1101 TAAACCCGCT GATCAGCCTC GACTGTGCCT TCTAGTTGCC AGCCATCTGT
1151 TGTTTGCCCC TCCCCCGTGC CTTCCTTGAC CCTGGAAGGT GCCACTCCCA
1201 CTGTCCTTTC CTAATAAAAT GAGGAAATTG CATCGCATTG TCTGAGTAGG
1251 TGTCATTCTA TTCTGGGGGG TGGGGTGGGG CAGGACAGCA AGGGGGAGGA
1301 TTGGGAAGAC AATAGCAGGC ATGCTGGGGA TGCGGTGGGC TCTATGGCTT
1351 CTGAGGCGGA AAGAACCAGT GGCGGTAATA CGGTTATCCA CAGAATCAGG
1401 GGATAACGCA GGAAAGAACA TGTGAGCAAA AGGCCAGCAA AAGGCCAGGA
1451 ACCGTAAAAA GGCCGCGTTG CTGGCGTTTT TCCATAGGCT CCGCCCCCCT
1501 GACGAGCATC ACAAAAATCG ACGCTCAAGT CAGAGGTGGC GAAACCCGAC
1551 AGGACTATAA AGATACCAGG CGTTTCCCCC TGGAAGCTCC CTCGTGCGCT
```

```
1601 CTCCTGTTCC GACCCTGCCG CTTACCGGAT ACCTGTCCGC CTTTCTCCCT
1651 TCGGGAAGCG TGGCGCTTTC TCATAGCTCA CGCTGTAGGT ATCTCAGTTC
1701 GGTGTAGGTC GTTCGCTCCA AGCTGGGCTG TGTGCACGAA CCCCCCGTTC
1751 AGCCCGACCG CTGCGCCTTA TCCGGTAACT ATCGTCTTGA GTCCAACCCG
1801 GTAAGACACG ACTTATCGCC ACTGGCAGCA GCCACTGGTA ACAGGATTAG
1851 CAGAGCGAGG TATGTAGGCG GTGCTACAGA GTTCTTGAAG TGGTGGCCTA
1901 ACTACGGCTA CACTAGAAGG ACAGTATTTG GTATCTGCGC TCTGCTGAAG
1951 CCAGTTACCT TCGGAAAAAG AGTTGGTAGC TCTTGATCCG GCAAACAAAC
2001 CACCGCTGGT AGCGGTGGTT TTTTTGTTTG CAAGCAGCAG ATTACGCGCA
2051 GAAAAAAAGG ATCTCAAGAA GATCCTTTGA TCTTTTCTAC GGGGTCTGAC
2101 GCTCAGTGGA ACGAAAACTC ACGTTAAGGG ATTTTGGTCA TGAGATTATC
2151 AAAAAGGATC TTCACCTAGA TCCTTTTAAA TTAAAAATGA AGTTTTAAAT
2201 CAATCTAAAG TATATATGAG TAACCTGAGG CTATGGCAGG GCCTGCCGCC
2251 CCGACGTTGG CTGCGAGCCC TGGGCCTTCA CCCGAACTTG GGGGGTGGGG
2301 TGGGGAAAAG GAAGAAACGC GGGCGTATTG GCCCCAATGG GGTCTCGGTG
2351 GGGTATCGAC AGAGTGCCAG CCCTGGGACC GAACCCCGCG TTTATGAACA
2401 AACGACCCAA CACCGTGCGT TTTATTCTGT CTTTTTATTG CCGTCATAGC
2451 GCGGGTTCCT TCCGGTATTG TCTCCTTCCG TGTTTCAGTT AGCCTCCCCC
2501 TAGGGTGGGC GAAGAACTCC AGCATGAGAT CCCCGCGCTG GAGGATCATC
2551 CAGCCGGCGT CCCGGAAAAC GATTCCGAAG CCCAACCTTT CATAGAAGGC
2601 GGCGGTGGAA TCGAAATCTC GTGATGGCAG GTTGGGCGTC GCTTGGTCGG
2651 TCATTTCGAA CCCCAGAGTC CCGCTCAGAA GAACTCGTCA AGAAGGCGAT
2701 AGAAGGCGAT GCGCTGCGAA TCGGGAGCGG CGATACCGTA AAGCACGAGG
2751 AAGCGGTCAG CCCATTCGCC GCCAAGCTCT TCAGCAATAT CACGGGTAGC
2801 CAACGCTATG TCCTGATAGC GGTCCGCCAC ACCCAGCCGG CCACAGTCGA
2851 TGAATCCAGA AAAGCGGCCA TTTTCCACCA TGATATTCGG CAAGCAGGCA
2901 TCGCCATGGG TCACGACGAG ATCCTCGCCG TCGGGCATGC TCGCCTTGAG
2951 CCTGGCGAAC AGTTCGGCTG GCGCGAGCCC CTGATGCTCT TGATCATCCT
3001 GATCGACAAG ACCGGCTTCC ATCCGAGTAC GTGCTCGCTC GATGCGATGT
3051 TTCGCTTGGT GGTCGAATGG GCAGGTAGCC GGATCAAGCG TATGCAGCCG
3101 CCGCATTGCA TCAGCCATGA TGGATACTTT CTCGGCAGGA GCAAGGTGAG
3151 ATGACAGGAG ATCCTGCCCC GGCACTTCGC CCAATAGCAG CCAGTCCCTT
3201 CCCGCTTCAG TGACAACGTC GAGCACAGCT GCGCAAGGAA CGCCCGTCGT
3251 GGCCAGCCAC GATAGCCGCG CTGCCTCGTC TTGCAGTTCA TTCAGGGCAC
3301 CGGACAGGTC GGTCTTGACA AAAAGAACCG GGCGCCCCTG CGCTGACAGC
3351 CGGAACACGG CGGCATCAGA GCAGCCGATT GTCTGTTGTG CCCAGTCATA
```

```
3401 GCCGAATAGC CTCTCCACCC AAGCGGCCGG AGAACCTGCG TGCAATCCAT
3451 CTTGTTCAAT CATGCGAAAC GATCCTCATC CTGTCTCTTG ATCGATCTTT
3501 GCAAAAGCCT AGGCCTCCAA AAAAGCCTCC TCACTACTTC TGGAATAGCT
3551 CAGAGGCCGA GGCGGCCTCG GCCTCTGCAT AAATAAAAAA AATTAGTCAG
3601 CCATGGGGCG GAGAATGGGC GGAACTGGGC GGAGTTAGGG GCGGGATGGG
3651 CGGAGTTAGG GGCGGGACTA TGGTTGCTGA CTAATTGAGA TGCATGCTTT
3701 GCATACTTCT GCCTGCTGGG GAGCCTGGGG ACTTTCCACA CCTGGTTGCT
3751 GACTAATTGA GATGCATGCT TTGCATACTT CTGCCTGCTG GGGAGCCTGG
3801 GGACTTTCCA CACCCTAACT GACACACATT CCACAGCTGG TTCTTTCCGC
3851 CTCAGGACTC TTCCTTTTTC AATAAATCAA TCTAAAGTAT ATATGAGTAA
3901 ACTTGGTCTG ACAGTTACCA ATGCTTAATC AGTGAGGCAC CTATCTCAGC
3951 GATCTGTCTA TTTCGTTCAT CCATAGTTGC CTGACTCCCC GTCGTGTAGA
4001 TAACTACGAT ACGGGAGGGC TTACCATCTG GCCCCAGTGC TGCAATGATA
4051 CCGCGAGACC CACGCTCACC GGCTCCAGAT TTATCAGCAA TAAACCAGCC
4101 AGCCGGAAGG GCCGAGCGCA GAAGTGGTCC TGCAACTTTA TCCGCCTCCA
4151 TCCAGTCTAT TAATTGTTGC CGGGAAGCTA GAGTAAGTAG TTCGCCAGTT
4201 AATAGTTTGC GCAACGTTGT TGCCATTGCT ACAGGCATCG TGGTGTCACG
4251 CTCGTCGTTT GGTATGGCTT CATTCAGCTC CGGTTCCCAA CGATCAAGGC
4301 GAGTTACATG ATCCCCCATG TTGTGCAAAA AAGCGGTTAG CTCCTTCGGT
4351 CCTCCGATCG TTGTCAGAAG TAAGTTGGCC GCAGTGTTAT CACTCATGGT
4401 TATGGCAGCA CTGCATAATT CTCTTACTGT CATGCCATCC GTAAGATGCT
4451 TTTCTGTGAC TGGTGAGTAC TCAACCAAGT CATTCTGAGA ATAGTGTATG
4501 CGGCGACCGA GTTGCTCTTG CCCGGCGTCA ATACGGGATA ATACCGCGCC
4551 ACATAGCAGA ACTTTAAAAG TGCTCATCAT TGGAAAACGT TCTTCGGGGC
4601 GAAAACTCTC AAGGATCTTA CCGCTGTTGA GATCCAGTTC GATGTAACCC
4651 ACTCGTGCAC CCAACTGATC TTCAGCATCT TTTACTTTCA CCAGCGTTTC
4701 TGGGTGAGCA AAAACAGGAA GGCAAAATGC CGCAAAAAAG GGAATAAGGG
4751 CGACACGGAA ATGTTGAATA CTCATACTCT TCCTTTTTCA ATATTATTGA
4801 AGCATTTATC AGGGTTATTG TCTCATGAGC GGATACATAT TTGAATGTAT
4851 TTAGAAAAAT AAACAAATAG GGGTTCCGCG CACATTTCCC CGAAAAGTGC
4901 CACCTGACGC GCCCTGTAGC GGCGCATTAA GCGCGGCGGG TGTGGTGGTT
4951 ACGCGCAGCG TGACCGCTAC ACTTGCCAGC GCCCTAGCGC CCGCTCCTTT
5001 CGCTTTCTTC CCTTCCTTTC TCGCCACGTT CGCCGGCTTT CCCCGTCAAG
5051 CTCTAAATCG GGGGCTCCCT TTAGGGTTCC GATTTAGTGC TTTACGGCAC
5101 CTCGACCCCA AAAAACTTGA TTAGGGTGAT GGTTCACGTA GTGGGCCATC
5151 GCCCTGATAG ACGGTTTTTC GCCCTTTGAC GTTGGAGTCC ACGTTCTTTA
```

```
5201 ATAGTGGACT CTTGTTCCAA ACTGGAACAA CACTCAACCC TATCTCGGTC
5251 TATTCTTTTG ATTTATAAGG GATTTTGCCG ATTTCGGCCT ATTGGTTAAA
5301 AAATGAGCTG ATTTAACAAA AATTTAACGC GAATTTTAAC AAAATATTAA
5351 CGCTTACAAT TTACGGAGCG CGCGTTGACA TTGAT
```

Appendix C

Table 1: Ringer's solution, used to defolliculate the oocytes by chemical treatment. 2mg/ml Collagenase is added to the buffer prior to treatment.

	Formula weight (g/mol)	Concentration (mM)
Sodium chloride (NaCl)	58.443	83
Potassium chloride (KCl)	74.515	2
Magnesium chloride ($MgCl_2$)	95.2115	2
HEPES	238.3059	5

Table 2: Storage solution, used to store the oocytes post-treatment. The following antibiotics were added to the buffer prior to use; gentamicin, tetracyclin, amikacin

	Formula weight (g/mol)	Concentration (mM)
Sodium chloride (NaCl)	58.443	83
Potassium chloride (KCl)	74.515	2
Calcium chloride ($CaCl_2$)	110.9848	1.8
Magnesium chloride ($MgCl_2$)	95.2115	2
HEPES	238.3059	5

Table 3: ND96 $2K^+$buffer. Physiological buffer titrated to pH6.0 or pH7.4 with Sodium Hydroxide

	Formula weight (g/mol)	Concentration (mM)
Sodium chloride (NaCl)	58.443	96
Potassium chloride (KCl)	74.515	2
Calcium chloride ($CaCl_2$)	110.9848	1.8
Magnesium chloride ($MgCl_2$)	95.2115	2
HEPES	238.3059	5

Appendix D

nature COMMUNICATIONS

ARTICLE

Received 9 Jan 2014 | Accepted 11 Jun 2014 | Published 8 Jul 2014

DOI: 10.1038/ncomms5377 OPEN

A hydrophobic barrier deep within the inner pore of the TWIK-1 K2P potassium channel

Prafulla Aryal[1,2,3], Firdaus Abd-Wahab[1], Giovanna Bucci[1], Mark S.P. Sansom[2,3] & Stephen J. Tucker[1,3]

Recent X-ray crystal structures of the two-pore domain (K2P) family of potassium channels have revealed a unique structural architecture at the point where the cytoplasmic bundle-crossing gate is found in most other tetrameric K^+ channels. However, despite the apparently open nature of the inner pore in the TWIK-1 (K2P1/KCNK1) crystal structure, the reasons underlying its low levels of functional activity remain unclear. In this study, we use a combination of molecular dynamics simulations and functional validation to demonstrate that TWIK-1 possesses a hydrophobic barrier deep within the inner pore, and that stochastic dewetting of this hydrophobic constriction acts as a major barrier to ion conduction. These results not only provide an important insight into the mechanisms which control TWIK-1 channel activity, but also have important implications for our understanding of how ion permeation may be controlled in similar ion channels and pores.

[1] Clarendon Laboratory, Department of Physics, University of Oxford, Oxford OX1 3PU, UK. [2] Department of Biochemistry, University of Oxford, Oxford OX1 3QX, UK. [3] OXION Initiative in Ion Channels and Disease, University of Oxford, Oxford OX1 3PT, UK. Correspondence and requests for materials should be addressed to M.S.P.S. (email: mark.sansom@bioch.ox.ac.uk) or to S.J.T. (email: stephen.tucker@physics.ox.ac.uk).

© 2014 Macmillan Publishers Limited. All rights reserved.

K2P potassium channels represent a structurally unique family of channels involved in physiological functions as diverse as cell-volume regulation, central chemosensitivity, apoptosis, vasodilatation, neuronal excitability and the perception of pain[1]. They also act as a major target of volatile anaesthetics and represent attractive therapeutic targets for the treatment of a variety of cardiovascular and neurological disorders[2,3]. In particular, the first mammalian member of this superfamily to be cloned, TWIK-1 (K2P1/*KCNK1*), has been implicated in having an important physiological role in the brain and the heart[4–6]. However, understanding the biophysical, pharmacological and functional properties of this particular channel has been difficult. This is mainly because of the extremely low levels of functional activity observed when TWIK-1 is expressed in heterologous systems, especially when compared with other members of the K2P family[7]. The precise reasons for this remain controversial and may involve a combination of either post-translational modification (sumoylation)[8,9] and/or rapid endocytosis[10–13]. However, it is clear that even when TWIK-1 channels are present in the plasma membrane they have very low levels of intrinsic functional activity and are effectively silent[10–12,14].

Two recent crystal structures of K2P channels (TWIK-1 and TRAAK) revealed that these channels assemble as a dimer with many similarities to classical K^+ channels including a 'pseudo-tetrameric' K^+ selective pore[15,16]. However, functional studies have indicated that K2P channels, unlike most other K^+ channels, do not utilize an intersection of the pore-lining helices or cytoplasmic 'bundle-crossing' as their primary gate. Instead, K2P channel gating is primarily the result of a gate located close to, or within, the selectivity filter[17–19]. It was therefore interesting to observe in the crystal structures of both TWIK-1 and TRAAK that the dimensions of the cytoplasmic entrance to the pore were comparable to other K^+ channel structures believed to represent functionally open conformations[20,21]. However, despite the apparently 'open' conformation of the TWIK-1 structure, the arrangement of the transmembrane helices at the cytoplasmic entrance to the pore remains unusual; the distal end of M4 is kinked parallel to the membrane forming an amphipathic 'C-helix' that has been proposed to have a role in channel gating[16]. In addition, the C-helix also contains Lys274, the residue proposed to be the site responsible for channel 'silencing' by post-translational sumoylation[8,9].

In this study we sought to investigate whether the structural features of TWIK-1 may provide an insight into the apparent lack of functional activity when this channel is expressed. We therefore employed multi-scale molecular dynamics (MD) tools to simulate the behaviour of the TWIK-1 crystal structure within a lipid membrane environment. Intriguingly, we found evidence for a hydrophobic gate deep within the inner cavity of the TWIK-1 pore, and we demonstrate that this hydrophobic barrier plays a key role in determining the functional activity of TWIK-1.

Results

MD simulation of TWIK-1 within a lipid bilayer. To simulate the behaviour of TWIK-1 within a lipid membrane environment we first used coarse-grain MD simulations (CGMD) to embed and equilibrate the experimentally determined channel structure in a phospholipid (POPC (1-palmitoyl,2-oleoyl-sn-glycero-3-phosphocholine)) bilayer. In the CGMD simulations and at the start of the subsequent atomistic simulations, the C-helix aligned parallel to the membrane and the side-fenestration between M2 and M4 was still visible (Fig. 1). At the end of the 100-ns atomistic simulation, movement of the transmembrane helices at the lipid interface resulted in a closure of the fenestration and a small upward movement of the distal end of M2. Nevertheless, the overall structure remained stable; in particular, the C-helix remained parallel to the plane of the membrane and the cytoplasmic gate and inner pore remained apparently open (Fig. 1; Supplementary Fig. 1).

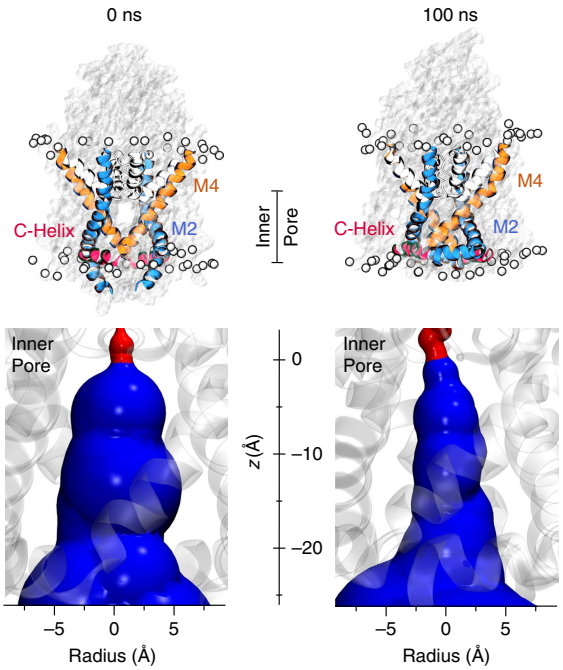

Figure 1 | TWIK-1 cytoplasmic gate remains open. Top: pore-lining structure and surface of TWIK-1 at the start (0 ns), and end (100 ns) of the MD simulation. The pore-lining helices and C-helix are highlighted. The position of the membrane is shown by the phosphorus atoms of POPC highlighted as light grey spheres. The C-helix remains stable and associated with the membrane throughout the simulation (Supplementary Fig. 1). Below each snapshot of the simulation is an expanded view of the inner-pore section indicated by the line in the top panel. Distances along the *z*-axis of the inner pore start below the S4 binding site. The pore radius dimensions show that the cytoplasmic mouth of the inner cavity remains open throughout the simulation. The HOLE surface profiles are coloured red ($r<1.2$ Å) or blue ($r>1.2$ Å).

Water dynamics within the inner pore. Closer examination of the simulation revealed an unusual behaviour of water molecules within the pore of the channel; a stochastic wetting and dewetting process was observed within the inner pore (Fig. 2; Supplementary Movie 1). Visualization of the averaged water density within the inner pore revealed that the water loss was most drastic around 5–10 Å below the selectivity filter (Fig. 2a). The number of water molecules within this region dropped to zero within a few nanoseconds of starting the simulation, followed by fluctuations throughout the simulation (Fig. 2a,b). An averaged distribution plot shows a clear absence of water within this region compared with the cytoplasmic entrance of the pore (Fig. 2c). Similar water dynamics were also observed in another separate 100-ns simulation and a fractional occupancy histogram shows that water was completely absent from this region of the inner pore for >50% of the duration of the simulations (Fig. 2d).

© 2014 Macmillan Publishers Limited. All rights reserved.

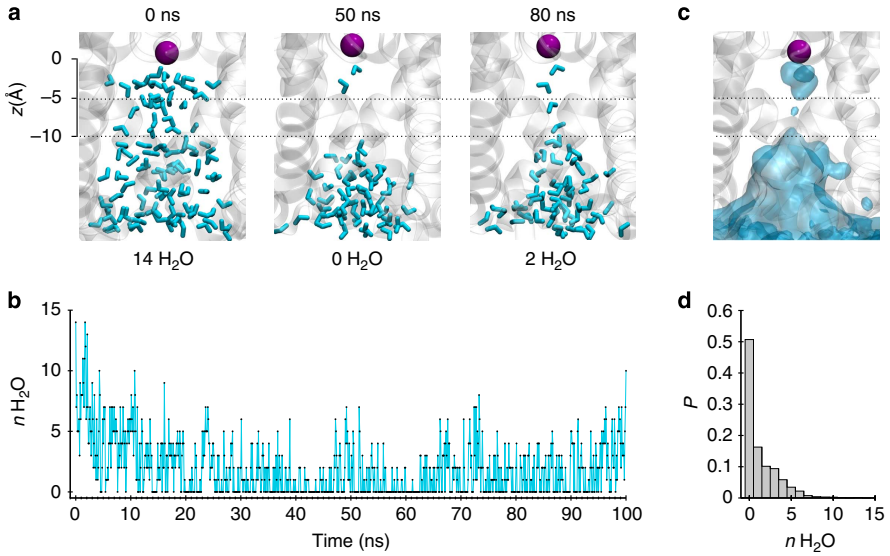

Figure 2 | Dewetting of the inner pore. (**a**) Snapshots of water molecules (cyan) inside the inner pore of TWIK-1 channel at different time points during the MD simulation. For orientation, the K^+ ion at the S4 site is shown as a purple sphere. Dashed lines (5–10 Å below the S4 site) indicate the location where dewetting is most prominent. The number of water molecules in this region is indicated below each snapshot. (**b**) Water count within this region of the inner pore sampled every 0.1 ns during the simulation. (**c**) Average water density inside the inner pore during the simulation is shown as transparent cyan surface contoured at 0.50 of bulk water density, overlaid on a snapshot of the inner pore at 100 ns. (**d**) Normalized probability histogram of the water count at this region for two 100-ns MD simulations. This reveals water molecules to be absent from this region of the inner pore for >50% of the duration of the simulation.

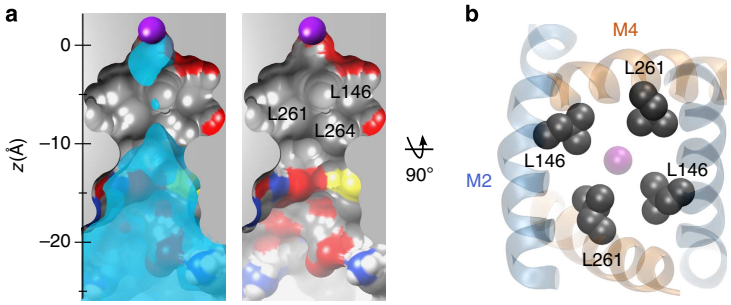

Figure 3 | Hydrophobic cuff within the TWIK-1 inner pore. (**a**) A longitudinal section through the centre of the TWIK-1 channel at the end of the MD simulation. Left, a section of the average water density is overlaid. The S4 K^+ ion is shown as a purple sphere. Note the hydrophobic nature residues lining the inner pore. Right, leucine residues contributing to the hydrophobic cuff are labelled. (**b**) Bottom-up view of the inner pore. Leu146 and Leu261 which form the hydrophobic cuff are shown as grey van der Waals spheres. M2 is shown in blue and M4 in orange.

Hydrophobic cuff deep within the TWIK-1 pore. To understand this dewetting process we examined the structure of the TWIK-1 pore. A section through the inner pore shows that the region where dewetting is most prominent is extremely hydrophobic (Fig. 3a). In particular, Leu146 and Leu261 from both subunits form a hydrophobic cuff around this region with their side chains pointing into the pore throughout the simulation (Fig. 3b). Another hydrophobic side chain (Leu264) also appears to contribute to this cuff, but this residue is located at the interface between M2 and M4, and so the side chain is not fully exposed to the conduction pathway. Interestingly, the hydrophobic nature of this inner cavity is in marked contrast to the cytoplasmic mouth of the pore which is lined by numerous polar side chains and which remains hydrated throughout the simulations (Fig. 3a).

Simulations of inner pore hydration. Confinement of water and ions at the molecular scale can strongly influence their behaviour and lead to effects not anticipated from macroscopic descriptions[22–26]. The dewetting process we observed within the hydrophobic cuff therefore led us to consider the influence of a possible 'hydrophobic gating' process within the TWIK-1 pore, and to ask whether this hydrophobic barrier might contribute to the very low basal levels of ionic currents which these channels appear to conduct. The principle of hydrophobic gating was first demonstrated in MD simulations of model nanopores with hydrophobic constrictions of radius <6 Å where water begins to evaporate and fluctuate between its liquid and vapour states. These fluctuations lead to an effective energy barrier for ion permeation even without physical occlusion of the pore and

© 2014 Macmillan Publishers Limited. All rights reserved.

therefore can function as a 'vapour-lock' gate[23–27]. This type of gating has now been shown to occur in several classes of ion channel including pentameric ligand-gated channels, the prokaryotic mechanosensitive MscS channel and voltage-gated K^+ channels[28–31].

Intriguingly, a previous study showed that the L146D mutation in M2 of TWIK-1 resulted in large currents when expressed in *Xenopus* oocytes[11]. This result is consistent with Leu146 contributing to a hydrophobic barrier within the pore and with disruption of this barrier by the L146D mutation. We therefore examined the water dynamics of a TWIK-1 channel with the L146D mutation during a 100-ns simulation. This mutation markedly altered the behaviour of water within the inner pore, which remained hydrated throughout the simulation (Fig. 4a; Supplementary Fig. 2). However, the L146D mutation introduces a negative charge into the pore. We therefore changed Leu146 to another hydrophilic, but non-charged side chain of similar size (L146N), and repeated the MD simulation. Analysis of water occupancy and density revealed that the L146N mutant also retained water within the inner pore, indicating that this effect is not just the result of introducing a negative charge into the pore (Fig. 4b; Supplementary Fig. 2).

As a further control, we also performed MD simulations of the wild-type (WT) and L146N-mutant TWIK-1 channels using a variety of different force fields. Importantly, dewetting was observed in the WT channel irrespective of the force field used, whereas the L146N-mutant simulations all remained fully hydrated (Supplementary Fig. 3). Furthermore, to determine whether this dewetting process was a result of subtle changes in pore structure during the simulations, we performed additional simulations in which the Cα backbone atoms of the protein were subjected to a soft positional restraint, thus keeping the channel conformation close to that in the crystal structure. For the WT structure, a similar dewetting process was also observed within the first few nanoseconds, followed by intermittent fluctuations of water within the inner cavity, whereas the L146N-mutant pore remained hydrated throughout (Fig. 5a–d). This demonstrates that dewetting of the WT channel is not a consequence of any of the minor structural changes which occur during the simulation. Furthermore, similar to the result seen during simulation of the NavMs sodium channel[32], even though the fenestrations remained open during this restrained simulation of TWIK-1, the alkyl chains of the surrounding lipid bilayer were not long enough to occlude the inner cavity.

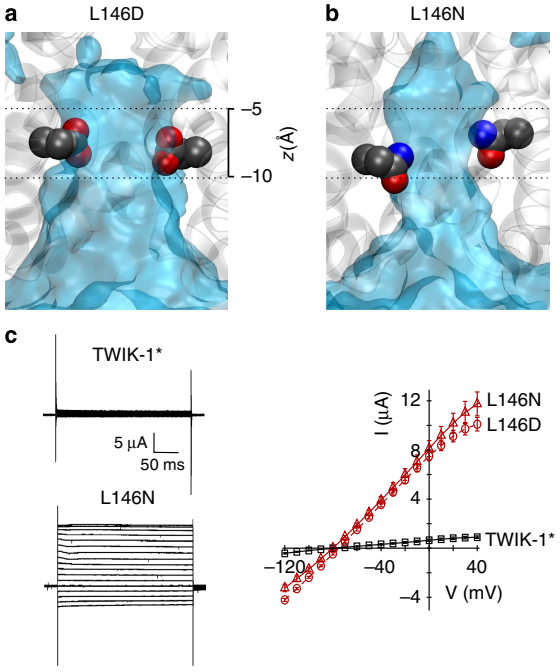

Figure 4 | Mutation of Leu146 hydrates the inner pore. Average water density from a 100-ns MD simulation of: (**a**) L146D and (**b**) L146N mutants. The heavy atoms of the mutant side chains are shown as van der Waals spheres at the end of the MD simulation (see also Fig. 2c). Dashed lines represent approximate position of the hydrophobic cuff (**c**) Left, representative whole-cell currents recorded from the WT TWIK-1* and L146N-mutant channels. Right, averaged current–voltage relationship for whole-cell currents of WT TWIK-1* (black), L146D and L146N TWIK-1* mutants (red) expressed in *Xenopus* oocytes.

Energetics of the hydrophobic barrier. We next reasoned that retention of water within the inner pore by the L146N mutation should also reduce the energetic barrier to the movement of a K^+ ion through the inner cavity. We therefore performed potential mean force (PMF) calculations, which provide an estimate of the free energy profile for the transit of a K^+ ion through the inner pore in equilibrated MD structures for WT and L146N-mutant structures (Fig. 5e). These results show that for the WT TWIK-1 structure there is a steadily increasing barrier to permeation as the ion approaches the hydrophobic cuff from the cytoplasmic entrance (Fig. 5f). This barrier continues towards the selectivity filter due to the associated dewetting of the region above the hydrophobic cuff. However, for the L146N mutation there is an overall reduction in this barrier (by about 4 kT), especially within the deep inner pore in the vicinity of this mutation. This demonstrates that the L146N mutation can directly influence the conduction pathway for K^+ ions.

L146N mutation increases channel activity. The result of these simulations therefore led us to test the effects of the hydrophilic L146N mutation on the functional activity of TWIK-1. To achieve this we used a variant of TWIK-1, which contains a trafficking mutation (I293A/I294A) within the cytoplasmic domain. This trafficking mutation (hereafter referred to as TWIK-1*) has been shown to prevent the endocytic retrieval of TWIK-1, thereby promoting stable expression of TWIK-1 channels within the plasma membrane[11,12]. As shown previously, we found that WT TWIK-1 produces no detectable channel activity when expressed in *Xenopus* oocytes and that the activity of the TWIK-1* mutant is barely detectable above background (Supplementary Fig. 4). This supports previous studies which show that even when TWIK-1 channels can reach the membrane they generally exhibit very low levels of channel activity[10–12].

However, when the L146N mutation was introduced into TWIK-1*, we observed high levels of whole-cell current, similar to reported effects of the L146D mutation (Fig. 4c). This demonstrates that introduction of an uncharged hydrophilic side chain into the hydrophobic inner pore of TWIK channel not only leads to an increase in hydration of the inner cavity *in silico* but also to enhanced whole-cell currents. This result is also consistent with the effects of introducing similar polar side chains into the hydrophobic gate of the MscS channels[29].

Direct effects on the ion conduction pathway. Previous studies have shown that mutation of Leu146 and other residues within M2 do not affect the protein expression levels of TWIK-1* in *Xenopus* oocytes[11]. However, to confirm that the enhancement of

© 2014 Macmillan Publishers Limited. All rights reserved.

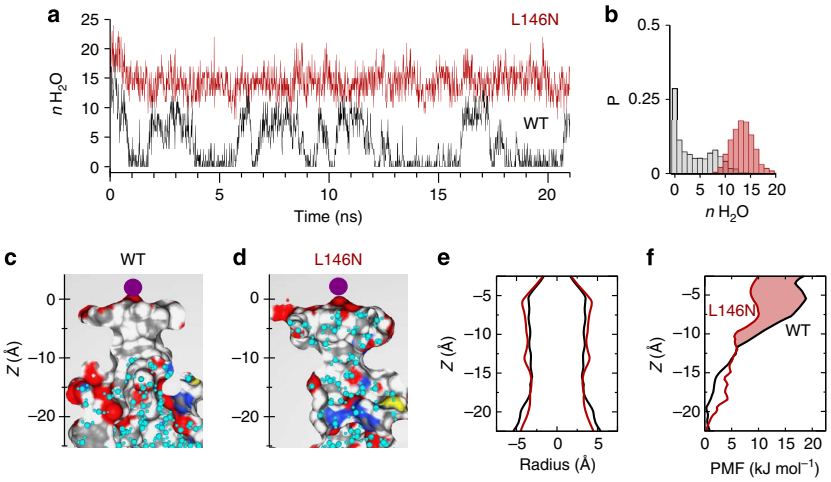

Figure 5 | Positional restraint simulations and energetic profiles. Dewetting precedes structural changes in the inner pore during the soft positional restraint simulation (**a**) Water count within the hydrophobic gate region (as in Fig. 2b) during a positional restraint simulation for WT (black) and L146N (red) sampled every 0.01 ns. Positional restraint with a force constant of 10 KJ mol^{-1} Å^{-2} were applied to the Cα carbons of WT and *in-silico* L146N mutants (**b**) Normalized probability histogram of the water count at the hydrophobic cuff during the positional restraint simulations. This shows that ~30% of the simulation time, there is no water in the hydrophobic region ($\Delta\mu$ $nH_2O_{(L146N-WT)} = 10.37$). (**c**) and (**d**) Cross-section of inner pore of the starting structures for probability mass function calculations where $nH_2O_{(WT)} = 0$ and $nH_2O_{(L146N)} = 12$. (**e**) The starting PMF structures, WT structure (black) and L146N structure (red) have a comparable radius profile. (**f**) Potential mean force profile for a K^+ ion translated along the *z*-axis of the inner pore of WT channel (black) and L146N-mutant channel (red). The shaded red area represents the additional free energy barrier experienced in the WT channel relative to the L146N-mutant within and above the hydrophobic cuff.

whole-cell currents seen with the L146N-mutant channel is primarily due to a direct effect on the structure of the inner pore, we recorded currents in giant excised patches. We have previously used this approach to demonstrate that some K2P channels are sensitive to intracellular block by large quaternary ammonium ions (for example, tetrahexylammonium (THexA)), which bind deep within the inner cavity just below the selectivity filter. This property can then be used as a direct measurement of the structure of the inner cavity which forms part of the conduction pathway[18,19].

We therefore first measured WT TWIK-1* currents in giant excised patches and found the channels to be essentially silent in symmetrical K^+ solutions (Fig. 6a). However, TWIK-1 currents have been shown to be enhanced in the presence of Rb^+ ions[14] and so we measured TWIK-1* currents using Rb^+ as a permeant ion. Under these conditions we were able to record outward currents through WT TWIK-1* channels at depolarized potentials (Fig. 6a,b). These currents were sensitive to block by quinine, a known TWIK-1 inhibitor[7,9], but were insensitive to block by 50-μM THexA (Fig. 6c, Supplementary Fig. 5).

We next measured currents for the L146N-mutant channel and unlike WT TWIK-1*, outward currents could be measured using K^+. These currents were also enhanced by Rb^+ (Fig. 6a). However, in marked contrast to WT TWIK-1*, the L146N channels were blocked >90% by 50-μM THexA and >70% by 1-μM THexA (Fig. 6c). Interestingly, we also observed that the Rb^+ currents through the WT TWIK-1* channel activated at higher voltages compared with the L146N-mutant (Fig. 6b). This result is consistent with the greater electrical driving force required to overcome the energetic barrier created by a hydrophobic versus hydrophilic nanopore[33]. Overall, these results therefore strongly support the idea that the L146N mutation directly influences the conduction pathway deep within the inner cavity.

Polar substitutions at Leu146 increase channel activity. To further support this hypothesis we introduced a series of different hydrophilic and hydrophobic residues at Leu146 and examined their effect upon the functional properties of TWIK-1*. Only very small whole-cell currents could be recorded from WT TWIK-1* channels (Supplementary Fig. 4a). However, we found that when polar substitutions were made at Leu146, very large whole-cell currents could be recorded, but that hydrophobic side chains of varying sizes had no effect (Fig. 7). For example, the hydrophobic substitution L146V is similar to WT TWIK-1*, whereas the isosteric, but hydrophilic threonine substitution (L146T) produces large whole-cell currents equal in size to L146D or L146N. Likewise, while the L146A mutation was similar to wild-type TWIK-1*, large currents were observed with the isosteric, but hydrophilic, L146S mutation (Fig. 7). These results strongly support a direct correlation between the ability to hydrate this inner cavity and the functional activity of TWIK-1.

Other polar substitutions within the hydrophobic cuff. To further validate the role of this hydrophobic cuff, we used identical *in silico* and *in vitro* mutagenesis strategies to examine the other major side chain which contributes to the cuff, that is, Leu261 located on M4. Similar to the results observed for Leu146, we also found that isosteric polar substitutions at Leu261 (L261D and L261N) led to retention of water within the inner pore during MD simulations (Fig. 8a; Supplementary Fig. 2c,d). Importantly, these mutations also produced large whole-cell currents (Fig. 8b,c). Moreover, similar to the effect observed with Leu146, other small but polar substitutions at Leu261 also markedly increased whole-cell current levels, whereas isosteric non-polar mutations did not, for example, L261A versus L261S (Fig. 8c).

To examine the role of this hydrophobic barrier even further, we next introduced mutations at both Leu146 and

© 2014 Macmillan Publishers Limited. All rights reserved.

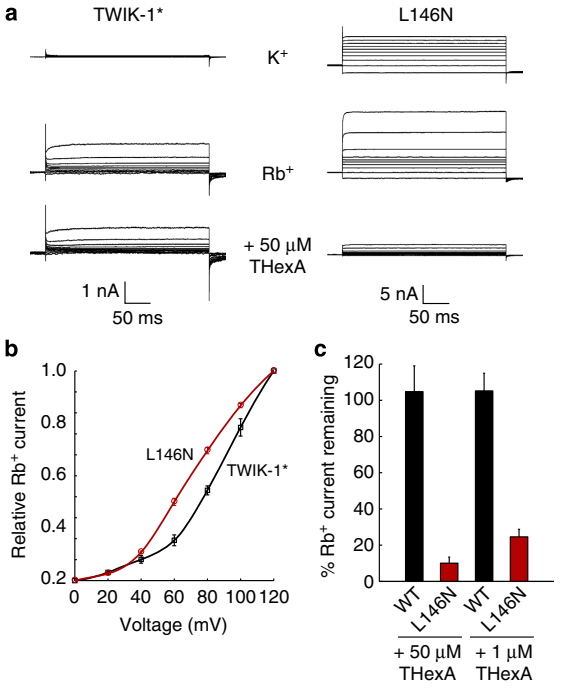

Figure 6 | L146N mutation directly alters conduction pathway. (**a**) Typical currents recorded from giant excised patches expressing WT TWIK-1*. Almost no current can be recorded with K^+ as the permeant ion in the intracellular bath solution. But replacing K^+ in the bath by Rb^+ produced large currents at depolarizing voltages. These TWIK-1* Rb^+ currents are sensitive to block by quinine (not shown), but are not inhibited by 50-µM THexA. Similar recordings of L146N-mutant channels exhibit larger currents with both K^+ and Rb^+ as the permeant ions, but the L146N Rb^+ currents are almost completely inhibited by 50-µM THexA applied intracellularly. (**b**) Voltage dependence of Rb^+ currents for both wild-type TWIK-1* and L146N normalized to activation at +120 mV. Note that L146N currents activate over a lower voltage range. (**c**) Percentage remaining current for WT TWIK-1* and L146N-mutant channels after block by 50-µM and 1-µM THexA; L146N channels exhibit a markedly enhanced sensitivity to THexA.

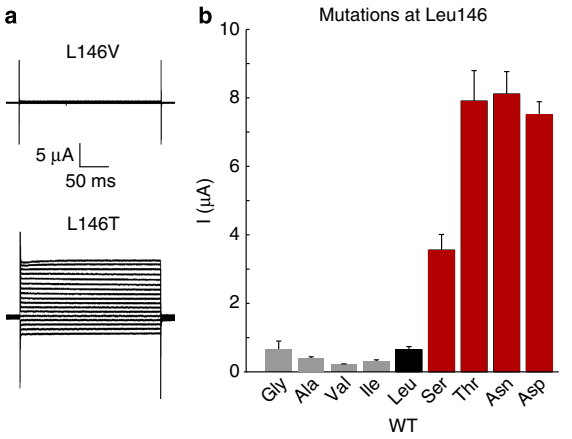

Figure 7 | Representative current traces of TWIK-1* channels with different hydrophilic or hydrophobic substitutions at Leu146. (**a**) Currents were recorded from a series of voltage steps between −120 and +40 mV with a holding potential of −80 mV. (**b**) Mean currents at 0 mV for a range of different of hydrophobic (grey) and hydrophilic (red) substitutions at the Leu146 position (WT TWIK-1* is shown in black).

Leu261, thereby allowing all four main side chains within the cuff to be changed. We found that the double polar substitutions (for example, L146S/L261S) produced large robust currents. However, a double non-polar alanine substitution (that is, L146A/L261A) did not increase currents, and even introduction of two glycines only led to a small enhancement of current levels (Fig. 8d).

Finally, we examined the effect of substitutions at Leu264, which also contributes to the hydrophobic cuff. The side chains of Leu264 are positioned at the interface between the M2 and M4 helices and so are not fully exposed to the conduction pathway; only one of the two δ-methyl groups of each side chain are exposed to the inner pore (Supplementary Fig. 6a). Nevertheless, we found that MD simulations of L264D mutant channels also led to retention of water within the inner pore (Supplementary Fig. 6b). Furthermore, hydrophilic substitutions at this position markedly increased whole-cell currents when compared with isosteric hydrophobic substitutions, consistent with a partial contribution of Leu264 to the hydrophobic nature of the inner pore.

Discussion

Utilizing a combination of computational approaches supported by experimental validation, we now provide evidence that the hydrophobic nature of the TWIK-1 pore restricts full hydration of the inner cavity and that this generates an energetic barrier restricting ion permeation through these channels. These results are therefore consistent with the presence of a hydrophobic gate which is now an emerging concept in the field of ion channel biophysics[23,25–31,34].

We validate this hypothesis by demonstrating, both computationally and functionally, that introduction of hydrophilic groups can directly disrupt this barrier. In particular, we demonstrate that the L146N mutation dramatically enhances the block of TWIK-1* currents by intracellular THexA. These quaternary ammonium ions have been shown to bind deep within the K2P channel pore in a region which would directly be affected by this hydrophobic barrier in TWIK-1 (ref. 18). The reduced voltage dependence of the L146N Rb^+ currents is also consistent with recent experimental studies of the behaviour of ions and water in hydrophobic nanopores, where dewetting can be overcome in a voltage-dependent manner to induce current flow[33,35]. Also the relative hydrophobicity of the nanopores increased the voltage required to induce hydration[33]. This therefore supports our hypothesis that the L146N mutation directly alters the hydrophobicity of the conduction pathway.

The L146N mutation also does not appear to alter regulation of the channel by extracellular pH or to affect inhibition by quinine (Supplementary Fig. 5), and it has been shown that mutation of L146 does not alter the levels of TWIK-1* expression in oocytes[11]. Therefore, although we cannot exclude additional effects of these mutations on other modalities of TWIK-1 channel gating, we conclude that polar substitutions within this hydrophobic cuff increase TWIK-1 currents by directly disrupting this hydrophobic barrier to water and hydrated ions.

Unlike classical tetrameric K^+ channels, the unusual dimeric architecture of the K2P channels places important structural constraints upon the ability of the pore-lining transmembrane helices to form a standard bundle-crossing gate. Evidence already exists that the selectivity filter plays a dynamic role in the control

© 2014 Macmillan Publishers Limited. All rights reserved.

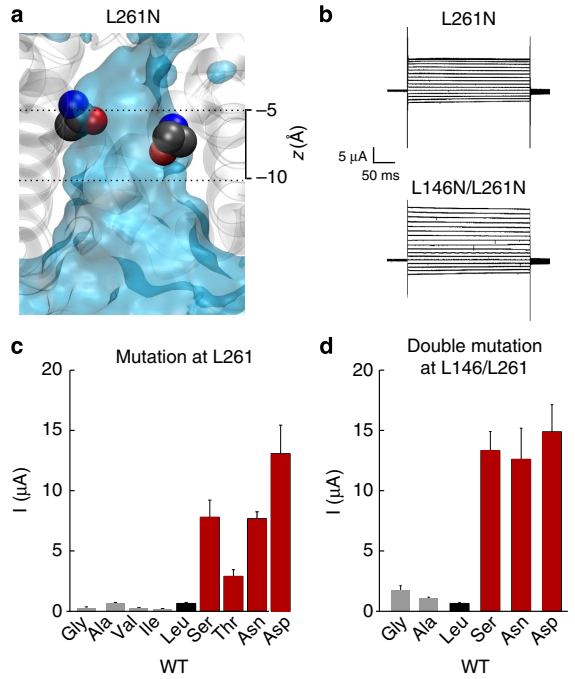

Figure 8 | Hydrophilic substitutions at Leu261 also hydrate the inner pore. (**a**) Average water density of the L261N-mutant channel structure. The heavy atoms of the mutant side chains at the end of the MD simulation are shown as van der Waals spheres (see also Fig. 2c). Dashed lines represent approximate position of the hydrophobic cuff. (**b**) Representative whole-cell currents recorded from L261N and L146N-/L261N-mutant TWIK-1* channels. (**c**) Mean whole-cell currents recorded at 0 mV for a series of hydrophobic (grey) and hydrophilic (red) substitutions at the Leu261 position. WT TWIK-1* is indicated in black. (**d**) Combining mutations at both Leu146 and Leu261 markedly enhances whole-cell currents for hydrophilic, but not hydrophobic substitutions.

of TWIK-1 channel function[5,6,11,14], but the role of additional structures in channel gating were unclear from the initial crystal structure of TWIK-1. Our demonstration that the C-helix remains stable, and that the cytoplasmic mouth of the pore remains open and hydrated in MD simulations, strongly suggests that the cytoplasmic mouth of the pore does not act as a gate as seen in Kv and Kir channels. Instead, our findings suggest that the hydrophobic inner pore of TWIK-1 acts as a strong barrier to ion permeation. In addition to the filter-gating mechanism, this may therefore contribute an additional mechanism to control the flow of ions through this channel.

It has been shown that in some cell types, post-translational sumoylation of Lys274 within the C-helix of TWIK-1 may account for its lack of functional activity[8,9]. However, when TWIK-1 is expressed in *Xenopus* oocytes, this effect still remains controversial[11–13] (Supplementary Fig 4). This does not preclude a role for sumoylation of TWIK-1 in other cell types, but our results clearly demonstrate that the hydrophobic barrier we have identified in this study contributes to the low basal levels of functional activity associated with TWIK-1.

The physiological mechanisms which regulate TWIK-1 currents *in vivo* are still poorly understood and so it is not yet possible to address how modulation of this hydrophobic barrier might occur. However, by analogy to other K2P channels which also possess a large C-terminal cytoplasmic domain connected to the end of the M4 helix[36], it is conceivable that regulatory inputs into this domain could induce subtle movements of the C-helix and pore-lining helices to modulate this hydrophobic barrier. It will also be interesting to examine whether similar hydrophobic barriers may exist in other K2P channels; these leucine residues are not highly conserved in other K2P channels, but there is an isoleucine residue at this position in M2 of THIK-2 and its mutation (I158D) markedly enhances channel activity[37]. Also, hydrophobic, but not polar, substitutions at the equivalent Leu146 position in M2 of the *Drosophila* KCNKØ channel cause reduced channel activity[38].

Hydrophobic barriers and the concept of hydrophobic gating were first observed during MD simulations of model nanopores[23–27]. Subsequently, this process has been shown to play a critical role in the gating of several ligand-gated Cys-loop channels[31,34], prokaryotic mechanosensitive channels[28,29] and even voltage-gated K^+ channels[30]. The biophysical basis of these hydrophobic gates has now been well-characterized; computational studies of Cys-loop channels show that the energy needed to hydrate a hydrophobic gate is greater than the energy needed to solvate an ion at this point, thereby allowing these regions to function as effective barriers to permeation[34]. Furthermore, in model nanopores hydration of the barrier can also be achieved by introduction of polar groups into the gate[27]. Similar results have been observed in both Cys-loop and MscS/MscL channels[28,29,31,34].

The hydrophobic barrier we observe in TWIK-1 may also share some similarities with the deep pore gating mechanisms found in the SK, BK and MthK Ca^{2+}-activated potassium channels[39–43] which also appear to lack a bundle-crossing gate. In summary, we believe that these results not only provide an important insight into the mechanisms which control TWIK-1 K2P channel activity, but also provide further evidence of how the unusual behaviour of water in a confined space is an increasingly important consideration for our understanding of ion channel structure and function.

Methods

MD simulations. The TWIK-1 crystal structure (PDB ID: 3UKM, chains A and B) was used as the starting structure for the simulations. Missing atoms and loops (residues 94–99 between E2 and P1 and residue 169–174 between M2 and M3 (Supplementary Fig. 1) were modelled using Modeller9.9 software[34,44]. The resultant TWIK-1 models were converted to CG (Martini v2.1) representations and CGMD simulations, then run for 500 ns at 323 K to permit the assembly and equilibration of a bilayer containing 298 POPC lipids around the embedded membrane protein[45,46]. The protein and lipids were next converted to atomistic structures using the CG2AT method described previously[47]. The initial system was solvated with simple point charge (SPC) water and 150-mM NaCl. K^+ ions were placed at positions S2 and S4 in the selectivity filter with an additional ion in the inner pore. Two water molecules were also added to the filter at the S1 and S3 positions. Initial atomistic simulations employed the GROMOS96 43a1 force field with SPC water at 323 K. The atomistic system was equilibrated for 1 ns with the non-hydrogen atoms of the protein restrained with a spring constant of 10 KJ mol^{-1} Å^{-2} at constant pressure (1 atm) and temperature, before the 100 ns unrestrained MD simulation with a timestep of 2 fs. Both the 1-ns positional restraint and 100-ns MD simulations were repeated by randomizing initial velocity to obtain two 100-ns simulation. *In silico* mutations were made using pyMOL mutagenesis scripts on the initial atomistic TWIK-1 system. The mutant systems were then energy minimized before the 1-ns positional restraint and 100-ns MD simulations.

To test the sensitivity of our MD findings, we repeated the atomistic simulations using two additional force fields, GROMOS 53A6 with SPC water, and optimized potentials for liquid simulations (OPLS) all-atom protein particles with united atom POPC lipids and TIP4P water. These simulations, along with our initial systems were also simulated at 310 K to also test temperature sensitivity. To determine whether dewetting precedes any alteration in inner pore structure, the Cα atoms were restrained with spring constant of 10 KJ mol^{-1} Å^{-2} and run for another 20 ns.

MD analysis. Snapshots of MD simulations were sampled at every 0.1 ns and visualized using VMD, Chimera or Pymol. HOLE radius profiles were generated

© 2014 Macmillan Publishers Limited. All rights reserved.

using MD analysis and HOLE[48,49]. Water occupancy at the hydrophobic constriction was analyzed by counting the number of water oxygen atoms at a region $-5\,\text{Å} < z < -10\,\text{Å}$ below the S4 ion binding site (Thr117 and Thr225, which define the 0 Å position on the *z*-axis, see Fig. 1). Water occupancy data from two 100-ns simulations were then combined to calculate the mean (μ) *n*H2O values and to generate fractional occupancy histograms. Average water density maps were generated by using the Volmap plugin tool with three-dimensional grids every 0.5 Å for each simulation. The maps were then normalized to bulk water density and visualized at an isovalue of 0.5. Water occupancy of mutant channels were compared with WT by obtaining the difference in mean occupancy values $\Delta\mu$ (Mutant–WT).

Potential mean force calculations. Starting structures for one-dimensional potential mean force calculations were obtained from snapshots at 50 ns of unstrained equilibrium simulations in OPLS all-atom force fields. We picked starting structures which had similar radius profile between WT and L146N-mutant channel, but contained $n\text{H2O} = 0$ for WT and $n\text{H2O} = 12$ for L146N mutant (Fig. 5b). Twenty-five umbrella-sampling windows were produced by placing a K^+ ion every 1 Å in the z direction from bulk water into the inner pore[24]. This K^+ ion was harmonically restrained by a force constant of 10 KJ mol^{-1} Å^{-2} in the z plane and the system was simulated for 1.25 ns. The z position of this K^+ ion, relative to centre-of-mass of the inner pore was sampled every 20 fs. WHAM v2.2 was used to calculate the probability mass function[50].

Molecular biology and electrophysiology. Wild-type and mutant TWIK-1 channel currents were studied by expression in *Xenopus* oocytes. The human TWIK-1 subunit was first cloned into the pBF oocyte expression vector, which adds the 5′ and 3′ untranslated regions of the *Xenopus* β-globin gene, and mutations were introduced by site-directed mutagenesis. The TWIK-1* channel has mutation of a dileucine trafficking motif (I293A/I294A), which permits stable expression in the plasma membrane, and was used as the background 'wild-type' template for all mutations[12]. Messenger RNA was transcribed *in vitro* and 15 ng of either wild-type or mutant subunits were injected. Oocytes were incubated for 12 h at 17 °C in ND96 buffer at pH 7.4 (96 mM NaCl, 2 mM KCl, 2 mM $MgCl_2$, 1.8 mM $CaCl_2$, 5 mM HEPES), followed by a further 12 h in an adjusted ND96 buffer, where all sodium is replaced with potassium[11]. Two-electrode voltage clamp recordings were taken 24 h after injection using an OC-725C Oocyte Clamp amplifier (Warner Instruments), Digidata 1440 interface and pClamp10 software. For the recordings, the oocytes are perfused with the standard ND96 buffer at pH 7.4. A step protocol from −120 mV to +40 mV was used to record the currents for 300 ms, from a holding potential of −80 mV. Excised patch recordings were performed using an Axopatch 200B amplifier. The pipette solutions contained 116 mM KCl, 4 mM NaCl, 1.8 mM CaCl2 and 10 mM HEPES, and the bath solution contained 119 mM KCl, 1 mM NaCl, 2 mM EGTA and 10 mM HEPES. Both solutions were adjusted to pH 7.2. Where indicated, KCl was replaced by RbCl in the bath solution. Currents were recorded in an inside-out configuration, using a step protocol from −100 to +100 mV, with a holding potential of −80 mV.

References

1. Enyedi, P. & Czirjak, G. Molecular background of leak K+ currents: two-pore domain potassium channels. *Physiol. Rev.* **90,** 559–605 (2010).
2. Mathie, A. & Veale, E. L. Therapeutic potential of neuronal two-pore domain potassium-channel modulators. *Curr. Opin. Investig. Drugs* **8,** 555–562 (2007).
3. Es-Salah-Lamoureux, Z., Steele, D. F. & Fedida, D. Research into the therapeutic roles of two-pore-domain potassium channels. *Trends. Pharmacol. Sci.* **31,** 587–595 (2010).
4. Zhou, M. *et al.* TWIK-1 and TREK-1 are potassium channels contributing significantly to astrocyte passive conductance in rat hippocampal slices. *J. Neurosci.* **29,** 8551–8564 (2009).
5. Ma, L., Zhang, X. & Chen, H. TWIK-1 two-pore domain potassium channels change ion selectivity and conduct inward leak sodium currents in hypokalemia. *Sci. Signal.* **4,** ra37 (2011).
6. Goldstein, S. A. K2P potassium channels, mysterious and paradoxically exciting. *Sci. Signal.* **4,** pe35 (2011).
7. Lesage, F. *et al.* TWIK-1, a ubiquitous human weakly inward rectifying K+ channel with a novel structure. *EMBO J.* **15,** 1004–1011 (1996).
8. Plant, L. D. *et al.* One SUMO is sufficient to silence the dimeric potassium channel K2P1. *Proc. Natl Acad. Sci. USA* **107,** 10743–10748 (2010).
9. Rajan, S. *et al.* Sumoylation silences the plasma membrane leak K+ channel K2P1. *Cell* **121,** 37–47 (2005).
10. Wang, W. *et al.* The contribution of TWIK-1 channels to astrocyte K(+) current is limited by retention in intracellular compartments. *Front. Cell. Neurosci.* **7,** 246 (2013).
11. Chatelain, F. C. *et al.* TWIK1, a unique background channel with variable ion selectivity. *Proc. Natl Acad. Sci. USA* **109,** 5499–5504 (2012).
12. Feliciangeli, S. *et al.* Potassium channel silencing by constitutive endocytosis and intracellular sequestration. *J. Biol. Chem.* **285,** 4798–4805 (2010).
13. Feliciangeli, S. *et al.* Does sumoylation control K2P1/TWIK1 background K+ channels? *Cell* **130,** 563–569 (2007).
14. Ma, L., Xie, Y. P., Zhou, M. & Chen, H. Silent TWIK-1 potassium channels conduct monovalent cation currents. *Biophys. J.* **102,** L34–L36 (2012).
15. Brohawn, S. G., del Marmol, J. & MacKinnon, R. Crystal structure of the human K2P TRAAK, a lipid- and mechano-sensitive K+ ion channel. *Science* **335,** 436–441 (2012).
16. Miller, A. N. & Long, S. B. Crystal structure of the human two-pore domain potassium channel K2P1. *Science* **335,** 432–436 (2012).
17. Zilberberg, N., Ilan, N. & Goldstein, S. A. KCNKO: opening and closing the 2-P-domain potassium leak channel entails 'C-type' gating of the outer pore. *Neuron* **32,** 635–648 (2001).
18. Piechotta, P. L. *et al.* The pore structure and gating mechanism of K2P channels. *EMBO J.* **30,** 3607–3619 (2011).
19. Rapedius, M. *et al.* State-independent intracellular access of quaternary ammonium blockers to the pore of TREK-1. *Channels (Austin)* **6,** 473–478 (2012).
20. Braun, A. P. Two-pore domain potassium channels: variation on a structural theme. *Channels (Austin)* **6,** 139–140 (2012).
21. Poulsen, H. & Nissen, P. Structural biology: the inner workings of a dynamic duo. *Science* **335,** 416–417 (2012).
22. Raviv, U., Laurat, P. & Klein, J. Fluidity of water confined to subnanometre films. *Nature* **413,** 51–54 (2001).
23. Hummer, G., Rasaiah, J. C. & Noworyta, J. P. Water conduction through the hydrophobic channel of a carbon nanotube. *Nature* **414,** 188–190 (2001).
24. Beckstein, O. & Tai, K. Sansom MSP. Not ions alone: barriers to ion permeation in nanopores and channels. *J. Am. Chem. Soc.* **126,** 14694–14695 (2004).
25. Beckstein, O. & Sansom, M. S. Liquid-vapor oscillations of water in hydrophobic nanopores. *Proc. Natl Acad. Sci. USA* **100,** 7063–7068 (2003).
26. Sansom, M. S. *et al.* Water in ion channels and pores—simulation studies. *Novartis. Found. Symp.* **245,** 66–78 discussion 79–83, 165–168 (2002).
27. Beckstein, O. *et al.* Ion channel gating: insights via molecular simulations. *FEBS Lett.* **555,** 85–90 (2003).
28. Anishkin, A. *et al.* Hydration properties of mechanosensitive channel pores define the energetics of gating. *J. Phys. Condens. Matter.* **22,** 454120 (2010).
29. Anishkin, A. & Sukharev, S. Water dynamics and dewetting transitions in the small mechanosensitive channel MscS. *Biophys. J.* **86,** 2883–2895 (2004).
30. Jensen, M. O. *et al.* Principles of conduction and hydrophobic gating in K+ channels. *Proc. Natl Acad. Sci. USA* **107,** 5833–5838 (2010).
31. Zhu, F. & Hummer, G. Drying transition in the hydrophobic gate of the GLIC channel blocks ion conduction. *Biophys. J.* **103,** 219–227 (2012).
32. Ulmschneider, M. B. *et al.* Molecular dynamics of ion transport through the open conformation of a bacterial voltage-gated sodium channel. *Proc. Natl Acad. Sci. USA* **110,** 6364–6369 (2013).
33. Powell, M. R. *et al.* Electric-field-induced wetting and dewetting in single hydrophobic nanopores. *Nat. Nanotechnol.* **6,** 798–802 (2011).
34. Zhu, F. & Hummer, G. Pore opening and closing of a pentameric ligand-gated ion channel. *Proc. Natl Acad. Sci. USA* **107,** 19814–19819 (2010).
35. Jiang, X., Huang, J., Sumpter, B. G. & Qiao, R. Electro-Induced dewetting and concomitant ionic current avalanche in nanopores. *J. Phys. Chem. Lett.* **4,** 3120–3126 (2013).
36. Bagriantsev, S. N., Clark, K. A. & Minor, Jr D. L. Metabolic and thermal stimuli control K(2P)2.1 (TREK-1) through modular sensory and gating domains. *EMBO J.* **31,** 3297–3308 (2012).
37. Chatelain, F. C. *et al.* Silencing of the tandem pore domain halothane-inhibited K+ channel 2 (THIK2) relies on combined intracellular retention and low intrinsic activity at the plasma membrane. *J. Biol. Chem.* **288,** 35081–35092 (2013).
38. Ben-Abu, Y., Zhou, Y., Zilberberg, N. & Yifrach, O. Inverse coupling in leak and voltage-activated K+ channel gates underlies distinct roles in electrical signaling. *Nat. Struct. Mol. Biol.* **16,** 71–79 (2009).
39. Bruening-Wright, A., Lee, W. S., Adelman, J. P. & Maylie, J. Evidence for a deep pore activation gate in small conductance Ca2+-activated K+ channels. *J. Gen. Physiol.* **130,** 601–610 (2007).
40. Cox, D. H. & Hoshi, T. Where's the gate? Gating in the deep pore of the BK(Ca) channel. *J. Gen. Physiol.* **138,** 133–136 (2011).
41. Thomson, A. S. & Rothberg, B. S. Voltage-dependent inactivation gating at the selectivity filter of the MthK K+ channel. *J. Gen. Physiol.* **136,** 569–579 (2010).
42. Thompson, J. & Begenisich, T. Selectivity filter gating in large-conductance Ca(2+)-activated K+ channels. *J. Gen. Physiol.* **139,** 235–244 (2012).
43. Shi, N. *et al.* Crucial points within the pore as determinants of K(+) channel conductance and gating. *J. Mol. Biol.* **411,** 27–35 (2011).
44. Sali, A. & Blundell, T. L. Comparative protein modelling by satisfaction of spatial restraints. *J. Mol. Biol.* **234,** 779–815 (1993).
45. Bond, P. J. & Sansom, M. S. Insertion and assembly of membrane proteins via simulation. *J. Am. Chem. Soc.* **128,** 2697–2704 (2006).
46. Scott, K. A. *et al.* Coarse-grained MD simulations of membrane protein-bilayer self-assembly. *Structure* **16,** 621–630 (2008).

© 2014 Macmillan Publishers Limited. All rights reserved.

47. Stansfeld, P. J. & Sansom, M. S. P. From coarse grained to atomistic: a serial multiscale approach to membrane protein simulations. *J. Chem. Theory Comp.* **7,** 1157–1166 (2011).
48. Michaud-Agrawal, N., Denning, E. J., Woolf, T. B. & Beckstein, O. MDAnalysis: a toolkit for the analysis of molecular dynamics simulations. *J. Comput. Chem.* doi:10.1002/jcc.21787 (2011).
49. Smart, O. S. *et al.* HOLE: a program for the analysis of the pore dimensions of ion channel structural models. *J. Mol. Graph.* **14,** 354–360 (1996).
50. Kumar, S. *et al.* The weighted histogram analysis method for free-energy calculations on biomolecules. I. the method. *J. Comput. Chem.* **13,** 1011–1021 (1992).

Acknowledgements

We would like to thank members of the SBCB for their computational expertise as well as Chris Miller for his helpful discussions and comments on the manuscript. This work was supported by grants from the Wellcome Trust, the BBSRC and Pfizer neusentis. P.A. is a Wellcome Trust OXION Training Fellow and F.A-W. is supported by a King's Scholarship from the Malaysian Government.

Author contributions

P.A. performed all computational studies. All other experimental work was performed by F.A-W. and G.B. The study was conceived by P.A. and supervised by M.S.P.S. and S.J.T. All authors were involved in the interpretation of the experimental studies. The manuscript was written by P.A. and S.J.T. with contributions from all other authors. P.A. and F.A-W. contributed equally to this study.

Additional information

Supplementary Information accompanies this paper at http://www.nature.com/naturecommunications

Competing financial interests: The authors declare no competing financial interests.

Reprints and permission information is available online at http://npg.nature.com/reprintsandpermissions/

How to cite this article: Aryal, P. *et al.* A hydrophobic barrier deep within the inner pore of the TWIK-1 K2P potassium channel. *Nat. Commun.* 5:4377 doi: 10.1038/ncomms5377 (2014).

This work is licensed under a Creative Commons Attribution 4.0 International License. The images or other third party material in this article are included in the article's Creative Commons license, unless indicated otherwise in the credit line; if the material is not included under the Creative Commons license, users will need to obtain permission from the license holder to reproduce the material. To view a copy of this license, visit http://creativecommons.org/licenses/by/4.0/

© 2014 Macmillan Publishers Limited. All rights reserved.

Supplementary Information

A Hydrophobic Barrier Deep Within the Inner Pore of the TWIK-1 K2P Potassium Channel

Aryal et al.

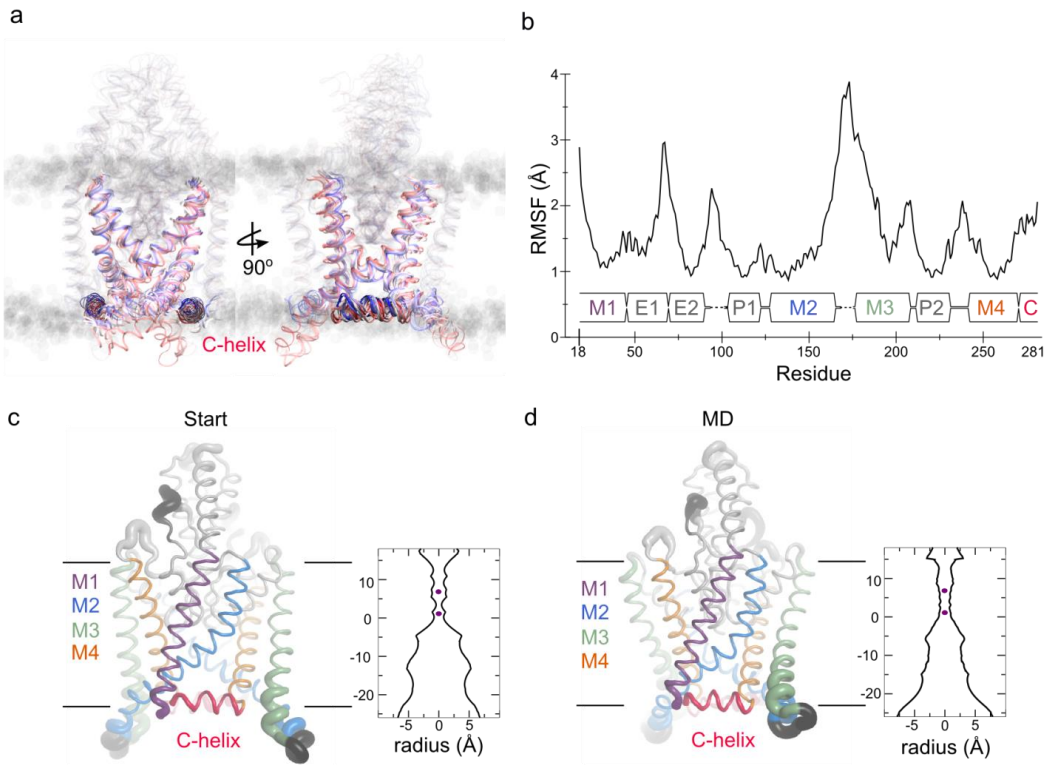

Supplementary Figure 1

TWIK-1 stability during MD simulations in a phospholipid bilayer. (a) Snapshots every 10 ns from a 100 ns MD simulation colored red (start) to blue (end) showing the positions of M2 M4 and the c-helix. Snapshots show the C-helix remains stable and parallel to the membrane. **(b)** Average root mean square fluctuations (RMSF) calculated for backbone atoms of both chains from two 100ns simulations with a schematic of the domain architecture of TWIK-1. Dashed lines represent missing regions of the original 3UKM crystal structure. **(c) left:** Schematic worm representation of the starting structure scaled to depict the range of fluctuations during two 100ns simulations with the TM domains. Largest fluctuations are away from the pore and near regions missing from the crystal structure (shown in black) **right:** radius profile of the ion conduction pathway at the start of MD simulation. The zero position on the z-axis is defined by the position of Thr117 and Thr225 which form the S4 binding site **(d) Left:** Worm representation of the average coordinates of the protein from 2x 100 ns MD simulations. **Right:** average radius during the MD simulation.

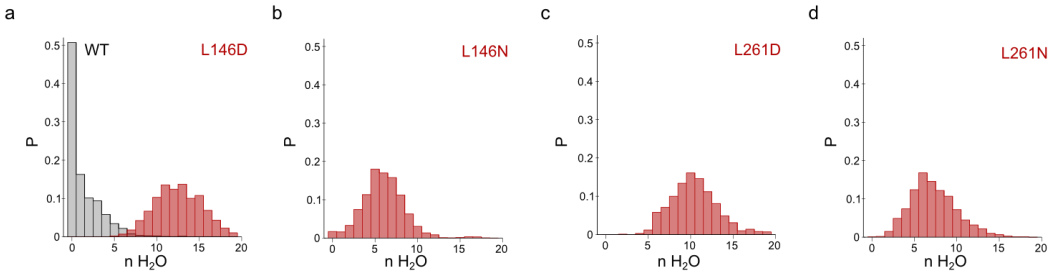

Supplementary Figure 2

Isosteric hydrophilic substitutions in the hydrophobic cuff of TWIK-1 increase water occupancy. Normalized histogram of water molecules present within the hydrophobic cuff region for two 100ns MD simulations sampled every 0.1 ns for **(a)** L146D (μ nH_2O = 13.2) overlaid on those for the WT simulation (grey, taken from Fig. 2c), **(b)** L146N (μ nH_2O = 6.97), **(c)** L261D (μ nH_2O =11.41), and **(d)** L261N (μ nH_2O = 9.44). For each mutant there is a large increase in the number of waters present and this region remains hydrated throughout the simulation. This contrasts to the WT channel where the average nH_2O is 1.95, and water is absent >50% of the time.

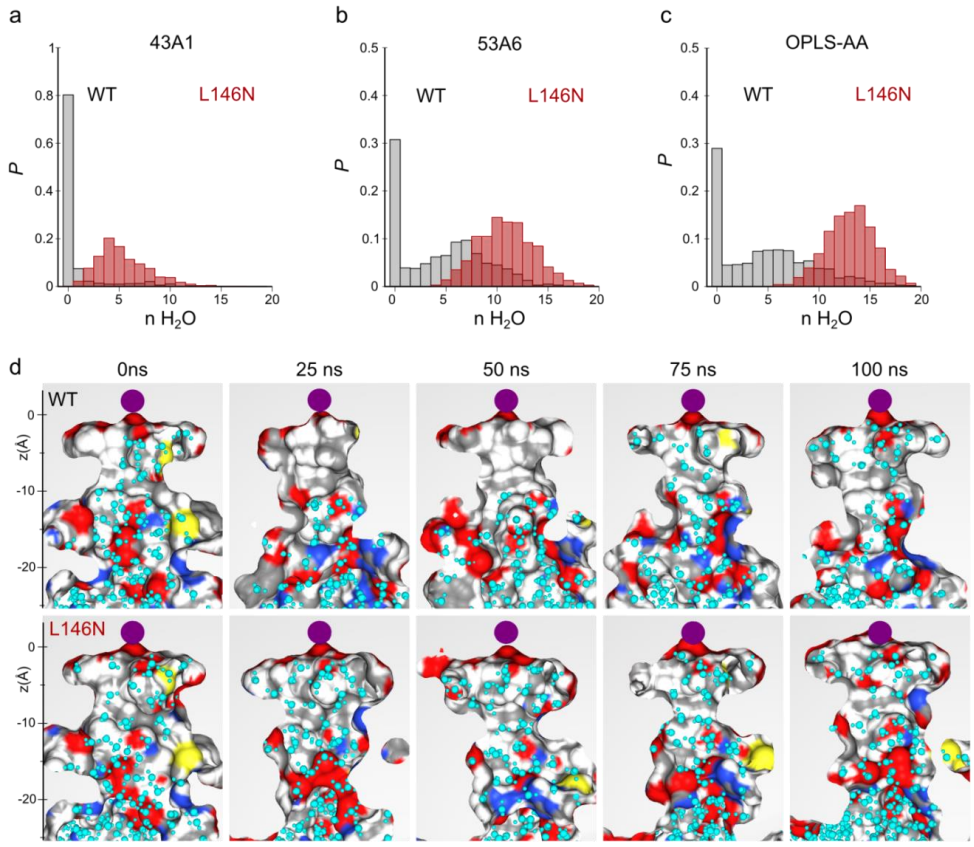

Supplementary Figure 3

Dewetting of the hydrophobic inner pore in different force fields. The principal findings of our simulations are reproducible in several different force fields. Normalized histograms of water within the hydrophobic cuff are shown for 100 ns MD simulations of WT and L146N mutants at 310K in **(a)** Gromos 43A1 with SPC water ($\Delta\mu$ nH_2O $_{(L146N-WT)}$ = 5.25) **(b)** 53A6 with SPC water ($\Delta\mu$ nH_2O $_{(L146N-WT)}$ = 6.5, and **(c)** the OPLS all atom force field with TIP4P water ($\Delta\mu$ nH_2O $_{(L146N-WT)}$ = 8.4. For each force field there is a large increase in the number of waters present for L146N mutant vs WT ($\Delta\mu$ nH_2O >5), and L146N mutant channels remains hydrated through the simulations. (**d**) Snapshots of sections through the inner pore during MD simulation using the OPLS all atom force field with TIP4P water for both WT TWIK-1 and L146N mutant structures. Dewetting of the inner pore is visible in the WT TWIK-1, but not the mutant L146N channel. Quantification of this effect is shown in panel (c). Note that in both structures the cytoplasmic mouth of the inner pore is hydrophilic and remains hydrated throughout the simulations.

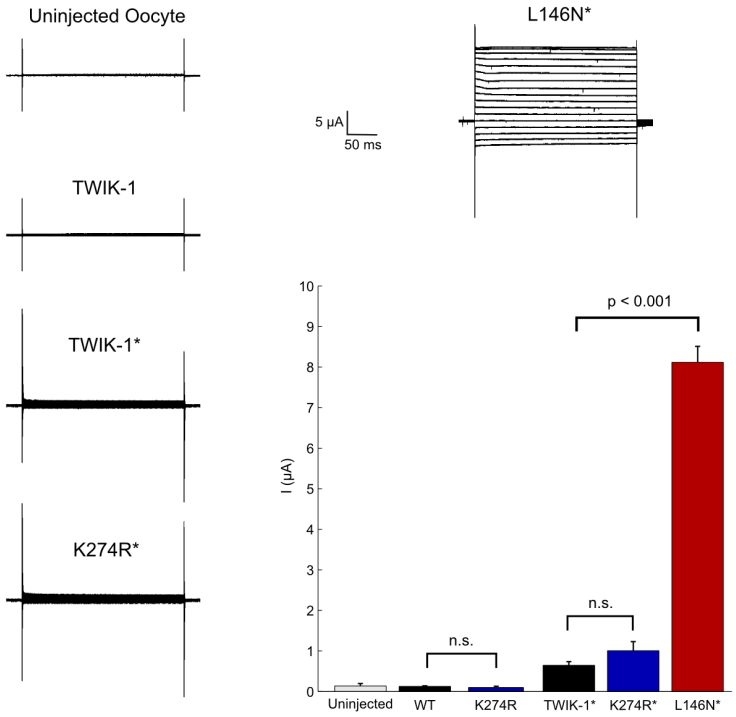

Supplementary Figure 4.

Mutation of Leu146 increases whole-cell currents. Representative whole-cell currents are shown for an uninjected oocyte and from oocytes expressing wild-type TWIK-1 or the trafficking mutant TWIK-1* (i.e. I293A/I294A) which prevents rapid endocytosis from the membrane (refs 10, 11). Currents recorded from wild-type TWIK-1 are not significantly different from uninjected oocytes. Very small currents (<0.5 µA) can be recorded from the wild-type TWIK-1* channels whereas the L146N TWIK-1* mutant channels (L146N*) express large whole-cell currents. When expressed in oocytes, the K274R mutation in WT TWIK-1 (which prevents sumoylation of Lys274) does not produce any increase in currents, nor does it produce any significant increase in the TWIK-1* mutant channel which is stable within the membrane (K274R*), therefore factors other than sumoylation must be responsible for the low levels of TWIK-1* basal currents in oocytes. All whole cell currents shown were recorded in ND 96 bath solution using voltage steps from -120 mV to +40 mV from a holding potential of -80 mV. Averaged currents values were measured at 0 mV and significance measured using a paired students t-test.

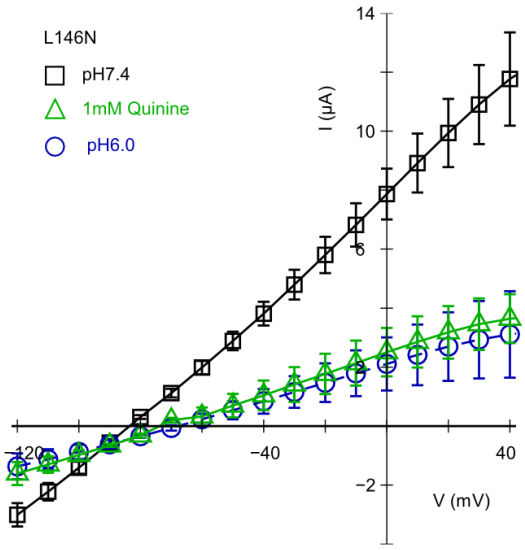

Supplementary Figure 5.

Mutation of Leu146 does not affect inhibition by quinine or external pH. Whole-cell currents recorded from L146N TWIK-1* mutant channels. Wild-type TWIK-1 can he inhibited by external acidification and quinine (refs. 5, 7, 9, 10). Here we show that the L146N mutant channels still exhibit inhibition by external acidification as well as application of 1 mM quinine. This demonstrates that mutations within the hydrophobic cuff do not affect the external pH-gating machinery which is thought to reside close to or within the selectivity filter.

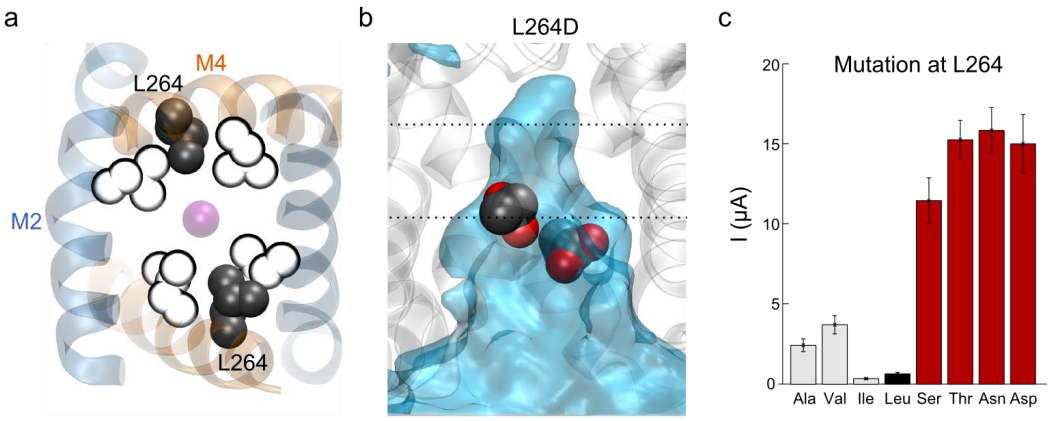

Supplementary Figure 6.

Leu264 also contributes to the hydrophobic cuff. (**a**) bottom-up view of the hydrophobic cuff with Leu264 shown in grey. Leu146 and Leu261 are shown (in white) as in Fig. 3b. Leu264 (in grey) is at the interface between M2 and M4 and only one δ-methyl group of the Leu264 side chain is exposed to the inner pore. (**b**) Average water density of the L264D mutant simulation represented as in Fig. 4a. (**c**) Mean currents at 0 mV of series of hydrophobic (grey) and hydrophilic (red) substitutions at Leu264 in TWIK-1*.

Supplementary Movie 1

Dewetting of the TWIK-1 inner pore. Snapshots of water molecules (cyan) inside the inner pore of TWIK-1 channel taken every 0.1 ns during a 100 ns MD simulation. For orientation, the K^+ ion at the bottom of the selectivity filter (S4) is shown as a purple sphere for orientation. Water loss is seen deep within the inner pore, but not at the cytoplasmic mouth of the channel.

ARTICLE ADDENDUM

Channels 9:1, 44–49; January/February 2015; Published with license by Taylor & Francis Group, LLC

Appendix E

Influence of lipids on the hydrophobic barrier within the pore of the TWIK-1 K2P channel

Prafulla Aryal[1,2,3], Firdaus Abd-Wahab[1], Giovanna Bucci[1], Mark SP Sansom[2,3,*], and Stephen J Tucker[1,3,*]

[1]Clarendon Laboratory, Department of Physics; University of Oxford; Oxford, UK; [2]Department of Biochemistry; University of Oxford; Oxford, UK; [3]OXION Initiative in Ion Channels and Disease; University of Oxford; Oxford, UK

Downloaded by [Radcliffe Infirmary] at 01:17 05 October 2015

Keywords: hydrophobic gating, K2P channel, lipid, Potassium channel, TWIK-1

© Prafulla Aryal, Firdaus Abd-Wahab, Giovanna Bucci, Mark SP Sansom, and Stephen J Tucker

*Correspondence to: Mark SP Sansom; Email: mark.sansom@bioch.ox.ac.uk; Stephen J Tucker; Email: stephen.tucker@physics.ox.ac.uk

Submitted: 10/23/2014

Accepted: 10/24/2014

http://dx.doi.org/10.4161/19336950.2014.981987

Addendum to: Aryal P, Abd-Wahab F, Bucci G, Sansom MSP, Tucker SJ. A hydrophobic barrier deep within the inner pore of the TWIK-1 K2P potassium channel. Nature Communications 2014; 5:4377.

This is an Open Access article distributed under the terms of the Creative Commons Attribution License (http://creativecommons.org/licenses/by/3.0/), which permits unrestricted use, distribution, and reproduction in any medium, provided the original work is properly cited. The moral rights of the named author(s) have been asserted.

Several recent ion channel structures have revealed large side portals, or 'fenestrations' at the interface between their transmembrane helices that potentially expose the ion conduction pathway to the lipid core of the bilayer. In a recent study we demonstrated that functional activity of the TWIK-1 K2P channel is influenced by the presence of hydrophobic residues deep within the inner pore. These residues are located near the fenestrations in the TWIK-1 structure and promote dewetting of the pore by forming a hydrophobic barrier to ion conduction. During our previous MD simulations, lipid tails were observed to enter these fenestrations. In this addendum to that study, we investigate lipid contribution to the dewetting process. Our results demonstrate that lipid tails from both the upper and lower leaflets can occupy the fenestrations and partially penetrate into the pore. The lipid tails do not sterically occlude the pore, but there is an inverse correlation between the presence of water within the hydrophobic barrier and the number of lipids tails within the lining of the pore. However, dewetting still occurs in the absence of lipids tails, and pore hydration appears to be determined primarily by those side-chains lining the narrowest part of the pore cavity.

Introduction

Ion channels are dynamic transmembrane proteins that reside within phospholipid bilayers. Thus a full understanding of their functional properties not only relies upon our knowledge of the channel structure itself, but also on those interactions which occur between the channel and its lipid environment.[1-3] There is now an increasing body of evidence that the interaction of membrane lipids with many classes of transmembrane proteins, including many ion channels, can profoundly influence their structure and function. Indeed, recent advances in X-ray crystallography,[4] mass spectrometry[5] and molecular dynamics simulations[6] have now been able to define these interactions with a high degree of accuracy and prediction.

The overall structural organization of most ion channels means that the sites which interact with membrane lipids typically reside on the outer surfaces of the protein. However, recent structures of several sodium and potassium channels have revealed relatively large side portals or 'fenestrations' between the transmembrane helices of these proteins.[7-9] These fenestrations connect the transmembrane pore to the lipid bilayer. In the case of the voltage-gated sodium channel the fenestrations are thought to be important for the access of lipophilic molecules such as local anesthetics into the ion conduction pathway.[9-11]

Fenestrations are also present in crystal structures of the K2P (*KCNK*) family of potassium channels.[7,8,12] These channels contain 2 pore domains per subunit and assemble as dimers to form a pseudo-tetrameric K^+ channel pore, thereby resembling other (tetrameric) potassium channels.[13] However, unlike most tetrameric K^+ channels they are not thought to gate via constriction of a cytoplasmic bundle-crossing gate.[14-17] The 2 pore-

Downloaded by [Radcliffe Infirmary] at 01:17 05 October 2015

lining helices (M2 and M4) are different in sequence and asymmetrical in their architecture. This asymmetry results in a gap at their interface that potentially exposes the central ion conduction pathway to the hydrophobic core of the lipid bilayer. Furthermore, in the crystal structure of TWIK-1, 2 tubular regions of electron density within the inner pore were attributed to alkyl chains, and it was proposed that these might represent co-purified lipids.[8] This led to a hypothesis that lipid tails within this section of the inner pore of the related TRAAK channel might be involved in channel gating via their insertion into the fenestrations and steric obstruction of the ion conduction pathway.[18] It was suggested that movement of lipid tails within the fenestrations might represent a mechanism for the direct sensing of mechanical tension in stretch-activated K2P channels.[18]

In order to understand the dynamic structural behavior of the TWIK-1 channel we recently performed molecular dynamics simulations of the TWIK-1 crystal structure in a phospholipid bilayer.[19] Interestingly, we observed that the inner pore of the channel was highly hydrophobic, and therefore prone to dewetting which creates a hydrophobic barrier within the ion conduction pathway.[20] The hydrophobic 'cuff' which forms this energetic barrier is comprised of leucine sidechains. We found that substitution of these residues with isosteric polar side-chains not only resulted in full wetting of the pore *in silico,* but also correlated with increased functional activity of the channel.[19]

We also reported that the fenestrations in TWIK-1 were dynamic and capable of closing during our simulations, but that when the fenestrations were open, the alkyl tails of the surrounding phospholipid bilayer were able to enter the fenestrations, though not far enough to sterically occlude the inner pore.[19] Interestingly, similar observations have been reported for MD simulations of prokaryotic voltage-gated sodium channel structures where it was found that lipid tails could also penetrate the fenestrations.[10,21]

However, even without steric occlusion of the inner pore, the presence of lipid tails within the fenestrations might be expected to contribute to the hydrophobicity of the TWIK-1 inner pore cavity and so influence the dewetting process. Therefore, to investigate the contribution of the surrounding lipids to the hydrophobic barrier in the TWIK-1 pore, we have now carried out longer simulations of TWIK-1 in a POPC lipid bilayer. Here we describe the dynamics of the interactions between the channel protein, membrane lipids, and the hydrophobic barrier.

Results and Discussion

Two distinct fenestrations within TWIK-1

Molecular surface representations of the TWIK-1 crystal structure reveal that the fenestration at the interface between subunits can be divided into 2 distinct regions we term the 'upper' and 'lower' fenestrations (**Fig. 1A**). This division is formed by the side chains of L146 on M2 and L264 on M4 (**Fig. 1B**). Interestingly these residues, along with L261, contribute to the hydrophobic cuff that promotes dewetting of the inner pore.[19] The upper fenestration is at the interface of the M2/M4 helices and is above the hydrophobic cuff. Tubular electron density was resolved in the crystal structure. This is thought to represent two 11-carbon alkyl chains penetrating the upper fenestrations and inner pore, (**Fig. 1B, C**).[8] The lower fenestration is between the hydrophobic cuff and the C-helix at the cytoplasmic entrance to the pore (**Fig. 1A, B**).

The TWIK-1 structure was embedded in a POPC (1-palmitoyl-2-oleoyl-*sn*-glycero-3-phosphocholine) bilayer and 2 simulations run, each for 200 ns. In our previous study we observed dewetting of the inner pore irrespective of whether the backbone was restrained or not.[19] Therefore, to ensure the fenestrations remained open and accessible throughout the simulations, a positional restraint was imposed on the Cα-atoms of the protein backbone. POPC was chosen because it represents a typical phospholipid containing both a saturated (palmitoyl, C16:0) and an unsaturated (oleoyl, C18:1) alkyl tail, and is routinely used for MD simulations of membrane proteins.

Interestingly, we found that throughout these simulations the upper fenestration was located at approximately the center of the bilayer. Consequently, tails of POPC lipids from both the inner and the outer-leaflet were able to line the subunit interface and upper fenestration, but were not long enough to fully penetrate and occlude the inner cavity (**Fig. 1C**). This suggests that direct lipid block of the inner pore is unlikely. However, some mammalian saturated phospholipids have tails up to 24 carbons in length,[22] and it remains possible that such longer phospholipid tails might penetrate further through the upper fenestration. It is interesting to note that the TWIK-1 crystal structure was solved using protein isolated from *Pichia pastoris* and that yeast contain very long (26:0) phosphosphingolipids.[22,23]

In marked contrast however, the lower fenestration is located near the middle of the inner leaflet, making it a more accessible portal for lipid tail entry (**Fig. 1A, C**). We observed that lipids tails from the inner leaflet occupied the lower fenestrations throughout the entire duration of the 200 ns simulation. Both the unsaturated oleoyl and the saturated palmitoyl lipid tails of POPC were able to occupy this fenestration. Lipid tails were capable of entering the inner cavity just below the hydrophobic cuff. However, they did not penetrate far enough to occlude the ion conduction pathway (**Fig. 1D**).

Influence of lipids on the hydrophobic barrier

Our previous study demonstrated that dewetting of the hydrophobic barrier deep within the inner pore of TWIK was dependent upon the relative hydrophobicity of the surface lining the pore.[19] Consequently, if the alkyl tails of the lipids are capable of entering the fenestrations and penetrating into the cavity then it might be anticipated that they could also influence the hydrophobic barrier in TWIK-1. We therefore next examined the correlation between the presence of such lipid tails and the behavior of water within the hydrophobic cuff.

Consistent with our previous studies, we observed dewetting of the hydrophobic inner pore of TWIK-1 within the first few nanoseconds of the simulation and this was concurrent with lipid tails entering

Downloaded by [Radcliffe Infirmary] at 01:17 05 October 2015

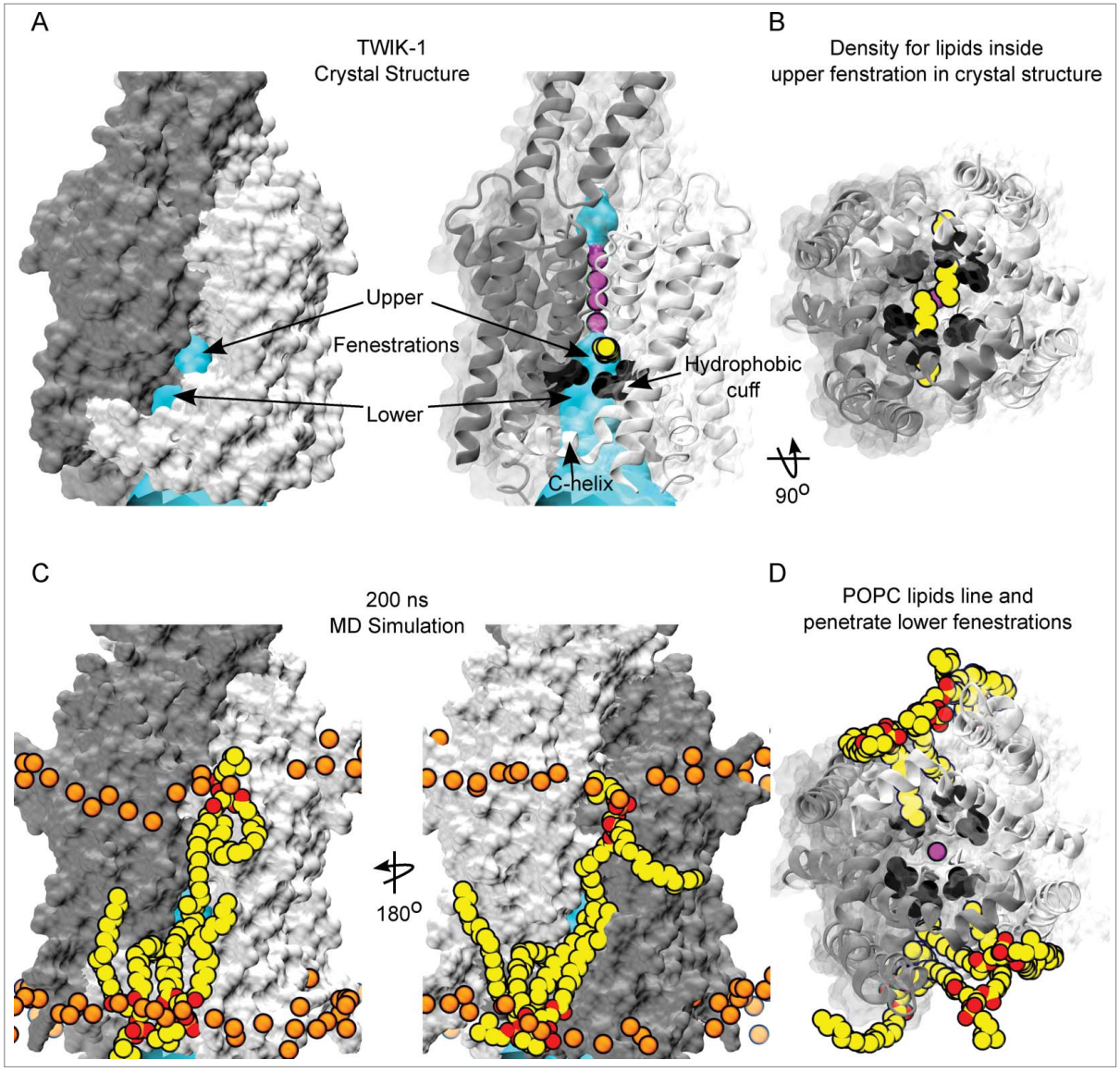

Figure 1. Interaction of lipids with the fenestrations of TWIK-1. (**A**) (left) Molecular surface representation of TWIK-1 crystal structure subunit interface shows 2 distinct gaps, termed upper and lower fenestrations. The channel is colored by subunit, with cyan HOLE surface depicting the ion conduction pathway. (right) Cartoon representation of the TWIK-1 crystal structure with side chain atoms of L146, L264 and L261 of the hydrophobic-cuff shown as black spheres. The upper fenestration is at the interface of pore-lining helices at the subunit interface, electron density attributed to alkyl chains (yellow) was found below selectivity filter (purple K^+ ions) and above the hydrophobic cuff, whereas the lower fenestration is below the hydrophobic cuff. (**B**) A bottom up view of the inner-pore of the TWIK-1 crystal structure shows that the alkyl chains found inside the upper fenestrations block the ion conduction pathway. (**C**) Relative position of the POPC lipids on the subunit interface of TWIK-1 at the end of a 200ns MD simulation of the channel embedded in a POPC bilayer. TWIK-1 is shown as in A; Carbons atoms of POPC are colored yellow, oxygen red and nitrogen blue. Phosphorus atoms of the bilayer lipids are shown as spheres and colored orange for orientation. The upper fenestration is approximately at the center of the bilayer, and lipid tails from both the upper and lower leaflet can approach the upper fenestration, but do not penetrate the cavity. By contrast, lipid tails fully occupy the lower fenestrations. (**D**) A bottom up view of the pore at the end of the MD simulation showing lipid tails from the lower leaflet occupying both of the lower fenestrations, with one lipid tail penetrating the pore.

the fenestration and thereby forming part of the lining of the pore (**Fig. 2A and B**). We also observed liquid-vapor transitions and fluctuating lipid penetration into the pore lining throughout the simulations (**Fig. 2A and B**).

We next compared the number of water molecules within the hydrophobic cuff, with the number of lipid carbon atoms present in the pore and its lining (**Fig. 2B**). Although both processes were subject to fluctuations, their time series

Downloaded by [Radcliffe Infirmary] at 01:17 05 October 2015

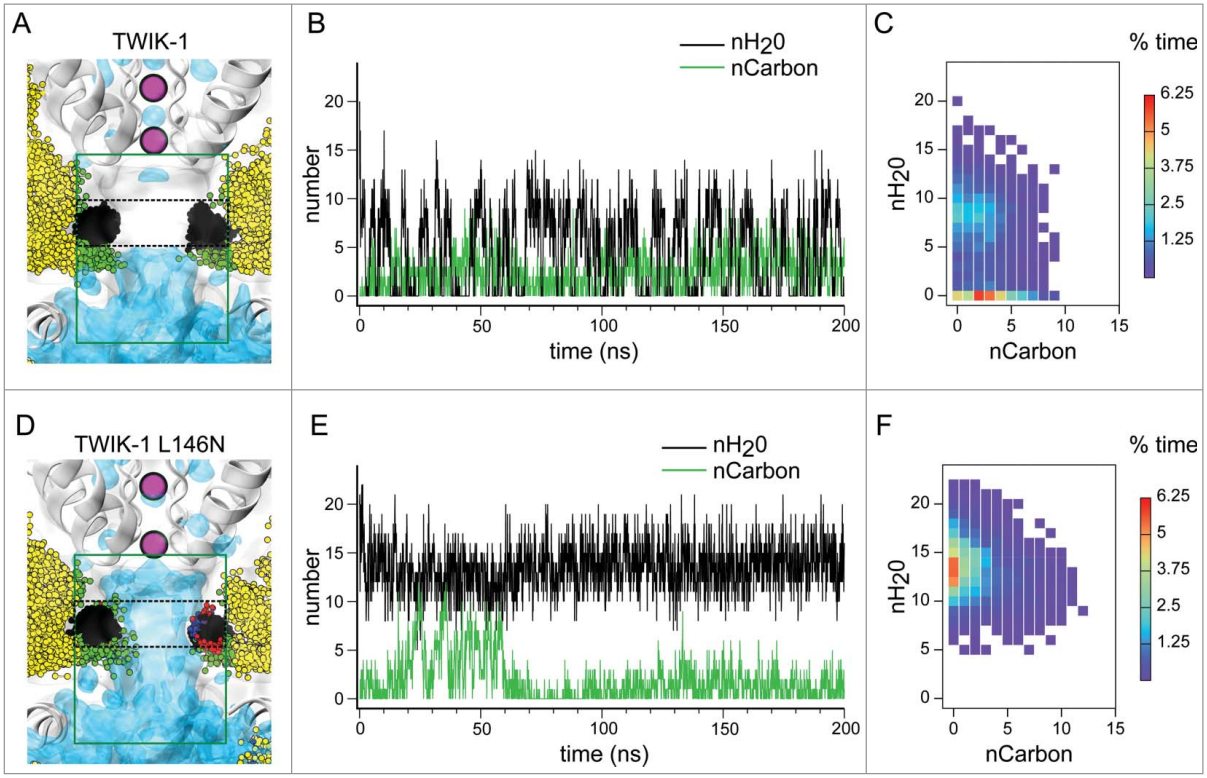

Figure 2. Influence of lipid tails in the ion conduction pathway of TWIK-1. (**A**) Average water density from a 200ns simulation inside the TWIK-1 ion conduction pathway. Snapshots (taken every 1ns) of lipid residues lining the pore, as well as the snapshots of the L146 and L264 sidechains from both subunits, are depicted as ball and sticks. Lipid carbon atoms lining and entering the pore (as defined by the green box) are colored green, whereas carbons outside of the lining are colored yellow. Carbons of the L146 and L264 side-chains are shown in black. Black dashes indicate the region within the green box used to count the number of waters within the hydrophobic cuff. The selectivity filter containing purple K^+ ions and C-helix at the start of the simulation are shown for orientation. (**B**) Number of water molecules within the hydrophobic cuff (black) taken every 0.1 ns during a 200 ns MD simulation. Also shown are the number of lipidic carbon atoms (green) which enter the pore cavity as defined by the green box in panel A. (**C**) Correlation heat map for the 2 traces shown in panel B. Data shown as percent of time. (**D–F**) As above but for the L146N mutant channel. Oxygen and nitrogen atoms colored red and blue respectively.

suggests some correlation between dewetting of the hydrophobic barrier and the presence of lipid tails exposed to the pore. We therefore generated a correlation heatmap; this shows that although dewetting can occur when lipids are completely absent from the cavity, the highest instance of dewetting occurs when 2 or 3 lipid tail carbons are present in the mouths of the fenestrations which line the central cavity (**Fig. 2C**).

Our previous study demonstrated that dewetting of the cavity was profoundly influenced by the hydrophobicity of residues within the hydrophobic cuff. For example, the L146N mutation was found to induce full hydration of the inner cavity.[19] We therefore examined 2 identical simulations of the L146N mutant channel structure. Interestingly, we observed that during the first 60 ns of the simulation up to 12 lipid carbon atoms penetrated into the cavity of the L146N mutant, but the cavity remained hydrated throughout the entire simulation (**Fig. 2D, E**). Furthermore, we found a decrease in the percent occupancy of carbons in the pore (35% for the L146N mutant vs 55% for WT in two 200ns simulations) (**Fig. 2F**). Therefore, polar substitutions in the hydrophobic cuff not only prevent dewetting of the cavity, but also decrease the overall occupancy of lipids.

In summary, these simulations demonstrate that the terminal carbons of the surrounding lipids can penetrate the fenestrations of TWIK-1 and contribute to the lining of the inner cavity, but not far enough to sterically occlude the pore. The presence of lipids within the fenestrations also influences the relative hydrophobicity of the surface lining the inner pore, and dewetting occurs most frequently when lipid tails line the cavity. However, dewetting still occurs in the absence of such lipid tails, and it is the relative hydrophobicity of residues at the narrowest constriction point (i.e. the hydrophobic barrier) that primarily determines the hydration status of the inner pore.

Future simulations with more physiological lipid head-group compositions, and mixed lipid tail length are clearly needed to fully understand the behavior of TWIK-1 and other K2P channels in complex bilayers. Hydrophobic lipid tails

might still regulate TWIK-1 channel activity by influencing this hydrophobic barrier. However, only long lipid tails (e.g. $\geq$24 carbon[22]) might be able to directly occlude the inner pore. TREK-1 and TRAAK channels retain their mechanosensitivity when reconstituted into a bilayer consisting primarily of 16 and 18 carbon lipid chains.[24] Therefore, mechanogating by dynamic modulation of a lipid block within the conduction pathway appears unlikely. Nevertheless, it remains possible that the presence of lipid tails within the fenestrations might influence the biophysical properties of ion conduction, as well as more global conformational changes involving movement of the transmembrane helices and closure of the fenestrations.[12,25]

In complex cellular membranes, K2P channel function is clearly affected by the composition of the surrounding lipids,[26-28] and lipid composition can vary dramatically between different intracellular organelles.[23] It is therefore possible that the interaction of different physiological lipids, and even lipophilic drugs with these fenestrations remains a potential mechanism for the control of K2P channel activity.

Methods

Molecular dynamics simulations were similar to those described previously.[19] Briefly, missing atoms and loops were modeled into the TWIK-1 crystal structure (PDBID: 3UKM).[8] To embed the protein into a bilayer, the structure was converted into coarse grain representation (Martini v2.1) and embedded into a POPC bilayer by running coarse grain self-assembly and equilibration simulations for 500 ns. The resultant protein embedded in a bilayer containing 212 POPC lipids was then converted into atomistic structure using the CG2AT method.[29,30] Atomistic simulations reported here employed GROMOS 53A6 with SPC water and 150 mM KCl. K^+ ions were placed at positions S2 and S4 in the selectivity filter with an additional ion in the inner pore. Two water molecules were also added to the filter at the S1 and S3 positions. Then 200 ns equilibration simulations were run at constant pressure (1 atm) and temperature (310K) with Cα atoms of the protein restrained with spring constant of 10 KJ mol^{-1} $Å^{-2}$. The simulations were repeated by randomizing the initial velocity to obtain two 200 ns simulations for TWIK-1 WT protein. Two additional 200 ns simulations were run for the L146N *in-silico* mutant, where both of the L146 residues of the dimer were mutated to asparagine using pyMOL mutagenesis script on the initial TWIK-1 WT system. HOLE radius profiles were generated using MD analysis and HOLE.[31] Average water density maps were generated by using the Volmap plugin tool with 3-dimensional grids every 0.5 Å for each simulation. The maps were then normalized to bulk water density and visualized at an isovalue of 0.5. Water occupancy at the hydrophobic constriction was analyzed by counting the number of water oxygen atoms in a box of 20 $\times$ 20 $\times$ 5 Å located -5 Å$<z<-10$ Å below the S4 ion binding site (Thr117 and Thr225, which define the 0 Å position on the *z*-axis, whereas the number of carbon atoms were counted in a box 20 $\times$ 20 $\times$ 20 Å below the S4 ion binding site using vmd tcl script.

Disclosure of Potential Conflicts of Interest

No potential conflicts of interest were disclosed.

Acknowledgments

We would like members of the SBCB for their computational expertise and helpful comments on the manuscript.

Funding

This work was supported by grants from the Wellcome Trust, the BBSRC and Pfizer Neusentis. P.A. is a Wellcome Trust OXION Training Fellow and F.A-W is supported by a King's Scholarship from the Malaysian Government.

References

1. Yeagle PL. Non-covalent binding of membrane lipids to membrane proteins. Biochimica et Biophysica Acta 2014; 1838:1548-59; PMID:24269542; http://dx.doi.org/10.1016/j.bbamem.2013.11.009
2. Tucker SJ, Baukrowitz T. How highly charged anionic lipids bind and regulate ion channels. J. Gen Physiol 2008; 131:431-8; http://dx.doi.org/10.1085/jgp.200709936
3. Logothetis DE, Petrou VI, Zhang M, Mahajan R, Meng XY, Adney SK, Cui M, Baki L. Phosphoinositide Control of Membrane Protein Function: A Frontier Led by Studies on Ion Channels. Ann Rev Physiol 2014; PMID: 25293526; http://dx.doi.org/10.1146/annurev-physiol-021113-170358
4. Whorton MR, MacKinnon R. Crystal structure of the mammalian GIRK2 K+ channel and gating regulation by G proteins, PIP2, and sodium. Cell 2011; 147:199-208; PMID:21962516; http://dx.doi.org/10.1016/j.cell.2011.07.046
5. Laganowsky A, Reading E, Allison TM, Ulmschneider MB, Degiacomi MT, Baldwin AJ, Robinson CV. Membrane proteins bind lipids selectively to modulate their structure and function. Nature 2014; 510:172-5; PMID:24899312; http://dx.doi.org/10.1038/nature13419
6. Schmidt MR, Stansfeld PJ, Tucker SJ, Sansom MS. Simulation-based prediction of phosphatidylinositol 4,5-bisphosphate binding to an ion channel. Biochem 2013; 52:279-81; http://dx.doi.org/10.1021/bi301350s
7. Brohawn SG, del Marmol J, MacKinnon R. Crystal structure of the human K2P TRAAK, a lipid- and mechano-sensitive K+ ion channel. Science 2012; 335:436-41; PMID:22282805; http://dx.doi.org/10.1126/science.1213808
8. Miller AN, Long SB. Crystal structure of the human two-pore domain potassium channel K2P1. Science 2012; 335:432-6; PMID:22282804; http://dx.doi.org/10.1126/science.1213274
9. Payandeh J, Scheuer T, Zheng N, Catterall WA. The crystal structure of a voltage-gated sodium channel. Nature 2011; 475:353-8; PMID:21743477; http://dx.doi.org/10.1038/nature10238
10. Kaczmarski JA, Corry B. Investigating the size and dynamics of voltage-gated sodium channel fenestrations: A molecular dynamics study. Channels 2014; 8; PMID:24632677; http://dx.doi.org/10.4161/chan.28136
11. Martin LJ, Corry B. Locating the route of entry and binding sites of benzocaine and phenytoin in a bacterial voltage gated sodium channel. PLoS Com Biol 2014; 10:e1003688; http://dx.doi.org/10.1371/journal.pcbi.1003688
12. Brohawn SG, Campbell EB, MacKinnon R. Domain-swapped chain connectivity and gated membrane access in a Fab-mediated crystal of the human TRAAK K+ channel. Proc Natl Acad Sci (U.S.A) 2013; 110:2129-34; PMID:23341632; http://dx.doi.org/10.1073/pnas.1218950110
13. Enyedi P, Czirjak G. Molecular background of leak K+ currents: two-pore domain potassium channels. Physiol Rev 2010; 90:559-605; PMID:20393194; http://dx.doi.org/10.1152/physrev.00029.2009
14. Bagriantsev SN, Peyronnet R, Clark KA, Honore E, Minor DL, Jr. Multiple modalities converge on a common gate to control K2P channel function. EMBO J 2011; 30:3594-606; PMID:21765396; http://dx.doi.org/10.1038/emboj.2011.230
15. Cohen A, Ben-Abu Y, Zilberberg N. Gating the pore of potassium leak channels. Eur Biophys J 2009; 39:61-73; PMID:19404634; http://dx.doi.org/10.1007/s00249-009-0457-6
16. Piechotta PL, Rapedius M, Stansfeld PJ, Bollepalli MK, Ehrlich G, Andres-Enguix I, Fritzenschaft H, Decher N, Sansom MS, Tucker SJ, et al. The pore structure and gating mechanism of K2P channels. EMBO J 2011; 30:3607-19; PMID:21822218; http://dx.doi.org/10.1038/emboj.2011.268
17. Rapedius M, Schmidt MR, Sharma C, Stansfeld PJ, Sansom MS, Baukrowitz T, Tucker SJ. State-independent intracellular access of quaternary ammonium blockers to the pore of TREK-1. Channels 2012;

Downloaded by [Radcliffe Infirmary] at 01:17 05 October 2015

6:473-8; PMID:22991046; http://dx.doi.org/10.4161/chan.22153
18. Nilius B, Honore E. Sensing pressure with ion channels. Trends Neurosci 2012; 35:477-86; PMID:22622029; http://dx.doi.org/10.1016/j.tins.2012.04.002
19. Aryal P, Abd-Wahab F, Bucci G, Sansom MS, Tucker SJ. A hydrophobic barrier deep within the inner pore of the TWIK-1 K2P potassium channel. Nat Comms 2014; 5:4377; http://dx.doi.org/10.1038/ncomms5377
20. Aryal P, Sansom MS, Tucker SJ. Hydrophobic Gating in Ion Channels. J Mol Biol 2014; 427:121-130; PMID:25106689
21. Ulmschneider MB, Bagneris C, McCusker EC, Decaen PG, Delling M, Clapham DE, Ulmschneider JP, Wallace BA. Molecular dynamics of ion transport through the open conformation of a bacterial voltage-gated sodium channel. Proc Natl Acad Sci (USA) 2013; 110:6364-9; PMID:23542377; http://dx.doi.org/10.1073/pnas.1214667110
22. Holthuis JC, Pomorski T, Raggers RJ, Sprong H, Van Meer G. The organizing potential of sphingolipids in intracellular membrane transport. Physiol Rev 2001; 81:1689-723; PMID:11581500
23. Holthuis JC, Menon AK. Lipid landscapes and pipelines in membrane homeostasis. Nature 2014; 510:48-57; PMID:24899304; http://dx.doi.org/10.1038/nature13474
24. Brohawn SG, Su Z, MacKinnon R. Mechanosensitivity is mediated directly by the lipid membrane in TRAAK and TREK1 K+ channels. Proc Natl Acad Sci (U.S.A) 2014; 111:3614-9; PMID:24550493; http://dx.doi.org/10.1073/pnas.1320768111
25. Bagriantsev SN, Clark KA, Minor DL, Jr. Metabolic and thermal stimuli control K(2P)2.1 (TREK-1) through modular sensory and gating domains. EMBO J 2012; 31:3297-308; PMID:22728824; http://dx.doi.org/10.1038/emboj.2012.171
26. Comoglio Y, Levitz J, Kienzler MA, Lesage F, Isacoff EY, Sandoz G. Phospholipase D2 specifically regulates TREK potassium channels via direct interaction and local production of phosphatidic acid. Proc Natl Acad Sci (U.S.A) 2014; 111:13547-52; PMID:25197053; http://dx.doi.org/10.1073/pnas.1407160111
27. Chemin J, Patel A, Duprat F, Zanzouri M, Lazdunski M, Honore E. Lysophosphatidic acid-operated K^+ channels. J Biol Chem 2005; 280:4415-21; PMID:15572365; http://dx.doi.org/10.1074/jbc.M408246200
28. Dedman A, Sharif-Naeini R, Folgering JH, Duprat F, Patel A, Honore E. The mechano-gated K(2P) channel TREK-1. Eur Biophys J 2009; 38:293-303; PMID:18369610; http://dx.doi.org/10.1007/s00249-008-0318-8
29. Bond PJ, Sansom MS. Insertion and assembly of membrane proteins via simulation. J Am Chem Soc 2006; 128:2697-704; PMID:16492056; http://dx.doi.org/10.1021/ja0569104
30. Scott KA, Bond PJ, Ivetac A, Chetwynd AP, Khalid S, Sansom MS. Coarse-grained MD simulations of membrane protein-bilayer self-assembly. Structure 2008; 16:621-30; PMID:18400182; http://dx.doi.org/10.1016/j.str.2008.01.014
31. Smart OS, Neduvelil JG, Wang X, Wallace BA, Sansom MS. HOLE: a program for the analysis of the pore dimensions of ion channel structural models. J Mol Graph 1996; 14:354-60, 76; PMID:9195488; http://dx.doi.org/10.1016/S0263-7855(97)00009-X

Downloaded by [Radcliffe Infirmary] at 01:17 05 October 2015

Appendix E

References

Armstrong, C.M. (1971). Interaction of Tetraethylammonium Ion Derivatives with the Potassium Channels of Giant Axons. The Journal of General Physiology *58*, 413–437.

Aryal, P., Abd-Wahab, F., Bucci, G., Sansom, M.S.P., and Tucker, S.J. (2014a). A hydrophobic barrier deep within the inner pore of the TWIK-1 K2P potassium channel. Nature Communications *5*, 1–9.

Aryal, P., Abd-Wahab, F., Bucci, G., Sansom, M.S.P., and Tucker, S.J. (2014b). Influence of lipids on the hydrophobic barrier within the pore of the TWIK-1 K2P channel. Channels *9*, 44–49.

Aryal, P., Sansom, M.S.P., and Tucker, S.J. (2014c). Hydrophobic gating in ion channels. Journal of Molecular Biology .

Ball, P. (2003). Chemical physics: How to keep dry in water. Nature *423*, 25–26.

Bavro, V.N., De Zorzi, R., Schmidt, M.R., Muniz, J.R.C., Zubcevic, L., Sansom, M.S.P., Vénien-Bryan, C., and Tucker, S.J. (2012). Structure of a KirBac potassium channel with an open bundle-crossing indicates a mechanism of channel gating. Nature Structural & Molecular Biology *19*, 158–163.

Beckstein, O., Biggin, P.C., and Sansom, M.S.P. (2001). A Hydrophobic Gating Mechanism for Nanopores. The Journal of Physical Chemistry B *105*, 12902–12905.

Beckstein, O. and Sansom, M.S.P. (2003). Liquid-vapor oscillations of water in hydrophobic nanopores. Proceedings of the National Academy of Sciences of the United States of America *100*, 7063–8.

Beckstein, O. and Sansom, M.S.P. (2004). The influence of geometry, surface character, and flexibility on the permeation of ions and water through biological pores. Physical Biology *1*, 42.

Beckstein, O. and Sansom, M.S.P. (2006). A hydrophobic gate in an ion channel: the closed state of the nicotinic acetylcholine receptor. Physical Biology *3*, 147.

Ben-Abu, Y., Zhou, Y., Zilberberg, N., and Yifrach, O. (2009). Inverse coupling in leak and voltage-activated K^+ channel gates underlies distinct roles in electrical signaling. Nature Structural & Molecular Biology *16*, 71–79.

Benarroch, E.E. (2009). Potassium channels: Brief overview and implications in epilepsy . Neurology *72*, 664–669.

Bichet, D., Blin, S., Feliciangeli, S., Chatelain, F., Bobak, N., and Lesage, F. (2014). Silent but not dumb: how cellular trafficking and pore gating modulate expression of TWIK1 and THIK2. Pflügers Archiv - European Journal of Physiology 1–11.

Bollepalli, M.K., Fowler, P.W., Rapedius, M., Shang, L., Sansom, M.S.P., Tucker, S.J., and Baukrowitz, T. (2014). State-dependent network connectivity determines gating in a K+ channel. Structure (London, England : 1993) *22*, 1037–46.

Brohawn, S.G., Campbell, E.B., and MacKinnon, R. (2013). Domain-swapped chain connectivity and gated membrane access in a Fab-mediated crystal of the human TRAAK K+ channel. Proceedings of the National Academy of Sciences *110*, 2129–2134.

Brohawn, S.G., Del Marmol, J., and MacKinnon, R. (2012). Crystal Structure of the Human K2P TRAAK, a Lipid- and Mechano-Sensitive K+ Ion Channel. Science *335*, 436–441.

Brohawn, S.G., Su, Z., and MacKinnon, R. (2014). Mechanosensitivity is mediated directly by the lipid membrane in TRAAK and TREK1 K(+) channels. Proceedings of the National Academy of Sciences of the United States of America *111*, 3614–3619.

Cai, M. and Jordan, P.C. (1990). How does vestibule surface charge affect ion conduction and toxin binding in a sodium channel? Biophysical Journal *57*, 883–891.

Chatelain, F.C., Bichet, D., Douguet, D., Feliciangeli, S., Bendahhou, S., Reichold, M., Warth, R., Barhanin, J., and Lesage, F. (2012). TWIK1, a unique background channel

with variable ion selectivity. Proceedings of the National Academy of Sciences of the United States of America *109*, 5499–504.

Chatelain, F.C., Bichet, D., Feliciangeli, S., Larroque, M.M., Braud, V.M., Douguet, D., and Lesage, F. (2013). Silencing of the tandem pore domain halothane-inhibited K+ channel 2 (THIK2) relies on combined intracellular retention and low intrinsic activity at the plasma membrane. The Journal of Biological Chemistry *288*, 35081–92.

Chen, H., Chatelain, F.C., and Lesage, F. (2014). Altered and dynamic ion selectivity of K(+) channels in cell development and excitability. Trends in Pharmacological Sciences *35*, 461–469.

Cheng, C.J., Kuo, E., and Huang, C.L. (2013). Extracellular Potassium Homeostasis: Insights from Hypokalemic Periodic Paralysis. Seminars in Nephrology *33*, 237–247.

Chiavazzo, E., Fasano, M., Asinari, P., and Decuzzi, P. (2014). Scaling behaviour for the water transport in nanoconfined geometries. Nature Communications *5*.

Choe, S. (2002). Potassium channel structures. Nature Reviews Neuroscience *3*, 115–121.

Cluzeaud, F., Reyes, R., Escoubet, B., Fay, M., Lazdunski, M., Bonvalet, J.P., Lesage, F., and Farman, N. (1998). Expression of TWIK-1, a novel weakly inward rectifying potassium channel in rat kidney. American Journal of Physiology Cell Physiology *275*, C1602–1609.

Cuello, L.G., Jogini, V., Cortes, D.M., Pan, A.C., Gagnon, D.G., Dalmas, O., Cordero-Morales, J.F., Chakrapani, S., Roux, B., and Perozo, E. (2010). Structural basis for the coupling between activation and inactivation gates in K(+) channels. Nature *466*, 272–275.

Decressac, S., Franco, M., Bendahhou, S., Warth, R., Knauer, S., Barhanin, J., Lazdunski, M., and Lesage, F. (2004). ARF6-dependent interaction of the TWIK1 K+ channel with EFA6, a GDP/GTP exchange factor for ARF6. European Molecular Biology Organization Reports *5*, 1171–1175.

Díaz-Franulic, I., Sepúlveda, R.V., Navarro-Quezada, N., González-Nilo, F., and Naranjo, D. (2015). Pore dimensions and the role of occupancy in unitary conductance of Shaker K channels. The Journal of General Physiology *146*, 133–46.

Dong, Y.Y., Pike, A.C.W., Mackenzie, A., McClenaghan, C., Aryal, P., Dong, L., Quigley, A., Grieben, M., Goubin, S., Mukhopadhyay, S., et al. (2015). K2P channel gating mechanisms revealed by structures of TREK-2 and a complex with Prozac. Science *347*, 1256–1259.

Doyle, D.A. (2004). Structural changes during ion channel gating. Trends in Neurosciences *27*, 298–302.

Doyle, D.A., Cabral, J.M., Pfuetzner, R.A., Kuo, A., Gulbis, J.M., Cohen, S.L., Chait, B.T., and MacKinnon, R. (1998). The Structure of the Potassium Channel: Molecular Basis of K+ Conduction and Selectivity. Science *280*, 69–77.

Egwolf, B. and Roux, B. (2010). Ion selectivity of the KcsA channel: a perspective from multi-ion free energy landscapes. Journal of Molecular Biology *401*, 831–42.

Eisenman, G. and Horn, R. (1983). Ionic selectivity revisited: The role of kinetic and equilibrium processes in ion permeation through channels. The Journal of Membrane Biology *76*, 197–225.

El-Jouni, W., Haun, S., and Machaca, K. (2008). Internalization of Plasma Membrane Ca(2+)-ATPase during Xenopus Oocyte Maturation. Developmental Biology *324*, 99–107.

Enyedi, P. and Czirják, G. (2010). Molecular background of leak K+ currents: two-pore domain potassium channels. Physiological Reviews *90*, 559–605.

Feliciangeli, S., Bendahhou, S., Sandoz, G., Gounon, P., Reichold, M., Warth, R., Lazdunski, M., Barhanin, J., and Lesage, F. (2007). Does sumoylation control K2P1/TWIK1 background K+ channels? Cell *130*, 563–569.

Feliciangeli, S., Chatelain, F.C., Bichet, D., and Lesage, F. (2015). The family of K2P channels: salient structural and functional properties. The Journal of Physiology *593*, 2587–2603.

Feliciangeli, S., Tardy, M.P., Sandoz, G., Chatelain, F., Warth, R., Barhanin, J., Bendahhou, S., and Lesage, F. (2009). Potassium channel silencing by constitutive endocytosis and intracellular sequestration. Journal of Biological Chemistry .

Fowler, P.W., Bollepalli, M.K., Rapedius, M., Nematian-Ardestani, E., Shang, L., Sansom, M.S.P., Tucker, S.J., and Baukrowitz, T. (2014). Insights into the structural nature of the transition state in the Kir channel gating pathway. Channels *8*, 551–555.

Gareau, J.R. and Lima, C.D. (2010). The SUMO pathway: emerging mechanisms that shape specificity, conjugation and recognition. Nature Reviews Molecular Cell Biology *11*, 861–871.

Geiss-Friedlander, R. and Melchior, F. (2007). Concepts in sumoylation: a decade on. Nature Reviews Molecular Cell Biology *8*, 947–956.

Goldstein, S.A., Bockenhauer, D., O'Kelly, I., and Zilberberg, N. (2001). Potassium leak channels and the KCNK family of two-P-domain subunits. Nature Reviews Neuroscience *2*, 175–184.

Goldstein, S.A.N. (2011). K2P Potassium Channels, Mysterious and Paradoxically Exciting. Science Signaling *4*, pe35–pe35.

Grossfield, A. (2005). Dependence of ion hydration on the sign of the ion's charge. The Journal of Chemical Physics *122*, 024506.

Hall, J.E. (2010a). Membrane Potentials and Action Potentials. In A.C. Guyton and J.E. Hall, eds., Guyton and Hall Textbook of Medical Physiology, chapter 5, 57–69 (Philadelphia: Elsevier Saunders), 12 edition.

Hall, J.E. (2010b). Renal regulation of potassium, calcium, phosphate, and magnesium; integration of renal mechanisms for control of blood volume and extracellular fluid volume. In A.C. Guyton and J.E. Hall, eds., Guyton and Hall Textbook of Medical Physiology, chapter 29, 363 (Philadelphia: Elsevier Saunders), 12 edition.

Heginbotham, L., Abramson, T., and MacKinnon, R. (1992). A functional connection between the pores of distantly related ion channels as revealed by mutant K+ channels. Science *258*, 1152–1155.

Henley, J.M., Craig, T.J., and Wilkinson, K.A. (2014). Neuronal SUMOylation: mechanisms, physiology, and roles in neuronal dysfunction. Physiological Reviews *94*, 1249–85.

Hille, B. (2001). Ionic channels of excitable membranes, volume 3 (Sinauer).

Hodgkin, A.L. and Keynes, R.D. (1955). The potassium permeability of a giant nerve fibre. The Journal of Physiology *128*, 61–88.

Hummer, G. (2014). Potassium ions line up. Science *346*, 303.

Hummer, G., Rasaiah, J.C., and Noworyta, J.P. (2001). Water conduction through the hydrophobic channel of a carbon nanotube. Nature *414*, 188–190.

Jha, A., Purohit, P., and Auerbach, A. (2009). Energy and Structure of the M2 Helix in Acetylcholine Receptor-Channel Gating. Biophysical Journal *96*, 4075–4084.

Ketchum, K.A., Joiner, W.J., Sellers, A.J., Kaczmarek, L.K., and Goldstein, S.A. (1995). A new family of outwardly rectifying potassium channel proteins with two pore domains in tandem. Nature *376*, 690–695.

Kjeldsen, K. (2010). Hypokalemia and sudden cardiac death. Experimental and Clinical Cardiology *15*, e96–e99.

Kofuji, P. and Newman, E.A. (2004). Potassium buffering in the central nervous system. Neuroscience *129*, 1045–1056.

Köpfer, D.A., Song, C., Gruene, T., Sheldrick, G.M., Zachariae, U., and de Groot, B.L. (2014). Ion permeation in K+ channels occurs by direct Coulomb knock-on. Science *346*, 352–355.

Kuo, A., Gulbis, J.M., Antcliff, J.F., Rahman, T., Lowe, E.D., Zimmer, J., Cuthbertson, J., Ashcroft, F.M., Ezaki, T., and Doyle, D.A. (2003). Crystal Structure of the Potassium Channel KirBac1.1 in the Closed State. Science *300*, 1922–1926.

Lesage, F., Guillemare, E., Fink, M., Duprat, F., Lazdunski, M., Romey, G., and Barhanin, J. (1996a). TWIK-1, a ubiquitous human weakly inward rectifying K+ channel with a novel structure. The European Molecular Biology Organization Journal *15*, 1004–1011.

Lesage, F., Reyes, R., Fink, M., Duprat, F., Guillemare, E., and Lazdunski, M. (1996b). Dimerization of TWIK-1 K+ channel subunits via a disulfide bridge. The European Molecular Biology Organization Journal *15*, 6400–6407.

Long, S.B., Campbell, E.B., and MacKinnon, R. (2005). Voltage Sensor of Kv1.2: Structural Basis of Electromechanical Coupling. Science *309*, 903–908.

Lu, Z., Klem, A.M., and Ramu, Y. (2001). Ion conduction pore is conserved among potassium channels. Nature *413*, 809–813.

Ma, L., Xie, Y.P., Zhou, M., and Chen, H. (2012). Silent TWIK-1 Potassium Channels Conduct Monovalent Cation Currents. Biophysical Journal *102*, L34–L36.

Ma, L., Zhang, X., and Chen, H. (2011). TWIK-1 two-pore domain potassium channels change ion selectivity and conduct inward leak sodium currents in hypokalemia. Science Signaling *4*, ra37.

MacKinnon, R. (2003). Potassium channels. FEBS Letters *555*, 62–65.

Manders, E.M.M., Verbeek, F.J., and Aten, J.A. (1993). Measurement of co-localization of objects in dual-colour confocal images. Journal of Microscopy *169*, 375–382.

Mason, A.K., Jacobs, B.E., and Welling, P.A. (2008). AP-2-dependent Internalization of Potassium Channel Kir2.3 Is Driven by a Novel Di-hydrophobic Signal. Journal of Biological Chemistry *283*, 5973–5984.

Millar, I.D., Taylor, H.C., Cooper, G.J., Kibble, J.D., Barhanin, J., and Robson, L. (2006). Adaptive downregulation of a quinidine-sensitive cation conductance in renal principal cells of TWIK-1 knockout mice. Pflügers Archiv *453*, 107–116.

Miller, A.N. and Long, S.B. (2012). Crystal structure of the human two-pore domain potassium channel K2P1. Science *335*, 432–6.

Miller, C. (2000). An overview of the potassium channel family. Genome Biology *1*, reviews0004.1–reviews0004.5.

Miyazawa, A., Fujiyoshi, Y., and Unwin, N. (2003). Structure and gating mechanism of the acetylcholine receptor pore. Nature *423*, 949–955.

Nie, X., Arrighi, I., Kaissling, B., Pfaff, I., Mann, J., Barhanin, J., and Vallon, V. (2005). Expression and insights on function of potassium channel TWIK-1 in mouse kidney. Pflügers Archiv *451*, 479–488.

Nimigean, C.M. and Allen, T.W. (2011). Origins of ion selectivity in potassium channels from the perspective of channel block. The Journal of General Physiology *137*, 405–413.

Nishida, M., Cadene, M., Chait, B.T., and MacKinnon, R. (2007). Crystal structure of a Kir3.1âĂŘprokaryotic Kir channel chimera. The European Molecular Biology Organization Journal *26*, 4005–4015.

Noori, H.R. (2011). The impact of the glial spatial buffering on the K+ Nernst potential. Cognitive Neurodynamics *5*, 285–291.

Noskov, S.Y. and Roux, B. (2007). Importance of Hydration and Dynamics on the Selectivity of the KcsA and NaK Channels. The Journal of General Physiology *129*, 135–143.

Ortega, B., Mason, A.K., and Welling, P.A. (2012). A Tandem Di-hydrophobic Motif Mediates Clathrin-dependent Endocytosis via Direct Binding to the AP-2 $\alpha\sigma$2 Subunits. The Journal of Biological Chemistry *287*, 26867–26875.

Palmer, B.F. (2015). Regulation of Potassium Homeostasis. Clinical Journal of the American Society of Nephrology *10*, 1050–1060.

Pérez-Hernández, N., Luong, T.Q., Febles, M., Marco, C., Limbach, H.H., Havenith, M., Pérez, C., Roux, M.V., Pérez, R., and Martín, J.D. (2012). The Mobility of Water Molecules through Hydrated Pores. The Journal of Physical Chemistry C *116*, 9616–9630.

Piechotta, P.L., Rapedius, M., Stansfeld, P.J., Bollepalli, M.K., Erhlich, G., Andres-Enguix, I., Fritzenschaft, H., Decher, N., Sansom, M.S.P., Tucker, S.J., et al. (2011). The pore structure and gating mechanism of K2P channels. The European Molecular Biology Organization Journal *30*, 3607–3619.

Plant, L.D., Dementieva, I.S., Kollewe, A., Olikara, S., Marks, J.D., and Goldstein, S.A.N. (2010). One SUMO is sufficient to silence the dimeric potassium channel K2P1. Proceedings of the National Academy of Sciences of the United States of America *107*, 10743–10748.

Plant, L.D., Zuniga, L., Araki, D., Marks, J.D., and Goldstein, S.A.N. (2012). SUMOylation Silences Heterodimeric TASK Potassium Channels Containing K2P1 Subunits in Cerebellar Granule Neurons. Science Signaling *5*, ra84–ra84.

Pohl, H., Wheeler, J., and Murray, H. (2013). Sodium and Potassium in Health and Disease. In A. Sigel, H. Sigel, and R.K.O. Sigel, eds., Interrelations between Essential Metal Ions and Human Diseases SE - 2, volume 13 of *Metal Ions in Life Sciences*, 29–47 (Springer Netherlands).

Posson, D.J., McCoy, J.G., and Nimigean, C.M. (2013). The voltage-dependent gate in MthK potassium channels is located at the selectivity filter. Nature Structural & Molecular Biology *20*, 159–166.

Posson, D.J., Rusinova, R., Andersen, O.S., and Nimigean, C.M. (2015). Calcium ions open a selectivity filter gate during activation of the MthK potassium channel. Nature Communications *6*.

Powell, M.R., Cleary, L., Davenport, M., Shea, K.J., and Siwy, Z.S. (2011). Electric-field-induced wetting and dewetting in single hydrophobic nanopores. Nature Nanotechnology *6*, 798–802.

Rajan, S., Plant, L.D., Rabin, M.L., Butler, M.H., and Goldstein, S.A.N. (2005). Sumoylation silences the plasma membrane leak K+ channel K2P1. Cell *121*, 37–47.

Reisser, S., Strandberg, E., Steinbrecher, T., and Ulrich, A.S. (2014). 3D hydrophobic moment vectors as a tool to characterize the surface polarity of amphiphilic peptides. Biophysical journal *106*, 2385–94.

Renigunta, V., Schlichthörl, G., and Daut, J. (2015). Much more than a leak: structure and function of K2P-channels. Pflügers Archiv - European Journal of Physiology *467*, 867–894.

Roth, R., Gillespie, D., Nonner, W., and Eisenberg, R.E. (2008). Bubbles, Gating, and Anesthetics in Ion Channels. Biophysical Journal *94*, 4282–4298.

Sendner, C., Horinek, D., Bocquet, L., and Netz, R.R. (2009). Interfacial Water at Hydrophobic and Hydrophilic Surfaces: Slip, Viscosity, and Diffusion. Langmuir *25*, 10768–10781.

Shi, N., Zeng, W., Ye, S., Li, Y., and Jiang, Y. (2011). Crucial points within the pore as determinants of K+ channel conductance and gating. Journal of Molecular Biology *411*, 27–35.

So, I., Ashmole, I., Davies, N.W., Sutcliffe, M.J., and Stanfield, P.R. (2001). The K(+) channel signature sequence of murine Kir2.1: mutations that affect microscopic gating but not ionic selectivity. The Journal of Physiology *531*, 37–50.

Stansfeld, P.J. and Sansom, M.S.P. (2011). From Coarse Grained to Atomistic: A Serial Multiscale Approach to Membrane Protein Simulations. Journal of Chemical Theory and Computation *7*, 1157–1166.

Sukharev, A.A., Akitake, B., Kamaraju, K., Chiang, C.S., and S (2010). Hydration properties of mechanosensitive channel pores define the energetics of gating. Journal of Physics: Condensed Matter *22*, 454120.

Tan, P.S., Perry, M.D., Ng, C.A., Vandenberg, J.I., and Hill, A.P. (2012). Voltage-sensing domain mode shift is coupled to the activation gate by the N-terminal tail of hERG channels. The Journal of General Physiology *140*, 293–306.

Trick, J.L., Wallace, E.J., Bayley, H., and Sansom, M.S.P. (2014). Designing a Hydrophobic Barrier within Biomimetic Nanopores. ACS Nano *8*, 11268–11279.

Varma, S., Rogers, D.M., Pratt, L.R., and Rempe, S.B. (2011a). Design principles for K(+) selectivity in membrane transport. The Journal of General Physiology *137*, 479–488.

Varma, S., Rogers, D.M., Pratt, L.R., and Rempe, S.B. (2011b). Perspectives on: ion selectivity: design principles for K+ selectivity in membrane transport. The Journal of General Physiology *137*, 479–88.

Wang, W., Putra, A., Schools, G.P., Ma, B., Chen, H., Kaczmarek, L.K., Barhanin, J., Lesage, F., and Zhou, M. (2013). The contribution of TWIK-1 channels to astrocyte K+ current is limited by retention in intracellular compartments .

Zhou, M., Xu, G., Xie, M., Zhang, X., Schools, G.P., Ma, L., Kimelberg, H.K., and Chen, H. (2009). TWIK-1 and TREK-1 Are Potassium Channels Contributing Significantly to Astrocyte Passive Conductance in Rat Hippocampal Slices. The Journal of Neuroscience *29*, 8551–8564.

Zhou, Y., Morais-Cabral, J.H., Kaufman, A., and MacKinnon, R. (2001). Chemistry of ion coordination and hydration revealed by a K+ channel-Fab complex at 2.0Å resolution. Nature *414*, 43–48.

Zhu, F. and Hummer, G. (2012). Drying Transition in the Hydrophobic Gate of the GLIC Channel Blocks Ion Conduction. Biophysical Journal *103*, 219–227.

Zilberberg, N., Ilan, N., and Goldstein, S.A. (2001). KCNKØ: opening and closing the 2-P-domain potassium leak channel entails "C-type" gating of the outer pore. Neuron *32*, 635–648.